Regulation of Ca^{2+}-activated Cl^- channel ANO1 (TMEM16A) by different Ca^{2+} sources in sensory neurons

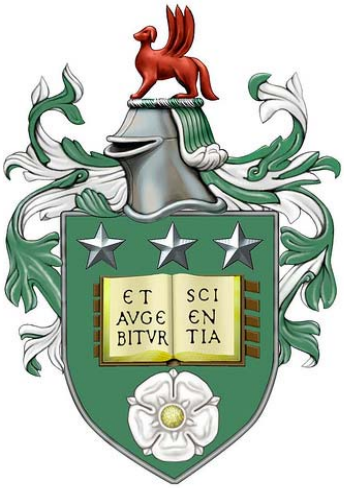

Xin Jin

Submitted in accordance with the requirements for the degree of
Doctor of Philosophy

The University of Leeds
School of Biomedical Sciences

March 2015

The candidate confirms that the work submitted is his/her own, except where work which has formed part of jointly authored publications has been included. The contribution of the candidate and the other authors to this work has been explicitly indicated below. The candidate confirms that appropriate credit has been given within the thesis where reference has been made to the work of others.

Chapter 4, 5, 6, 7 are based on work from jointly authored publication: Activation of the Cl- channel ANO1 by localized calcium signals in nociceptive sensory neurons requires coupling with the IP3 receptor. Jin X, Shah S, Liu Y, Zhang H, Lees M, Fu Z, Lippiat JD, Beech DJ, Sivaprasadarao A, Baldwin SA, Zhang H, Gamper N. Sci Signal. 2013 Aug 27; 6 (290):ra73.

Xin Jin et al planned experiments; Xin Jin et al performed experiments; Xin Jin et al analyzed data; Figure 4.5 in panels A-C was contributed by Yani Liu, Figure 5.2 was contributed by Huiran Zhang, Figure 6.1 was contributed by Shihab Shah and Nikita Gamper.

Acknowledgements

I would like to thank my supervisor, Dr Nikita Gamper for giving me the opportunity to work on such an exciting project, for his advice, encouragement, critical inputs and continuous guidance throughout this project.

I am thankful to past and present members of the Gamper group for their valuable discussions and practical help. I would also like to sincerely thank Prof. Hailin Zhang and his group for continuous generous help and practical support. I am extremely grateful to Dr Rao Sivaprasadarao and Dr Stephen Baldwin for their excellent advice, and general help. As it is impossible to mention everyone who has helped me during the course of this project, I would like to say a big thanks to the people in neuroscience and ion channels groups at Leeds.

I would like to acknowledge the Faculty of Biological Sciences and University of Leeds for funding.

I am grateful to my family, for their encouragement, advice and support throughout my life.

Abstract

Proteins of anoctamin (TMEM16) family are the candidate subunits for Ca^{2+}-activated Cl^- channels (CaCC). In recent years, studies have shown that anoctamin-1 (TMEM16A or ANO1) plays important physiological roles in processes including epithelial fluid secretion, muscle contraction and olfactory transduction. How the Ca^{2+} regulates the activity of ANO1 in different tissue is still not clear.

In this study, I showed that the excitatory CaCC in nociceptors (small-diameter sensory neurons that are responsible for transmission of painful stimuli) was activated by the release of Ca^{2+} from the 1, 4, 5-trisphosphate (IP_3)-sensitive intracellular stores in response to bradykinin (BK) or proteases (through protease activated receptor 2). Interestingly, while in the majority of nociceptors, CaCC was induced by Ca^{2+} release from the stores, only in a few neurons CaCC was activated by the Ca^{2+} influx through the voltage-gated Ca^{2+} channels (VGCC). Chelating intracellular Ca^{2+} with the slow Ca^{2+} buffer EGTA did not affect CaCC activation by protease activated receptor 2 (PAR2), while BAPTA abolished such activation, suggesting a close proximity of the Ca^{2+} release sites and CaCC. Membrane fractionation demonstrated that in the dorsal root ganglion (DRG), ANO1, bradykinin receptor 2 (B_2R) or PAR2, were co-purified with lipid raft marker caveolin-1. Using various biochemical approaches I further demonstrated that ANO1 physically interacted with the IP_3 receptor 1 (IP_3R1) in DRG. Moreover, IP_3R1, ANO1, B_2R, and/or PAR2 were all assembled into functional signalling complexes and the plasma membrane components of the complex which contained ANO1 and GPCRs were tethered to the juxtamembrane regions of the endoplasmic reticulum. Disruption of the membrane microdomains by methyl-beta-cyclodextrin (MβCD) or competitive peptides partially restored coupling of CaCC to VGCC but disrupted coupling between B_2R or PAR2 signaling and ANO1. Thus, such molecular complexes dichotomize different Ca^{2+} sources to provide ANO1-mediated excitation in response to specific ambient signals but protect the channels from global changes in intracellular Ca^{2+} and prevent sensory neurons from overexcitability.

Table of contents

List of figures

List of tables

Abbreviations

Abbreviations	Full names
5-HT	5-hydroxytryptamine
$[Ca^{2+}]_i$	Intracellular free Ca^{2+} concentration
2-APB	2-Aminoethoxydiphenylborate
αCD	α-cyclodextrin
A9C	Anthracene-9-carboxylic acid
AC	Adenylate cyclase
AP	Action potential
ATP	Adenosine triphosphate
B_1R	Bradykinin receptor B_1
B_2R	Bradykinin receptor B_2
BK	Bradykinin
CaCCs	Calcium (Ca^{2+}) -activated chloride (Cl^-) channels
CaM	Calmodulin
CaMKII	Calmodulin-dependent protein kinase II
CaMKs	Calmodulin-dependent kinases
cAMP	Cyclic Adenosine monophosphate
$cAMP_i$	Cytosolic cAMP
Cav-1	Caveolin-1
CF	Cystic fibrosis
CFTR	Cystic fibrosis membrane conductance regulator
CGRP	Calcitonin-gene related peptide
cGMP	Cyclic guanosine monophosphate
CHO	Chinese hamster ovary
C-MAD	C-terminal membrane-attachment domain
CNG	Cyclic nucleotide-gated
CNS	Central nervous system
CRAC	Ca^{2+} release activated channel
CREB	cAMP response element binding protein
CSD	Caveolin scaffolding domain
DAG	Diacylglycerol
dBK	desArg9-BK
DCPIB	4-(2-Butyl-6,7-dichloro-2-cyclopentyl-indan-1-on-5-yl) oxobutyric acid
DIDS	4,4'-Diisothiocyano-2,2'-stilbenedisulfonic acid
DIGs	Detergent-insoluble, glycolipid-enriched complexes
DMEM	Dulbecco's Modified Eagle's Medium
DPC	Diphenylamine-2-carboxylic acid
DRG	Dorsal root ganglia
DRMs	Detergent-resistant membranes
DTT	Dithiothrietol
EC_{50}	Half-maximal concentration

E_{Cl}	Equilibrium potential for Cl^-
ENaC	Epithelial Na^+ channel
ER	Endoplasmic reticulum
FBS	Fetal bovin serum
FFA	Flufenamic acid
FRET	Fluorescence resonance energy transfer
FRT	Fischer rat thyroid
$GABA_A$	γ-aminobutyric acid type A
$GABA_ARs$	$GABA_A$ receptors
GFP	Green fluorescent protein
GlyR	Glycine receptor
GPCRs	G protein-coupled receptors
GPI	Glycosyl-phosphatidylinositol
GST	Glutathione S-transferase
HEK293	Human Embryonic Kidney 293
HUVEC	Human Umbilical Vein Endothelial Cell
HVA	High-voltage gated Ca^{2+} channels
IL-4	Interleukin 4
IB	Immunoblotting
I_{CaCC}	Ca^{2+}-activated Cl^- channel current
IK	Intermediate-conductance Ca^{2+}- activated K^+ channel
IP	Immunoprecipitation
IP_3	Inositol 1, 4, 5-triphosphate
IP_3R	IP_3 receptor
I-V	The current-voltage relationship
KChIP	Voltage-gated K^+ channel-interacting protein
KCC2	K^+-Cl^- cotransporter2
Kd	Equilibrium binding constant
Kv	Voltage-gated K^+ channel
LVA	Low-voltage gated Ca^{2+} channels
MTSET	2-(Trimethylammonium)ethyl methanethiosulfonate, bromide
MTSEA	2-Aminoethyl methanethiosulfonate hydrobromide
MAPK	Mitogen-activated protein kinase
mGluR	Metabotropic glutamate receptor
MS	Mechano-gated channel
MβCD	Methyl-β-cyclodextrin
NBD	Nucleotide-binding domain
NFA	Niflumic acid
NFAT	Nuclear factor activated T-cells
NKCC1	Na^+-K^+-Cl^- cotransporter1
N-MAD	The amino-terminal membrane-attachment domain
NPPB	5-nitro-2-(3-phenylpropylamino)-benzoate
NMDA	N-methyl-D-aspartate
OD	Oligomerization domain

PAG	Peri aqueductal grey
PAGE	Polyacrylamide gel electrophoresis
PASMCs	Pulmonary artery smooth muscle cells
PAR2	Protease activated receptor 2
PAR2-PL	Protease activated receptor 2 peptide ligand
PARs	Protease activated receptors
PCR	Polymerase chain reaction
PI3K	Phosphoinositide-3-kinase
PIP_2	Phosphatidylinositol 4, 5-bisphosphate
PKA	Protein kinase A
PKC	Protein kinase C
PLA	*In situ* proximity ligation assay
PLA2	Phospholipase A2
PLC	Phospholipase C
PM	Plasma membrane
PSD-95	Postsynaptic density protein-95
RCA	Rolling circle amplification
RPE	Retinal pigment epithelial
RT-PCR	Reverse Transcription-Polymerase Chain Reaction
RVM	Rostroventral medulla
RyRs	Ryanodine receptors
SCG	Superior cervical ganglia
SERCA	Ca^{2+}-ATPase
SITS	4-acetamido-4-isothiocyanatostilbene-2,2-disulfonic acid
SK	Small-conductance Ca^{2+}- activated K^+ channel
Slo1 or $K_{Ca1.1}$	Large-conductance Ca^{2+}- activated K^+ channel
SMC	Smooth muscle cell
SILAC	Stable isotope labeling by amino acids in cell culture
SOCE	Store-operated Ca^{2+} entry
SP	Substance P
SR	Sarcoplasmic reticula
$\tau_{0.5}$	Time required to reach the half-maximal current
TG	Trigeminal ganglia
TGF-α	Transforming growth factor alpha
TM	Trans-membrane
TMB	Transmembrane domain
VAMP3	Vesicle-associated membrane protein 3
VGCC	Voltage-gated Ca^{2+} channel
VM	Vesicle membrane
VRCC	Volume regulated Cl^- channel
VSM	Vascular smooth muscle
VSMC	Vascular smooth muscle cell
YFP	Yellow Fluorescent Protein

Chapter 1 General introduction

1.1 Nociceptors and pain transmission

Nociception is the neural process of encoding painful (noxious) stimuli [1]. Such stimuli can be mechanical (e.g. pressure, punctures or cuts to the skin), thermal or chemical (e.g. chili powder or burns). Normally nociception is initiated at the free nerve endings of the specialized nociceptive sensory fibers. Most nociceptive fibers are either small-diameter, non-myelinated C fibers, or thinly-myelinated, medium-diameter Aδ fibers, although a small proportion of larger Aβ fibers also contributes to nociception [2]. Aδ fibers have higher conduction velocity and, thus, they normally mediate acute "fast" pain responses, while C fibers are responsible for the slower "second" pain [3]. Most nociceptors (nociceptive neurons) are polymodal: they respond to heat, mechanical and chemical stimuli. They can, however, be further subdivided into various subpopulations depending on the modality of response or expression of specific markers. Thus, "peptidergic" C nociceptors express calcitonin-gene related peptide (CGRP) and substance P (SP), while "non-peptidergic" nociceptors bind specific plant isolectin IB4. Cell bodies of nociceptive fibers reside within peripheral sensory ganglia such as dorsal root ganglia (DRG) and trigeminal ganglia (TG) [4]. Once stimulated, nociceptors send the action potentials (APs) to the superficial laminae of the spinal cord where first synaptic connection takes place. Most C fibers synapse in laminae I and II, while Aδ fibers synapse in laminae II and V [3, 5]. The main neurotransmitter used at the first synapse is glutamate, but peptidergic nociceptors also abundantly release SP (see Fig. 1.1 inset). Both glutamate and SP are excitatory neurotransmitters. Second order nociceptive neurons decussate and ascend contralaterally within the spinothalamic and spinoreticulothalamic tracts to the thalamus. Third-order neurons in the thalamus project to the somatosensory cortex where nociceptive information is finally processed. There are several other projections besides this main pathway, such as the projection to the periaqueductal grey or amygdala. It should be

noted that the amygdala is responsible for processing the emotional components of the perception of pain (Fig 1.1) [3, 5].

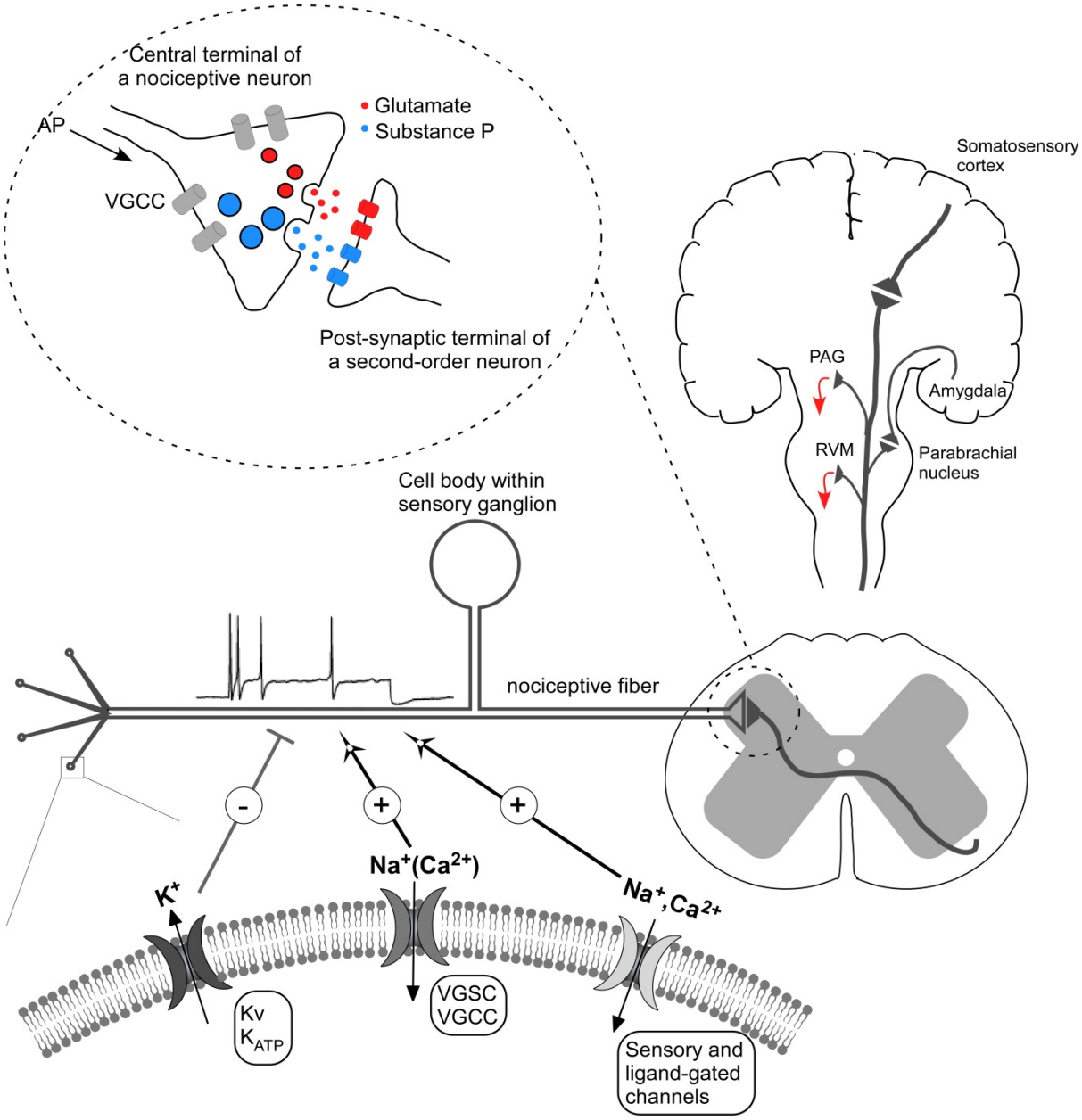

Figure 1.1 Schematic representations of nociceptive pathways. The plasma membrane of the free nerve ending of the nociceptive fiber (enlarged in the lower part of the figure) is equipped with a specific set of ion channels that produce APs in response to noxious stimuli. The nociceptive fibers synapse in the superficial laminae of the spinal cord (synaptic terminal is enlarged in the insert above), and second order nociceptive neurons project into the thalamus. Third order neurons in the thalamus then project

to the somatosensory cortex. Several auxiliary projections, such as those to the rostroventral medulla (RVM), the parabrachial nucleus and the periaqueductal grey (PAG) are also indicated. Red arrows represent descending inhibitory pathways (based on [3, 5-7]).

1.2. Inflammatory pain

A specific type of pain develops following local tissue inflammation. When peripheral tissue is injured, different types of immune cells will migrate to the injury area releasing multiple chemical agents that orchestrate the immune response. These agents released include prostaglandins, histamines, adenosine triphosphate (ATP), protons, bradykinin (BK) and many other factors which are often referred to as "inflammation mediators". These inflammation mediators not only act on the immune cells, but also often directly excite or sensitize peripheral fibers. This direct excitation results in acute pain, hyperalgesia (increased sensitivity to painful stimuli) and allodynia (painful sensation from normally non-painful stimuli) [8]. Some inflammatory mediators excite or sensitize peripheral nerves by acting directly on ion channels (e.g. ATP can activate P2X2 and P2X3 channels expressed in nociceptive neurons [9-11] while protons act on the TRPV1 channel [12, 13]). Other inflammatory mediators use intracellular signaling cascades by acting via their specific receptors such as the G protein-coupled receptors (GPCRs) or receptor tyrosine kinases (e.g. Trk A and TrkB receptors for nerve growth factor (NGF) and glial cell line-derived neurotrophic factor respectively [14, 15]). One particularly well-recognized mechanism of inflammatory hyperalgesia is the sensitization of TRPV1 channels by signaling cascades that activate protein kinase A (PKA) and C (PKC). These kinases then phosphorylate TRPV1 and reduce its temperature activation threshold, thus increasing sensitivity to noxious heat [16, 17].

Another mechanism of inflammatory pain that has recently received attention is the activation of Ca^{2+}-activated Cl^- channels (CaCCs) and the subsequent efflux of Cl^- that depolarizes and excites sensory neurons because of their unusually high intracellular Cl^-

concentrations. As recently demonstrated, inflammatory mediator BK, acting via its receptor B_2 (B_2R), activates a signaling cascade involving depletion of plasma membrane phosphatidylinositol 4, 5-bisphosphate (PIP_2) and release of Ca^{2+} from stores in the endoplasmic reticulum (ER) (see chapter 5 for detail). Together, these effects inhibit anti-excitatory M-type K^+ channels and activate pro-excitatory CaCC [7], thus delivering a strong excitatory impact. Such depolarization of the nerves innervating the inflamed tissue further facilitates the release of neuropeptides such as SP and CGRP from the peripheral endings of nociceptive neurons themselves [18-20] (Fig 1.2). This may lead to a further enhancement of the nociceptive signals (positive feed-back). Over longer periods, inflammatory stimulation can increase expression and/or trafficking of voltage-gated Na^+ channels and TRPV1 [21, 22], and down-regulate expression and/or activity of K^+ channels [23-25]. These effects result in a sustained overexcitability of the inflamed nerves [26-28]. It is evident that the primary target for inflammatory modulation of sensory nerve activity and sensitivity is the pool of ion channels that controls sensory neuron excitability. The ion channels of sensory neurons (with particular focus on the Cl^- channels which are the focus of this work) will be considered in detail in the next sections. Some inflammatory mechanisms are outlined in Figure 1.2.

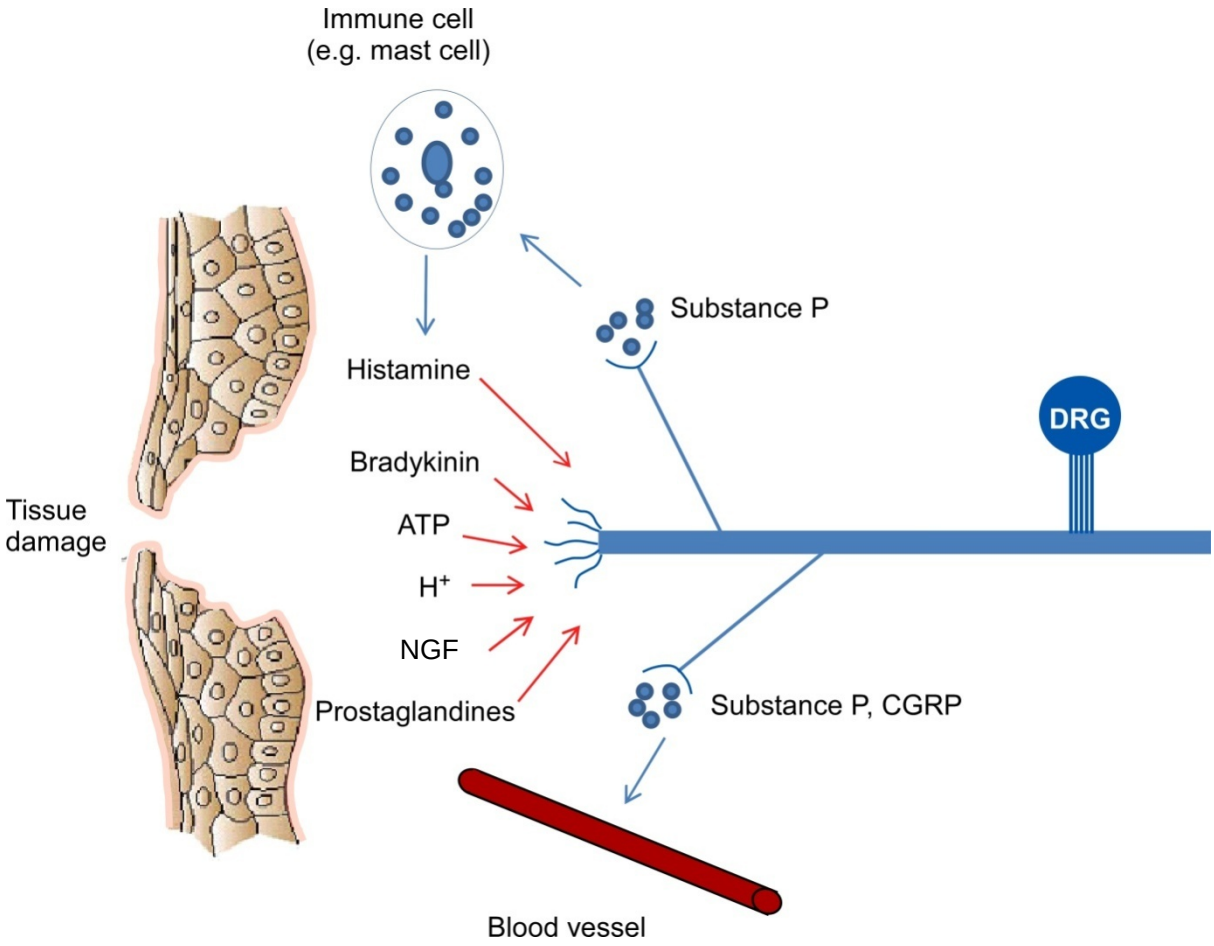

Figure 1.2 Interactions between inflammatory and nociceptive responses to tissue injury. Tissue injury causes inflammatory cells like mast cells or neutrophils to release a variety of chemical mediators, such as ATP, BK, H^+, nerve growth factor (NGF), prostaglandins and vascular endothelial growth factor. These factors bind their specific receptors expressed by nociceptors and excite or sensitize the nociceptors. The nociceptors not only transmit painful stimuli to the spinal cord, but also release neuropeptides, such as CGRP and similar substances that cause the local tissue response known as "neurogenic inflammation".

1.3 Ion channel diversity

Ion channels are a superfamily of ubiquitous proteins that are expressed in virtually every cell. They are integral membrane proteins that form transmembrane pores, which provide a pathway for diffusion of ions across the membrane. Ion channels are different from other transport proteins such as ATP-binding cassette transporters or ion pumps, in that they have continuous pores through which ions can flow unobstructed when the channel is open. This

results in much faster ion transport rates through ion channels (millions of ions per second) as compared to transporters (hundreds of ions per second; [29]).

Ion channels can be subdivided into such large families as ligand-gated channels, voltage-gated channels, and mechanosensitive channels. According to their particular range of ion selectivity, channels can be grouped into Na^+, Ca^{2+}, K^+, non-selective anion, and non-selective cation channels. They can then be further sub-divided into groups based on such functional properties such as regulatory mechanism (e.g., Ca^{2+}-activated) or biophysical characteristics (e.g., inward rectifiers).

1.3.1 Ligand-gated channels

Ligand-gated channels open in response to the binding of an extracellular signal molecule, or "ligand," which induces a series of conformational changes in the channel protein prompting it to open. Ligand-gated channels can be further divided into cation channels, such as acetylcholine, glutamic acid and 5-hydroxytryptamine (5-HT) receptors, and anion channels, such as glycine and GABA receptors (see below).

1.3.2 Voltage-gated channels

Voltage-gated channels are regulated by changes in the membrane potential, which controls the channel gate. The sequence and structural analysis of voltage-gated, Na^+, K^+, and Ca^{2+} channels suggests they evolved independently, but from the same ancestral structure. Evolution from a common chemical ancestor is likely because of significant conservation of homologous structures within 3 kinds of channels. A prototypic voltage-gated K^+ channel is formed by four identical subunits, each having 6 transmembrane segments (S1 - S6) with N and C terminals located in the cytoplasm [30, 31]. Voltage-gated Na^+ and Ca^{2+} channels have more complex structures, as their pore-forming subunits usually have a single polypeptide with

four homologous domains. Each domain contains six transmembrane α helices (S1-S6) [30, 31]. Despite the difference in primary structure, voltage-gated Na^+, K^+, and Ca^{2+} channels have essentially the same basic design: four subunits or domains, each of which has 6 transmembrane segment architecture, combine to form a functional channel complex. One of the six transmembrane segments (S4) in each subunit or domain acts as a voltage sensor with a typical hydrophobic structure containing a number of positively charged lysine and arginine residues [32]. A domain connecting the S5 and S6 segments by a hairpin turn is thought to constitute the pore-forming region (P-loop) which allows ions to diffuse through the membrane [33-35]. The S4 segment controls the gate, possibly via the S4–S5 linker [36]. Recent advances in X-ray crystallography have revealed the detailed structures of several major voltage-gated ion channels, shedding light on their operation principles [37-42]. A meaningful treatment of these operation principles is, however, outside the scope of this thesis.

1.3.3 Cyclic nucleotide-gated (CNG) channels

Cyclic nucleotide-gated (CNG) channels are gated by intracellular cyclic nucleotides such as cyclic guanosine monophosphate (cGMP) or cyclic adenosine monophosphate (cAMP). These channels play important roles in sensory perception, including vision and olfaction. CNG channels are structured like voltage-gated channels. Specifically, every subunit has six transmembrane segments, with intracellular N and C termini, and a P-loop region, between S5 and S6, that forms the pore [43]. The P loop and S6 segments regulate CNG channel gating and ion conduction. The cyclic nucleotide-binding site is located in the C-terminal region [44]. CNG channels are non-selective cation channels for such monovalent cations as K^+ and Na^+, as well as divalent cations like Ca^{2+}. Selective permeability, as measured with salamander rod CNG channels [45], was determined to be $Li^+ > Na^+ \sim K^+ > Rb^+ > Cs^+$ (CNG channels are particularly well studied in chemoreceptors and photoreceptors, which convert

extracellular signals into membrane currents [45]). Olfactory chemoreceptors, for example, contain specific olfactory GPCRs that, when bound to a specific odor, activate adenylate cyclase (AC), producing cAMP, and opening the cAMP-gated cation channels. The activated CNG channel, in turn, elicits inward Na^+ and Ca^{2+} currents, leading to depolarization of the membrane and formation of the olfactory signal.

1.3.4 Mechano-gated channels

Cells can be mechanically stimulated by such things as friction, pressure, pulling force, gravity, and shear stress. Some cells are capable of translating mechanical stimulation into electrochemical signals, a process which is called mechanical signal transduction (mechanotransduction). There are several types of mechano-gated channel (MS) including stretch-activated and stretch-inactivated ion channels [46]. Recent works have suggested that the epithelial Na^+ channel (ENaC/DEG) family and TRP family channels [47] are plausible candidates as mechano-gated channels. A new family of mechanosensitive ion channels, the piezo family, has also been identified [48]. In mammals, this family consists of two members, piezo-1 and piezo-2, with the latter isoform expressing at high levels in the peripheral somatosensory neurons [48, 49]. Several models purport to explain MS channel gating, particularly the lipid bilayer and the tethered models [50]. In the bilayer model, MS channels can be directly activated by the membrane stretch or lipid bilayer tension. In the tethered model, MS channels directly connect with cytoskeletal or extracellular matrix proteins such deflect of the tether by external forces causes the channel to open [51]. This model has been proposed for ion channels in hair cells and in chick skeletal muscle [52, 53]. Mechano-gated channels have been identified in both prokaryotes and eukaryotes, where they have been shown to play roles in heat sensation, hearing, touch, taste, smell, and osmotic and cell swelling.

1.3.5 Water channels

In the past, it was generally believed that intracellular and extracellular water molecules diffused through the lipid bilayer membrane directly. This assumption was challenged in 1988, when Peter Agre's group found a 28 kDa hydrophobic transmembrane protein [54]. This membrane, which they called CHIP28 (channel-forming integral membrane protein 28 kDa), turned out to be the first member of the water channel (aquaporin, or AQP) family. When CHIP28 was injected into *Xenopus* oocytes in a hypotonic solution, the oocytes expanded rapidly and ruptured within several minutes. This phenomenon was inhibited by Hg^{2+}, which is known to decrease the permeability of cells to water. At the present time at least 11 aquaporins like CHIP28 have been found in human cells. These aquaporins selectively mediate the passage of allow water molecules through the plasma membrane [55].

1.3.6 Cl^- channels

There is also a large group of channels that are permeable to anions. Under physiological conditions, most of these anionic channels conduct Cl^- currents, and therefore are commonly referred to as Cl^- channels. This is true even though most of them are actually non-selective anion channels. Cl^- channels have been divided into the following six families: 1) CLC channels, 2) amino acid receptor Cl^- channels, 3) Ca^{2+}-activated Cl^- channels, 4) large conductance Cl^- channels, 5) volume regulated Cl^- channels (VRCCs), and 6) cystic fibrosis membrane conductance regulators (CFTRs).

Cl^- channels are widely distributed, being found in cell membranes, lysosomes, mitochondria, and the ER. Excitable cells such as neurons and skeletal muscle mostly express CLC channels, CaCC, VRCC and amino acid receptor Cl^- channels [56, 57].

In most adult mammalian neurons the concentration of Cl^- in the cytosol is very low (below 10 mM) relative to the extracellular space (over 100 mM), which permits

hyperpolarized (viz., more negative than -80 mV) equilibrium potentials in neurons [58]. This property of the Cl^- gradient makes the opening of Cl^- channels in an adult central nervous system (CNS) inhibitory –it hyperpolarizes the membrane potential and inhibits AP generation. However, the Na^+-K^+-Cl^- cotransporter 1 (NKCC1) is expressed at high levels in early development of central neurons and adult peripheral neurons, which differ from adult central neurons [59, 62-63]. Because NKCC1 transports Cl^- ions from the extracellular space into the cytoplasm [64], intracellular Cl^- concentration in neonatal CNS neurons and in primary sensory neurons (at all ages) remains high, in the range of 30-50 mM [65-71]. This high Cl^- concentration establishes an equilibrium potential for Cl^- (E_{Cl}) in the range of -35 to -40 mV in DRG neurons [7], which are more positive than the resting membrane potential. Thus, Cl^- channel activation in sensory neurons leads to depolarization and excitation [7, 72-76].

Apart of their role in excitability, Cl^- channels also have major roles in the regulation of cell volume, cell homeostasis, acidification of organelles, and in assisting the transport of substance across cell membranes.

1.3.6.1 CLC channels

CLCs are the only voltage-gated Cl^- channels discovered to date. The first member of the family (CLC-0) was cloned from Torpedo marmorata [571]. At present, nine CLC or CLC-like proteins have been cloned in mammals. According to the gene and protein sequences, mammalian CLC channels have been divided into the following three subclasses [77]:

- The first subclass includes CLC-0, CLC-1 (CLCN), CLC-2, and CLC-K (CLC-Ka and CLC–Kb) isoforms.
- The proteins from the second subclass have structures similar to the yeast CLC channel (ScCLC). Channels in this second subclass include mammalian CLC-3, CLC-4, and CLC-5.

- The proteins from the third subclass (CLC-6 and CLC-7) are structurally similar to plant CLC protein. Channels that localize to the plasma membrane include CLC-0, CLC-1, CLC-2, CLC-3, CLC-Ka, and CLC-Kb. Channels CLC-4, CLC-5, CLC-6, and CLC-7 localize to intracellular membranes, where and they are thought to play roles in facilitating the acidification of intracellular compartments (Fig 1.3) [78].

These CLC channels are likely assembled from dimers, in which each subunit forms an independent pore and the dimeric channel complex functions as a "double-barreled" channel [79-82]. It is assumed that all CLC channels have similar topology [83, 84], with each subunit having D1-D12 intramembrane helices that span the plasma membrane 10-12 times. The D9–D12 region spans the lipid bilayer 3 to 5 times, and D4 does not cross bilayer. Therefore each subunit has a total of 10 or 12 transmembrane helices, with N and C termini being located in the intracellular space (Fig 1.4) [84].

The X-ray structures of two prokaryotic CLC Cl^- channels from bacteria have been determined [85]. The topology structure of the entire CLC channels is needed to be revised: the bacterial CLC protein is composed of 18 helices, many of which do not span the membrane entirely. Most of the helices are not perpendicular to the membrane plane, but severely tilted [85]. CLC proteins have two identical pores, each pore being formed by a separate subunit, which is related by a two-fold axis of symmetry perpendicular to the membrane plane [85]. Individual subunits are composed of two roughly repeated halves that span the membrane with opposite orientations [85]. Each subunit forms its own independent pore and selectivity filter [85].

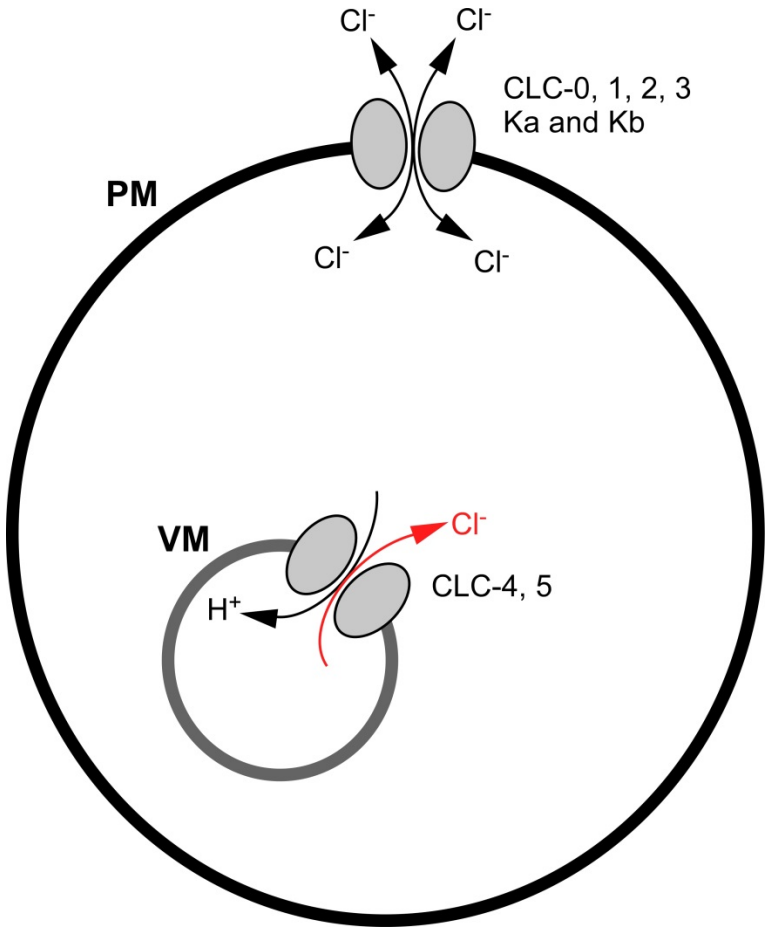

Figure 1.3 Schematic illustration of the cellular localization of CLC proteins. CLC-0, 1, 2, 3, Ka and Kb are Cl^- ion channels that are localized to the plasma membrane (PM). CLC-4 and CLC-5 appear to be Cl^-/H^+ antiporters and mediate Cl^-/H^+-exchange across intracellular vesicle membranes (VM). Arrows indicate the direction of ion transport.

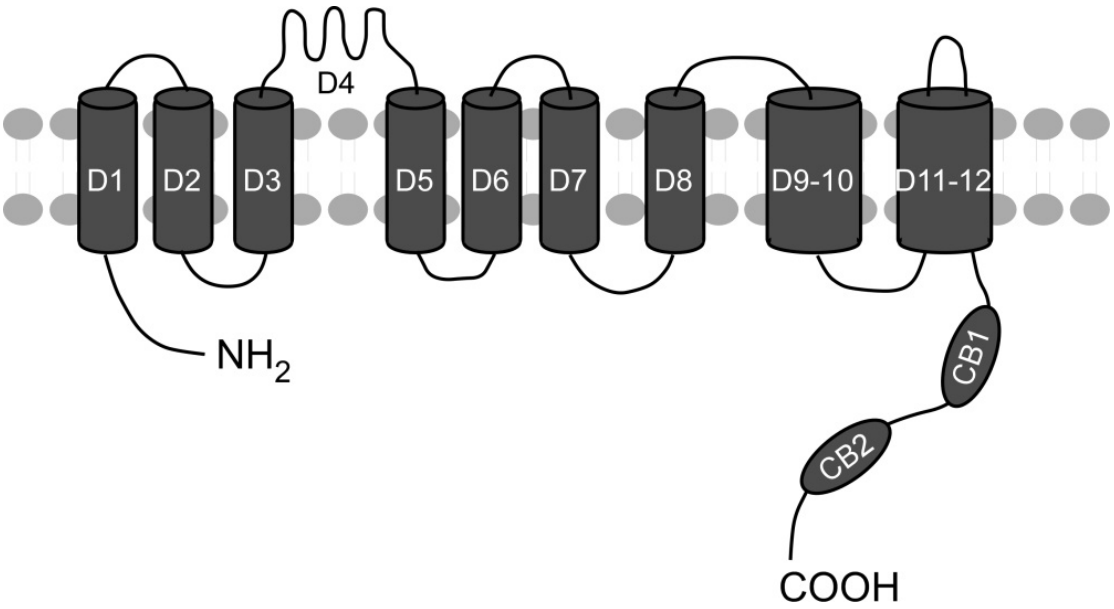

Figure 1.4 The transmembrane topology model of CLC channels [84]. The cylinders represent transmembrane helices. The membrane-associated domains contain 10 or 12 α-helices (the D9–D12 region spans the lipid bilayer 3 or 5 times). Because the number and arrangement of transmembrane helices from D9-D12 is difficult to determine, two larger cylinders are shown in the figure. The carboxy terminus of all eukaryotic CLC proteins has two CBS domains, each of which contains a three-stranded, antiparallel β-sheet with two α-helices on one side. These CBS domains play roles in protein-protein interaction through their β-sheets.

The CLC channel has two relatively independent pores which have different gating kinetics and voltage-dependency [86]. At least two independent gating mechanisms have been proposed, “slow” and “fast” gates. The slow gate operates on both pores simultaneously and facilitates pore opening at negative voltages on a time scale of seconds. The fast gate operates independently in each pore, promoting pore closing at negative voltages on a timescale of milliseconds. The fast gate is influenced mainly by movement of the Cl^- ion across the transmembrane voltage gradient.

CLC channels have a wide variety of physiological roles and biophysical properties. Thus, CLC-1 is expressed in adult skeletal muscle fibers and conducts a large Cl^- current at resting potential [87]. CLC-2 is expressed widely in cardiac myocytes and contributes to the

inwardly rectifying Cl^- conductance in these cells [88]. CLC-2 is probably involved in the regulation of neuronal and cardiac excitability [88, 89]. CLC-3 is thought to be a VRCC [90] (see Section 1.3.6.3). CLC-4 and CLC-5 have similar sequences and functions, and are expressed in intracellular membranes like the anion channels CLC-5 forms in endosomes. Anion channels like those formed by CLC-5 play a role in the acidification of organelles [91-93]. CLC-6 and CLC-7 are widely expressed in different tissues, but little is known of their functional roles or physiological properties.

CLC channels have divergent biophysical properties. Thus CLC-0 and CLC-1 are open at 0 mV, and conduct hyperpolarization-activated currents [94]. Overexpressed CLC-0 channels display linear current-voltage relationships, while hCLC-1 displays an inwardly rectifying current-voltage relationship. CLC-2 is closed at positive potentials and conducts hyperpolarization-activated currents. The current-voltage relationship of the open channel is linear. Human CLC-4 displays outwardly rectifying current-voltage relationship, and is activated by membrane depolarization [94]. All CLC channels are actually poorly selective for anions and conduct Cl^-, Br^-, NO_3^-, I^- and SCN^- currents. The permeability sequence of many CLC channels is: $Cl^- > Br^- > I^-$ [94].

Mutation within CLC channel genes can lead to various human diseases. For example, mutations within CLC-1 and CLC-2 can lead to muscle stiffness and systemic epilepsy, respectively. Moreover, CLC-2 channel dysfunction can lead to testicular and retinal degeneration, and vacuolization in the brain and in the white matter of the spinal cord. Deficiencies of CLC-3 and CLC-5 can also cause severe disease. Mice with a deleted CLC-3 gene develop monogenetic lipid disorders and epilepsy shortly after birth. A functional deficiency of CLC-5 may lead to low protein urine and nephrolithiasis. CLC-7 is highly expressed in osteoclast folds, and is closely related to osteoclast function. Accordingly, CLC-7 deficiency in mice results in development of severe bone sclerosis and retinal degeneration.

Mutations in CLC-7 were also found to cause infantile malignant osteopetrosis.

1.3.6.2 Amino acid receptor Cl^- channels

This superfamily of Cl^- channels includes ligand-gated anion channels. $GABA_A$ receptors ($GABA_ARs$) are important inhibitory ionotropic receptors in the CNS. $GABA_A$ channels are formed by various combinations of different types of α (α1 – α6), β (β1 – β3), γ (γ1 – γ3), δ, ε, π, θ and ρ (ρ1 – ρ3) subunits assembled in a pentameric fashion. Each subunit consists of four transmembrane domains, with corresponding sites for binding ligands and regulatory molecules. $GABA_A$ mediated Cl^- currents are selectively blocked by the antagonists bicuculline, SR-95531 and picrotoxinin [95]. $GABA_ARs$ can exhibit both outward and inward rectification, depending on subunit composition [96-103]. Such drugs as benzodiazepines, barbiturates, anesthetics, alcohol, and some steroids potentiate $GABA_ARs$, usually by increasing the open probability of $GABA_ARs$ [56]. Mutations in GABA receptor subunits are associated with epilepsy. GABA receptor dysfunction has also been associated with depression and affective disorders.

The glycine receptor (GlyR) is another inhibitory ligand-gated Cl^- channel. It is widely expressed in the CNS and plays important roles in different physiological processes. Like $GABA_AR$, a functional GlyR contains five subunits: either three α_1 subunits and two β subunits [104], or four α_1 subunits and one β subunit [105], arranged symmetrically around a central pore. Each subunit is composed of four α-helical transmembrane domains. The α subunits play an essential role in ligand binding, while the β subunits contribute to intracellular trafficking and channel clusterings. The GlyR displays different biophysical properties in different tissues. Thus, rat GlyR (either overexpressed in Human Embryonic Kidney 293 (HEK293) cells or native channels in rat olfactory bulb) displays no voltage dependence [106-108], while the human GlyR (either overexpressed in *Xenopus* oocytes or native channels in ciliary ganglion

or hypothalamus neurons) exhibits an outward rectification at hyperpolarized membrane potentials [109]. The GlyR is selectively antagonized by strychnine and cesium [110]. Ethanol and isoflurane potentiates glycine activation of the GlyR [110]. Mutations in the α_1 subunit of the GlyR cause Startle disease (hyperekplexia), which is characterized by attacks of muscular rigidity in response to unexpected auditory, visual or somatosensorial stimuli [111].

1.3.6.3 Volume regulated Cl^- channels (VRCC)

Cell volume regulation is important for cells as they need to maintain a constant size. The VRCCs play an important role in the regulation of cell volume in many cell types [112]. In addition, VRCCs are involved in many physiological processes, including cell proliferation and apoptosis. VRCCs have been found in different cell types. The major biophysical and pharmacological characteristics of VRCCs include current activation in a hypotonic solution, time-dependent inactivation at positive potentials, and a moderate tendency to be outwardly rectifying. Anion selectivity displays the following sequence: $I^->Br^->Cl^->F^-$>gluconate. VRCCs are inhibited by 5-Nitro-2-(3-phenylpropylamino)benzoic Acid (NPPB), 4,4'-Diisothiocyano-2,2'.-stilbenedisulfonic acid (DIDS), anthacene-9-carboxylic acid (A9C), niflumic acid (NFA), tamoxifen and 4-(2-Butyl-6,7-dichloro-2-cyclopentyl-indan-1-on-5-yl) oxobutyric acid (DCPIB), with DCPIB being the most effective blocker of this channel [113-116]. There are, however, some differences in voltage dependence and signaling mechanisms of VRCCs among different cell types. Cytosolic cAMP ($cAMP_i$), for example, enhances VRCCs in canine atrial myocytes and in human atrial and ventricular myocytes [117, 118], while $cAMP_i$ inhibits the outwardly rectifying VRCC currents in native cardiac myocytes in both guinea-pig and canine hearts [119].

The molecular correlates of VRCC currents are unclear. Although CLC-2 is implicated in cell volume regulation [120], CLC-2 can be activated by hyperpolarization and acidic

solutions [121, 122], its current-voltage (I-V) relationships are inwardly rectifying, and the channel cannot be inhibited by DIDS. Such characteristics differ from native VRCC [113]. CLC-3 is another candidate for VRCC [90, 123]. When expressed in NIH3T3 cells, CLC-3 currents display outward rectification, voltage-dependent inactivation at positive potentials, and modulation by cell volume, with an anion selectivity sequence of I^-> Cl^-> Asp, and inhibition by NPPB, DIDS, A9C, as seen with native VRCCs [123]. Moreover, intracellular dialysis with an antibody against CLC-3 inhibited native VRCC currents in guinea pig cardiac cells and canine pulmonary arterial smooth muscle cells. Other facts consistent with CLC-3 being responsible for regulation of cell volume include the following:

- Oligonucleotides antisense to CLC-3 has been shown to reduce native VRCC currents and to decrease regulated volume in bovine non-pigmented ciliary epithelial cells [124], HeLa cells and *Xenopus laevis* oocytes [125].
- CLC-3 siRNA inhibited native VRCC currents and caused regulatory volume decreases in human corneal keratocytes and human fetal lung fibroblasts [126].

This positive evidence for CLC-3 being responsible for regulation of cell volume is, however, contradicted by the findings of Matsuda and colleagues. The Matsuda group showed that when hCLC-3 was expressed in Chinese hamster ovary (CHO) cells, it displayed strong outward rectification and failure to conduct at negative voltages. The channels were insensitive to NPPB and were more selective to Cl^- than to I^- [127]. These features are inconsistent with the documented behavior of VRCCs.

Another study suggested that the Ca^{2+}-activated Cl^- channel subunit named ANO1 contributes to VRCC activity [128]. The picture has been made even cloudier by the recent cloning of a previously unknown protein named SWELL1. The necessity for SWELL1 in cell volume regulation has been demonstrated by the fact that SWELL1 knock-down abolishes the VRCC current entirely [129, 130]. It is, however, not known whether SWELL1 is itself a

channel, or merely a necessary complement to some other macromolecule that constitutes the actual channel.

1.3.6.4 Cystic fibrosis membrane conductance regulator

Cystic fibrosis (CF) is a lethal exocrine gland disease with autosomal recessive inheritance. The main clinical symptoms of CF are gastrointestinal and pancreatic dysfunction, progressive bronchiectasis and respiratory failure. CF is caused by the CFTR gene mutation. The CFTR is a low conductance Cl^- ion channel, which is regulated by cAMP and ATP. Although over 200 mutations can lead to CFTR Cl^- ion channel defects, about 90% of patients with CF have the ΔF508 mutation, which consists of the deletion of phenylalanine at 508 positions in one or both CFTR gene alleles [131].

The CFTR is an anion channel that physiologically conducts Cl^- and HCO_3^-. CFTR belongs to a family of ATP-binding cassette transporters. A single polypeptide constitutes the entire CFTR channel. The cytosolic N-terminal region is connected to the first transmembrane domain (TMD1) which has six helices, and helix 6 forms the pore [132]. The first nucleotide-binding domain (NBD1) is connected to helix 6, and is then followed by the regulatory (R) domain [132]. This R domain then connects with helix 7 of the second transmembrane domain (TMB2) [132]. Channel opening depends upon the binding of ATP, and the subsequent hydrolysis of ATP closes the channel. The NBD1/NBD2 complex binds two molecules of ATP. When ATP binds to the NBD1/NBD2 complex, it triggers a conformational change that induces channel opening [133]. The hydrolysis of ATP on NBD2 disrupts the interaction between NBD1 and NBD2, resulting in channel closure [134]. The R domain is phosphorylated by PKA which, in turn, facilitates the ATP-dependent opening of the CFTR channel [135, 136]. In the resting state, the channel has a very low probability of being open (<0.003); phosphorylation increases this probability substantially. PKC also phosphorylates the R domain, but this

phosphorylation does not affect the likelihood of the opening of a functional pore [135, 136].

Many inhibitors block the CFTR channel, including NPPB, A9C, clofibric acid, and disulfonic stilbenes. Glibenclamide also inhibits the CFTR channel [56]. It is significant that all of these blockers are non-specific and can inhibit other anion channels. Suramin is a more effective and specific blocker, although even it is not completely specific, as shown by its ability to block P2X receptors [56].

1.3.6.5 Ca^{2+}-activated Cl^- channels (CaCCs)

As most other Cl^- channels, the Ca^{2+}-activated Cl^- channel (CaCC) is an anion channel permeable to various anions including I^-, NO_3^-, and HCO_3^-. However, because Cl^- is the most abundant anion in biological fluids, the largest fractional currents conducted by CaCC under physiological conditions is a Cl^- current. CaCCs were first characterized in *Rana pipiens* eggs and photoreceptors, salamander retinas and *Xenopus* oocytes [137-139]. In recent decades, CaCC has been observed in many different cell types and tissues, such as neurons, and epithelial and smooth muscle cells (SMCs), where it plays a role in controlling excitability, contractility, secretion and proliferation.

1.3.6.5.1 CaCC in the nervous system

The role of CaCC in the neurons seems to consist in the control of excitability, although the effect of CaCC activation may be either inhibitory or excitatory depending on the type of neuron that carries it. Thus, CNS neurons from adult mammals have a low intracellular Cl^- concentration, and the E_{Cl} is in the more negative voltage range relative to resting membrane potential [140]. However, immature CNS neurons as well as adult peripheral somatosensory neurons accumulate significant amounts of intracellular Cl^- [69, 141, 142]. Therefore,

activation of CaCC in these neurons will depolarize the plasma membrane and may cause AP firing. Intracellular Cl^- concentration depends on the balance between Cl^- uptake and Cl^- extrusion pathways. As mentioned before, the transporter NKCC1 provides the main route for Cl^- uptake in neurons, while K^+-Cl^- cotransporter 2 (KCC2) is an important Cl^- extrusion pathway. In rodent CNS cells (e.g. neurons in cortex and hippocampus), NKCC1 expression level is high during early postnatal days (the first week), but decreases during postnatal development (from P14 onward), and is found at low level in adults. The expression of KCC2, on the other hand, is minimal at birth, but increases dramatically with age [59-61]. Thus, in development, the E_{Cl} shifts from values near -40 mV to values of -80 mV or even more negative. These facts imply that CaCC activation causes Cl^- extrusion, membrane depolarization and excitation in the immature CNS, but Cl^- influx, hyperpolarization, and an inhibitory effect in the mature CNS.

In contrast to NKCC1 in CNS neurons, NKCC1 expression in the primary afferent neurons of the peripheral nervous system (e.g. somatosensory neurons and olfactory sensory neurons) does not change significantly during maturation [62, 63]. Importantly, KCC2 expression could hardly be detected in the peripheral nervous system during maturation [60]. It is also noteworthy that NKCC1 was co-localized with TRPV1, a specific marker for nociceptive neurons [143]. Thus, in both the immature and mature peripheral somatosensory system, CaCC activation results in Cl^- efflux and depolarization [71, 144, 145].

In accord with these general principles, CaCC activation was reported to hyperpolarize the membrane potential and play inhibitory roles in the adult Purkinje neurons [140] and in hippocampal neurons [146]. Conversely, in immature cortical neurons and in adult peripheral neurons, CaCC activation depolarized the membrane potential and played an excitatory role [141, 142, 147]. In olfactory neurons, CaCCs can amplify the odorant-induced signal by enhancing depolarization in response to Ca^{2+} influx through the CNG channels [148]. In DRG

neurons, CaCC activation leads to prolonged depolarization and occasionally to burst firing [149].

1.3.6.5.2 CaCCs in other tissues

CaCC currents are important for regulation of excitability in vascular smooth muscles (VSMs). There are a number of Cl^- channels expressed in SMCs [150], and there are at least two types of CaCCs, a type that produces a "classical" CaCC current with voltage-dependent gating and mediation by ANO1 [151, 152] (see below); and an "unorthodox" CaCC current that requires intracellular cGMP for activation [153, 154] and is possibly dependent on bestrophins [150, 155]. Like sensory neurons, SMCs accumulate high intracellular Cl^- concentrations (in the range of 30 to 50 mM) [150, 156-158]. Accordingly, CaCC activation in smooth muscles induces depolarization and vasoconstriction.

CaCCs play an important role in epithelial tissues where these channels (together with CFTR and other Cl^- channels) control secretion [159, 160]. Another cell type where CaCCs play an important excitatory role are the interstitial cells of Cajal, specialised cells of the gastrointestinal tract, which control phasic contractions of gastrointestinal smooth muscle.

1.3.6.5.3 Properties of endogenous CaCCs

Although several types of native CaCC currents exist, the field agrees that a "classical" CaCC satisfies the following conditions [161, 162]:

1) Sensitivity to intracellular free Ca^{2+} concentration ($[Ca^{2+}]_i$), at submicromolar and low micromolar concentrations (0.2–1.0 μM).
2) Interrelated voltage- and Ca^{2+} sensitivities: lower intracellular Ca^{2+} activates an outwardly rectifying Cl^- current while at several micromolar $[Ca^{2+}]_i$ the current becomes voltage-

independent and displays linear current-voltage relationships. Another manifestation of the same phenomenon is the fact that the Ca^{2+} sensitivity of the channel is much weaker at negative voltages than at positive voltages (e.g. ~2-5 μM at -100 mV as opposed to ~500 nM at +100 mV).

3) The channels are preferentially permeable to large anions, with I^- and SCN^- being more permeable than Cl^-. The permeability sequence to anions is $SCN^- > I^- > Br^- > Cl^- > F^-$ [163, 164].
4) The currents are blocked by Cl^- channel blockers such as DIDS, NPPB, and NFA.

Despite these generally accepted bench mark features, native CaCCs in various tissues do differ in their properties. For example, CaCC shows low Ca^{2+} sensitivity (equilibrium binding constant (K_d) for Ca^{2+} at +120 mV was ~900 nM) when the CaCC occurs in *Xenopus* oocytes [165], as well as when the CaCC occurs in superior cervical ganglion (SCG) neurons [166]. In contrast, the Ca^{2+} sensitivity in parotid acinar cells is much higher – K_d for Ca^{2+} at +70 mV ~60 nM [167]. In pulmonary artery myocytes, medullary collecting duct cells, and bovine endothelial cells, CaCCs have intermediate levels of Ca^{2+} sensitivity [168-170]. In the sheep parotid gland, the permeability sequence of CaCC is $SCN^- > I^- > Cl^- > Br^-$, which differs from the $SCN^- > I^- > Br^- > Cl^-$ sequence seen in most native tissues [171].

The unitary conductance of CaCC in rat pulmonary artery smooth muscle cells (PASMCs) measured via single-channel recordings was ~3 pS. A similar value was obtained in single-channel recordings from rabbit PASMCs and other VSM cell types [163, 172]. In contrast, the single-channel conductance for ANO1 (a strong candidate for CaCC in the following introduction) was reported to be ~8.3 pS [202].

In rabbit PASMCs and rabbit portal vein myocytes, NFA has a dual effect on Ca^{2+}-activated Cl^- channel current (I_{CaCC}). This is seen by the fact that concentrations of NFA of 10 μM or more increase inward I_{CaCC} at negative potentials but decrease outward I_{CaCC} under

positive potentials ($[Ca^{2+}]_i$ is either 250 or 500 nM) [173, 174]. It is hypothesized that NFA might increase the probability of Cl^- channel opening in addition to blocking Ca^{2+}-activated Cl^- conductance. At negative potentials and low $[Ca^{2+}]_i$, the probability of ANO1 opening is small, and NFA increases the current. On the other hand, with $[Ca^{2+}]_i$ at high concentration (1 μM), the probability of ANO1 opening is much higher, and therefore the blocking effect of NFA is predominant [173, 174]. The other possible reason for dual effect is that NFA is reported to induce the release of Ca^{2+} from the sarcoplasmic reticulum in PASMCs [175]. CaCC in vascular smooth muscle cells (VSMCs) can be activated by NS1619 and isopimaric acid and blocked by paxilline, tamoxifen, penitrem A, and iberiotoxin, but these modulators also have an effect on K^+ channel ($K_{Ca}1.1$) [555, 572].

Phosphorylation/dephosphorylation has effects on native CaCC in different tissues, I will discuss this in the following section.

1.3.6.5.4 Molecular correlates of CaCCs

Despite the fact CaCCs have been studied in various cell types for over 30 years, the molecular identity of CaCCs began to emerge only recently. There are three main reasons for that. Firstly, many popular expression systems, particularly *Xenopus* oocytes, express endogenous CaCC, which makes such systems unsuitable for expression cloning; heterologous expression of Cl^- channel candidates often result in upregulation of endogenous anion currents, producing false-positives [161, 162]. Secondly, most pharmacological modulators of CaCC are not very specific. For example, NFA increases CLC-Ka and CLC-Kb currents in the 10~1000 μM range [573]. NPPB is an effective inhibitor of the K^+/Cl^- co-transporter and the lactate transporter [574]. Thirdly and finally, homology cloning is difficult since the gene that finally was identified as CaCC (ANO1 or TMEM16A, see below) has no sequence similarity to other ion channel genes [161].

Several candidate proteins were proposed as potential molecular candidates for CaCCs in earlier studies. CLCA channels were considered candidates in several studies [172, 176-178]. The CLCA subfamily of CLC Cl^- channels includes two bovine isoforms (bCLC1; bCLCA2), three mouse (mCLCA1; mCLCA2; mCLCA3) and four human (hCLCA1; hCLCA2; hCLCA3; hCLCA4) isoforms. When transiently expressed in HEK293 cells, the CLCA proteins bCLCA1, mCLCA1, hCLCA1, and hCLCA2 produce Cl^- channels that are activated by high (~2 mM) intracellular Ca^{2+} concentrations. Currents of these isoforms reverse at 0 mV, exhibit some outward rectification, and are inhibited by the classic Cl^- conductance inhibitor DIDS at 300 mM, as well as by tamoxifen at 10 mM and NFA at 100 mM) [176, 179-181]. Likewise, mCLCA4 also produced Ca^{2+}-dependent currents activated by the application of Ca^{2+} ionophore ionomycin (10 μM) [182].

But much evidence suggests that CLCA channels are not true CaCCs. Firstly, the currents observed in HEK293 cells expressing CLCA needed higher concentrations of Ca^{2+} for activation (2 mM) as compared to native CaCC [183-185]. Secondly, there are also striking differences in the voltage and time dependence of CLCA versus endogenous CaCCs. Most of studies show that CLCA currents exhibit time- and voltage-independent kinetics and linear or only mildly outwardly rectified current–voltage relationships [183-185], while endogenous CaCC shows outward rectification at subsaturating Ca^{2+} concentrations. In addition, CLCA current can be inhibited by the reducing agent Dithiothreitol (DTT), while native CaCCs are insensitive to this compound [176, 179-181]. Thirdly, in some instances CLCA channels produced Cl^- currents that were not inhibited by NFA [176]. Finally, some studies reported that CLCA proteins are soluble, secreted proteins which do not form ion channels themselves [186].

Another candidate CLC channel that was considered to be CaCC was CLC-3. The currents evoked by recombinant hCLC-3 channels stably expressed in TsA cells show Ca^{2+}-dependent gating [177], but CLC-3 has also been associated with the activity of cell swelling-

activated Cl^- channels. Moreover, CLC-3 knockout mice show normal Ca^{2+}- activated Cl^- conductances [178, 187], which ruled out CLC-3 from the CaCC candidate list.

Another group of proteins that were long thought to generate CaCC currents in some situations is a family of transmembrane proteins called bestrophins. An isoform of bestrophin (Best1-4) has been found in humans [188-190]. Heterologously expressed bestrophins recapitulate Cl^- channels that are activated by physiological levels of Ca^{2+} [191, 192]. Mouse mBest1 overexpressed in HEK293 generates a Cl^- current which is activated by nanomolar concentrations of intracellular Ca^{2+} without the involvement of kinases. This is likely because a Ca^{2+} binding site has been localized to the C-terminal region of Best1 [193]. The currents show modest outward rectification but otherwise are largely time and voltage- independent (Fig. 1.5). The mBest1 channel has an anion selectivity sequence of $SCN^- > I^- > Cl^-$, and mutation of the predicted pore domain decreases the anion permeability; the current is blocked by 100 μM NFA and DIDS [194, 195]. Channels from mBest2 and mBest3 have similar biophysical properties. Although these properties are broadly consistent with some form of CaCC, as with the CLCA family, there are differences between "classical" CaCC (see above) and bestrophin currents. Firstly, classical CaCCs exhibit voltage-dependent kinetics and outward rectification that is not seen with bestrophin channel currents [196]. Secondly, CaCC currents are still present in some tissues of Best1 knockout mice [197-199]. Thus, Best1 is expressed at high levels in the basolateral membrane of retinal pigment epithelial (RPE) cells [200], but the RPE cells show normal Cl^- conductance in Best1 knockout mice [201].

Recently, a new family of ionic channels, anoctamins (TMEM16) was identified as a candidate membrane protein family for the CaCC currents [202-204]. Anoctamins (the term derived from 'anion' and 'octo', designating their function as anion channels and also reflecting the fact that these proteins have eight transmembrane domains) comprise a large protein family currently consisting of 10 members (ANO1-10). The functions of 8 anoctamin isoforms are

unknown or debated, but two members (ANO1 and ANO2) recapitulate most properties of native CaCCs and are increasingly being considered to be the main CaCC subunits in most mammalian cell types. The ANO1 CaCC is considered in detail in the next section.

1.4 Anoctamins

1.4.1 ANO1

Expression of ANO1 in mammalian cell lines or amphibian oocytes results in a CaCC current closely resembling the native CaCC current [202-204]. When expressed in HEK293 cells, ANO1 channel currents exhibit slow kinetics and are activated by increases in cytosolic free Ca^{2+} in submicromolar to micromolar ranges [151, 205-207] (see Fig. 1.5). When cytosolic free Ca^{2+} is less than ~1 μM, depolarizing voltage steps elicit two components of currents [151, 205-207]: an instantaneous current, indicating that channels are open at the holding potential, followed by a time-dependent current, due to the channels opened by depolarization (Fig. 1.5). The time-dependent currents can be well fit by a single-exponential function. The currents have an activation time constant in the range of 250 ms at +70 mV with 500 nM $[Ca^{2+}]_i$ [151]. As the $[Ca^{2+}]_i$ increases, the activation time constants decrease [151, 205-207]. The deactivation of CaCC also follows a time course that is described by a single exponential, with a time constant that is voltage-dependent [151, 205-207]. As $[Ca^{2+}]_i$ increases or at less negative voltages (depolarization), the deactivation time constants increase, while the deactivation is slowing. ANO1 currents are inhibited by typical CaCC blockers, such as NFA and 5-nitro-2-(3-phenylpropylamino)-benzoic acid (NPPB) [195, 202-204]. These properties of ANO1 are in good agreement with those of native CaCCs.

ANO1 (and native CaCCs) have interacting voltage- and Ca^{2+}-dependence that make the channel more sensitive to Ca^{2+} at depolarizing voltages. Accordingly, the $[Ca^{2+}]_i$ half-maximal concentration (EC_{50}) for ANO1 activation at −60 mV and + 60 mV was reported to

be 2.6 μM and 0.4 μM, respectively [202]. Transfection of HEK293 cells with ANO1 along with GPCRs such as angiotensin II receptor 1 or endothelial receptor produced an agonist-induced inward current which has typical properties of native I_{CaCC} induced by the appropriate GPCR ligands [202]. Importantly, ANO1 knockout mice had diminished CaCC currents, providing additional evidence that ANO1 is a strong candidate for native CaCCs [128, 208].

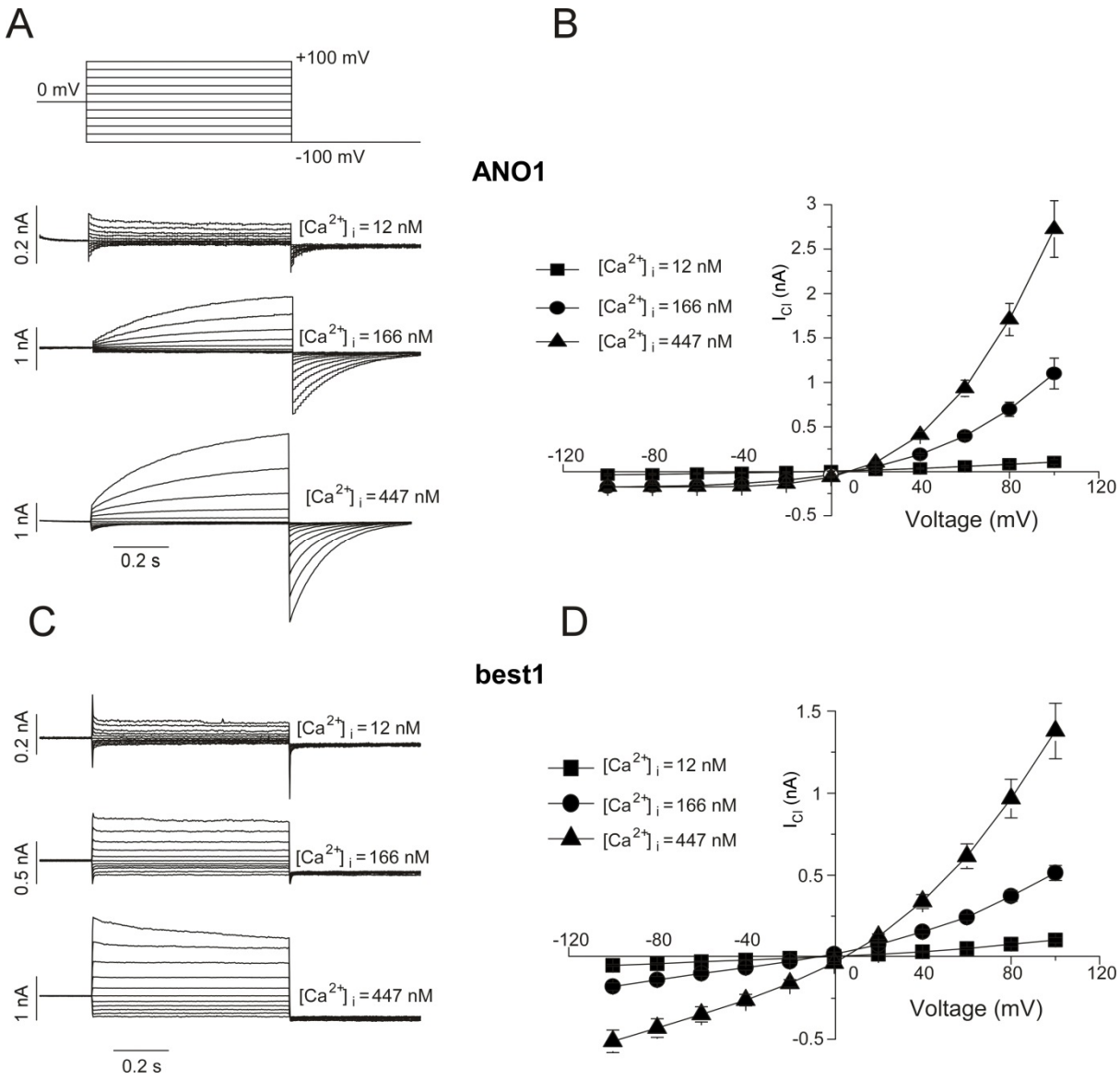

Figure 1.5 Electrophysiological properties of the currents produced by ANO1 (A-B) and best1 (C-D) stably overexpressed in CHO cells; adapted from reference [195].

Genetic knockout or ex vivo siRNA-based downregulation of ANO1 suppresses native CaCC and abolishes some CaCC-dependent cellular functions. For example, knockdown of ANO1 with siRNA strongly attenuated CaCC in human cardiac fibroblasts and rat PASMCs [209], as well as in rat sensory neurons [7]. Similarly, ANO1 siRNA reduced vasopressin–induced contraction of rat mesenteric small arteries via reduced depolarization [210]. In the

cerebral vascular bed, ANO1 siRNA knock-down inhibited vascular contraction [152]. In the intrahepatic biliary epithelial cell CFTR and ANO1 are both expressed and thought to provide the driving force for ion and water secretion [211]. SiRNA knock-down of ANO1 but not CFTR abolished CaCC current in these cells thus providing evidence that ANO1 plays a critical role in biliary epithelial secretion and bile formation [211].

ANO1 was found to be present in cells and tissues associated with CaCC expression. These included epithelial cells, smooth muscle and most sensory neurons [160, 161]. In epithelial tissues, Cl^- channels localize in the apical and basolateral membranes of the epithelial cells; cAMP and Ca^{2+} activate CFTR and CaCC, respectively, thus stimulating Cl^-secretion across the apical membrane due to intracellular accumulation of Cl^- by NKCC1 [212, 213]. CFTR contributes to Cl^- secretion in epithelial cells of airways, intestine, and the ducts of pancreas and sweat gland while CaCC was reported to contribute to Cl^- secretion in pancreatic acini, salivary and sweat glands [56, 214, 215]. Recent studies show that ANO1 contributes to Cl^- secretion in these tissues under some conditions [160]. For example, ANO1 knockout mice revealed that ANO1 plays major roles in Cl^- secretion in the superficial epithelium of neonatal murine airways [216]. Likewise, carbachol-induced Cl^- secretion was severely reduced in the colon of ANO1 knockout mice [217]. ANO1 also moderately contributes to the Cl^- secretion in airway and intestinal epithelia [218]. It was also reported that some inflammatory mediators such as interleukin 4 (IL-4) can upregulate the expression of ANO1 in epithelial cells [203]. Epidermal growth factor also can regulate the expression of ANO1 in the intestinal epithelium [219].

In exocrine glands, studies have shown that ANO1 contributes to CaCC current in salivary gland acinar cells and contributes to Cl^- efflux and fluid secretion [208]. ANO1 was clearly detectable in cells of the submucosal glands and it is important for the mucociliary clearance in human airways. Accordingly, mucus accumulations, impaired mucociliary

clearance, and low Cl^- secretion in the airways were found in ANO1 knockout mice (Fig 1.6) [216, 217].

The role and expression of CaCC in SMCs have been reported by many groups [152, 170, 173, 220-224]. As discussed above, SMCs, like sensory neurons, accumulate high intracellular Cl^- levels. Therefore CaCC activation (e.g. in response to Ca^{2+} release from intracellular stores) enables Cl^- efflux, which causes membrane depolarization and vasoconstriction [163, 225, 226]. Many groups have found ANO1 expressed in SMCs; accordingly, it is not surprising that siRNA ANO1 knock-down was shown to reduce CaCC currents in SMCs [151, 152]). The expression of ANO1 was shown to correlate with vascular remodeling and hypertension. Because of this correlation, the overexpression of ANO1 in basilar VSMC is thought to decrease expression of Cyclins D1 and E, thereby inhibiting the proliferation of SMCs [227]. Chronic hypoxia upregulated ANO1 expression in PASMCs and in a rat model of pulmonary hypertension, and ANO1 in PASMCs contributes to the CaCC currents and contractile responses [228, 229]. Chronic inflammation in airway smooth muscle cells increased ANO1 expression along with contractility [230]. In most of the cases, ANO1 inhibitors had a relaxant activity on SMCs [231].

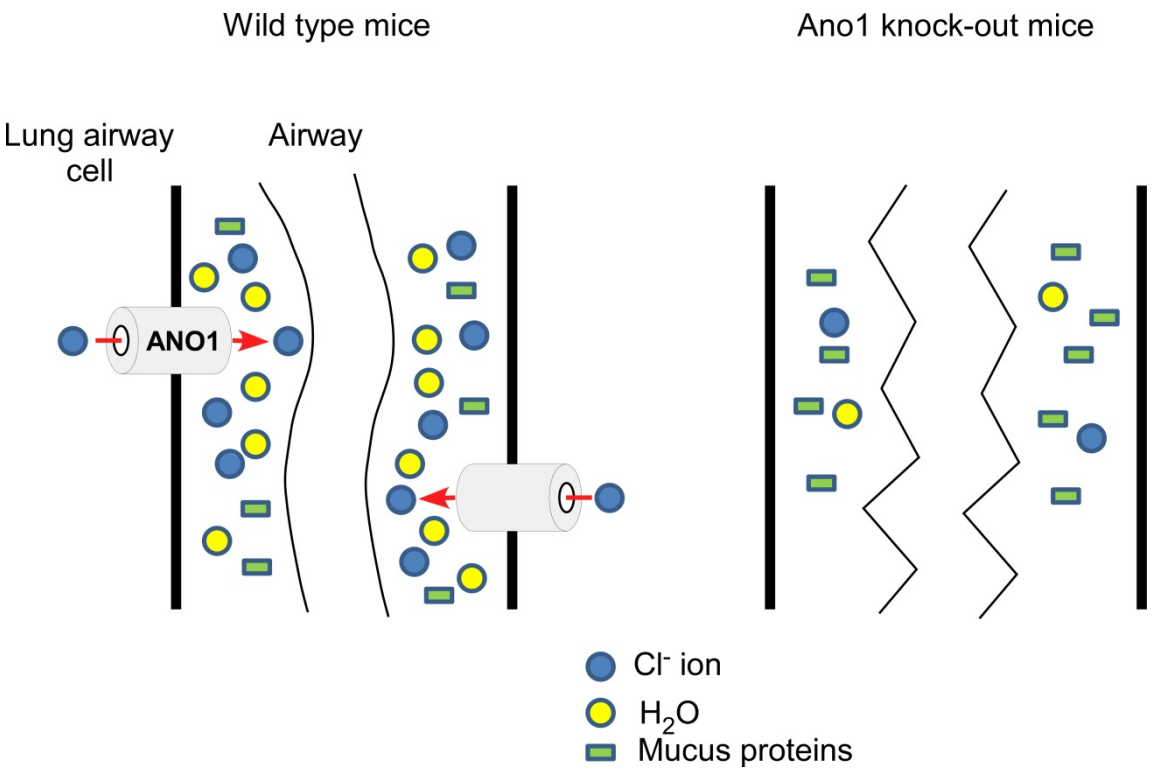

Figure 1.6 Effect of ANO1 knock out on the airways. Permeability for Cl^- via CaCC/ANO1 channels allows for water transport due to large transepithelial osmotic gradients in normal airways. Flow of water clears mucus proteins. In contrast, the surface liquid layer in ANO1 knockout mice is reduced due to small transepithelial osmotic gradients and mucociliary clearance is largely impaired. The red arrows in Figure 1.6 indicate the direction of Cl^- transport.

1.4.1.1 Structure-functional relationships of ANO1 protein

ANO1 functions as homodimers [232, 233]. Coexpression in HEK293 cells of ANO1 subunits differentially tagged with fluorescence resonance energy transfer (FRET) paired fluorescent proteins demonstrated a significant amount of energy transfer, which is indicative of a close physical interaction between ANO1 subunits. Chemical cross-linking and coimmunoprecipitation (co-IP) was also used to demonstrate dimer formation. Another study has shown that ANO1 proteins form homodimers prior to transport to the plasma membrane [233]. Recently, a dimerization domain of ANO1 was localized to the channel's N-terminus [234]. Whether ANO1 can form heteromultimers with other anoctamins is currently unknown.

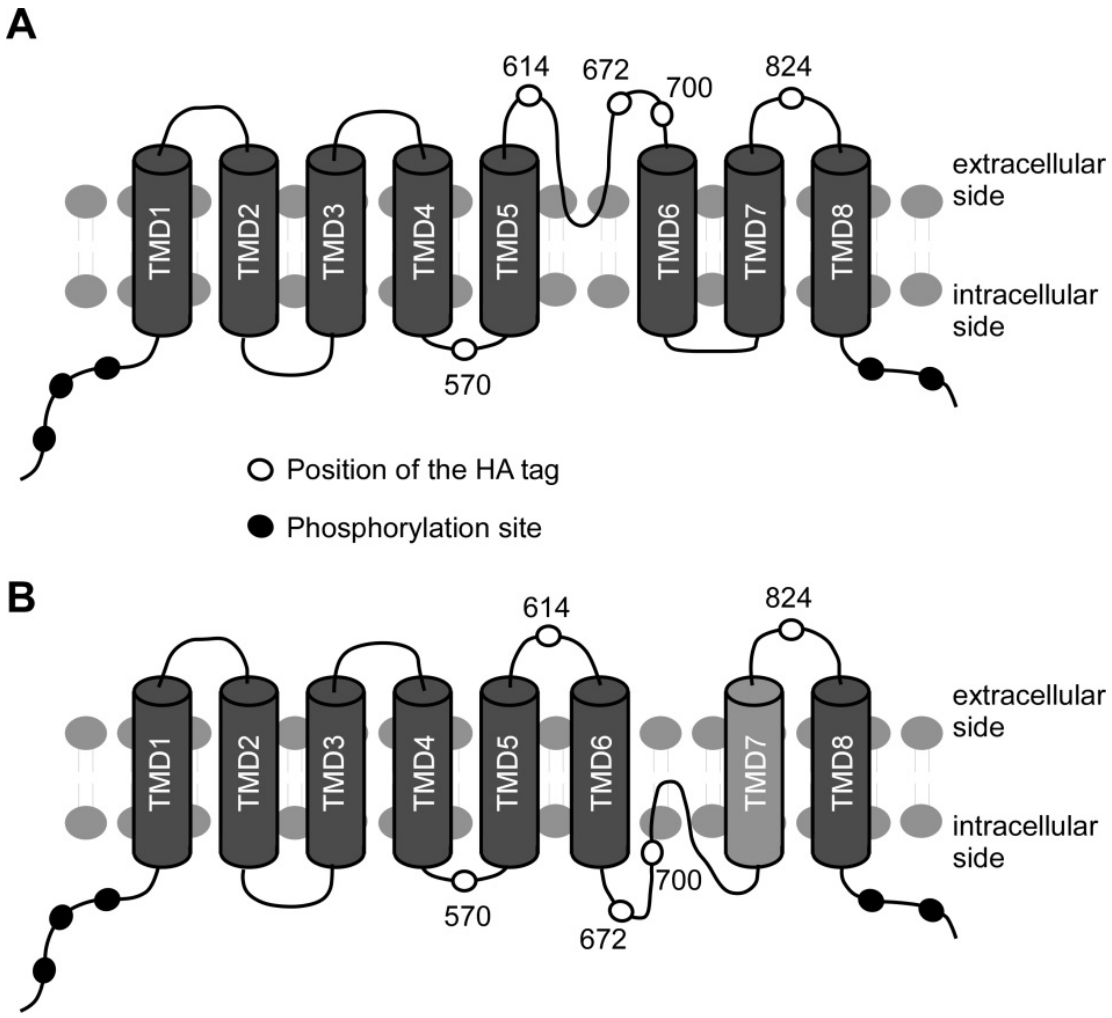

Figure 1.7 Current topology models of ANO1. (A) = Originally proposed topology; (B) = revised topology. The ANO1 protein has eight putative transmembrane domains (TMD1-8), and a re-entrant loop between the TMD5 and TMD6 that is suggestive of a channel pore. Some consensus phosphorylation sites are labelled (dark ovals). White ovals depict HA tags that were inserted into the channel in study [206]. Their appearance relative to the plasma membrane was tested by immunostaining of non-permeabilized cells. These experiments led to the revised topology shown in (B). Positions 614 and 824 can be accessed by extracellular anti-HA antibody. Other positions are not accessible, suggesting that the fragment between positions 672 and 700 is located intracellularly.

The predicted topology shows that ANO1 has at least eight putative transmembrane segments, with both NH_2 and COOH termini located intracellularly (Fig 1.7A). The predicted re-entrant loop is located between the fifth (TMD5) and the sixth (TMD6) transmembrane segments (Fig 1.7A). Yang and colleagues [202] suggested the re-entrant loop (amino acids

from 620 to 650) might form the channel pore. They used mutations of positively charged amino acids to change the ionic selectivity of the channel [202]. However, this topology model of ANO1 has been challenged by Yu and colleagues [206] (Fig 1.7B). Using the HA epitope accessibility method, these authors suggested that the 're-entrant' loop of ANO1 in fact fully crosses the phospholipid bilayer, and then generates a cytosolic loop important to Ca^{2+} binding (Fig 1.7B). They also used cysteine accessibility mutagenesis of the putative "re-entrant" loop, and replaced each amino acid between 620 and 646 with cysteines and then conducted electrophysiological testing of the resulting mutants for the effects of the cysteine-modifying agents 2-(trimethylammonium)ethyl methanethiosulfonate, bromide (MTSET) or 2-aminoethyl methanethiosulfonate hydrobromide (MTSEA). These mutants generally responded to MTSET/MTSEA with decreased current amplitude but no changes in ion selectivity as compared with the wild-type ANO1. These results suggested that the re-entrant loop of ANO1 may contribute to the permeation pathway, but is not critical for forming the selectivity filter [206]. Another study has shown that the re-entrant loop region does not form the entire pore, but may instead consist of a trafficking domain [235].

As native CaCCs, ANO1 also has permeability to other anions. The permeability sequence is: NO_3^-> I^-> Br^-> Cl^-> F^- [202]. Another study has shown that ANO1 has different open states with different ion selectivities and, thus, the ion selectivity of the channel is not rigid [236]. Jung and colleagues reported that the permeability of recombinant ANO1 to anions (e.g. HCO_3^- and Cl^-) can be dynamically modulated by Ca^{2+}. At submaximal cytosolic Ca^{2+} levels of ~1 μM, ANO1 was more readily permeable to Cl^- than to HCO_3^-, but when $[Ca^{2+}]_i$ raised to 3 μM, the HCO_3^- permeability of ANO1 increased greatly, exceeding that of Cl^-. Because similar results were found in mouse salivary gland acinar cells, the authors concluded that ANO1 may play an important role in cellular HCO_3^- transport, especially in transepithelial HCO_3^- secretion [236].

It has been shown that the intracellular N- and C-termini of ANO1 contain multiple phosphorylation sites [160]. This may explain why some native CaCCs, such as these in colonic, airway and pancreatic epithelial cells, require Ca^{2+}-dependent phosphorylation or calmodulin-dependent kinases (CaMKs) for activation [162, 237-240]. Other studies, however, show that CaMK or phosphorylation actually has an inhibitory effect on CaCCs in other tissues [170, 222, 241]. For example, in tracheal and arterial smooth muscle cells, inhibitors of CaMK augment CaCC. Likewise, CaMK in smooth muscle causes desensitization of CaCCs, so that CaCC was inhibited when intracellular Ca^{2+} increased. Moreover, internal dialysis with active Calmodulin-dependent protein kinase II (CaMKII) inhibited I_{CaCC} in pulmonary artery myocytes, while Ca^{2+}-dependent dephosphorylation stimulates I_{CaCC} in rabbit pulmonary artery smooth muscle [170, 222, 241]. The Ca^{2+}-dependent phosphatase activity of calcineurin has been shown to exert a stimulatory effect on CaCC [223]. In summary, there is no unifying theory of the effect of phosphorylation on CaCC activity, although a recent study suggested that phosphorylation is not a prerequisite for ANO1 activation [242].

1.4.1.2 Pharmacology of ANO1

Classical Cl^- channel inhibitors including A9C, NPPB, DIDS, Diphenylamine-2-carboxylic acid (DPC) and 4-acetamido-4-isothiocyanatostilbene-2, 2-disulfonic acid (SITS) inhibit CaCC in a voltage-dependent manner by interfering within the anion permeation pathway in an unselective manner. For example, DIDS not only inhibits CaCCs, but also blocks Na^+/HCO_3^- co-transporters [243] and Cl^-/HCO_3^- exchangers [244]. The most common blockers for native CaCCs are NFA and flufenamic acid (FFA) (representative CaCC inhibitors are listed in Fig. 1.8). These substances effectively inhibit CaCC currents in epithelial cell and *Xenopus* oocytes at concentrations ranging from 5 to 100 μM [195, 203, 245]. NFA inhibits spontaneous CaCC currents in rabbit portal vein smooth muscle cells with an IC_{50} of

around 2–5 μM [246], while DPC inhibits CaCC effectively in millimolar concentrations [204]. When human ANO1 is expressed in HEK293 cells, NFA and A9C inhibit ANO1 currents with IC_{50} values of 12 and 58 μM, respectively [247]. At concentrations ranging from 16 to 250 μM, 2 to 44 μM and 10 to 1000 μM, respectively, DIDS, NFA and A9C effectively inhibited the endogenous CaCC current in *Xenopus* oocytes [162]. NFA is often considered a relatively specific blocker, and is often used to identify CaCCs in different tissues. However, NFA is not a perfect tool to identify CaCCs. First of all, NFA also affects other ion channels, such as N-methyl-D-aspartate (NMDA) and $GABA_A$ receptors [56]. Secondly, like A9C, NFA has a bimodal effect on ANO1 activation [173, 174, 248, 249]; in vascular myocytes, 100 μM NFA inhibits CaCC current at positive potentials incompletely, and even stimulates I_{CaCC} at negative potentials (when recorded with $[Ca^{2+}]_i$ of either 250 or 500 nM). A similar phenomenon was observed for recombinant ANO1 [195]. A9C, FFA and NPPB were also reported to have bimodal effect on ANO1 activation [195, 248]. It was hypothesized that at low $[Ca^{2+}]_i$, when the open probability of ANO1/CaCC is small, a stimulatory effect of NFA predominates, whereas higher (over 1 μM) $[Ca^{2+}]_i$ greatly increases the probability of the channel being open. Under these high $[Ca^{2+}]_i$ conditions, the blocking effect of NFA is predominant [173]. It is possible that these compounds have multiple binding sites on ANO1, and that these different binding sites may have different affinities for the "bimodal" drugs, thereby mediating opposing effects on the channel activity. A similar phenomenon was reported for the CFTR channel [250].

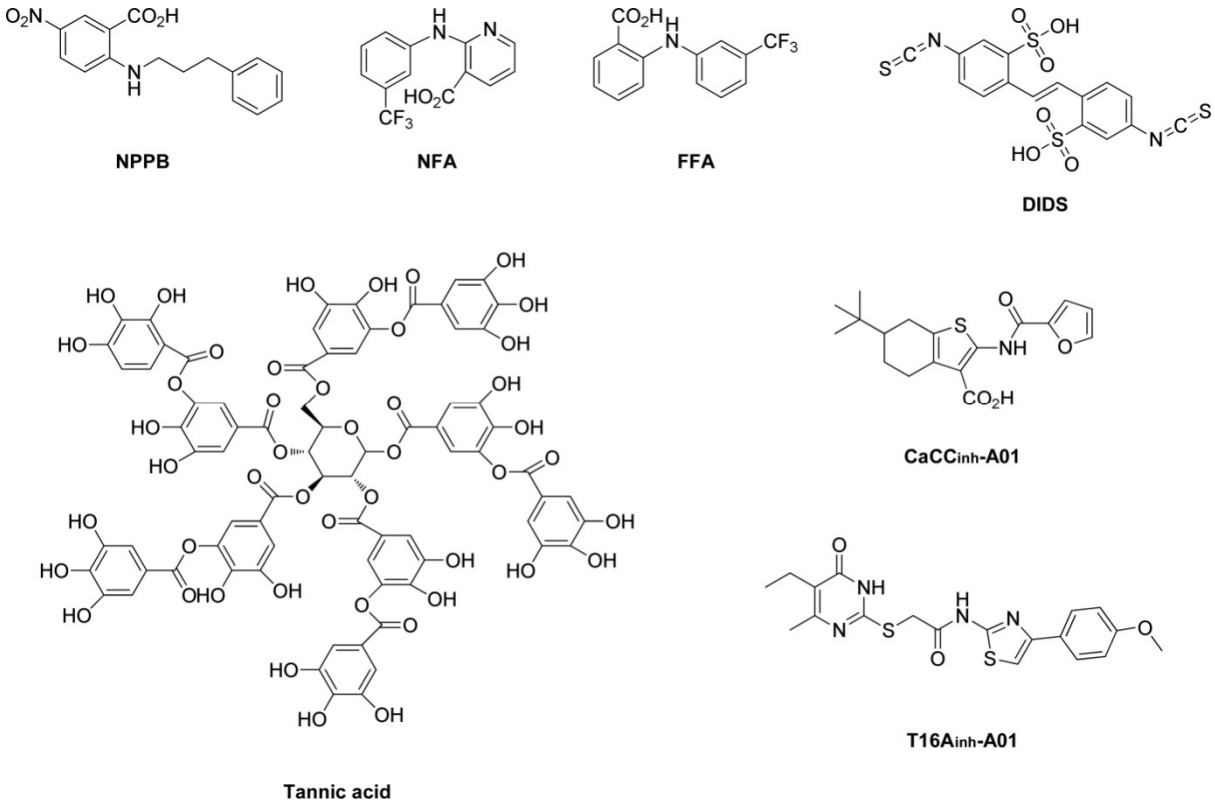

Figure 1.8 Chemical structures of the most widely used CaCC/ANO1 inhibitors (adapted from [195]).

Recently, a series of more selective ANO1 modulators has been developed. Such compounds as $CaCC_{inh}A01$, tannic acid and related compounds have given rise to a new line of ANO1 blockers (Fig. 1.8) [218, 251]. $CaCC_{inh}A01$ inhibits heterologously-expressed ANO1 channels in a voltage-independent manner with IC_{50} below 10 μM; it also blocks Best1 mediated CaCC currents with similar potency [195, 218].

T16Ainh-A01 is the most recent CaCC inhibitor and is more selective for ANO1, having little effect on other Cl^- channels, including CFTR and Best1 [195]. It was originally reported to block recombinant ANO1 almost completely with IC_{50} ~1 μM [218, 231, 252]. However, in another study, this inhibitor had much lower efficacy, blocking only ~30% of mouse ANO1 (mANO1) and ~50% of human ANO1 (hANO1) currents at maximal concentrations [195]. Likewise, T16Ainh-A01 reportedly has variable efficacy in native tissues, blocking CaCC current poorly in human bronchial epithelial cells. Nevertheless,

T16inh-A01 has been successfully used as specific tool to identify the molecular identity of native CaCCs in several tissues including transepithelial cells, SMCs, and cancer cells [219, 228, 231, 253].

Recently, small-molecule activator/potentiators of ANO1 have been also reported including N-aroylaminothiazole and tetrazolylbenzamide. Aroylaminothiazole compounds strongly activated heterologous ANO1 in the absence of cytosolic Ca^{2+}, producing outwardly rectifying currents which became more linear at higher $[Ca^{2+}]_i$. In contrast, tetrazolylbenzamide compounds did not activate ANO1 in the absence of cytosolic Ca^{2+}, but increased Cl^- current at submaximal Ca^{2+}. It is possible that tetrazolylbenzamide potentiates the ANO1 current by increasing channel sensitivity to Ca^{2+} [252].

1.4.1.3 ANO1 and nociceptive neurons

Accumulating evidence indicates that excitability of sensory neurons is supported by the activity of Cl^- channels. More specifically, Cl^- fluxes have been shown to be important in the setting of cell membrane resting potential, and in the maintenance of proper cell volume in sensory neurons. In sensory neurons, as in other cell types, Cl^- fluxes may also play other cellular roles including pH and volume homeostasis, transport of organic solutes, and so on [56, 144, 254, 255]. ANO1 is abundantly expressed in most DRG sensory neurons [202], particularly in small-diameter nociceptors [202, 256]. In the context of small-diameter nociceptors, it is interesting to note that earlier studies showed that CaCC currents activated by Ca^{2+} influx through voltage-gated Ca^{2+} channels (VGCCs) was found in medium- and large-diameter sensory neurons, but not in small DRG neurons [202, 257]. It was also found that nerve injury increased CaCC currents in medium-diameter DRG neurons, best1 and best3 were found to mediate this increase [258]. Recently, Liu and colleagues found that BK can induce CaCC in small DRG neurons [7]. This action of BK was mediated by a G_q-coupled bradykinin

receptor B_2 (B_2R and phospholipase C (PLC)) cascade, involving inositol 1, 4, 5-triphosphate (IP_3) production and release of Ca^{2+} from intracellular stores. It was found that depolarizing CaCC current, along with voltage-gated K^+ channel (KCNQ) inhibition (also through the PLC-dependent pathway), contributed to membrane depolarization and to the increase of AP firing of nociceptive sensory afferents [7]. Knock-out and gene silencing experiments demonstrate that CaCC activity in small DRG neurons depends on ANO1 expression [7, 256].

1.4.1.4 Role of ANO1 in human disease

Relative expression levels of ANO1 are associated with several types of cancers. ANO1 strongly contributes to breast cancer tumorigenesis, ANO1 can activate CaMKII, subsequently inducing activation of Akt and mitogen-activated protein kinase (MAPK) signaling. These inductions can lead to increased secretion of epidermal growth factor and transforming growth factor alpha (TGF-α), substances that have been implicated in breast cancer tumorigenesis [253, 259]. Gene expression and immunobiochemistry experiments suggest that ANO1 is highly expressed in oral and head and neck squamous cell carcinomas, gastrointestinal stromal tumors, and prostate cancers [260-262]. It is certainly noteworthy that overexpression of ANO1 is associated with a poor prognosis for human patients with certain cancers [253]. Thus, ANO1 may become a good diagnostic biomarker for some forms of cancer. While it is not yet clear how ANO1 expression is regulated on the transcription level, it was found that epidermal growth factor increases ANO1 expression in colonic epithelial cells, both at the mRNA and protein levels, and PKCδ was found to mediate epidermal growth factor-induced ANO1 expression [219, 263].

ANO1 regulates cell proliferation and has been implicated in the spread of cancer. This has been shown by studies that ANO1 overexpression promoted the proliferation of cancer cells in vitro, just as knockdown or pharmacological inhibition of ANO1 significantly slowed

the growth of cancer cells [253, 262]. Other studies have shown that ANO1 can regulate the expression of cyclin D1 through the MAPK/ERK pathway, which is linked to the G1 cell cycle checkpoint [253]. In some cases, CaCCs promotes cell migrations as well as cell growth in vitro. It is therefore possible that ANO1 plays a role in metastases. Finally, some studies suggested that ANO1 is a negative regulator of hypertension and vascular remodeling, and that the expression of ANO1 can decrease the proliferation of vascular cells [227].

1.4.2 Other anoctamins

The anoctamin family has 10 members. The ANO2 sequence is ~60% identical to the ANO1 sequence; other anoctamins are considerably less similar, with sequence similarities of 30% or below. ANO2 has also been identified as CaCC, although it has some distinct properties. Specifically, ANO2 has lower Ca^{2+} sensitivity and much faster activation kinetics than ANO1. In inside-out patches, the half-maximal concentrations of Ca^{2+} needed for ANO2 activation are 4.9 μM at −50 mV, and 3.3 μM at +50 mV [264]. Other studies reported similar values [265, 266], all of which are lower than the Ca^{2+} sensitivity of ANO1 [202, 205, 267]. In addition, ANO2 lacks voltage dependence in the absence of Ca^{2+} [266], whereas ANO1 can be activated by much depolarized voltages (~200 mV) under Ca^{2+}-free conditions [205]. The activation kinetics of ANO2 are voltage independent and become faster by increasing $[Ca^{2+}]_i$. This is shown by an activation time constant of 8.1 ± 0.8 ms at 1.5 μM $[Ca^{2+}]_i$ and +100 mV [266]. By comparison, the activation time constant of ANO1 is around 250 ms at +70 mV and 500 nM $[Ca^{2+}]_i$ [207]. The deactivation of ANO2 is also relatively faster than the deactivation of ANO1; the time required to reach the half-maximal current ($\tau_{0.5}$) for the deactivating tail current of ANO2 was 2.5 ms upon repolarisation to -60 mV, while the comparable figure for ANO1 was 41 ms [207]. The magnitude of the whole-cell currents elicited from heterologously expressed ANO1 was six times larger than that from ANO2 [207]. In spite of

these differences, the anion permeability sequence for both of these CaCCs is similar: SCN^-> I^-> Br^-> Cl^-> F^-.

ANO2 can be inhibited by NFA but is insensitive to SITS [268]. ANO2 is highly expressed in central neurons, microvilli of mouse vomeronasal sensory neurons, and photoreceptor synaptic terminals. It also contributes to endogenous CaCC in cilia, vomeronasal sensory neurons, and retinal synapses [268, 269]. The role of ANO2 in olfaction transduction is, however, unclear. Many previous studies show that the opening of ANO2/CaCCs causes the depolarization of olfactory neurons and induction of APs that reach the olfactory bulb [270, 271]. Although the high expression of ANO2 in mouse vomeronasal sensory neurons suggests a role in vomeronasal transduction [272], the fact that ANO2 knockout mice retain near-normal olfactory function shows that that Ca^{2+}-activated Cl^- currents and/or ANO2 are not required for olfaction [273].

Other studies suggest that ANO2 regulates AP and synaptic responses in hippocampus neurons [146], to understand the molecular identity of CaCCs in hippocampal neurons, the authors analysed the expression of ANO1 and ANO2 [146]. Only ANO2 was detected at mRNA and protein levels; accordingly, knockdown of ANO2 by siRNA significantly inhibited the neuronal CaCC current in hippocampal pyramidal neurons. The neural circuit is such that the postsynaptic terminals of these neurons in the CA1 region of the hippocampus receives information from CA3 pyramidal neurons and sends the information out of the hippocampus. Since adult CNS neurons have low $[Cl]_i$ and very negative E_{Cl}, activation of CaCC in these cells is inhibitory. Therefore the presence of ANO2/CaCC in hippocampal neurons can decrease neuronal activity. It was shown that, indeed, ANO2-mediated CaCC in hippocampal neurons is activated by Ca^{2+} influx via VGCC during the depolarization phase of the AP (note the difference with ANO1 coupling in DRG neurons). This activation mechanism raises the AP threshold and inhibits synaptic transmission, such that ANO2 acts as a brake on neuronal

excitability in the CNS [146].

Much less is known about the physiology and biophysics of other members of the family. Although Duran and colleagues did not find membrane expression or Ca^{2+}-activated Cl^- currents for ANO3–7 [274], other groups have demonstrated plasma membrane expression for ANO1, 2, 5, 6, 7 and 9 when these were overexpressed in HEK293 and Fischer rat thyroid (FRT) cells [275]. One anoctamin which attracted much attention is ANO6, a protein is linked to Scott syndrome, a rare congenital bleeding disorder caused by a defect in blood coagulation. The root of Scott syndrome is an aberrant phospholipid composition of the outer membrane leaflet of platelets which is attributed to a deficit in phospholipid scrambling. Suzuki et al. found that many patients with Scott syndrome have a mutation in ANO6 [276], and hypothesized that ANO6 has a lipid scramblase activity. Accordingly, ANO6 knockout mice have impaired coagulation, like that seen in patients with Scott syndrome [277]. The same group also reported that ANO6 was localized to the plasma membrane, and conferred Ca^{2+}-dependent scrambling of phospholipids [276, 278]. However, many facts about this protein are disputed in the current literature. Thus, Yang and colleagues suggest that ANO6 is a Ca^{2+}-activated cation channel required for lipid scrambling in platelets, even though it is not itself a scramblase [277]. Martins and colleagues suggested that ANO6 is an essential component of the outwardly rectifying Cl^- channel [279]. Another study showed that ANO6 constitutes a Ca^{2+}-activated anion channel [280].

It has recently been suggested that the anoctamin family should be divided into two subfamilies: a family characterized by Ca^{2+}-dependent Cl^- channels (ANO1 and 2), and a family comprised of Ca^{2+}-dependent lipid scramblases (3, 4, 5, 6 and 7) [278]. Another anoctamin, ANO3, was found to play a role in nociception. ANO3 is expressed in the central and peripheral nervous systems (including DRGs), but apparently does not form an ion channel by itself. Rather, it somehow enhances the expression of the Na^+-activated K^+ channel of Slack,

thus causing hyperpolarization of the cell membrane and playing an overall anti-nociceptive role in pain pathways [281].

1.5 Working hypothesis and aims of the study

Previous experiments from our group and others have identified ANO1 as a novel pro-algesic ion channel in DRG neurons that mediates noxious responses to inflammation [7, 256]. The evidence for this contention includes the following six observations:

1. ANO1 is highly expressed in small-diameter DRG neurons in rats;
2. Activation of ANO1 in these neurons is excitatory;
3. The inflammatory mediator BK activates CaCC in small DRG neurons via PLC- and IP_3-mediated Ca^{2+} release from intracellular stores;
4. Native CaCC activated by BK in DRGs is reduced by siRNA against ANO1;
5. Knock-out, knock-down or pharmacological inhibition of ANO1 in DRGs reduces BK-induced pain in vivo; and
6. Ca^{2+} influx via the VGCC in small-diameter DRG neurons were surprisingly ineffective in activating CaCC. Such poor coupling to a particular Ca^{2+} source was not expected from the ANO1 overexpression studies.

These findings point to the central question of this study:

Why do Ca^{2+} transients produced by BK activate ANO1/CaCC in DRG neurons, while Ca^{2+} influx from VGCCs fail to do so (activate ANO1/CaCC in DRG neurons)?

My hypothesis is based on the following observations and assumptions:

1) The Ca^{2+} sensitivity of ANO1 at voltages near the rest potential of a DRG neuron is low (~2-5 μM), suggesting that the channel must be in close proximity to the source of intracellular Ca^{2+} to be activated by an endogenous signal;

2) Specific molecular interactions coupling ANO1 to a particular Ca^{2+} source must exist; and

3) Specific coupling of ANO1 to Ca^{2+} release sites may play an important role in conferring specificity and fidelity of inflammatory signaling in nociceptive neurons.

The aims of the study are therefore the following.

1) To investigate the signaling pathway for ANO1 activation by PLC-coupled inflammatory mediators in small-diameter DRG neurons, with special attention given to the source of Ca^{2+} for ANO1 activation;

2) To probe the molecular mechanisms for preferential coupling of ANO1 channels in small-diameter DRG neurons to intracellular Ca^{2+} stores; and

3) To explore the physiological role of the preferential coupling of ANO1 to Ca^{2+} sources in DRG neurons.

2.1 Materials

All cell culture reagents were obtained from Gibco BRL (Paisley, UK). All other reagents were of the highest obtainable grade. Unless stated otherwise, all chemicals were from Sigma-Aldrich.

2.2 DRG culture

All procedures were approved by the Animal Care Committee of the University of Leeds. DRG were extracted from all spinal levels of 21-day-old Wistar rats as described previously [6]. In brief, animals were euthanized according to schedule 1 protocol, and the spinal column was removed and cut in halves along the saggital plane. After removal of the spinal cord, DRG were extracted from either side of spinal column with roots cut. Ganglia were then incubated in HBSS solution (137.93 mM NaCl, 5.33 mM KCl, 4.17 mM $NaHCO_3$, 0.441 mM KH_2PO_4, 0.338 mM Na_2HPO_4, 1.26 mM $CaCl_2$, 0.493 mM $MgCl_2$, 5.56 mM D-Glucose) supplemented with 1 mg/ml collagenase and 10 mg/ml dispase for 30 minutes at 37^oC. The digestion was stopped by addition of 10 ml ice-cold Dulbecco's Modified Eagle's Medium (DMEM) supplemented with 10% fetal bovin serum (FBS) and antibiotics (Penicillin-Streptomycin, 100 U/mL penicillin, and 100 µg/mL streptomycin). The cell suspension was collected by centrifugation at 900x g for 5 min, followed by two washes with the DMEM media. After the last wash, the pellet was resuspended in DMEM (with FBS and antibiotics) and plated onto cover slips pre-coated with poly-D-lysine and laminine. DRG cultures were used from 48 hours (hr) and up to one week after plating. No growth factors were added to the culture media (Fig 2.1).

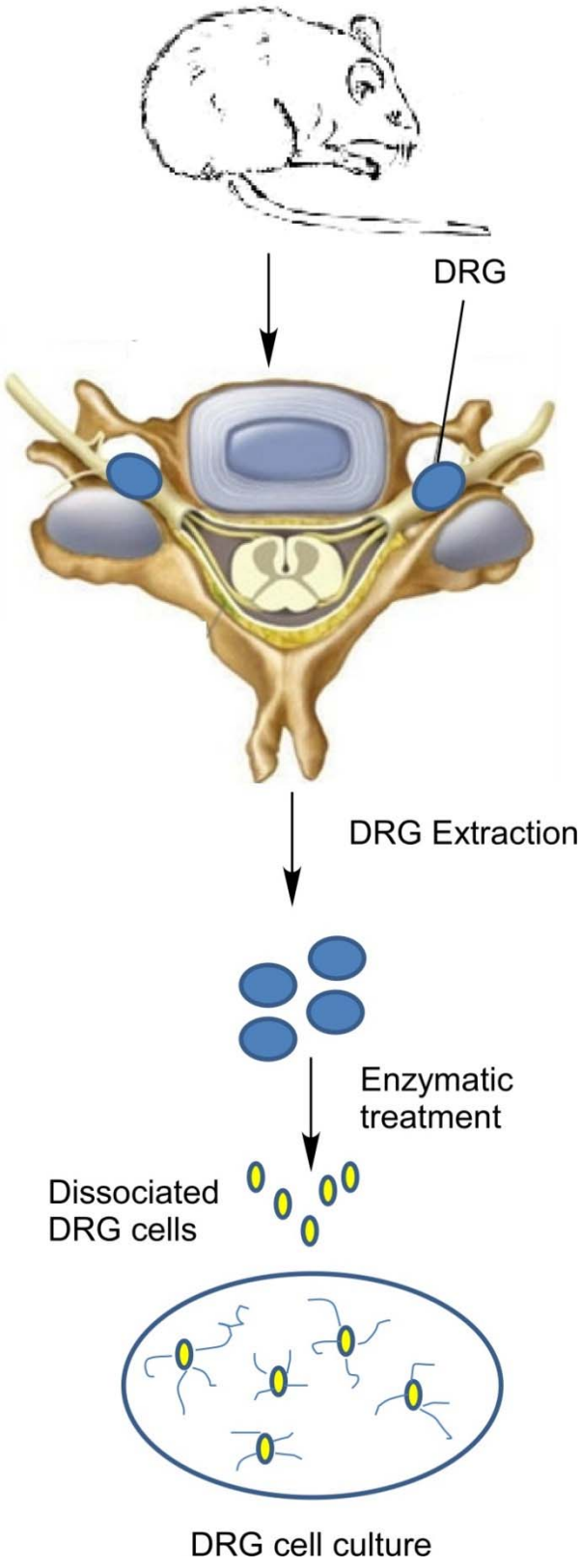

Figure 2.1 Schematic of the DRG dissociation process. The cell bodies of DRG neurons (blue ovals) are located outside the spinal cord in ganglia, the ganglia are located along the spinal nerves. Dissociation procedure involves removing of the spinal cord (including white and gray matter) and extracting DRGs, once carefully dissected, DRGs can be dissociated by enzyme digestion and

dissociated cells (yellow ovals) seeded onto culture dishes. Primary cultures from DRG grow well on a coverslip surface covered with laminin, an extracelluar matrix protein.

HEK293 cells were maintained on tissue culture plates at 37ºC and 5% CO_2 in a humidified atmosphere. Cells were cultured in DMEM: F12 (DMEM/Nutrient Mix F12 (1:1)) with Glutamax ITM containing 10% FBS, 100 U/mLpenicillin, 100 µg/mL streptomycin, and passaged cells when confluent.

2.3 Generation DNA constructs

For construction of plasmids expressing the glutathione S-transferase (GST)-fused ANO1 C-terminus, N-terminus, and the loop between TMD2 and TMD3, different parts of rat ANO1 were amplified by reverse transcription polymerase chain reaction (RT-PCR) from rat mRNA using the appropriate sets of primers (Table 2.1). RNA was extracted from rat DRG tissue using Trizol Reagent. Reverse transcription was conducted using Superscript-II RT (Invitrogen) according to manufacturer's instructions. Briefly, 50 ng of random primers were mixed with 500 ng total RNA and dNTP; the mixture was heated to 65°C for 5 min and quickly chilled on ice. DTT (10 mM) and reaction buffer were then added to the mixture; the mixture was incubated at 25°C for 2 min, then 1 µL (200 units) of SuperScript™ II RT was added and the mixture was further incubated at 25°C (10 min) followed by another incubation at 42°C (50 min). Finally, reaction was inactivated by heating to 70°C for 15 min.

PCR amplification was performed from rat cDNA according to the following protocol: 5 min preincubation at 95°C followed by 30 amplification cycles each consisting of 30 sec denaturing at 95°C, 30 sec primer annealing at 55°C, and 45 sec elongation at 72°C. The last cycle consisted of incubation at 72°C for 10 min. The details of primers are shown in Table

2.1. The PCR fragments were sub-cloned into pGEX-KT (GE Healthcare) using BamHI (sense) and EcoRI (antisense) site, to make pGST-C/ANO1, N/ANO1 and Loop/ANO1 plasmids.

Table 2.1 Details of primer used in this study

Fragment	**Primer sequence**
pIRES2 EGFP ANO1C-terminal sense	GCG CGA ATT C AT GAT GGA CTG GGT GAT C
pIRES2 EGFP ANO1C-terminal antisense	GCC GGA TCC CTA CAG CGC GCC CCC ATG G
pIRES2 EGFP ANO1Loop sense	CCG GAA TTC ATG ATG GAG CAC TGG AAA CG
pIRES2 EGFP ANO1Loop antisense	CGC GGA TCC TTA GAA ATA GGC TGG GAA T
pIRES2 EGFP ANO1N-terminal sense	CCG GAA TTC ATG CAG GAC ACA CAG GA
pIRES2 EGFP ANO1N-terminal antisense	CGC GGA TCC TCA AAG CCA GGC AAA GTA
pGST ANO1C-terminal sense	GCG CGG ATC C AT GAT GGA CTG GGT GAT C
pGST ANO1C-terminal antisense	GCG CGA ATT C CTA CAG CGC GCC CCC ATG G
pGST ANO1Loop sense	GCG CGG ATC C TG CGA GCA CTG GAA ACG GAA
pGST ANO1Loop antisense	GCG CGA ATT C GC AGA AAT AGG CTG GGA ATC
pGST ANO1N-terminal sense	GAG AGG ATC CAT GCA GGA CAC ACA G
pGST ANO1N-terminal antisense	GAG AGA ATT CAA GCC AGG CAA AGT AC

The PCR fragments were purified by gel extraction kit (Invitrogen) and ligation was done using T4 ligase (NEB) at room temperature overnight. The ligation product was transformed into competent cells and plated out on Luria Bertani-ampicillin (LB-Amp) plates. After 16 hr, several colonies were picked and confirmed by PCR amplification. Finally, the plasmids were prepared by plasmid mini-prep kit (Invitrogen) and sequenced to validate the sequence of the constructs. Thus, three plasmid constructs were made. For construction of pIRES2 EGFP plasmids expressing the same ANO1 fragments, these were amplified by PCR from pGST-C/ANO1, N/ANO1 and Loop/ANO1 plasmids using the appropriate primer pairs (Table 2.1) and sub-cloned into pIRES2 EGFP vectors (Clonetech) using BamHI (antisense) and EcoRI (sense) sites. Colonies expressing the fragment were identified by kanamycin resistance.

2.4 Electrophysiology

Whole-cell, and current clamp recordings were performed as described in [6, 7]; an EPC-10 patch clamp amplifier in combination with Patchmaster V2.2 software (HEKA) was used to amplify and record currents and potentials. In intracellular solutions with basal physiological $[Ca^{2+}]_i$, intracellular free Ca^{2+} was adjusted to 100 nM using the Maxchelator program (Stanford University). For high concentration of intracellular free Ca^{2+}, intracellular free Ca^{2+} was adjusted to 1 or 10 μM using the Maxchelator program (Stanford University). In the 'fast' whole cell experiments for testing the activation of CaCCs by GPCRs or VGCC, the internal pipette solution contained (in mM): 150 CsCl, 5 $MgCl_2$, 1 K_2ATP, 0.1 NaGTP, 1 EGTA, 10 HEPES (pH 7.4 with CsOH). The external solution contained (in mM): 145 TEACl, 2 $CaCl_2$, 10 HEPES (pH 7.4 with CsOH). In Ca^{2+} clamping experiments the internal solution contained (in mM): 135 CsCl, 5 $MgCl_2$, 5 HEPES, 1 K_2ATP, 0.1 NaGTP, and 10 of either EGTA or BAPTA, pH 7.35 with CsOH. The external solution contained (in mM): 145 TEACl, 2 $CaCl_2$,

10 HEPES (pH 7.4 with CsOH). In a 'Ca^{2+}-free' external solution $CaCl_2$ was omitted and 1 mM EGTA added to chelate residual free Ca^{2+}. For recordings with voltage ramp protocols used to measure activation of CaCC by GPCR the external solution contained (in mM):155 TEACl, 2 $CaCl_2$, 0.1 $CdCl_2$, 10 HEPES (pH 7.4 with CsOH). For recordings with voltage ramp protocols used to measure voltage-gated Ca^{2+} channel-induced CaCC, the internal pipette solution contained (in mM): 150 CsCl, 5 $MgCl_2$, 1 K_2ATP, 0.1 NaGTP, 1 EGTA, 10 HEPES (pH 7.4 with CsOH). The external solution contained (in mM): 140 NMDG, 2 $CaCl_2$, 1.5 $MgCl_2$, 10 HEPES, 10 glucose (pH 7.4 with HCl). In these experiments CaCC was measured as inward tail current following a square pulse to 0 mV from the holding potential of -80 mV with a subsequent second pulse to 80 mV. This second pulse activated VGCCs but caused little net Ca^{2+} influx due to the small driving force. CaCC amplitude was calculated as a difference in the peak tail current amplitudes after the depolarizing pulses with and without Ca^{2+} influx. VGCC current often displayed rapid run-down so the CaCC current amplitude was calculated from the first sweep. Current clamp experiments were performed in whole-cell patch mode with extracellular solution containing (in mM): 160 NaCl, 2.5 KCl, 2 $CaCl_2$, 1 $MgCl_2$, 10 HEPES, pH 7.4 with NaOH; intracellular solution contained 150 KCl 5 $MgCl_2$, 1 K_2ATP, 0.1 NaGTP, 1 EGTA, 10 HEPES. In a 'low $[Cl^-]_i$' pipette solution 140 mM KCl was replaced by equimolar K-acetate.

2.5 Immunocytochemistry

DRG neurons from 21-days rats were cultured on the cover slips for 2 days, fixed and permeabilised with acetone: methanol (1:1) at -20^{o}C for 20 min. To reduce nonspecific antibody binding, the sections were treated with 2% normal donkey serum in PBS for 15 min. For ANO1 staining, the sections were incubated in anti-ANO1 antibody (Santa Cruz) in PBS containing 2% normal horse serum, and 0.2% Na azide at 4^{o}C overnight followed by the incubation with the Alexa Fluor 488 donkey anti-goat IgG (Molecular Probes) for 1.5 hours at room temperature. For IP_3 receptor 1 (IP_3R1) staining, anti-IP_3R1 (Calbiochem) and Alexa Fluor 555 donkey anti-mouse IgG (Molecular Probes) were used. The antibody dilutions are shown in Tables 2.2 and 2.3. Confocal images were taken with an LSM510 META microscope (Zeiss). Human umbilical vein endothelial cells (HUVECs) were transfected with green fluorescent protein (GFP) along with the ANO1 plasmids using Fugene HD transfection kit (according to manufacturer's instructions). Approximately $1x10^6$ cells were seeded onto cover slips in 60 mm cell culture dishes 24 hours before transfection, and cells were transfected with 600 ng of each plasmid (GFP and ANO1). Cells were cultured for 36 hr in DMEM:F12 medium and then cells were fixed and permeabilised with acetone: methanol (1:1) and labelled with anti-ANO1 (Santa Cruz) and Alexa Fluor 488 donkey anti-goat IgG (Molecular Probes) as shown in DRG protocol. Confocal images were taken with an LSM510 META microscope (Zeiss).

2.6 Immunoprecipitation and Western blotting

Generally the procedures were performed as described by previous investigators [282, 283]. Briefly, entire DRGs (from all levels) from 21 day old Wistar rats were homogenized in non-denaturing lysis buffer (20 mM TrisHCl pH 8, 137 mM NaCl, 10% glycerol, 1% Triton X-100, 2 mM EDTA) with protease and phosphatase inhibitor cocktail including AEBSF at 104

mM, Aprotinin at 80 μM, Bestatin at 4 mM, E-64 at 1.4 mM, Leupeptin at 2 mM and Pepstatin A at 1.5 mM (Sigma-Aldrich), and incubated for 2 hr at 4°C before centrifugation for 20 min at 12,000 rpm (13,000 x g). For immunoprecipitation, 30 μl supernatants (5% of total lysate) were saved as input sample and the rest was used for immunoprecipitation. The resultant supernatant was incubated overnight at 4°C with 500 ng antibody at a dilution of 1:300. On the following day 100 μl protein G sepharose beads (GE Healthcare, London, UK) was added and incubation continued at 4°C under rotary agitation for 4 hr. Beads were then washed four times with lysis buffer (with inhibitors) and centrifuged; supernatants were discarded. Bound proteins were eluted from the beads with 25 μl 2X Laemmli buffer (4% SDS, 20% glycerol, 10% 2-mercaptoethanol, 0.004% bromphenol blue and 0.125 M Tris HCl, pH 6.8) at 95°C for 5 min before immunoblotting (IB).

For Western blotting analysis, total DRG lysate samples were eluted from protein G beads or membrane fractions (20 μg) and boiled for 5 min in 2X SDS–polyacrylamide gel electrophoresis (PAGE) sample buffer (4% SDS, 20% glycerol, 10% 2-mercaptoethanol, 0.004% bromphenol blue and 0.125 M Tris HCl, pH 6.8). Proteins were then separated by SDS-PAGE, followed by transfer to PVDF membrane by electroblotting. The membranes were incubated in blocking buffer (TBS: 50 mM Tris.HCl, pH 7.4 and 150 mM NaCl) supplemented with 5% skimmed milk and 0.1% Tween-20 for 2 hr followed by incubation with primary antibody diluted in the same buffer at 4°C overnight. The membranes were washed in TBS containing 0.1% Tween-20 before incubation with an appropriate secondary antibody (horseradish peroxidase-conjugated anti-IgG or IRDye®-conjugated anti-IgG). Bound antibodies were detected using the super-signal chemiluminescence system (ECL, Thermo) or Odyssey 9120 Infrared Imaging System (LI-COR, Lincoln, NE). In co-immunoprecipitation experiments, 5% of total lysate protein was run on the same gel for input control. The complete list of antibodies used in this study can be found in Tables 2. 2 and 2. 3.

Table 2.2 List of primary antibodies

Primary Antibody	Company	Dilution	Cat. number
ANO1	Santa Cruz	1:500(Western blotting); 1:100(immunofluorescence)	sc-69343
IP_3R	Cell signaling technology	1:800(Western blotting); 1:200(immunofluorescence)	#3760
CD71	Santa Cruz	1:500	sc-59112
B_2R	BD Biosciences	1:1000	610452
PAR2	Santa Cruz	1:1000	sc-13504
Caveolin- 1	BD Biosciences	1:1000	610406
GST	Santa Cruz	1:500	sc-138
Pan-VGCC	Sigma	1:400	C1103
SERCA	Badrilla Ltd	1:1000	A010-21AP

Table 2.3 List of secondary antibodies

Secondary Antibody	Company	Diluted times	Cat. number
donkey anti-goat IgG-HRP	SantaCruz	1:5000	sc-2020
donkey anti-mouse IgG-HRP	SantaCruz	1:5000	sc-2096
donkey anti-rabbit IgG-HRP	SantaCruz	1:5000	sc-2077
Alexa Fluor 488 donkey anti-goat IgG	Molecular Probes	1:1000	A-11055.
Alexa Fluor 555 donkey	Molecular Probes	1:1000	A-31570

2.7 Lipid Raft Isolation

Lipid raft isolation was performed as described in reference [284]. All steps were carried out at 4°C. Entire DRG were isolated from 21 days old Wistar rats (from all spinal levels) and frozen at -80°C until use. Lipid rafts were isolated by sucrose gradients. Briefly, frozen ganglia were thawed and homogenized using glass *Potter-Elvehjem* homogenizer in 1.5 ml MBST buffer (50 mM MES, 150 mM NaCl, pH 7.35, 1% Triton X-100, 5 µg/ml leupeptin, 5 µg/ml aprotinin and 2 µg/ml pepstatin A). The homogenate was then mixed with 1.5 ml of 80% sucrose in MBS buffer (50 mM MES, 150 mM NaCl, pH 6.5, 5 µg/ml leupeptin, 5 µg/ml aprotinin and 2 µg/ml pepstatin A) before overlaying successively with 3 ml volumes of 35% sucrose in MBS buffer and 5% sucrose in MBS buffer. For lipid raft isolation, the resultant gradients were ultracentrifuged (100000 g, 18 hr, 4°C), and 9 fractions were collected from each (from the top to the bottom of the tube, fractions 1–9). Samples were analysed by SDS-PAGE followed by Western blotting.

2.8 GST Pulldown Assays

GST pull-down assays were performed as described previously [285]. Briefly, rat ANO1 (UniProt accession D4A915) N terminus (1-407), TMD2-3 loop (505-568) and C terminus (963-1040) were PCR cloned from rat DRG cDNA and subcloned into the vector pGEX-KT. All constructs were expressed in *Escherichia coli* strain BL21-gold cells (Stratagene) and purified with Glutathione Sepharose 4B beads (GE Healthcare, London, U.K.) at 4°C overnight with gentle rotation. For GST pull-down, rat DRG ganglia were homogenized in non-denaturing lysis buffer (20 mM TrisHCl pH 8, 137 mM NaCl, 10% glycerol, 1% Triton X-100, 2 mM EDTA) with protease and phosphatase inhibitors and incubated for 2 hr at 4°C. Insoluble debris was removed by centrifugation for 20 min at 12,000 rpm (13,000 x g). GST protein and GST fusion proteins (bound to Glutathione sepharose, GE Healthcare, London,

UK) were incubated with rat DRG tissue homogenate overnight at 4°C. The beads were washed and bound proteins were eluted in SDS-PAGE sample buffer, and analysed by Western blotting.

2.9 Fluorescent Imaging

Point mutations H148Q and I152L [286] were introduced intothe pEYFP-N1 vector (Clontech) by QuikChange mutagenesis kit (Stratagene). The H148Q/I152LEYFP mutant was then subcloned into pcDNA6-V5/His vector (Invitrogen); subcloning was performed by Honling Rong. Transfection of DRG was performed as described previously [6, 7] using the Nucleofector device and rat neuron Nucleofector Kit (Lonza). Yellow fluorescent protein (YFP) fluorescence measurements were recorded using a Nikon Swept Field confocal microscope equipped with a 488 nm argon laser, an EM-CCD camera and controlled by the NIS Elements 3.2 software (Nikon). The extracellular solution for these experiments contained (in mM): 160 NaCl, 2.5 KCl, 2 $CaCl_2$, 1 $MgCl_2$, 10 HEPES (pH 7.4 with NaOH). To produce iodide influx 30 mM NaCl was replaced with 30 mM NaI. Ca^{2+} imaging was performed as described previously [7, 287]; briefly, neurons were loaded with fluo-4 AM (2 μM) in the presence of Pluronic F-127 (0.02%). DRG cultures were treated with 10 mM methyl-β-cyclodextrin (MβCD) or vehicle for 45 min during the loading with fluo-4 AM and imaged immediately using a Nikon TE2000E microscope in epi-fluorescence mode (these experiments were contributed by Shihab Shah and Nikita Gamper).

2.10 *In Situ* Proximity Ligation Assay (PLA)

Proximity ligation assay (also referred to as '*in situ* co-immunoprecipitation') allows specific labelling of closely associated proteins *in situ* [288, 289]. The principle of the assay is depicted in Fig. 2.2. Briefly, two primary antibodies (raised in different species) recognize the target antigens within proteins under investigation. After the primary antibodies bind the

antigen(s), a set of secondary antibodies covalently conjugated with unique oligonucleotide sequences is used. If these secondary antibodies label proteins that are no more than 30-40 nm apart, the conjugated oligonucleotides from both secondary antibodies can be bound by complementary connector oligonucleotides and ligated to form a unique circularstructure. This structure can be amplified by means of rolling circle amplification (RCA). The oligonucleotide of one of the proximity probes acts as a primer for RCA, and DNA-circle acts as template, while the oligonucleotide of the other proximity probe is inhibited. The RCA product is detected by hybridization with fluorescencently labeled oligonucleotides that tag a sequence in the RCA product. If the targeted proteins are indeed in close proximity *in situ*, the PLA produces bright fluorescent "puncta" of 0.5 – 1 μm in diameter which can be detected using a confocal microscope (Fig 2.2).

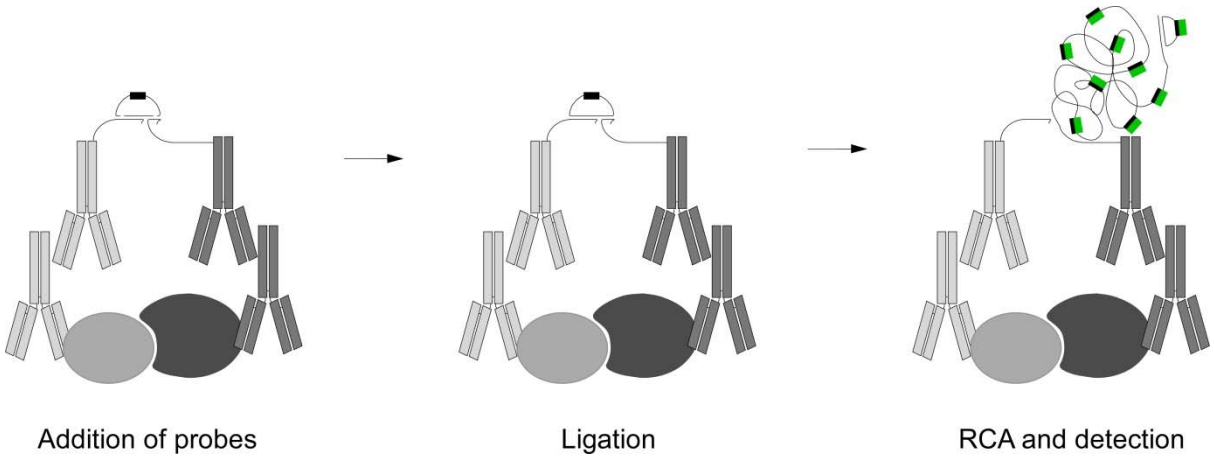

Figure 2.2 Schematic illustrating the PLA principle. When two proteins are in close proximity, antibodies connected to specific DNA fragments are close enough to bind in a complementary connector oligonucleotides, forming a circular structure amplified in the RCA process. The RCA product is detected by hybridization of dye-conjugated oligonucleotides complementary to a tag sequence in the RCA product (based on [288, 289]).

For PLA assay, cultured DRG neurons were fixed on the round coverglasses and permeabilised with acetone: methanol (1:1) for 20 minutes at -20^{o}C. The proximity ligation

assays were performed according to manufacturer's (OlinkBioscience) instructions. Briefly, after adding the blocking solution supplied as part of the PLA kit, the cover glasses were incubated for 30 minutes at 37°C. After treatment with the blocking solution, the coverglasses were incubated with the primary antibodies – anti-ANO1 and anti-IP_3R–overnight at 4°C using the same dilutions as in the immunocytochemistry experiments. The coverglasses were washed twice with buffer A (DuoLink II Detection Reagents Green Kit) for 5 min and a solution containing oligo-conjugated secondary antibodies (anti-goat PLUS, anti-rabbit MINUS PLA probes; 1:5 dilution as per manufacturer's protocol) was added. The coverglasses were then incubated for 60 min at 37°C and then washed twice with buffer A (5 min). For ligation, a solution containing 1:5 dilutions of Ligation Solution (DuoLink II Detection Reagents Green Kit) and 1:40 ligase (in high purity water) was used and coverglasses were incubated for 30 minutes at 37°C. After that, coverglasses were washed twice with buffer A (2 min) and the amplification stage (100 minutes at 37°C) was performed in Amplification Solution (1:5 dilution in high purity water) containing polymerase (1:80 dilution in high purity water). Coverglasses were then washed twice with buffer B (10 min) followed by 1 minute in 1:100 diluted buffer B. The coverglasses were then mounted with mounting medium containing DAPI. Confocal images were taken with an LSM510 META microscope (Zeiss). I used Z-stacking to quantify number of PLA puncta; each stack consisted of one layer in the nuclear focus plane (DAPI) and 16 layers separated by 0.475 nm, 8 above and 8 below that plane. The number of PLA puncta per captured multilayer image was analyzed using the Carl Zeiss software ZEN. In theory, each PLA spot represents one interaction. Although the *in situ* PLA signal is proportional to the amount of interactions, only a fraction of interactions gives a signal [290, 291]. As a negative control for the PLA assay, I tested proximity of ANO1 and VGCC using pan-VGCC antibody (Table 2.2, also see Chapter 6).

2.11 Data Analysis

All data are given as means ± standard error of the mean (SEM). Unless indicated otherwise, only values from responsive cells are included into reported means. Differences between groups were assessed by Student's two-tailed t-test, with the significance level set at $p<0.05$ or 0.01. A X^2 test was used to determine whether there were differences in the proportions of cells responding to a treatment.

3.1 Introduction

3.1.1 Ca^{2+} sensing and gating mechanisms of ion channels

Ca^{2+} has a major role in regulation of such cellular functions as neurotransmitter release in neurons, excitation-contraction coupling in muscles, gene expression, intracellular signaling mediation, and so on. The specificity, speed, reliability and spatial localisation of the Ca^{2+} signals determine the exact physiological response. Ca^{2+} is also needed for Ca^{2+}-binding proteins to perform their functions. One ubiquitous Ca^{2+}-binding protein is calmodulin (CaM), which binds Ca^{2+} through its four EF-hand domains. Other Ca^{2+}-binding proteins include calbindins/calneurins, parvalbumine and the neuronal Ca^{2+} sensor protein family [292].

One of the best understood examples of ion channel activation by Ca^{2+} can be found in Ca^{2+}- activated K^+ channels. Ca^{2+}-activated K^+ channels are a family of K^+ channels that include large-conductance (Slo1 or $K_{Ca1.1}$) channels, intermediate-conductance (IK) channels, and small-conductance (SK) channels. The Slo1 channel has a very large carboxy-terminus that includes the channel's own Ca^{2+}-binding sites. The high-affinity Ca^{2+}-binding site called the "Ca^{2+} bowl" contains a domain of five consecutive aspartic acid residues which act as high-affinity Ca^{2+} binding sites and respond to global Ca^{2+} [293-295]. The low-affinity Ca^{2+} binding site is located in the proximal part of C-terminus, close to the S6 domain. Low-affinity binding sites are believed to respond to local Ca^{2+} signals – that is, highly localised areas near the opening of a Ca^{2+} release point or entry pathway where high a Ca^{2+} concentration can be generated temporarily [296, 297].

By contrast, the Ca^{2+}-sensitivity of the IK and SK channels depends on the CaM. In comparison with the Slo1 channels, $K_{Ca3.1}$ (IK) is much more sensitive to Ca^{2+} and can thus respond to the global level of Ca^{2+}. This high affinity for Ca^{2+} depends upon four resident CaM

molecules bound to the cytoplasmic tails of α-subunits. Channel opening is activated in a synergistic manner by both depolarization and by an increase in intracellular Ca^{2+}.

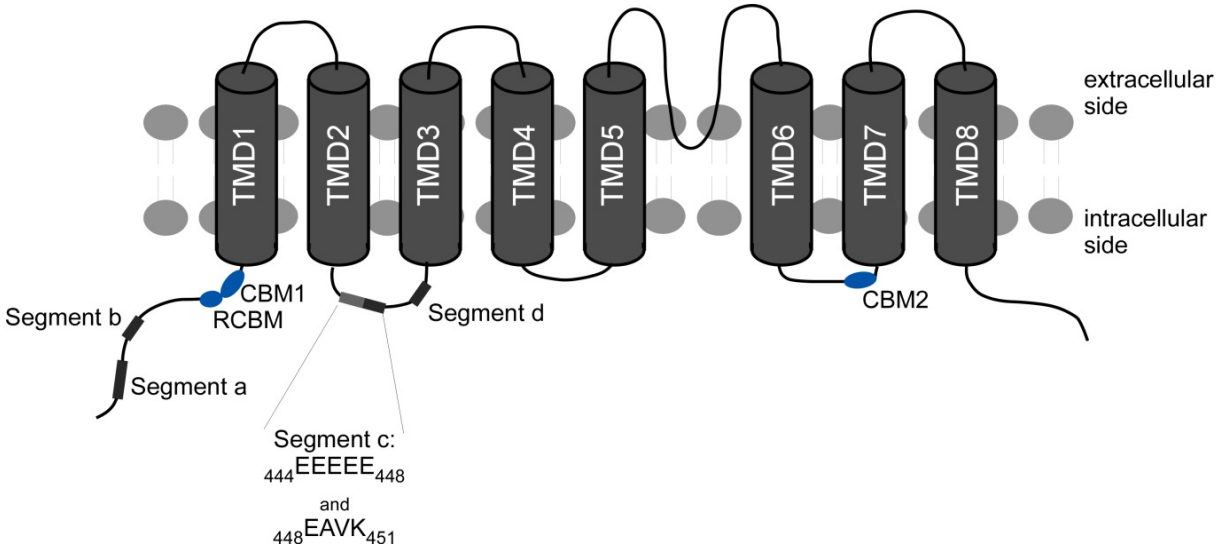

Figure 3.1 Topology model of ANO1 featuring alternative splicing variants and putative Ca^{2+}-sensitivity sites. The figure shows four alternatively spliced segments. Segment *a* codes for 116 amino acids located in the N terminus. Alternative splicing of this segment affects channel voltage dependence. Segment *b* codes for 22 amino acids located in the N terminus and is important for Ca^{2+}-sensitive gating. Segment *c* codes for four amino acids ($_{448}$EAVK$_{451}$) within the first intracellular loop of ANO1. There is a sequence of five consecutive glutamates in the loop that ends with E448, which was suggested to be important for the Ca^{2+} sensitivity of the channel [267]. The sequence $_{444}$EEEEEAVK$_{451}$ contributes to coupling of voltage and Ca^{2+}-dependent gating mechanisms. Two putative CaM-binding motifs (CBM1-2) are shown as blue ovals. An additional regulatory CaM binding site (RCBM) suggested by Vocke and colleagues [298] is also depicted.

In contrast to Ca^{2+}-activated K^+ channels, ANO1 does not have canonical Ca^{2+} binding domains or full-feature CaM-binding sites such as EF hands, and IQ domains (however see below). In addition, Ca^{2+} binding appear to be cooperative [165, 202], suggesting that ANO1 should have more than one Ca^{2+} binding domain. It has been reported that ANO1 can be directly activated by Ca^{2+}, and the first cytosolic loop between TMD2 and TMD3 has a short contiguous sequence of acidic amino residues ($_{444}$EEEEEAVK$_{451}$) which may be the possible Ca^{2+}-binding

region [161, 205, 299]. Five consecutive glutamates ($_{444}$EEEEE$_{448}$) may be a binding pocket for Ca^{2+}, as proposed for the "Ca^{2+} bowl" of Ca^{2+}-dependent K^+ channels [160, 295, 300]. But mutation of these amino acids did not alter Ca^{2+} sensitivity significantly [205]. In contrast, deletion of $_{448}$EAVK$_{451}$ in the first intracellular loop decreased the Ca^{2+} sensitivity [205, 267]. It was recently suggested that the third intracellular loop, which contains two glutamic acid residues ($_{702}$E and $_{705}$E), binds Ca^{2+} directly, and is a main domain controlling the Ca^{2+} sensitivity of ANO1 and ANO2. This hypothesis is based on chimeras of ANO1 and ANO2 and mutagenesis of these specific residues [301]. Yu and colleagues found that point mutations of $_{702}$E and $_{705}$E caused nearly 100-fold decreases in Ca^{2+} sensitivity [206].

Despite good evidence for direct activation of ANO1 by Ca^{2+}, several studies identified the direct association between ANO1 and CaM. Two putative CaM-binding motifs (CBM1-2; Fig. 3.1) were identified. These sites are different from canonical Ca^{2+} binding domains, but both CBM1 and CBM2 were shown to bind CaM in vitro [236]. These two putative CaM-binding motifs were implicated in the Ca^{2+}/CaM-dependent regulation of the ANO1 permeability to bicarbonate [236].

Vocke and colleagues identified another CaM binding site (RCBM), which is located in the first intracellular loop of ANO1 in close proximity to CBM1 (Fig 3.1) [298]. Tian and colleagues proposed two CaM-binding sites (CAMBD1 and CAMBD2) in ANO1; CAMBD2 shows an overlap with the distal part of the RCBM domain [242]. Tian and colleagues reported that CaM interacts with ANO1 and regulates its activity, while Jung and colleagues showed that CaM only interacted with ANO1 under very high Ca^{2+} concentrations [236]. Finally, it has to be pointed out that the role of CaM in ANO1 functioning has been disputed, because the channel retains normal Ca^{2+} sensitivity in the experimental conditions in which CaM is excluded [302, 303]. It also has been shown that ANO1 can be activated without ATP,

suggesting that channel phosphorylation is not required [303]. Clearly, further studies are needed to improve our understanding of the structural basis of ANO1 activation by Ca^{2+}.

3.1.2 Voltage gating mechanisms of ANO1

ANO1 does not have known voltage sensing region such as S4 in voltage-gated K^+ or Na^+ channels. However Ca^{2+} sensitivity of ANO1 displays strong voltage dependence, such that higher sensitivity is reported at positive membrane potentials as compared to more physiological, negative membrane potentials (see Chapter 1). It is likely that Ca^{2+} binding domain lies within the membrane electric field and couples both voltage and Ca^{2+} binding to channel gating [205]. As mentioned above, there are five consecutive glutamic acids ($_{444}$EEEEE$_{448}$) localized to the first intracellular loop of ANO1 (Fig 3.1). The last glutamic acid of this cluster-$_{448}$E, is the first residue of a naturally occurring alternatively spliced segment, $_{448}$EAVK$_{451}$ (Fig 3.1) [267]. Exclusion of $_{448}$EAVK$_{451}$ was reported to reduce the voltage dependence of ANO1 activation significantly [267]. However, another study reported that the deletion of $_{448}$EAVK$_{451}$ decreased apparent Ca^{2+} affinity of the channel [205]. In contrast, mutating the adjacent four glutamic acids to alanines ($_{444}$EEEE/AAAA$_{447}$) abolished intrinsic voltage dependence without altering the apparent Ca^{2+} affinity [205]. In light of these results the authors suggested that residues of $_{444}$EEEEEAVK$_{451}$ do not encompass the true Ca^{2+} binding site, but may instead be important to the coupling between voltage and Ca^{2+} sensitivity of the channel [205]. The authors hypothesized that the depolarization change the Ca^{2+} binding site, and drive Ca^{2+} into the binding site under the electrical field [205]. The mechanisms for voltage-dependent control of ANO1 channel gating and gating cooperation between Ca^{2+} and voltage require further investigation.

3.1.3 ANO1 gating by heat

Temperature is another gating mechanism which regulates the activity of ANO1. As discussed, ANO1 is expressed in nociceptive neurons in the DRG which are excited by noxious heat and express a noxious heat sensor, TRPV1. Interestingly, ANO1 was also found to be activated by high temperature with a threshold of ~44°C [256, 304]. Heat-induced opening of ANO1 depolarized DRG neurons. In addition, pharmacological block or deletion of ANO1 was found to reduce thermal hyperalgesia; mice with reduced ANO1 levels by siRNA or tissue-specific gene disruption displayed reduced sensitivity to hot temperatures. These results suggest that ANO1 is a heat sensor that mediates the perception of noxious heat [256].

3.1.4 Interaction of ANO1 with other proteins

Perez-Cornejo and colleagues identified potential accessory subunits of ANO1 by a highly sensitive quantitative proteomic approach (stable isotope labeling by amino acids in cell culture (SILAC) proteomics). The authors made a HEK293 cell line stably expressing ANO1, tagged a triple FLAG epitope, and then stabilized the ANO1 protein complex by using a crosslinking approach. They found that ANO1 interacted with the actin-based cytoskeleton network, including the actin-binding regulatory ERM proteins ezrin, radixin, moesin, and RhoA, all of which link actin to the plasma membrane and coordinate cell signaling events [305]. The actin cytoskeleton may regulate ANO1 function by modulating ANO1 channel gating, directing trafficking ANO1 to the membrane, or assembling ANO1 into signaling networks [305]. The same group also identified another group of proteins interacting with ANO1, included a SNARE protein complex containing vesicle-associated membrane protein 3 (VAMP3), syntaxins-2 and -4, and the syntaxin-binding proteins munc18b and munc18c. The role of these interactions are presently unknown but may include regulation of ANO1 trafficking [305].

3.1.5 Regulation of ANO1 properties by alternative splicing

Alternative splicing may also provide us with some clues about the ANO1 function and regulation. ANO1 splice variants containing different combinations of four alternatively-spliced segments, termed *a*, *b*, *c* and *d* were reported [203] (Fig 3. 1). There are 1,008 amino acid residues in ANO1 segments a through d. Segments *a* and *b* are located on the N terminus while segments *c* and *d* are in the first intracellular loop connecting TMD2 and TMD3. Segment *a* codes for 116 amino acid residues and has been considered to role in channel voltage dependence [267]. This function was suggested because an ANO1 splice variant lacking this segment displays reduced voltage dependence. Segment b is important for Ca^{2+}-sensitive gating. The variant (*ac*) shows higher Ca^{2+} sensitivity as compared to the variant (*abc*). In addition, high Ca^{2+} inhibits the activity of the variant (*ac*), although the exact reasons for this phenomenon are not clear [267]. Segment c is located in the first intracellular loop and codes for four amino acids ($_{448}$EAVK$_{451}$). The splice variant with exclusion of segment *c* has a 50-fold lower affinity to cytosolic Ca^{2+} [205]. However, another group found that the splice variant lacking segment *c* resulted in channels with reduced activation at positive membrane potentials [267]. The first intracellular loop includes five consecutive glutamates ($_{444}$EEEEE$_{448}$), including E448 of segment *c*. It has been suggested that this domain participates in Ca^{2+} sensing, but studies show that these glutamate residues have no or very little effect on apparent Ca^{2+} affinity, and are more likely involved in sensitivity of ANO1 to voltage [205]. Finally, alternative exon 15 codes for 26 amino acids (segment *d*) in the first extracellular loop, but the physiological significance of this segment is unclear [267]. These results show how alternative splicing of ANO1 might provide us with explanations of why CaCCs in various cell types have different biophysical properties [162].

3.2 Aims

The aim of this part of the study was to investigate activation by Ca^{2+} of ANO1 channels heterologously expressed in HEK293 cells and activation by Ca^{2+} of native CaCCs in small-diameter DRG neurons.

3.3 Results

3.3.1 Ca^{2+}-activated Cl^- currents recorded in HEK293 cells transfected with ANO1

HEK293 cells were transfected with mouse ANO1 cDNA, and recorded using the whole-cell patch clamp technique using pipette solutions with free intracellular Ca^{2+} concentration buffered to either 100 nM (control condition) or 1 μM. When untransfected HEK293 cells were recorded with 100 nM Ca^{2+} or 1 μM Ca^{2+} pipette solutions, steady-state currents at a holding potential of –60 mV were negligible (Fig. 3.2A). A different picture was observed in ANO1 transfected cells. At 100 nM free intracellular Ca^{2+}, the steady-state inward current was still very small – 12 ± 2.5 pA; n=5; Fig. 3.2B. In contrast, when recordings were made using 1 μM Ca^{2+} pipette solution, 13 of 13 ANO1-transfected HEK293 cells displayed large inward currents of a mean amplitude of 550 ± 20.8 pA at –60 mV (Fig. 3.2C-D). Five of thirteen cells demonstrated a transient activation of the current followed by a decrease in inward current amplitude (Fig. 3.2C), while a plateau was seen in the remaining eight cells (Fig. 3.2D). When recorded with 1 μM free Ca^{2+} in the pipette, voltage steps from −120 to 120 mV (in 10 mV increment) elicited a typical I_{CaCC} characterized by a slow exponentially developing current at +120 mV that generally reached a steady-state level at the end of 1 second steps (Fig. 3.2E, n=2). ANO1 current-voltage relationships were analysed using voltage ramp protocol (Fig. 3.2F). The currents in ANO1-transfected cells were recorded with 17, 225 and 600 nM free Ca^{2+} pipette solutions, and currents were evoked by voltage ramps from −60 to 100 mV (n=5, contributed by Yani Liu). These currents displayed hallmarks of CaCC currents:

the reversal potential was about 0 mV as expected (n=5, Fig. 3.2F). Elevating the pipette free Ca^{2+} concentration from 225 nM to 600 nM increased Cl^{-} current density and induced outward rectification, increasing the mean rectification index (I_{60}/I_{-60}) from 2.11 ± 0.1 to 4.47 ± 1.5 (n=5, Fig. 3.2G).

NFA (100 μM), a common CaCC blocker, potently inhibited such currents (Fig. 3.2E, n=3). Shown in Fig. 3.2G is a time series of the steady-state inward current recorded from the ANO1-transfected HEK293 cell maintained at a holding potential of –60 mV with 1 μM Ca^{2+} pipette solution. Bath application of NFA reversibly inhibited the Ca^{2+}-activated current (90% ± 15%, n=4).

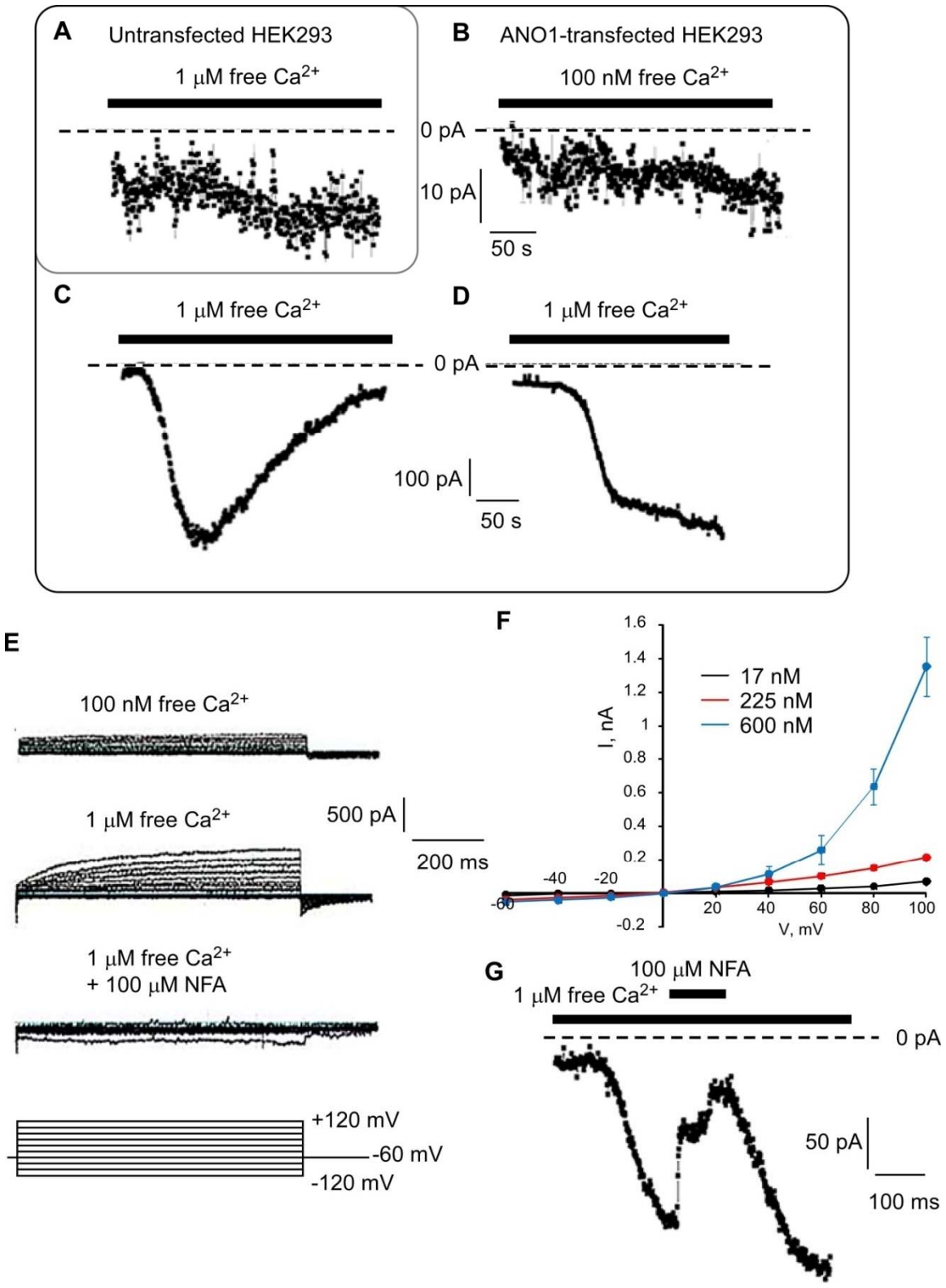

Figure 3.2 Ca^{2+} activates a current in HEK293 cells transfected with ANO1. (A) Whole-cell currents recorded in untransfected HEK293 cell at a holding potential of –60 mV in the presence of 1 μM free Ca^{2+} in the recording electrode. (B) Whole-cell currents recorded in HEK293 cell transfect with ANO1 plasmid at a holding potential of –60 mV in the presence of 100 nM free Ca^{2+} in the recording electrode.

(C, D) Whole-cell currents recorded in HEK293 cells transfected with ANO1 plasmid at a holding potential of –60 mV in the presence of 1 μM free Ca^{2+} in the recording electrode. Representative current traces showing inward currents induced by intracellular Ca^{2+} shown in (E). Representative current traces recorded in ANO1-transfected cells during 120 ms voltage steps from –120 to +120 mV in the presence of 100 nM or 1 μM free Ca^{2+} in the recording pipette (top and middle panels, as indicated). Also shown are current responses in after bath application of NFA (1 μM free Ca^{2+} in the pipette; lower panel). (F) Whole-cell currents recorded in an ANO1-transfected HEK293 cell at a holding potential of –60 mV in the presence of 1 μM free Ca^{2+} in the recording electrode. Bath application of 100 μM NFA was performed during the period indicated by the bar. (G) Whole-cell currents recorded from HEK293 cells expressing ANO1 in the presence of 17, 225 or 600 nM $[Ca^{2+}]_i$, (as indicated) in response to voltage ramps from -60 to +100 mV (n=7). Data are given as mean ± SEM.

3.3.2 Activation of CaCC in DRG neurons by global Ca^{2+} elevation

We next analysed CaCC current in cultured small DRG neurons. Recordings were made from cultured small-diameter (~20 μm) DRG neurons with whole-cell; as characterised by the Gamper's group earlier, these neurones are predominantly (~70%) capsaicin-sensitive [6, 306]. Thus, we consider this neuronal population as predominantly nociceptive. Majority of these neurons also express ANO1 and display CaCC [7]. We used high concentration of Ca^{2+} (10 μM) in the patch pipette to test if high global Ca^{2+} rise can activate CaCC in these neurons. As shown in Fig. 3.3A, CaCCs were activated in only about ~15% of the small DRG by being exposed to high global Ca^{2+}. It is possible that ANO1 was either not expressed or expressed at a very low level in the majority of small DRG neurons under our experimental conditions. In order to exclude this possibility, 1 μM BK was bath-applied to voltage-clamped DRG neurons. Previous evidence from our own laboratory has indicated that stimulation of BK elicits an increase $[Ca^{2+}]_i$ in DRG neurons [7]. As shown in Fig. 3.3B and C, 12 neurons in which dialysis of 10 μM global free Ca^{2+} did not induce inward current responded to BK with a prominent inward current. Some studies suggest that at very high concentrations Ca^{2+} may inhibit ANO1 [205]. In order to exclude this possibility, we used 1 μM free Ca^{2+} pipette solution. However,

at 1 μM global free Ca^{2+}, there was still no inward current activation (Fig 3.3 B and D). Our data therefore suggested that for whatever reason endogenous ANO1 channels in DRG neurons are very poorly sensitive to global Ca^{2+} elevations.

3.4 Discussion

In this chapter, we found that heterologous expression of mouse ANO1 in HEK293 cells produced CaCC with properties similar to those of recombinant ANO1 currents reported by other studies [151, 205-207], such as Ca^{2+} dependence and outward rectification. When holding HEK293 cells at -60 mV, dialysis of 1 μM of free Ca^{2+} via patch pipette activated inward current which was sensitive to the "classical" CaCC inhibitor, NFA. These results were expected.

After ANO1 was identified as a CaCC candidate in 2008, numerous groups found that ANO1 contributed to CaCC current in many native cells, including VSM cells, salivary acinar cells, DRG neurons and others [151, 202, 208, 210, 224, 229, 307-309].

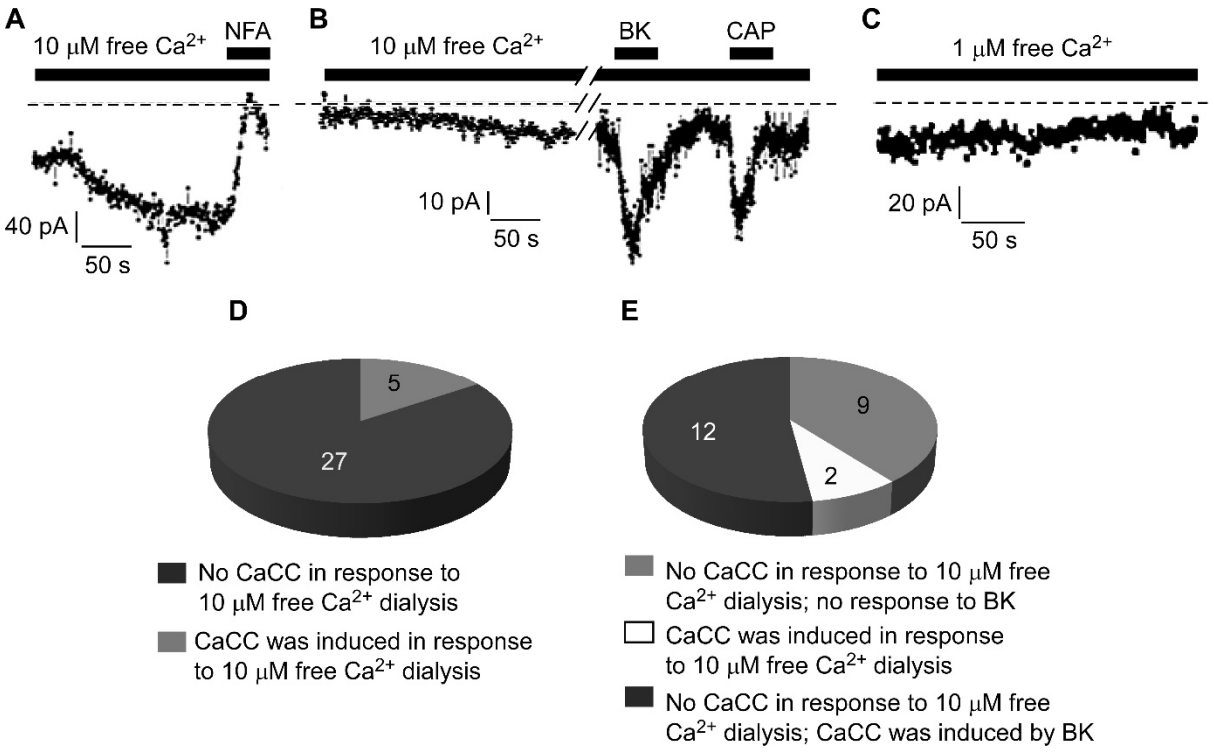

Figure 3.3 Ca^{2+} activates an NFA-sensitive inward current in small DRG neurons. (A) Example steady state current at –60 mV recorded from a neuron in which pipette dialysis of 10 μM free Ca^{2+}induced an NFA-sensitive inward current. Bath application of 100 μM NFA was performed during the period indicated by the bar. (B) Representative current traces showing a neuron in which inward current was not induced by 10 μM free Ca^{2+} but induced by BK (BK, 1 μM), and capsaicin (CAP, 1 μM) in the same neuron. Traces were obtained by continuous recording at a holding potential of –60 mV. (C) Example of the whole-cell recording from a neuron in which at dialysis of 1 μM free Ca^{2+} did not induce an inward current. (D) Summary data for the (A) showing the proportion of the neurons responded to the dialysis of 10 μM free Ca^{2+} with an inward current. (E) Summary data for (B) showing that in a significant proportion of DRG neurons in which dialysis of 10 μM free Ca^{2+} was unable to produce an inward current BK did induce CaCC.

Most of the reported biophysical properties of recombinant ANO1 channels are largely in agreement with the properties of native CaCCs in many tissues (see also Chapter 1 and the introduction to this chapter). In my study, I used rat DRG tissue to study ANO1 regulation. Unfortunately thus far I have been unable to clone a full-length rat ANO1, although I have

successfully cloned three intracellular regions of the rat ANO1 channel (see Chapter 6). The amino acid sequences of rat ANO1 are 96% identical to the mouse ANO1 and, therefore, the mouse ANO1 clone has been used here. However, differences between mouse and rat clones are mostly localized to the intracellular N-termini of ANO1. It is therefore possible that this divergence affected ANO1 regulation. Therefore, in future, plasmids containing the full-length rat ANO1 will be needed to complement studies performed on rat DRGs.

This study made use of symmetrical Cl^- concentrations for intra-and extra-cellular solutions. For intracellular solutions, K^+ was replaced by Cs^+ (impermeable for K^+ channels), while in extra-cellular solutions Na^+ was replaced by TEA (impermeable for most ion channels). Thus the permeable ions in our system were Cl^- and Ca^{2+} although only for Cl^- was the equilibrium potential near 0 mV. Reversal potentials of the Ca^{2+}-activated currents in ANO1-transfected HEK293 cells were all near 0 mV (Fig. 3.2F), confirming that these were indeed Cl^- currents.

As expected, Cl^- current in ANO1-transfected HEK293 cells was blocked by the CaCC blocker NFA. We found that inward currents could be reactivated by washing out NFA in the presence of 1 μM intracellular Ca^{2+}. A similar effect has also been reported by others [173, 310]. It is possible that NFA binds to the intracellular pore region of ANO1, and so that the anion flux is reduced, while anions still go through from the pore after removing NFA [310]. Here we used only a 100 μM concentration of NFA, because our group has determined that 100 μM NFA can block CaCC in DRG neurons. Similar results have been observed in other tissues [7, 307, 311]. Ni and colleagues [310] obtained the dose-dependency of NFA inhibition of ANO1 in excised patches. In HEK293 cells transfected with ANO1, the IC_{50} of NFA was in the range of 18–20 μM upon 20 μM Ca^{2+} at +40 mV [247]. Interestingly, in vascular myocytes, NFA had paradoxical effects on CaCC: at 100 μM, NFA partly inhibits CaCC at positive potential, but increased inward current upon repolarization to negative potentials [173, 174].

This biphasic effect of NFA on recombinant ANO1 has also been reported [195]. It will be important to clarify the mechanism of NFA action on ANO1 and native CaCCs in the future.

Kunzelmann's group has found that HEK293 cells have some endogenous ANO1 [312], but we did not find any currents upon dialysis of high concentration of Ca^{2+} into the untransfected HEK293 cells using the ramp protocol from -60 to +80 mV. This suggests that the levels of endogenous ANO1 expression and/or activity must be low. Similar results were obtained by others [195]. HEK293 is a widely used expression system for studying properties of recombinant ANO1 [233, 305].

In some ANO1-transfected HEK293 cells, Cl^- current evoked by pipette solutions containing 1 μM free Ca^{2+} exhibited a rapid rundown immediately after reaching maximal amplitude, and then remained constant at a lower steady-state amplitude level (Fig. 3.2C). Another group also reported similar results, finding that the CaCC current in *Xenopus* oocytes undergoes a prominent rundown at $[Ca^{2+}]_i$>1 μM [165]. There are several possible mechanisms that could account for ANO1 rundown, perhaps one involving a co-factor that is being diluted during the whole-cell experiment. For example, PIP_2-sensitive ion channels often run-down in whole-cell or excised patch experiments due to the loss of membrane PIP_2 [313]. Although ANO1 channels were reported to be inhibited by PIP_2 [314], diffusion of another co-factor could be involved here. Similarly, channel phosphorylation status can be affected during the dialysis of cytosol during the whole-cell recording which, in turn, could cause the rundown of channel activity.

Although previous reports showed the presence of CaCC in sensory neurons [315-317], our group and others observed that Ca^{2+} influx through VGCC is largely ineffective in activating CaCC in small DRG neurons [7, 257]. Strikingly, while in HEK293 cells overexpressing ANO1 dialysis of 1 μM Ca^{2+} or less (Fig. 3.2) induced channel activation. A rather different picture was observed in DRG neurons, in which dialysis of as high a

concentration of free Ca^{2+} as 10 μM was relatively ineffective in activating CaCC in cultured small-diameter DRG neurons; only a small minority (10-15%) of the neurons were observed to be activated by this procedure (Fig. 3.3).

It is possible that small DRG neurons do not express ANO1. However, our group and others have reported robust expression and functional activity of ANO1 in the sensory neurons and particularly in nociceptors [7, 202, 256]. Another possibility is that excessively high concentrations of intracellular Ca^{2+} can inhibit ANO1/CaCC. Such a phenomenon has indeed been reported [165, 221]. CaCCs have been reported to have several sub-conductance states: 3.5, 1.8 and 1.2 pS [221], indicating different open states. It has been hypothesized that Ca^{2+} binds site (s) that can be located within the channel pore. Therefore, the binding of Ca^{2+} ions may obstruct the flow of Cl^- ions through the channel. As more and more Ca^{2+} ions are bound, the unitary conductance is reduced, such that when three Ca^{2+} ions bind the pore, the conductance for Cl^- is lower than the conductance with a single Ca^{2+} ion [165, 221]. However, two observations contradict such Ca^{2+}-dependent inhibition of ANO1/CaCC in our DRG recordings: 1) whole-cell dialysis of 1 or 10 μM free Ca^{2+} was also largely ineffective in inducing CaCC current; 2) application of BK induced CaCC in the same neurons in which dialysis of 10 μM Ca^{2+} was unable to induce inward current. ANO1 was shown to underlie CaCC in small DRG neurons with the use of siRNA knock-down [7] and by knocking-out ANO1 gene in mice [256]. Our previous studies have shown that BK can activate ANO1 in small DRG neurons [7]. Therefore, the most likely explanation for the results reported here is that while ANO1 is expressed in most small-diameter DRG neurons and is functional, global Ca^{2+} is, for some reason, unable to activate ANO1. Such an interpretation is in agreement with the poor coupling between the VGCC and CaCC in small DRG neurons, but it also implies that Ca^{2+} signals produced in DRG neurons by BK represent a different type of Ca^{2+} signal which is preferentially coupled to ANO1/CaCC (and therefore in this sense is not “global”). The

mechanisms underlying this specificity will be investigated in the next chapters. Of note here is the fact that the percentage of neurons responding to BK with inward current under the high global Ca^{2+} conditions was ~50%, which is similar to the proportion of neurons in which BK induced CaCC under physiological Ca^{2+} concentration [7].

Chapter 4. Activation of ANO1 by GPCR

4.1 Introduction

4.1.1 GPCR families

The GPCRs comprise a large superfamily of membrane proteins that respond to different extracellular stimuli and are expressed in cells of virtually every tissue and organism, from yeast to mammal. All GPCRs have a common basic structure: seven membrane-spanning regions, an N-terminus facing the extracellular space, a C-terminus lying in the cytoplasm, three cytoplasmic loops and three extracellular loops [318]. GPCRs are involved in a wide variety of physiological processes such as regulation of behavior and mood, the sense of smell, control of cell division/proliferation, regulation of neuronal firing, modulation of ion channels, modulation of homeostasis and modification of cell morphology. Ligands of GPCRs bind to a pocket formed by membrane-spanning regions, thereby inducing conformational changes that activate the receptor. Associated with the receptor is a trimeric G protein complex which includes three subunits: α, β and γ. At rest the complex is inactive and is reversibly bound to GDP. The G-protein complex is allosterically activated by the binding of a ligand to the receptor, which entails the exchange of GDP for GTP at the G-protein's α-subunit. The GDP-GTP exchange causes the subunits of the G-protein complex to dissociate into a Gα-GTP monomer and a Gβγ dimer, which are now free to trigger their corresponding intracellular signaling cascades [319, 320]. There are thousands of genes encoding GPCRs in the mammalian genome. Based on structural and functional similarities, GPCRs are split into 6 classes (A-F or 1-6).

The Gα subunits trigger two main signal transduction pathways: the cAMP signalling pathway and the IP_3/diacylglycerol (DAG) signalling pathway [321, 322] (Fig. 4.1). In addition, some signalling events are mediated by Gβγ; for example, Gβγ activates phosphoinositide-3-kinase (PI3K) isoforms which modulate the activity of VGCC and K^+ channels [323].

GPCRs regulate the activity of many ion channels and signalling molecules in sensory neurons including TRPV1 and TRPA1, ATP-gated P2X channels, acid-sensing ion channels, Tetrodotoxin-resistant Na^+ channels, voltage-dependent Ca^{2+} channels, and M-type K^+ channels [324-329]. These mechanisms are responsible for modulation of neuronal excitability, and therefore are closely associated with the modulation of pain transmission.

4.1.2 The BK receptor and inflammation pain

BK is a short, pro-inflammatory peptide which consists of nine amino acids (H-Arg-Pro-Pro-Gly-Phe-Ser-Pro-Phe-Arg-OH) [330]. Carboxypeptidase removes carboxy-terminal Arg from BK to generate another active metabolite, desArg9-BK (dBK) [331]; the actions of BK are mediated through the activation of B_2R, while dBK is the agonist of the bradykinin receptor B_1 (B_1R) [331]. An important difference between the two receptor types is the fact that B_2Rs are expressed constitutively, while B_1Rs are normally absent from tissues unless induced by phenomena associated with inflamed and/or damaged tissues [332-334].

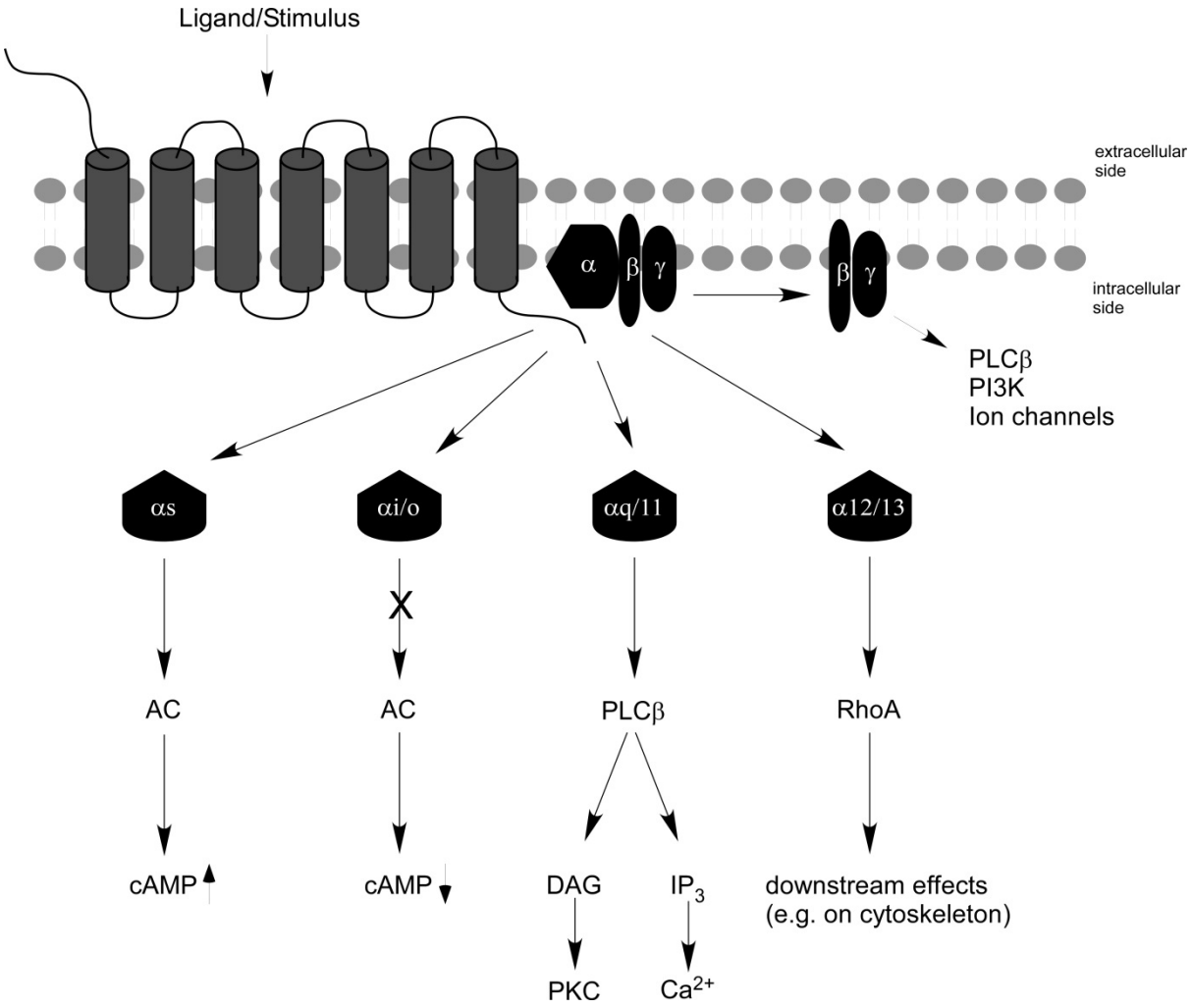

Figure 4.1 Schematic summary of heterotrimeric G protein signaling. GPCR forms reversible associations with a trimeric G protein complex comprising of α, β, and γ subunits. The activation of GPCR induces a conformational change in the receptor that triggers an exchange of GDP for GTP at the α-subunit, and a dissociation of βγ subunits. Gα and Gβγ trigger specific intracellular signaling pathways. G_{α} subunits include $G_{\alpha s}$, $G_{\alpha i/o}$, $G_{\alpha q/11}$ and $G_{\alpha 12/13}$. $G_{\alpha s}$ enhances the activity of adenylyl cyclase (AC) and produces cAMP, which affects the activity of ion channels and PKA isoforms.$G_{\alpha i/o}$ inhibits AC activity and decreases cAMP levels. $G_{\alpha q/11}$ activates PLCβ, which cleaves PIP_2 into the IP_3 and DAG. IP_3 induces release of Ca^{2+} from the ER, while $G_{\alpha 12/13}$ activates the small GTPase, Rho, which participates in multiple intracellular cascades including cytoskeletal rearrangements. $G_{\beta\gamma}$ modulates the activity of such ion channels as G-protein-regulated inwardly rectifying K^+ channels, VGCC, as well as PLCβ and PI3K.

The B_1Rs and B_2Rs are coupled to G_q or G_{11} types of Gα, and act primarily by stimulation of PLCβ and phospholipase A2 (PLA2) pathways [335-337] (Fig. 4.1). Activation of PLCβ leads to hydrolysis of PIP_2 into IP_3 and DAG. IP_3 increases in intracellular Ca^{2+} and DAG activates PKC [338]. B_1R also leads to activation of PLA and release of prostaglandins [339, 340]. Activation of B_1Rs has been shown to have an effect on renal function and vasodilatation of blood vessels [341]. B_2Rs have many effects in a number of tissues. Stimulation of B_2R contributes to such immune responses as local tissue inflammation in rheumatoid arthritis, local tissue inflammation, and vasodilatation of blood vessels.

In nociceptive somatosensory pathways, most effects of BK, including acute inflammatory reactions, oedema, pain and hyperalgesia, are mediated by the B_2Rs that are constitutively expressed in the peripheral terminals of sensory nerve fibers [342-345]. Tissue damage causes local BK production by the kinin-kallikrein system, and the activation of B_2Rs within peripheral terminals of nociceptive fibers leads to their excitation and the release of SP and CGRP. SP and CGRP further amplify local immune responses [346]. Moreover, BK can enhance release of prostaglandins, cytokines and nitric oxide from sensory neurons, endothelial and immune cells or fibroblasts [3, 342, 347]. The increase of BK-induced release of neuropeptides is augmented by prostaglandins, a positive feedback that modulates the activity of ion channels and the excitability of sensory neurons [3, 342, 347]. By acting on B_2Rs, BK sensitizes and depolarizes the peripheral terminals of sensory nerve fibers, thereby promoting hyperalgesia [342]. B_2Rs play roles in acute inflammation pain, while B_1Rs play roles in the chronic phase of inflammatory pain processes, because B_1R expression is upregulated after long-term exposure to inflammatory mediators. Recent studies suggest that B_1R expression in sensory fibrosisis induced by pro-inflammatory cytokine networks such as IL-1β [348-350]. B_1R and B_2R knockout mice show hypoalgesia against painful stimuli [351,

352], which is strong evidence that BK receptors are potent regulators of local inflammation which also contribute to inflammatory pain.

4.1.3 Protease activated receptors (PARs) and inflammation pain

Protease activated receptors (PARs) are a subfamily of related GPCRs that are activated by cleavage of their N-terminal domains by serine proteases [353]. Hydrolysis reveals a tethered peptide ligand, which binds to the ligand binding domain in a second extracellular loop [354] and activates downstream signaling (Fig. 4.2). Most of the PAR family act through the actions of $G_{\alpha i}$ (cAMP system), $G_{\alpha 12/13}$ (Rho and Ras activation), and $G_{\alpha q}$ (Ca^{2+} signalling) to cause cellular actions [353]. These receptors are highly expressed in platelets, but also in endothelial cells, myocytes, and neurons [353]. Four PAR family members have been identified to date: PAR1, PAR2, PAR3 and PAR4. PAR1, PAR3 and PAR4 are thrombin receptors; PAR2 is not activated by thrombin, but can be activated by trypsin or trypsin-like protease. PAR4 needs 10 to 100-fold higher concentrations of thrombin as compared to PAR1 and PAR3 [355-357]. Synthetic peptides corresponding to the "tethered ligand domains of PARs are often used as pharmacological activators of these receptors in experiments. Thus, the peptide SLIGKV-NH2 (Ser-Leu-Ile-Gly-Lys-Val-NH2) selectively activates PAR2; the peptide TFLLR-NH2 selectively activates PAR1; and peptide AYPGKV-NH2 is specific for PAR4 [358, 359]. In my thesis, I used the peptide SLIGKV-NH2 to activate the PAR2 receptors, and I will refer to it as the "PAR2 peptide ligand" or "PAR2-PL". Like BK receptors, the signal transduction pathway of PAR2 is mediated by the activation of phospholipase C through Gαq/11 protein (Fig 4. 3).

Like B_2Rs, PAR2 is also found in sensory neurons, especially in C-fibers [360]. Mounting evidence suggests that direct activation of PAR2 in sensory neurons contributes to inflammatory nociceptive pathways [6]. Intraplantar injection of PAR2-PLs induced the release of neuropeptides such as SP and CGRP [361]. Intraplantar injection of sub-inflammatory doses

of PAR2-PL induced hyperalgesia in response to a thermal or mechanical stimulation [362]. Other studies have shown that PAR2 agonists enhanced capsaicin-evoked release of CGRP in isolated DRG neurons [363]. Interestingly, PAR2 is functionally coupled to TRPV1 channels in nociceptive neurons. Thus, PAR2 was shown to potentiate responses of TRPV1 to capsaicin [364]. In addition, activation of PAR2 decreased the temperature threshold for TRPV1 activation in HEK293 cells expressing both PAR2 and TRPV1. In accordance with these observation, activation of PAR2 leads to amplification and persistence of pain responses, producing thermal hyperalgesia [364, 365]. The TRPV1 antagonist capsazepine was able to inhibit PAR2-induced thermal hyperalgesia [364, 365].

In summary, both B_2R and PAR2 are coupled to the $G_{\alpha q11}$-type of G proteins, which causes robust release of IP_3 and Ca^{2+}. Both receptor types have been found to express in small DRG neurons. Peripheral injections of PAR2-PL or BK produce pain and hyperalgesia. During inflammation, CaCCs are recorded in small DRG neurons and genetic knock-out or knock-down experiments demonstrated that CaCC activity in small DRG neurons depends on ANO1 expression [7, 256]. It has also been shown that BK activates ANO1 in DRG neurons which, in turn, leads to depolarization and an increase in AP firing frequency [7]. Finally, inhibition of ANO1 channels in peripheral nociceptive terminals in vivo reduces BK-induced pain [7, 366].

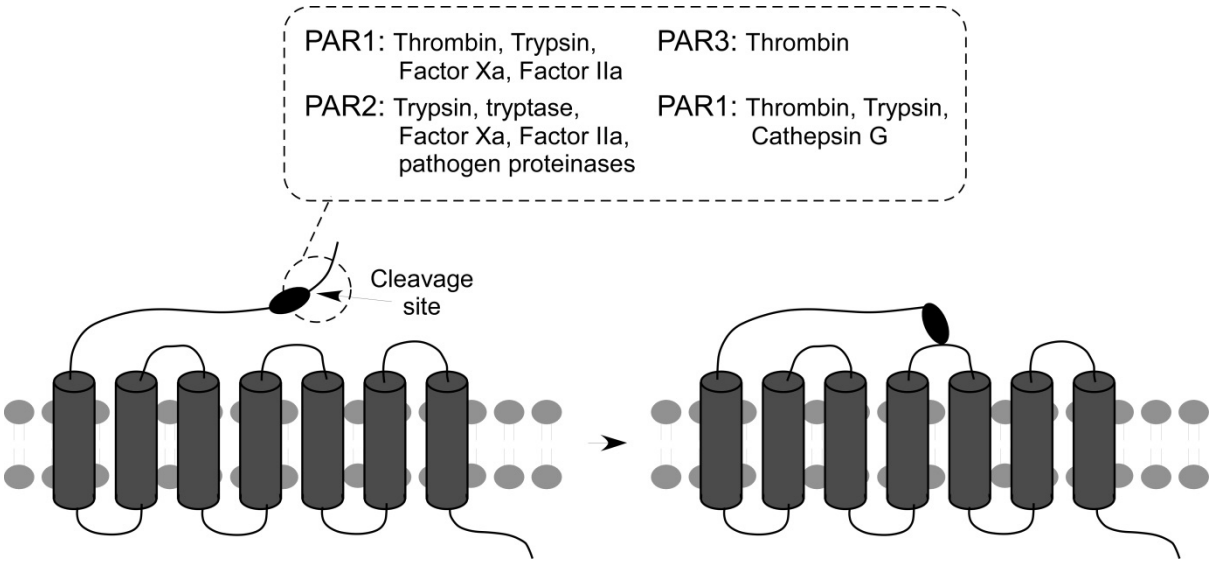

Figure 4.2 Mechanism of activation of PARs by proteinase [367]. PARs are a subfamily of GPCRs activated via proteolytic cleavage of their N-terminal domain by serine proteinases. Cleavage reveals a "hidden" N-terminal sequence that binds to and activates the receptor. Proteases specific to each PAR subtype are listed in the box above.

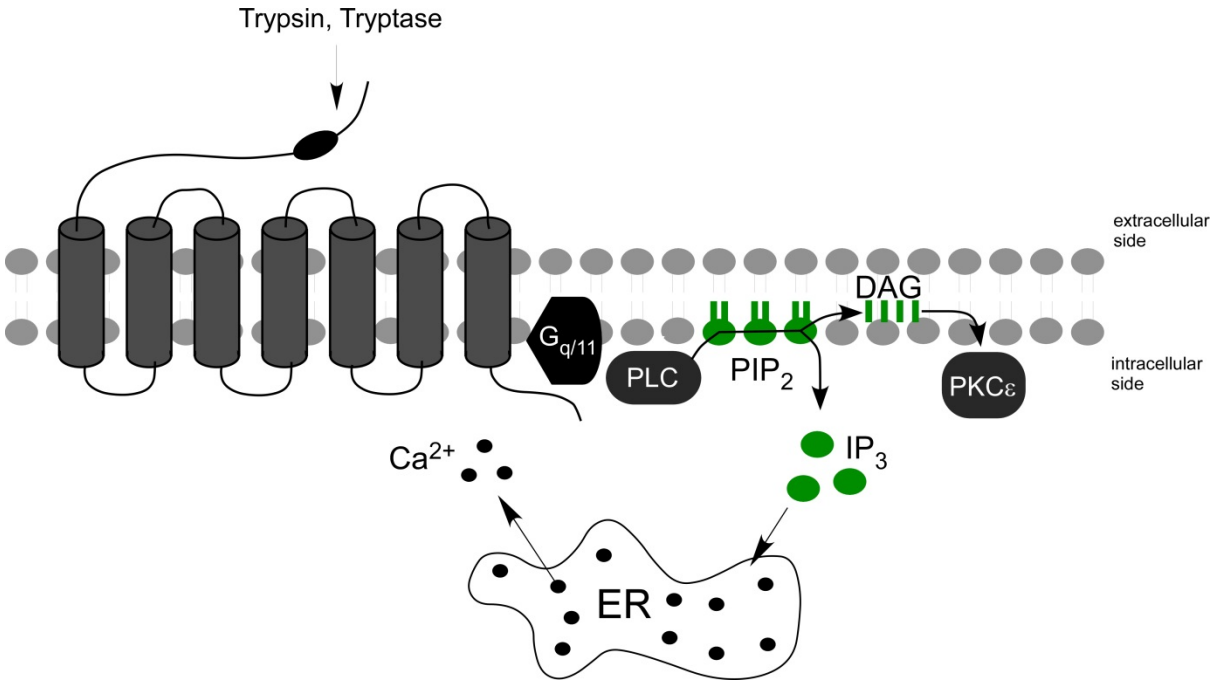

Figure 4.3 PAR2 and its downstream signaling pathways (PLC, PKA, and PKCε) [368]. Activation occurs through proteolytic cleavage by trypsin or tryptase, which leads to the dissociation of $G\alpha_{q/11}$ from βγ subunits, and activation of PLCβ. PLCβ then cleaves PIP_2 into IP_3 and DAG. IP_3 binds to the IP_3Rs in the ER and triggers Ca^{2+} release, while DAG activates the PKCε.

4.2 Aims

In our previous studies, we found that BK induced CaCC in small DRG neurons via B_2R. B_2R is coupled to the same signaling pathways as PAR2 (Fig. 4.3), and PAR2 is also abundantly expressed in DRG neurons. Before this work, it was not known that PAR2 could activate CaCC in these neurons.

The experiments in this chapter have two purposes: 1) to test whether PAR2, like B_2R, can activate CaCC in small-diameter DRG neurons; and 2) to further investigate preferential coupling of ANO1/CaCC in DRG neurons to Ca^{2+} release from the ER.

4.3 Results

4.3.1 BK-and Ca^{2+}-activated Cl^- current in HEK293 and small DRG neurons

In our previous study we found that BK induced an inward current in small DRG neurons, and that this current was a Cl^- current associated with CaCC/ANO1 [7]. In order to test if exogenously expressed ANO1 channels can also be activated by BK, we expressed ANO1 and B_2R in HEK293 cells along with GFP for visual identification of transfected cells, and tested the current response to BK stimulation in whole-cell patch clamp recordings. The pipette solution contained 100 nM free Ca^{2+}. Under these conditions, application of 1 μM BK to cells expressing B_2R only evoked negligible inward currents (Fig. 4.4A, n=5). By contrast, application of 1 μM BK to ANO1/B_2R-expressing cells evoked robust inward currents (218 ± 70 pA, n=3) when the membrane potential was held at -60 mV. This inward current was completely inhibited by 100 μM NFA (Fig. 4.4B). Next we tested the response of small DRG neurons to BK stimulation in whole-cell patch clamp recordings. As shown in Fig. 4.4C and D, application of 1 μM BK to small DRG neurons evoked inward currents when the membrane potential was held at -60 mV (131 ± 17 pA, n=11). We then compared the BK-activated Cl^- current in B_2R-expressing HEK293 cells and in DRG neurons using the voltage ramp protocol (1s voltage ramp form −60 to +80 mV). As shown in Fig. 4.5A, BK-activated Cl^- currents in B_2R-expressing HEK293 cells which were not overexpressing ANO1 was very small (negligible currents, n=8). By contrast, BK activated prominent Cl^- currents in ANO1/B_2R-expressing cells (Fig. 4.5B and C). These currents displayed hallmarks of CaCC currents, such as outward rectification and reverse potential at ~0 mV. The mean rectification index (I_{60}/I_{-60}) was 1.52 ± 0.47 (n=3). Very similar BK-activated Cl^- currents were also recorded in small DRG neurons (Fig. 4.5D and E). These currents also displayed hallmarks of CaCCs such as outward rectification, the reversal of potential at 0 mV, and a mean rectification index (I_{60}/I_{-60}) of 5.21

± 0.08 (n=3). In these experiments we used TEA to replace Na^+, Cs^+ to replace K^+, and Cd^{2+} to block Ca^{2+} current. Thereby the membranes were only permeable to Cl^-.

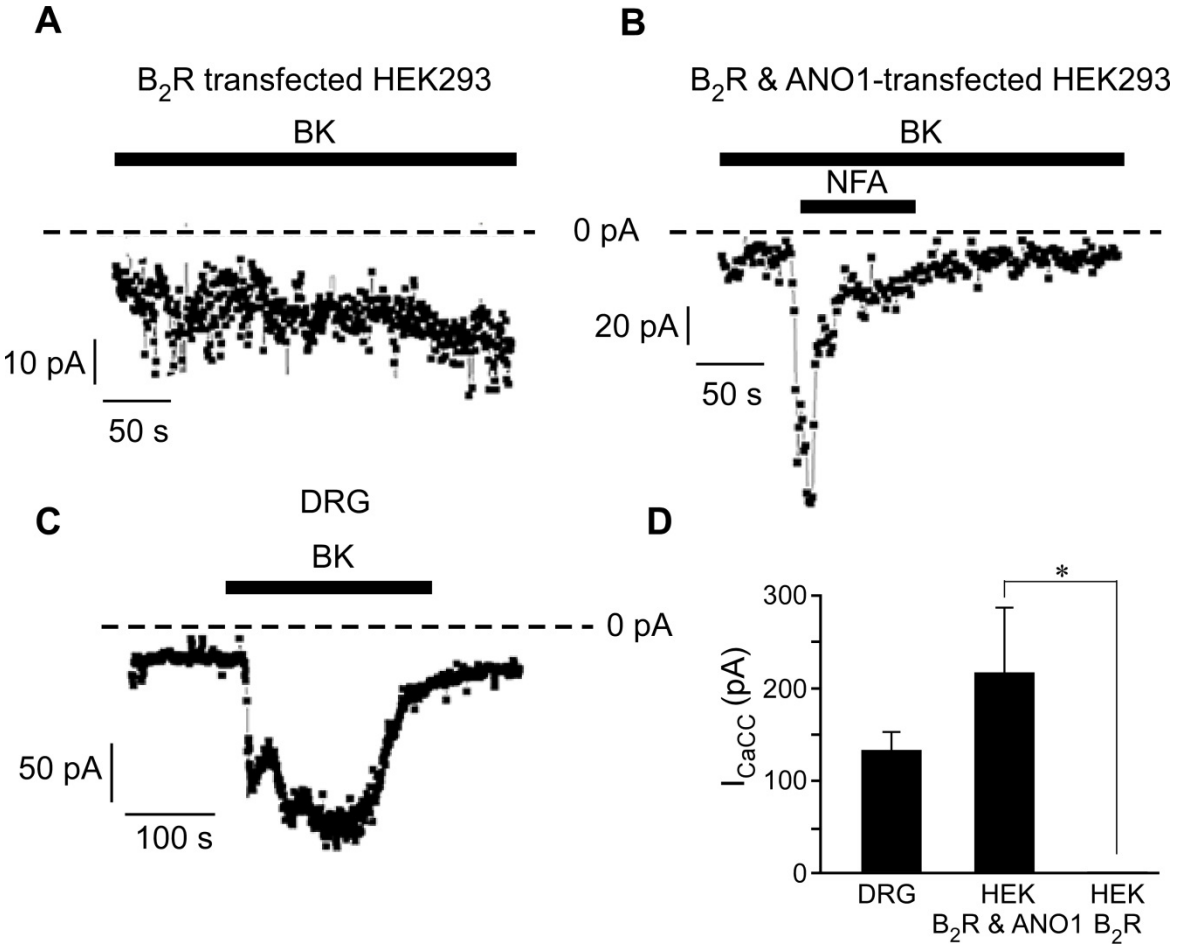

Figure 4.4 BK activates Ca^{2+}-activated Cl^- current. (A) HEK293 cells transfected with B_2R only. In the presence of 100 nM free Ca^{2+} in the recording electrode, 1 μM BK indicated negligible inward currents. (B) HEK293 cells transfected with ANO1 and B_2R. In the presence of 100 nM free Ca^{2+} in the recording electrode, 1 μM BK induced prominent inward current which was inhibited by 100 μM NFA. (C) Representative current trace recorded from small DRG neuron showing inward current induced by BK (1 μM). Traces were obtained by continuous recording at a holding potential of –60 mV. (D) Summary of the amplitudes of BK-induced CaCC current for (A), (B), and (C). Data are presented as mean ± SEM. * P<0.05 vs. HEK293 cells transfected with B_2R only.

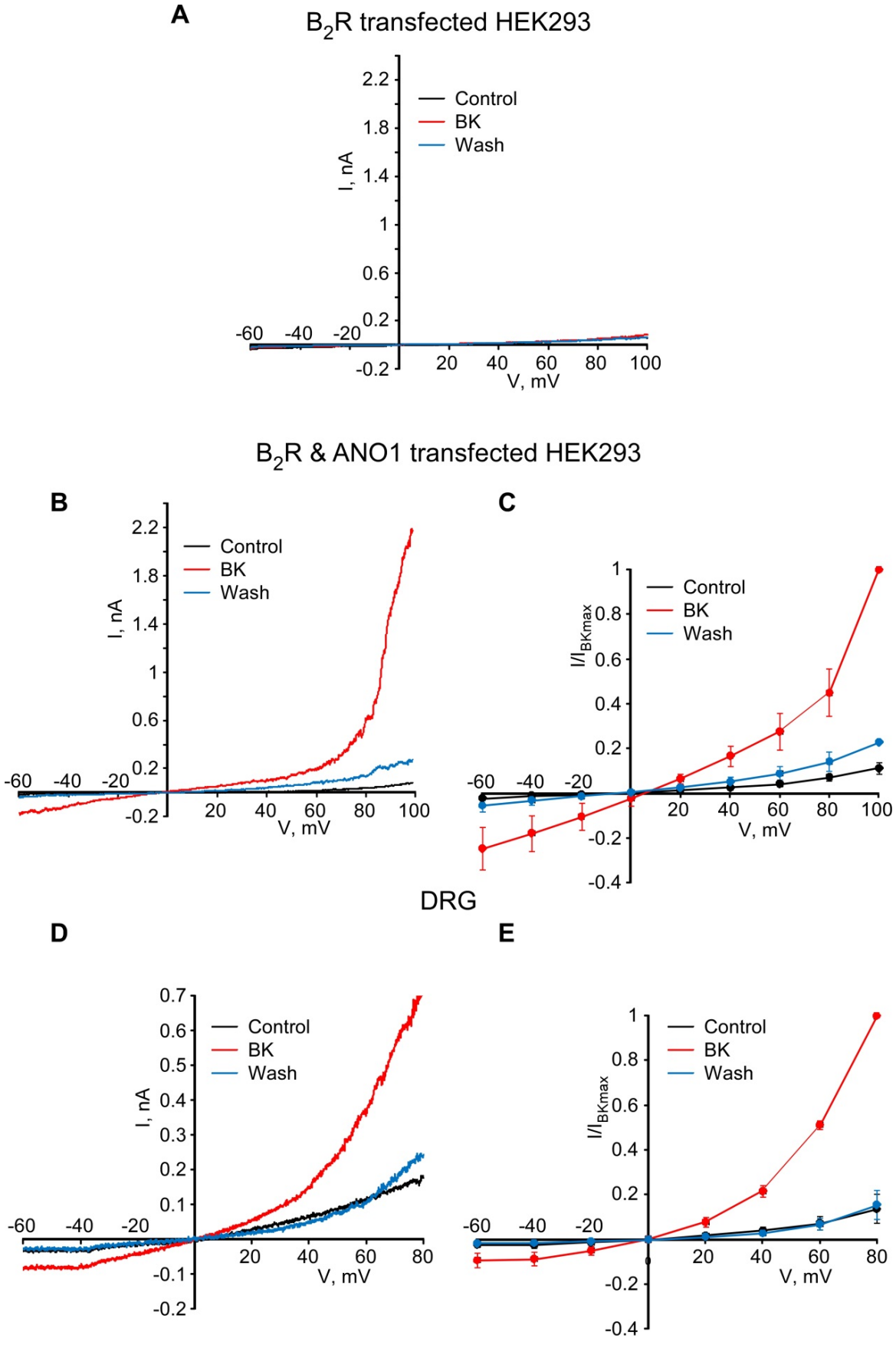
A
B2R transfected HEK293
Control
BK
Wash
I, nA
V, mV
B2R & ANO1 transfected HEK293
B
C
I/IBKmax
DRG
D
E

Figure 4.5 Ca^{2+}-activated Cl^- currents evoked by voltage ramp protocol. (A) HEK293 cells transfected with B_2R only. In the presence of 100 nM free Ca^{2+} in the recording electrode, voltage ramps –60 to +100 mV induced negligible currents with or without 1 μM BK. (B) HEK293 cells transfected with ANO1 and B_2R. In the presence of 100 nM free Ca^{2+} in the recording electrode, 1 μM BK induced robust outwardly-rectifying currents. (C) Summary of the I-V relationship of BK-induced CaCC current for (B) (n=8); data are given as mean ± SEM. (D) Representative current traces recorded from small, capsaicin-sensitive DRG neuron showing currents induced by BK (1 μM). Traces were obtained by ramp step protocols from –60 to +80 mV. (E) Summary of the I-V relationship of BK-induced CaCC current for (D) (n=7). Data are given as mean ± SEM. (Data shown in panels A-C was contributed by Yani Liu). From [Jin, X., et al., Sci Signal, 2013. 6(290): p. ra73.] Reprinted with permission from AAAS.

4.3.2 PAR2-PL activated Ca^{2+}-activated Cl^- current in HEK293 and small DRG neurons

Since PAR2 signaling is very similar to that of B_2R in DRG [6], we investigated whether PAR2 can also induce CaCC activation. First, we expressed ANO1 and PAR2 in HEK293 cells along with GFP for visual identification of transfected cells and tested the responses to PAR2 agonist (PAR2-PL) application in a whole-cell patch clamp recording. The pipette solution contained 100 nM free Ca^{2+}. Under these conditions, application of 10 μM PAR2-PL to PAR2 expressing cells evoked negligible inward currents at a holding potential of –60 mV (Fig. 4.6A, n=5). In contrast, application of 10 μM PAR2-PL to ANO1/PAR2-expressing cells evoked robust inward currents when the membrane potential was 181 ± 45pA (Fig. 4.6B, n=3). This inward current was strongly inhibited by 100 μM NFA (Fig. 4.6B and D). NFA was applied after the inward current reached its maximal amplitude. Next, we tested PAR2-PL can activate CaCC in small DRG neurons.

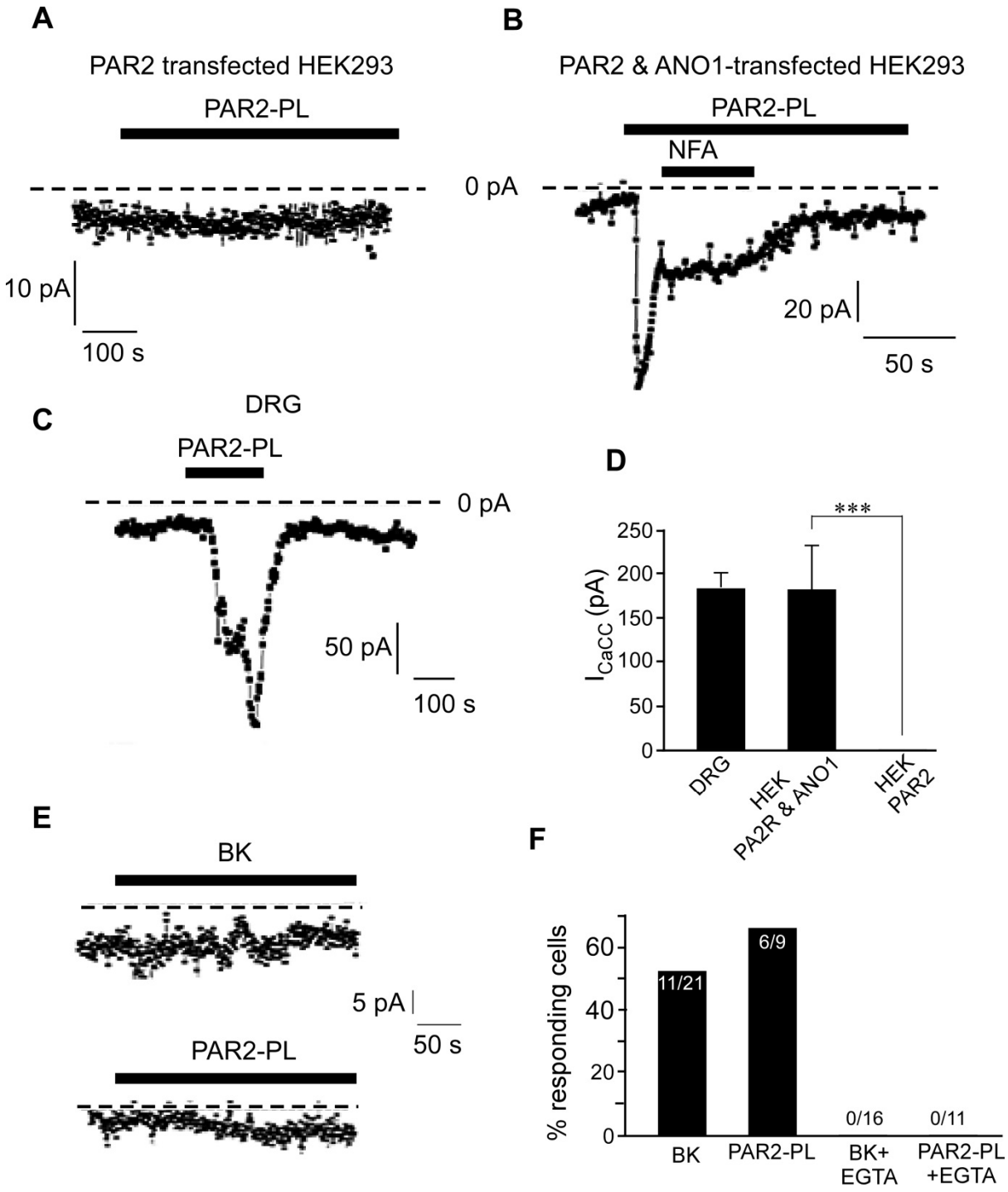

Figure 4.6 PAR2-PL activates Ca^{2+}-activated Cl^- current. (A) HEK293 cells transfected with PAR2 only. In the presence of 100 nM free Ca^{2+} in the recording electrode, 10 μM PAR2-PL induced negligible inward currents. (B) HEK293 cells transfected with ANO1 and PAR2. In the presence of 100 nM free Ca^{2+} in the recording electrode, 10 μM PAR2-PL induced prominent inward current which was inhibited by 100 μM NFA. (C) Representative current trace recorded from small DRG neuron showing inward current induced by PAR2-PL (10 μM). HEK293 cells transfected with PAR2 only. (E) Representative current trace recorded from small DRG neurones dialyzed for 10 min with 10 mM EGTA. Neither BK

nor PAR2-PL was able to induce an inward current under such conditions. (F) The number of neurons responsive to either PAR2-PL or BK in control conditions and after 10 min EGTA dialysis.

As shown in Fig 4.6C and D, application of 10 μM PAR2-PL to such neurons evoked robust inward currents of 185 ± 15 pA (n = 6; holding potential of -60 mV). In order to confirm that the Cl^- currents induced by BK or PAR2-PL are dependent on Ca^{2+}, we depleted intracellular Ca^{2+} stores with high concentration of EGTA. Dialysis with high levels of EGTA or BAPTA for a sufficiently long time depletes the intracellular stores of Ca^{2+} [369, 370]. Indeed, dialysis of the cytosol with 10 mM EGTA for 10 min completely abolished the inward currents induced by both BK and PAR2-PL (Fig. 4.6E and F).

4.4 Discussion

In this chapter we found that BK and PAR agonists activated ANO1 in HEK293 cells transfected with ANO1 along with B_2R or PAR2. We also found that both agonists activated ANO1-like inward currents in small DRG neurons. These currents were sensitive to the Cl^- blocker NFA and also to chelation of cytosolic and ER Ca^{2+}.

In our previous study [7], we characterized the BK-induced inward current in small DRG neurons as true CaCC, and determined that ANO1 is the most likely molecular correlate of this CaCC current. The following evidence was obtained: i) BK-induced inward current was inhibited by Cl^- channel blockers NFA and NPPB; ii) the reversal of potential of BK-induced inward currents was ~-35 mV in gramicidin-perforated patches, which was similar to the reversal of potential of Cl^- currents induced by GABA under the same conditions; iii) substitution of intracellular Cl^- with acetate abolished the BK-induced inward current; iv) various techniques that blocked ER Ca^{2+} release also abolished or reduced the BK-induced

inward current. Finally, v) ANO1 siRNA strongly reduced the amplitude of the inward current in response to BK in DRG neurons.

Both PAR2 and B_2R belong to GPCR that is mainly couple to $G_{q/11}$ type of Gα. These receptors activate the PLCβ signalling cascade, which results in Ca^{2+} release from the ER. Accordingly, in our previous study, we found that BK-induced CaCC in DRG neurons by means of IP_3-mediated Ca^{2+} release from ER Ca^{2+} stores [7]. In the present study, we further characterised the BK-induced currents in DRG neurons and compared these to the currents activated by BK in HEK293 cells overexpressing ANO1 through B_2R. The I-V relationship showed that the BK-activated currents in DRG neurons have approximately the same voltage dependence as compared with BK-induced current in HEK293 cells overexpressing ANO1 and B_2R. Both currents displayed outward rectification and reversed at 0 mV under conditions in which Cl^- is the only ion with equal concentrations across the plasma membrane. Although we applied the same concentration of BK in both the DRG and HEK293 experiments, we observed stronger outward rectification in DRG neurons as compared to HEK293 transfected with B_2R and ANO1 (Fig. 4.5). As ANO1 rectification depends on intracellular Ca^{2+}, such that at higher intracellular Ca^{2+} levels the inward current increases and the rectification becomes less prominent [151, 152], it is reasonable to propose that overexpressed B_2R in HEK293 cells produce stronger Ca^{2+} transients as compared to the DRG neurons.

Recently a novel nociceptive pathway mediated by PAR2 has received much attention. Stimulation of PAR2 has been reported to decrease nociceptive thresholds and evoke prolonged mechanical and thermal hyperalgesia in an inflammatory pain model (hindpaw injection of formalin or capsaicin) [362]. As discussed in the introduction, PAR2 is self-activated by proteolytic cleavage of the extracellular amino terminus. The tethered peptide ligands are produced during the process of cleavage. This cleavage produces soluble synthetic peptides matching the sequences of their cognate tethered ligands which activate PAR2 [371], a

phenomenon that we have exploited in the present study. Indeed, we found that PAR2-PLs induced an inward current in small DRG neurons, and this current was inhibited by the Cl^- channel blocker NFA and by Ca^{2+} chelation. This current was very similar to that induced by BK; thus, we identified it as CaCC. Interestingly, CaCC currents in response to both BK and PAR2-PL were transient in nature. This transience matches well with the shape of Ca^{2+} transients triggered by these agonists in DRG neurons [6, 7]. The likely reasons for the transient nature of Ca^{2+} and CaCC responses are the limited capacity of the intracellular stores and receptor desensitization [372-375].

The observed overall 67% response rate of DRG neurons to PAR2-PLs fits well with the report that approximately 60% of these neurons express PAR2 [6, 361, 376]. Similarly, over 50% of DRG neurons displayed CaCC in response to BK, which is also consistent with previous data on the distribution of BK receptors in DRG [377]. In the following chapters, I will describe experiments that further probe coupling of CaCC to the B_2R and PAR2. Particular attention will be given to the functional interactions between ANO1/CaCC and the IP_3-sensitive Ca^{2+} stores, and to the role such interactions might play in CaCC activation.

Chapter 5. Identification of a source of Ca^{2+} for ANO1 activation in small diameter DRG neurons

5.1 Introduction

There are many ways in which intracellular Ca^{2+} concentration can be altered. Ca^{2+} can enter the cell through numerous Ca^{2+}-permeable channels such as voltage-gated Ca^{2+} channels, ligand-gated (e.g. P2X) cation channels, sensory channels (e.g. TRPV1) or store-operated channels. In addition, Ca^{2+} can be released from the ER stores via IP_3 or ryanodine receptors. Other intracellular sources of Ca^{2+} (e.g. mitochondria) can also contribute to Ca^{2+} transients. Potentially, all of these pathways may result in activation of ANO1/CaCC. Since activation of CaCC in nociceptors is excitatory [7], a mechanism is required to ensure selective coupling of CaCCs to Ca^{2+} signals of particular physiological relevance. Nociceptors are normally silent and fire APs only in response to potentially damaging mechanical, thermal or chemical stimuli. Since excitation of these neurons may result in pain, it is necessary for such a neuron to be able to specifically respond to Ca^{2+} signals originating only from the relevant sensory events. On the other hand, it is useful for a CaCC in nociceptive neuron to be able to "ignore" Ca^{2+} transients originating from electrical activity itself (i.e. via VGCC activation during AP firing). Therefore, in the following chapters I have investigated the source of Ca^{2+} for the physiological activation of ANO1 in small DRG neurons. The three major pathways for generating cytosolic Ca^{2+} signals are VGCC, ER release channels, and non-selective cation channels of the plasma membrane. These pathways are discussed in the next section.

5.1.1 Voltage-gated Ca^{2+} channels

Voltage-gated Ca^{2+} channels (VGCCs) are widely expressed in different cell types, including the central and peripheral neurons, skeletal muscle, and cardiac myocytes. VGCCs play key roles in many physiological processes, including cell proliferation, apoptosis, neurotransmitter release, cell migration, gene transcription, and muscle contraction [378]. In neurons, one of the most important roles of VGCCs is regulation of synaptic transmission. In brief, the APs arriving to the presynaptic terminals cause depolarization which opens the VGCC and trigger Ca^{2+} influx. This, in turn, leads to the activation of synaptic vesicle release machinery. For peripheral nociceptors, this would result in release of excitatory neurotransmitter glutamate and a peptide co-transmitter SP [379].

As discussed below, VGCCs can be classified into L, N, P/Q, R and T-type channels. In addition, VGCCs can be divided into, high-voltage activated (HVA) channels that require membrane depolarizations of ~ -40 mV, or low-voltage activated (LVA) channels, which can be activated by smaller depolarizations of around −60 mV or even more negative [380]. HVA channels include L-($Ca_V1.1$-4), P/Q-($Ca_V2.1$), N-($Ca_V2.2$) and R-($Ca_V2.3$) type channels, while LVA channels include T-type ($Ca_V3.1$-3) channels. VGCCs consist of an assembly of multiple subunits that form a functional channel. Subunits include a pore-forming α_1-subunit as well as auxiliary β-, $\alpha_2\delta$ and γ-subunits. The cytosolic β subunits can help the α_1 subunit trafficking to the plasma membrane, as well as adjusting the activation and inactivation properties of the channel [381].

The α_1 subunit of a VGCC consists of four domains (I-IV), each containing six transmembrane segments (S1–S6), cytoplasmic N- terminal, C-terminal, and a number of intracellular loops. The pore is formed by the loop between S5 and S6 of each of four domains. These loops contain conserved glutamic acid residues that make the pore permeable and

selective for Ca^{2+} [382]. The S6 segment causes channel inactivation [383], while the S4 segments voltage sensors [384]. N- and C- terminals are largely responsible for channel modulation and regulation.

L-type channels have been found in VSM, skeletal muscle, cardiac tissue, the CNS, and peripheral sensory neurons. Neuronal L-type channels are predominately found at postsynaptic membranes and in the somata [385]. These channels were reported to localize to microdomains along dendritic spines which enables them to modulate some Ca^{2+}-dependent processes quickly and accurately [386]. In some cases, L-type channels can regulate gene expression [387]. P/Q-type channels (CaV2.1) are found in DRG [388] and TG; studies show the P/Q-type channel blocker ω-agatoxin IVA does not have much effect on the APs along Aδ-fibers. Instead it strongly inhibits nociceptive input to the spinal cord [389]. In the dorsal spinal cord, P/Q-type channels are strongly expressed in interneurons, and play a role in modulating synaptic transmission in the spinal dorsal horn [390].

N-type channels are ubiquitously expressed in neurons and in some other cell types, e.g.in neuroendocrine cells, where they regulate neurotransmitter release like P/Q-type channels [391].

T-type channels (Cav3.1-Cav3.3) are another VGCC subtype that is abundantly expressed in cell bodies, axons and peripheral terminals of nociceptive DRG neurons [392]. The Cav3.2 type is the dominant isoform [392]. In nociceptors, unlike P/Q and N-type channels, T-type channels play a larger role in excitability than in neurotransmission [393]. As T-type channels activate at voltages near or even below -60 mV, they also may display a significant window current at voltages near the neuronal resting membrane potential [393].

5.1.2 Inositol 1, 4, 5-triphosphate receptors (IP_3Rs), and Ryanodine receptors (RyRs)

The release of Ca^{2+} from the ER is mediated by two types of receptors/channels, IP_3Rs and RyRs. Most of the IP_3Rs are expressed in the ER, although the Golgi apparatus, nucleus and some secretory vesicles also express IP_3Rs. There are three different receptor isoforms of IP_3Rs: 1, 2 and 3. All isoforms have similar biophysical properties, such as IP_3-binding sites, Ca^{2+}-gating, and ion conduction [394]. IP_3R1 is the most widely expressed in all tissue types and at all developmental life stages. Functional IP_3Rs are large (~1200 kDa), tetrameric proteins, composed of four identical subunits [395]. Each subunit has membrane-spanning domains, an N-terminal domain and a C-terminal region, and an IP_3- binding site located at the N-terminal domain [396, 397]. The last pair of trans-membrane domains together with the intervening luminal loop from each of the four subunits forms the central pore [398]. The binding of IP_3 with the IP_3-binding core (IBC, residues 224–604) in the N-terminal domain initiates the conformational change that promotes channel opening [396].

IP_3 is generated from PIP_2 in response to agonist binding to plasma membrane receptors that activate PLC (see Fig. 4.3 in the previous chapter). IP_3 is a soluble molecule which diffuses through the cell to the ER and binds to the IP_3R. IP_3-triggered channel opening causes a rapid increase in cytosolic Ca^{2+} [399]. Although IP_3 is necessary to open native IP_3Rs, activation of these channels is also regulated by Ca^{2+} concentration. At concentrations up to ~500 nM, Ca^{2+} works synergistically with IP_3 to activate IP_3Rs, but higher cytosolic Ca^{2+} concentrations inhibit IP_3R opening [400]. The inhibition of IP_3R by Ca^{2+} is thought to be a crucial mechanism for ending channel activity and thus preventing cytosolic Ca^{2+} overload. Because Ca^{2+} signals can be encoded in both temporal and spatial domains, the oscillatory nature of IP_3-evoked Ca^{2+} release can carry important functional significance. In general, cytosolic Ca^{2+} diffusion from the IP_3R is rather limited. This limitation is mainly attributable

to the strong Ca^{2+} buffering capacity of the cytosol, which creates a steep concentration gradient originating from the ER release site. Ca^{2+} buffering in the cytosol is attributable to many cytosolic Ca^{2+}-binding proteins, like CaM and parvalbumins and many other proteins. These endogenous Ca^{2+} buffers bind free Ca^{2+} ions and decrease the amplitude of Ca^{2+} transients. At the mouth of IP_3R, the Ca^{2+} concentration can surpass 100 μM, whereas the concentration may be below 1 μM only a few micrometers away [401].

While DRG neurons mostly express IP_3R, RyRs are also expressed and contribute to Ca^{2+} signalling [402]. Both RyRs and IP_3R belong to the same receptor family. Like IP_3R, RyRs are also large tetrametric proteins with each monomer consisting of ~5000 amino acid residues [403, 404]. RyRs include three family members: RyR1, RyR2, and RyR3. RyRs are similar in structure to the IP_3R, particularly in the channel pore region. RyRs can release Ca^{2+} from the endo- and sarcoplasmic reticula (ER and SR respectively), and thus control many Ca^{2+}-dependent processes within the cell. The RyR1 is mostly expressed in skeletal muscles where it plays a major role in excitation-contraction coupling and muscle contraction [405]. The RyR2 is widely expressed in cardiac muscle and the brain. The RyR3 is found in striated, smooth, and cardiac muscle, as well as in the brain, particularly in regions involved in learning and memory like the cortex and hippocampus [406, 407]. Ca^{2+} controls RyR opening, and indeed, the binding of Ca^{2+} is a fundamental requirement for channel activation. When Ca^{2+} enters the cytosol, Ca^{2+} sensors within RyRs bind Ca^{2+} and facilitate opening, resulting in release of Ca^{2+} from the SR [408]. The RyR is also positively regulated by ATP and negatively regulated by Mg^{2+} [409]. As with the IP_3Rs, numerous signaling cascades can also regulate RyR function. These cascades include kinases such as PKA, PKC, cGMP-dependent protein kinase, and Ca^{2+}/CaMKII [409]. The activity of RyR is also modulated by presenilin, an ER-localized protease that cleaves a variety of type I membrane proteins [410, 411]. CaM also modulates

RyRs. At high Ca^{2+} levels, CaM inhibits both RyR1 and RyR2; at low Ca^{2+} levels, CaM activates RyR1 and inhibits RyR2 [412].

5.1.3 Non-selective cation channels

The mobilization of Ca^{2+} from internal stores or the influx of Ca^{2+} from the extracellular space, are the two major methods of raising Ca^{2+} concentrations such that downstream signal transduction pathways are activated. However, Ca^{2+} can also enter the cells not only through Ca^{2+}-selective channels, but also through a number of other channels generally referred to as "non-selective cation channels." Normally, these channels are permeable to cations like Na^{+}, K^{+}, and Ca^{2+} instead of anions. Generally, Ca^{2+} influx from VGCCs induces secretion or plasticity in neurons, but Ca^{2+} entry from non-selective cation channels causes inflammatory responses, morphological changes (e.g. a growth cone turning in spinal neurons), cell death and other effects [413-416].

TRP channels form a large superfamily of non-selective cation channels permeable to Ca^{2+}. They are encoded by 28 different genes, many of which produce multiple splice variants. TRP channels have six transmembrane segments, as do voltage-gated K^{+} channels. The domain between S5 and S6 is believed to form a pore. Like voltage-gated channels, TRPs form tetrameric complexes. The two main mechanisms of TRP channel activation are 1) store operation, via conformational coupling between TRP and the ER [417]; and 2) store-independent mechanisms, including activation by external ligands or plasma membrane receptors. Thus, many TRPs are activated by lipid-dependent signaling pathways following the activation of GPCRs or receptor-tyrosine kinases [418], such as by the activation of PLC and the production of second messengers like DAG.

TRP channels that are specifically activated by extracellular chemicals or physical stimuli exist in sensory neurons, hair cells, spindle organs, retinal rods, and taste cells. Sensory

TRP channels in nociceptive neurons, like the noxious heat sensor TRPV1 or the cold sensors TRPA1 and TRPM8, mediate heightened pain sensitivity and are often sensitized by pro-inflammatory agents [419-421]. TRPV1, TRPV3, TRPV4, TRPA1, and TRPM8 are distributed in nociceptors and respond to physical and chemical stimuli. TRPV1 is activated by temperatures above 43°C and capsaicin, as well as by such stimuli as protons or oxidised lipid metabolites [422]. TRPV2 is activated by very high temperatures (>52°C), and is sensitized by repetitive heating [423]. TRPV3 is activated by warm temperatures (threshold of ~33°C), TRPM8 is activated by cold with a threshold temperature of 25°C, and TRPA1 is activated by cold, with a mean threshold of 17°C [424-426]. TRPM8 is also the receptor for the compound menthol.

Ionotropic P2X purinoreceptors are another family of non-selective, Ca^{2+}-permeable cation channels. P2X2, P2X3 and P2X2/3 are expressed in primary sensory neurons that mediate nociception. These channels have also been implicated in peripheral pain transmission and inflammatory pain responses. P2X receptors are gated by ATP and have been found to form homo- and heterotrimers [427-429]. It is suggested that P2X3 and P2X2/3 are sensitive to changes in Phosphatidylinositol 3, 4, 5- trisphosphate and PIP_2 levels [430].

There are a number of additional Ca^{2+}-permeable channels like glutamate receptors, acid-sensing ion channels, or store-operated Ca^{2+} channels, all of which also modulate cytosolic Ca^{2+} levels. Detailed coverage of these pathways is, however, outside the scope of this thesis.

5.2 Aims

Although there are many pathways by which Ca^{2+} can enter and leave the cytosol, my work to date indicates three things regarding Ca^{2+} flux and its effects:

1. Heterologously expressed ANO1 channels can be activated by global cytosolic Ca^{2+} levels;
2. Native CaCCs in small-diameter DRG neurons is poorly sensitive to global cytosolic Ca^{2+}, but can be activated by ER Ca^{2+} release. The CaCC in small-diameter DRG neurons is probably mediated by ANO1 (see Chapter 4); and finally,
3. Gamper's previous work establishes the fact that activation of ANO1/CaCC channels in DRG neurons is excitatory, and can result in pain [7].

Therefore I hypothesize linking relevant Ca^{2+} signals directly to the excitation requires that ANO1/CaCC channels in small-diameter DRG neurons be directly coupled to specific Ca^{2+} sources. The aim of this chapter is to investigate coupling of ANO1/CaCC in small DRG neurons to two types of Ca^{2+} sources: IP_3Rs and VGCCs.

5.3 Results

5.3.1 VGCCs fail to activate CaCC in the majority of DRG neurons

To test whether Ca^{2+} influx through VGCC can activate the CaCC in DRG neurons, I used a patch-clamp recording protocol in which VGCC and CaCC could be measured simultaneously. A double-pulse voltage protocol was used to activate VGCC and induce Ca^{2+} influx (Fig. 5.1A). In this procedure, the first pulse was from a holding potential of -80 mV to 0 mV. The second pulse, from -80 mV to +80 mV, activated VGCC but did not produce Ca^{2+} influx because the driving force for Ca^{2+} was too small at this voltage (E_{Ca}~ +100 mV). The

CaCC current was calculated as a difference in peak tail current amplitudes between these two pulses:

$I_{CaCC} = I_{tail(0\ mV)} - I_{tail(+80\ mV)}$ [7, 257, 431].

We considered neurons displaying less than 40 pA as not displaying activation of CaCC by VGCC; since it is difficult to unambiguously identify inward tail current below 40 pA. We restricted our analysis to small-diameter, TRPV1-positive neurons, which were identified by exposure to 1 μM capsaicin at the end of the recording (Fig 5.1B). In 1 of 20 (5%) small DRG neurons an inward tail current (Fig. 5.1A; red line) was activated on repolarisation to -80 mV after the first pulse indicating activation of CaCC [257]. However, in 19 out of 20 (95%) cases, such tail currents in small DRG neurons were not observed (Fig. 5.1A; black line). Thus, we concluded that in most small DRG neurons Ca^{2+} influx through VGCC is not coupled to CaCC activation. This observation confirmed previous findings from our laboratory [7]. The lack of coupling between VGCC and CaCC was striking, particularly because BK and PAR2-PL induced CaCC in a large proportion of small-diameter DRG neurons (see chapter 4 and Fig. 4.6). In order to ensure that lack of coupling between VGCC and CaCC does not in fact reflect lack of functional CaCC, we performed measurements in which we applied a double-pulse protocol in order to measure VGCC-CaCC coupling. Then, in the same cells, we applied BK or PAR2-PL and measured CaCC responses at -60 mV (Fig. 5.1C-E). In neurons in which PAR2-PL and BK induced inward currents of 145 ± 47 pA (n = 4) and 259 ± 158 pA (n = 6), respectively, VGCC activation failed to induce any measurable CaCC. These experiments confirmed that lack of VGCC-CaCC coupling is not due to the lack of CaCC. We also took advantage of a recently developed specific ANO1 blocker, T16inh-A01 [218, 231], to further confirm the identity of BK-induced current. T16inh-A01 (50 μM) inhibited BK-induced current by 88 ± 6% (n = 6), (Fig 5.1F). Lower concentrations of T16inh-A01 were less

efficacious. The reasons for moderately less potent effect of T16inh-A01 (as compared with its almost complete inhibition of ANO1 in some studies [209, 218]), is currently unclear, however, poor block of heterologous ANO1 channels by T16inh-A01 has also been reported [195].

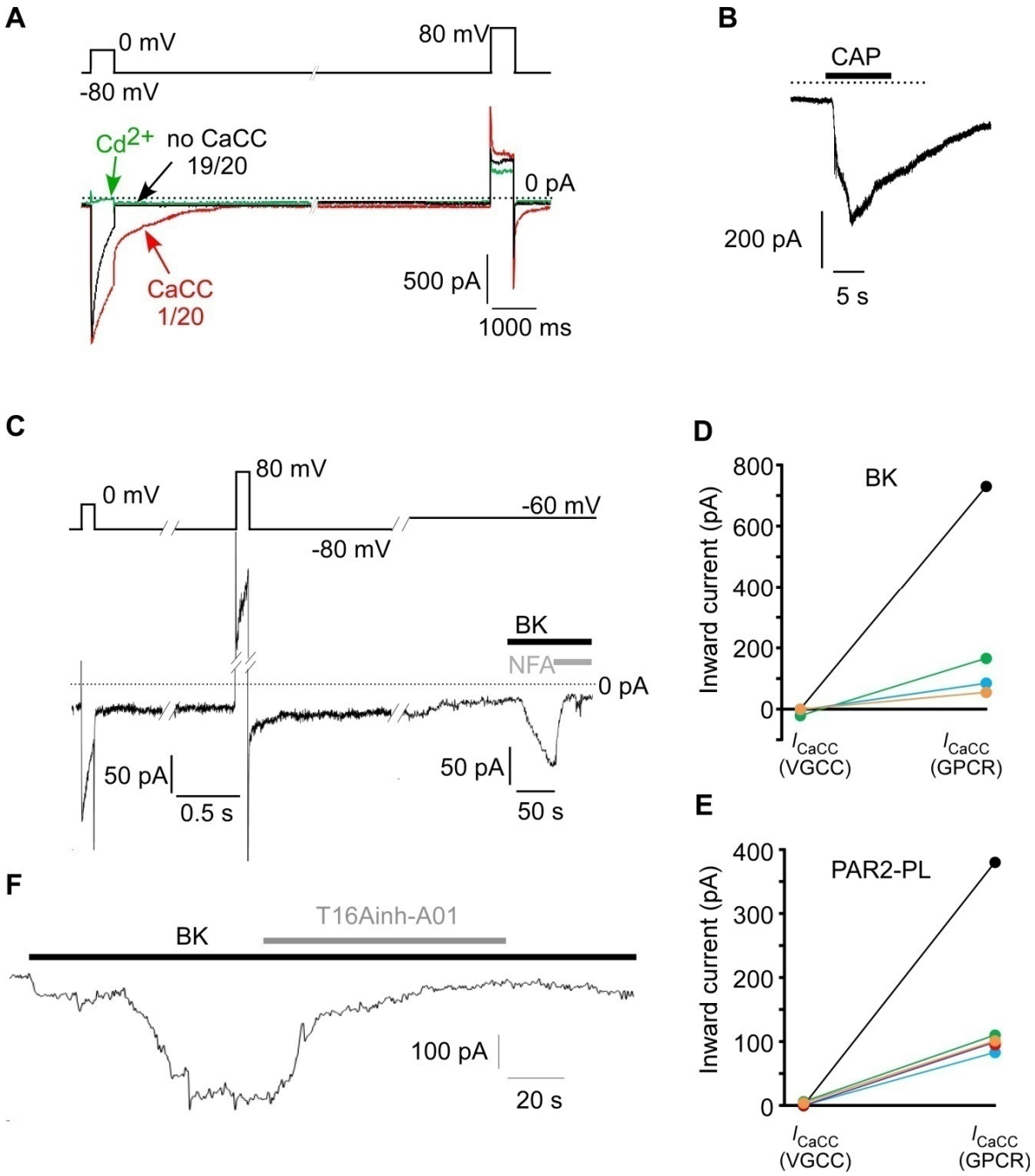

Figure 5.1 VGCC rarely activates ANO1 in small DRG neurons. (A) Majority of small DRG neurons (19/20) did not display inward tail current following the activation of VGCC by the voltage steps to 0 mV (black line); only one such neuron displayed a measurable inward tail current (red line). The Ca^{2+} current via VGCC was blocked by Cd^{2+} (100 μM, green line). (B) At the end of the recording neurons were tested for response to capsaicin (1 μM, CAP) to identify TRPV1-positive neurons. (C) Representative traces from the experiment in which coupling of CaCC to VGCC and GPCR was tested on the same cell. Double-pulse voltage protocol failed to induce measurable tail current following the VGCC activation while BK did induce CaCC. (D, E) Summary data from experiments similar to (C); amplitudes of VGCC-induced CaCC (I_{CaCC} (VGCC)) and the GPCR-induced CaCC (I_{CaCC} (GPCR) from the same neurons are connected by the lines of the colored lines. (D) Summarizes data for BK (n=4)

and (E) summarizes data for PAR2-PL (n=6). (F) Depicts example trace exemplify inhibition of the BK-induced CaCC by T16inh-A01. From [Jin, X., et al., Sci Signal, 2013. 6(290): p. ra73.] Reprinted with permission from AAAS.

It is well documented that the Ca^{2+}-dependence of ANO1 is voltage dependent, such that at depolarised voltages the channel is more sensitive to Ca^{2+} [205]. Thus, it is possible that Ca^{2+} influx through VGCC could activate ANO1 at positive potentials. In order to test this, a ramp voltage protocol was used in which ramps from a holding potential of -80 mV to +80 mV were applied at a rate of one per second. This rapid sampling rate caused an inactivation of VGCCs and, thus, the run-down of the VGCC current (seen as disappearance of the "hump" in the middle of the traces shown on Fig. 5.2A). As shown in Fig 5.2A, such voltage ramps induced a prominent outward current at positive voltages. This outward current was, however, completely unrelated to the amplitude of the inward "hump" produced by VGCC activation. Indeed, the first sweep (Fig 5.2A, red trace) and the 7^{th} sweep (Fig 5.2A; green trace) produced identical outward currents, yet the inward "hump" was prominent during the first sweep and almost completely absent during the 7^{th}. Thus, while the nature of this outward current remains unknown, it is certainly not a Ca^{2+}-dependent current and therefore is not a CaCC.

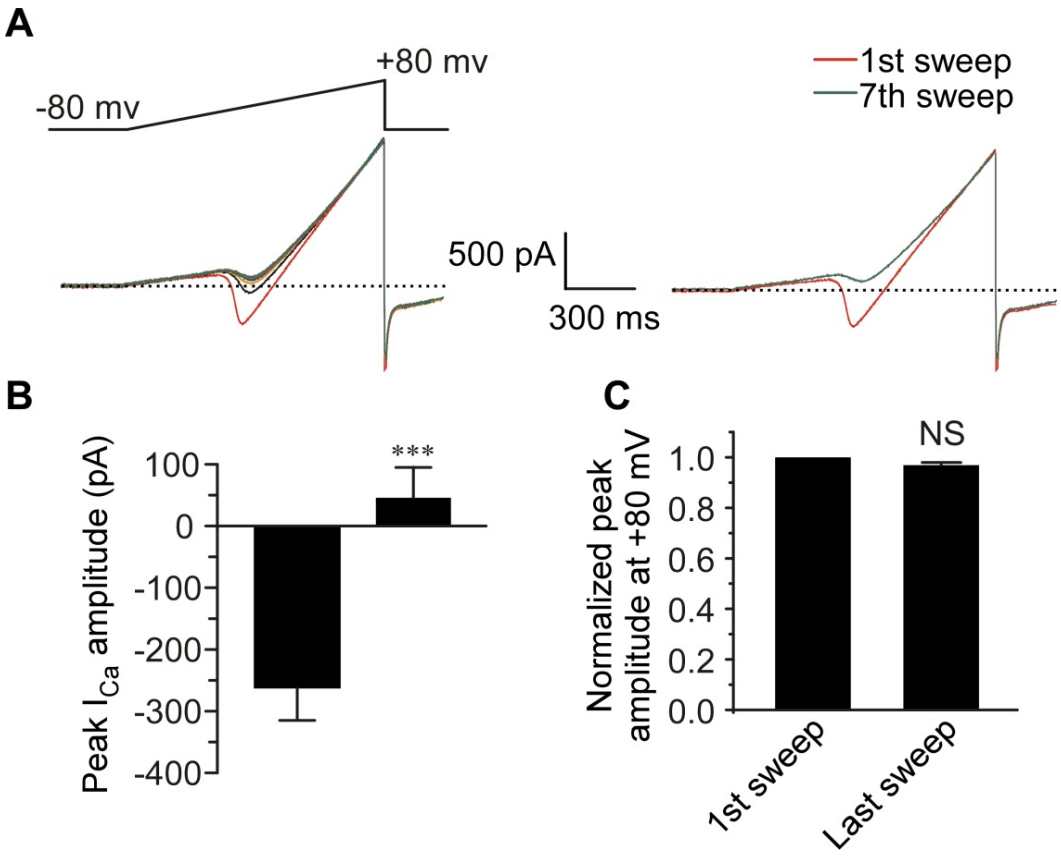

Figure 5.2 Outward currents which are not CaCC. (A) Small DRG neurons display outward currents at positive voltages as measured by the voltage ramp from -80 mV to 80 mV (panel above the traces on the left). The first trace is indicated by the red line; the 7th trace is indicated by the green line. (B) Summary data for the Ca^{2+} current amplitude (the "hump") between 1st and the last sweeps. (C) Summary data for the amplitudes of outward current at +80 mV between at 1st and the last sweeps. The experiments were contributed by Huiran Zhang. From [Jin, X., et al., Sci Signal, 2013. 6(290): p. ra73.] Reprinted with permission from AAAS.

5.3.2 Ca^{2+} release from IP_3R activates CaCC

Experiments discussed to this point established the following:

- Ca^{2+} influx via VGCC is mostly ineffective in activating CaCC in small-diameter DRG neurons;
- $G_{q/11}$-coupled GPCR reliably activates CaCC in such neurons.

Previous evidence from our laboratory indicated that stimulation of BK and PAR2-PL elicits an increase in cytosolic Ca^{2+} [6, 7] in DRG neurons. The most straightforward conclusion from current and past experiments is that $G_{q/11}$-PLC-induced Ca^{2+} release from the ER is the predominant source of Ca^{2+} for CaCC activation under our experimental conditions. Ca^{2+} influx from the store-operated Ca^{2+} channels could, however, potentially contribute to the GPCR-induced Ca^{2+} transients and therefore might also activate CaCC. In order to test this possibility, we applied BK to DRG neurons perfused with Ca^{2+} free bath solution. Under these conditions, application of 1 μM BK to small DRG neurons still induced robust inward currents when the membrane potential was held at -60 mV. This was not statistically different from that induced by BK in the control neurons perfused with a regular, Ca^{2+}-containing bath solution (187 ± 49 pA in Ca^{2+} free, n=5 vs. 159 ± 19 pA in Ca^{2+}-containing, n=16, $p>0.05$, Fig. 5.3A and C). Previous work in the laboratory confirmed that both BK [7] and PAR2-PL [6] prompt release of Ca^{2+} from the ER. To further confirm these findings, we depleted intracellular Ca^{2+} stores by incubating DRG cultures with 2 μM thapsigargin for 3 min. Thapsigargin is an irreversible inhibitor of the sarcoplasmic reticulum Ca^{2+}-ATPase pump. We then performed whole-cell patch recordings of CaCC currents induced by PAR2-PL. We found that thapsigargin pre-treatment strongly inhibited the effect of PAR2-PL (Fig. 5.3B and D). We also found that 78% (7/9) of the neurons did not respond to PAR2-PL after thapsigargin pre-treatment (Fig 5.4B and C, inward current of 215.4 ± 11.2 pA, n=16 in control vs. 52 pA in two thapsigargin-treated and responding neurons). All of these results indicated that Ca^{2+} release from the ER via the IP_3Rs is the most probable Ca^{2+} source for ANO1 activation in small DRG neurons under the experimental conditions used.

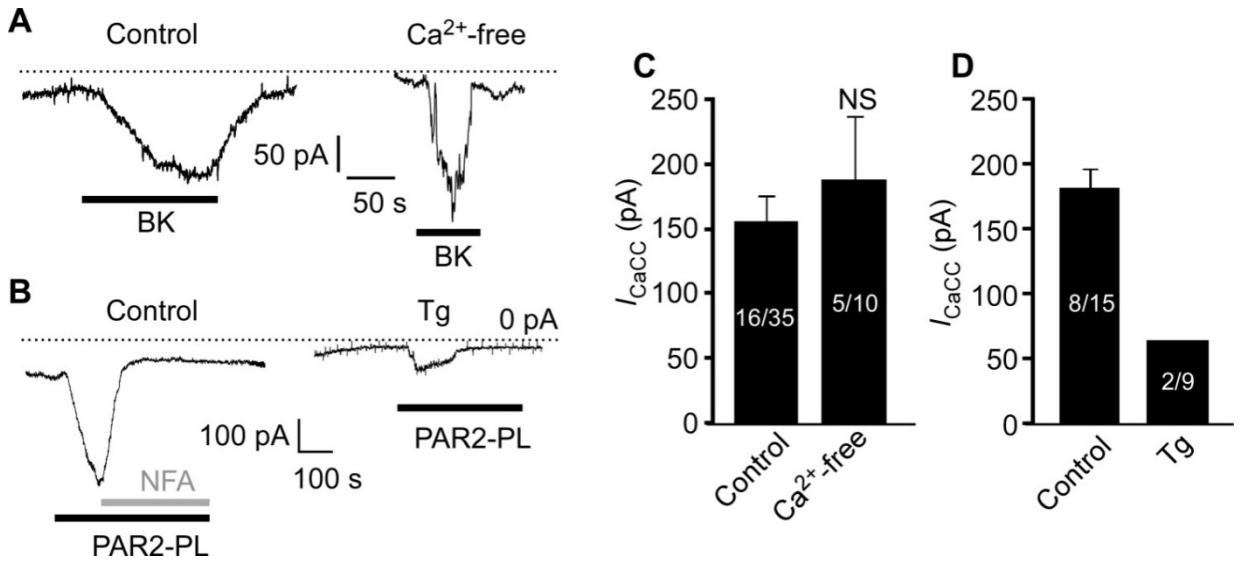

Figure 5. 3. Depletion of Ca^{2+} in the ER inhibits the activation of CaCC in small DRG neurons. (A) Representative traces of the whole-cell patch clamp recordings of small DRG neurons performed in control (left) and Ca^{2+} free (right) bath solution. (B) Representative traces of the whole-cell patch clamp recordings of small DRG performed after 3 min of bath application of 2 μM thapsigargin. (C, D) Summary data for (A) and (B). Data (bar graphs) are presented as mean ± SEM. From [Jin, X., et al., Sci Signal, 2013. 6(290): p. ra73.] Reprinted with permission from AAAS.

5.4 Discussion

The major conclusion from the experiments in this chapter is that $G_{q/11}$- and PLC-coupled GPCRs (B_2R and PAR2) reliably activate ANO1/CaCC in small DRG neurons, but that Ca^{2+} influx through the VGCC was generally ineffective in activating ANO1/CaCC in these neurons. It was also concluded that the major source of Ca^{2+} for ANO1 activation by the GPCR is Ca^{2+} release from the ER, but not store-operated Ca^{2+} influx. Thus, we found that Ca^{2+} store depletion abolishes GPCR-induced CaCC, while exclusion of Ca^{2+} from the extracellular milieu does not abolish GPCR-induced CaCC.

These data unambiguously confirm that GPCR, such as B_2R and PAR2, activate CaCC via the ER-mediated Ca^{2+} release from the IP_3R. This is in agreement with previous evidence from our lab demonstrating that blocking IP_3Rs with the specific blocker Xestospongin C

strongly reduces BK-induced CaCC [7]. Yet store-operated Ca^{2+} entry (SOCE) cannot be completely ruled out as a source of Ca^{2+} for CaCC activation. Therefore, while the amplitude of Ca^{2+} transients recorded in Ca^{2+}-free extracellular solution was not smaller relative to control conditions, the duration of transients was often reduced (Fig. 53A). Thus SOCE can be a secondary factor in supplying Ca^{2+} for CaCC/ANO1 activation. In this connection, it was recently suggested that in *Xenopus* oocytes, Ca^{2+} entering from the extracellular media through the STIM1/Orai1-mediated SOCE first needs to be channelled into the ER and then out through the IP_3Rs in order to be able to activate endogenous ANO1 [432]. It was further observed that a direct Ca^{2+} influx through STIM1/Orai1 into the cytosol did not activate ANO1, presumably because of lack of proximity between the ANO1 and the STIM1/Orai1 complexes.

Published evidence suggests that in the ER IP_3Rs are in more abundant than RyR [406], and that DRG neurons express moderately more IP_3R1 than IP_3R2 and IP_3R3 [433]. Therefore we focused on the IP_3R1 as a possible major source of Ca^{2+} for ANO1 activation in small DRG neurons.

Another important outcome of the experiments reported in this chapter is that Ca^{2+} influx through VGCC is poorly (if at all) coupled to CaCC in small, capsaicin-sensitive DRG neurons. Here we used a double-pulse protocol to test if VGCC activates CaCC. In most small neurons tested, VGCC activation did not activate CaCC as measured by the appearance of slow tail currents at – 80 mV. One of the hallmarks of ANO1 is that its sensitivity to Ca^{2+} is voltage-dependent. Thus, we investigated if VGCC could activate CaCC in small DRG neurons at positive voltages. We found that this was not the case. VGCC were shown to be able to activate other Ca^{2+}-dependent channels, like Slo1 channels in cardiac myocytes [434]. Ca^{2+} sensitivity of Slo1 channels is relatively low [294], but is within a range similar to that of ANO1. Thus, in order to be able to activate Slo1 channels, VGCC must be co-localized with Slo1 channels in tightly-coupled microdomains [435]. Lack of coupling between the VGCC and CaCC therefore

may suggest that in small DRG neurons VGCC do not co-localize with ANO1/CaCC. By the same logic, however, the tight coupling between ER Ca^{2+} release and CaCC activation in DRG neurons may suggest close spatial colocalization of IP_3R and ANO1/CaCC. This hypothesis will be tested in the next chapter.

Chapter 6. ANO1 activation in small DRG neurons requires local Ca^{2+} microdomains

6.1 Introduction

6.1.1 What are the local Ca^{2+} microdomains

Ca^{2+} is a ubiquitous intracellular messenger and a great number and variety of intracellular processes are regulated by changes in intracellular Ca^{2+} concentrations. Therefore, appropriate molecular mechanisms must exist to confer the needed specificity to Ca^{2+} signaling. Indeed, Ca^{2+} signaling is often precision-tuned in terms of spatial localization and temporal coding. Normally, the concentration of free Ca^{2+} in the cytosol at rest is in the range of 50 - 100 nM [436]. The most effective mechanism of increasing $[Ca^{2+}]_i$ is an inflow from the extracellular space via Ca^{2+}-permeable channels. An alternative mechanism is by releasing Ca^{2+} from intracellular Ca^{2+} stores, such as the SR, the ER or mitochondria. In some cases, cytoplasmic Ca^{2+} signals are restricted to certain regions of the cell. This spatial organization of Ca^{2+} into segregated microdomains is a recognized mechanism for enhancing the versatility and specificity of Ca^{2+} signaling system [437]. The global Ca^{2+} signal, as measured in the cytoplasm, is the average of highly focused, transient, elementary changes of Ca^{2+} concentrations. This mechanism is limited by the diffusion of Ca^{2+} in the cytoplasm, which is hindered by cytoplasmic proteins and neighboring membranes [438]. For example, localized IP_3-induced local Ca^{2+} release (10^{-6} to 10^{-4} M) far exceeds that of the global Ca^{2+} signal, measured over the whole cell. This allows Ca^{2+} to regulate even the low Ca^{2+} affinity effectors. The term microdomain is usually applied to transient fluctuations of Ca^{2+} in strictly localized areas (diameter of 10–100 nm) [437, 439, 440]. The term "Ca^{2+} microdomain" was first introduced to denote instances of close spatial colocalization of Ca^{2+} channels and an appropriate Ca^{2+}-sensitive proteins (e.g. Ca^{2+}-activated K^+ channel) that are regulated by Ca^{2+} influx from the Ca^{2+} channels [441, 442]. Recently a new term, "nanodomain," has been

coined, referring to multi-protein structures in which proteins are <100 nm from each other [443]. Studies show proteins within micro- or nano-domains are often tightly arranged by various adaptors and scaffolding proteins, including PDZ domain containing adaptors such as homers, SNARE and neurexin [444-446]. For example, α-neurexins at synapses are involved in the coupling between Ca^{2+} channels and synaptic Ca^{2+} sensor synaptotagmin and other components of the Ca^{2+}-sensitive synaptic vesicle release machinery [446].

Different local Ca^{2+} signals triggered in the cell by activating different signaling pathways result in targeting different intracellular effectors. In some cases it is possible to clearly demonstrate specificity of particular Ca^{2+} signals; for instance, local Ca^{2+} influx through Ca^{2+} release activated Ca^{2+} (CRAC) channels in mast cells stimulates Ca^{2+}-dependent PLA2 and 5-lipoxygenase, which generate the intracellular messenger cascades resulting in cytokine secretion. Stimulation of these cells with thapsigargin or carbachol applied in Ca^{2+}-free solution elicited significant rises in global $[Ca^{2+}]_i$, but these concentration increases were totally ineffective in activating cPLA2 or leukotriene C4 secretion [447, 448]. Another example of local Ca^{2+} influx tightly controlling a plasma membrane-restricted enzyme has come from work on T lymphocytes [449]. Agonists such as 2-Aminoethoxydiphenylborate (2-APB) increases Ca^{2+}-ATPase activity by an effect on local $[Ca^{2+}]_i$, which at low concentration enhances CRAC channel activity, and stimulates plasma membrane Ca^{2+}-ATPase activity through local changes in $[Ca^{2+}]_i$. The resultant rise in global cytoplasmic Ca^{2+} does not, however, enhance the activity of Ca^{2+}-ATPase.

Some scaffolding proteins have been found to be involved in the assembly of local Ca^{2+} microdomains. Thus, Ca^{2+} signaling complex in fly photoreceptors are assembled with the aid of the PDZ-containing scaffolding protein inaD, which couples the light-activated GPCR rhodopsin to TRP, PLC (norpA) and PKC (ninaC) [450, 451]. Mutating PDZ domains of InaD protein disrupted the entire microdomain assembly and severely impeded signal transduction.

Homer proteins are another type of scaffolding proteins that regulate local Ca^{2+} signaling. Homer proteins are predominantly localized at the postsynaptic densities in mammalian neurons, where they can form protein complexes with other postsynaptic density proteins through their N-terminal domains containing an EVH domain. The EVH domain is a protein module of ~115 amino acids which binds to proline-rich sequences present in many proteins involved in Ca^{2+} signaling, including GPCRs, IP_3Rs, RyRs, L-type Ca^{2+} channels and TRPC channels [452]. The C-terminal domains of Homer proteins contain a coiled-coil structure and leucine zipper motif which are involved in multimerization. Homer-mediated protein clustering facilitates signal transduction or cross-talk between different proteins. For example, Homer mediates the coupling of glutamate receptors to N-Type Ca^{2+} channel and regulates synaptic activity in superior cervical ganglia (SCG) neurons [453]. In the CNS, Homer1 has been shown to interact with metabotropic glutamate receptors (mGluRs) and IP_3R and to bridge the PM to ER into junctional microdomains [454]. Homer1 also interacts with GPCRs and TRPC channels at the PM and IP_3Rs at the ER [452], which may play a role in cellular memory by modulating the fidelity of GPCR signaling to reflect stimulation history. In the present work I discovered a junctional microdomain in DRG neurons which also involve IP_3Rs in the ER and GPCRs and ion channels at the plasma membrane (see below). Thus, I hypothesize that Homer proteins may play roles in the assembly of these microdomains. Preliminary data will be presented in the Chapter 8.

6.1.2 Functions of local Ca^{2+} microdomains

Although there are reasons to believe that Ca^{2+} microdomains represent a ubiquitous mechanism of signal transduction, I will discuss below several of the most well researched examples of such microdomain Ca^{2+} signaling.

6.1.2.1 Neurotransmitter release

Neurotransmitter release requires high $[Ca^{2+}]_i$, which is achieved in the presynaptic terminals by opening of VGCC in response to depolarization created by the arriving AP. In some experiments, local hot spots of high $[Ca^{2+}]_i$ have been shown to relate to neurotransmitter vesicle fusion events [455, 456]. Research has shown that "hot-spots" of Ca^{2+} (200–300 μM) appear in presynaptic terminals of the squid giant synapse following an AP [457]. In neuromuscular junctions of *Xenopus laevis,* APs also evoke Ca^{2+} hot-spots in presynaptic terminals [458]. Thus, in synapses, Ca^{2+} influx appear to be very tightly coupled with transmitter release. Using flash photolysis of caged Ca^{2+}, it has been shown that local $[Ca^{2+}]_i$ at the release sites is in the range 10–300 μM in different neurons. The "slow" Ca^{2+} buffer EGTA usually does not affect synaptic vesicle release, while the "fast" buffer BAPTA inhibits neurotransmitter release [459]. This is evidence that local domains of high $[Ca^{2+}]_i$ are necessary for transmitter release. Indeed, if the distance between Ca^{2+} channels and Ca^{2+} sensors of exocytosis is short (less than 100 nm), only the fast Ca^{2+} chelator BAPTA, but not the slow chelator EGTA (at millimolar concentrations), will have enough time to capture the Ca^{2+} on its way from the Ca^{2+} channels to the Ca^{2+} sensors and impair transmission. By contrast, if the coupling distance is longer, both the fast and the slow Ca^{2+} chelator will be effective [460]. On the other hand, some studies showed that Ca^{2+} channels are not as tightly coupled to exocytosis in these synapses. Borst and Rozov, for example, demonstrated that

EGTA can in fact reduce evoked neurotransmitter release in CNS synapses [461, 462]. Thus, further research is required to resolve this controversy.

6.1.2.2 Regulation of adenylyl cyclases

Although two isoforms of adenylyl cyclases are activated by a rise in cytoplasmic Ca^{2+}, robust releases of Ca^{2+} from intracellular stores in response to thapsigargin and the ionophore ionomycin were both unable to activate these Ca^{2+}-dependent isoforms [463, 464]. By contrast, store-operated Ca^{2+} influx significantly increased enzyme activity, even though it caused bulk Ca^{2+} to rise to a lesser degree than that achieved by Ca^{2+} release. Hence it was concluded that these isoforms are regulated by a subplasmalemmal (microdomain) $[Ca^{2+}]_i$ rise instead of a global increase.

6.1.2.3 Regulation of gene expression

It has been shown that the activation of the transcription factor cAMP-response-element-binding protein (CREB) needs Ca^{2+} hot spots in neurons [465]. Direct injection of BAPTA into the nucleus (which has no effect on cytoplasmic Ca^{2+} elevation) prevented CREB stimulation. Ca^{2+} microdomains arising from voltage-gated Ca^{2+} channels [466, 467] or Ca^{2+}-permeable NMDA receptors [468] might be capable of impacting nuclear events and inducing CREB phosphorylation. Another example of microdomain Ca^{2+} signaling can be found in the nuclear factor of activated T-cell (NFAT) signaling. Thus, it was shown that local $[Ca^{2+}]_i$ signals from L-type VGCC (CaV1.3) activate calcineurin (CaN) bound to AKAP79/150 in specific microdomains. AKAP79/150 then directs CaN to activate NFAT, which translocates to the nucleus and regulates gene expression [469]. This process is, for instance, capable of upregulating the expression of anti-excitatory KCNQ2 and KCNQ3 genes in response to excessive excitation of sympathetic and hippocampal neurons [469].

6.1.3 Ion channels and local Ca^{2+} microdomain

Ca^{2+} influx across the plasma membrane is essential for the regulation of some Ca^{2+}-dependent channel activity. In some cases, this activity entails the formation of microdomains. The relationship between Ca^{2+} channels and Ca^{2+}-sensitive channels in the immediate neighborhood will depend on peak local $[Ca^{2+}]_i$, on the distance between the components of the microdomain, and on the diffusion characteristics of Ca^{2+} in the local environment. What can affect the latter parameter? First, endogenous buffers like calbindin and CaM can impede diffusion [443]. Second, the intracellular characteristics of buffers like diffusion rates, affinities, and reaction kinetics play vital roles in determining the distribution of free Ca^{2+} [470]. It was suggested that the Ca^{2+}-binding rate of CaM is similar to or higher than exogenous fast chelators such as BAPTA [443]. Thus, the expression level or location of CaM may interfere with local Ca^{2+} signaling [443].

The physical interaction between a Ca^{2+} channel and its target Ca^{2+}-sensitive channel often facilitates signaling within Ca^{2+} microdomains. For example, the coupling between the Ca^{2+}-activated K^+ channel (Slo1) and P/Q-type VGCCs contributes to the activation of Slo1 in many cell types [471], such as vestibular hair cells [472], adrenal chromaffin cells [473] and frog neuromuscular junctions [474]. Some studies show that rapid activation of Slo1 channels is controlled by P/Q-type channels in *Xenopus* oocytes expressing recombinant Slo1 and P/Q-type channels [441]. Accordingly, high concentrations of cytoplasmic EGTA cannot inhibit the coupling between Slo1 and P/Q-type channels, but BAPTA inhibits Slo1–P/Q-type channel coupling. It was further found that Slo1channels are co-assembled with L-, P/Q- and N-type Ca^{2+} channels as tested by affinity purification in rat brain [442]. All these studies suggest that large-conductance Ca^{2+}-activated K^+ channels and VGCCs form a macromolecular complex with tight coupling. The authors also conclude that local Ca^{2+} concentration was about ~10 μM

around the mouth of VGCCs, and that the physical distance between VGCCs and Ca^{2+}-activated K^+ channels is a uniform coupling distance in the range of 10–15 nm [441].

Other studies have shown that store-operated Ca^{2+} channels couple with the Cl^- channels in a prostate cancer cell line [475]. Ca^{2+} influx from store-operated channels partially inhibited a VRCC current, while dialysis with 1 μM free Ca^{2+} failed to inhibit VRCC. These results suggest that store-operated Ca^{2+} channels were colocalized with these Cl^- channels. TRPC7 channels were also suggested to couple with the sarco-endoplpasmic Ca^{2+}–ATPase (SERCA) [476]. Activation of TRPC7 channels by DAG was blocked by the SERCA pump inhibitor thapsigargin. Even whole cell dialysis with high concentrations of BAPTA failed to affect this coupling, suggesting an intimate interaction between TRPC7 and SERCA pumps.

Interestingly, the Ca^{2+} affinity of both Slo1 and ANO1 channels is rather low (EC_{50} in the low micromolar range, [202, 477]). This may suggest that ANO1, like Slo1 channels, requires a local Ca^{2+} microdomain for activation.

6.2 Aims

In chapter 5 I found that Ca^{2+} release from IP_3R activated ANO1 in small-diameter DRG neurons, but that Ca^{2+} but from other sources, such as VGCC, was unable to activate ANO1. As discussed in this chapter, local microdomains might achieve relatively high local $[Ca^{2+}]_i$, and thereby efficiently couple sources of intracellular Ca^{2+} with their effectors. Since Ca^{2+} sensitivity of ANO is low, I hypothesize that ANO1 also requires a microdomain environment for its activation in small DRG neurons. The experiments in this chapter were designed to probe this hypothesis.

6.3 Results

6.3.1 Imaging of I^--sensitive YFP supports finding that VGCC cannot activate CaCC in small DRG neurons

We previously found that VGCC couples poorly to ANO1 in small DRG neurons, while GPCR activation ANO1 is clearly detectable in over 50% of such cells. In order to verify this finding with an independent technique that does not depend on selection of the "best" cells for a measurement, DRG neurons were transfected with I^--sensing yellow fluorescent protein YFP H148Q/I152L. Since ANO1 is permeable to I^- ions [299] and H148Q/I152L EYFP fluorescence is quenched by I^- (a property based on the capability of halides to quench the fluorescence by a collision mechanism [478]), overexpressed H148Q/I152L EYFP can be used as a tool to measure ANO1 activity [479]. We transfected DRG cultures with YFP H148Q/I152L and investigated ANO1 activation by BK and VGCC using fluorescent imaging. As shown in Fig. 6.1A and B, perfusion of DRG neurons transiently transfected with YFP H148Q/I152L with an external solution in which 30 mM NaCl was substituted by 30 mM NaI induced a slow decrease in fluorescence. In control neurons (vehicle, NaI only) the fluorescence decreased to 73 ± 5% of initial value after 300 s of application, presumably due to the presence of various background anion permeabilities. BK evoked much stronger fluorescence quenching reflecting an accelerated I^- influx compared with vehicle control (50 ± 4% of initial value). The effect of BK was blocked by NFA. In contrast, activation of VGCC by application of extracellular solution in which 50 mM NaCl has been replaced by 50 mM KCl (depolarization to ~ -25 mV according to the Nernst equation) did not produce significant quenching when compared to the vehicle control. In separate Ca^{2+} imaging experiments, we have confirmed that both BK and "high-K^+" solutions induced comparable Ca^{2+} transients in DRG neurons (not shown).

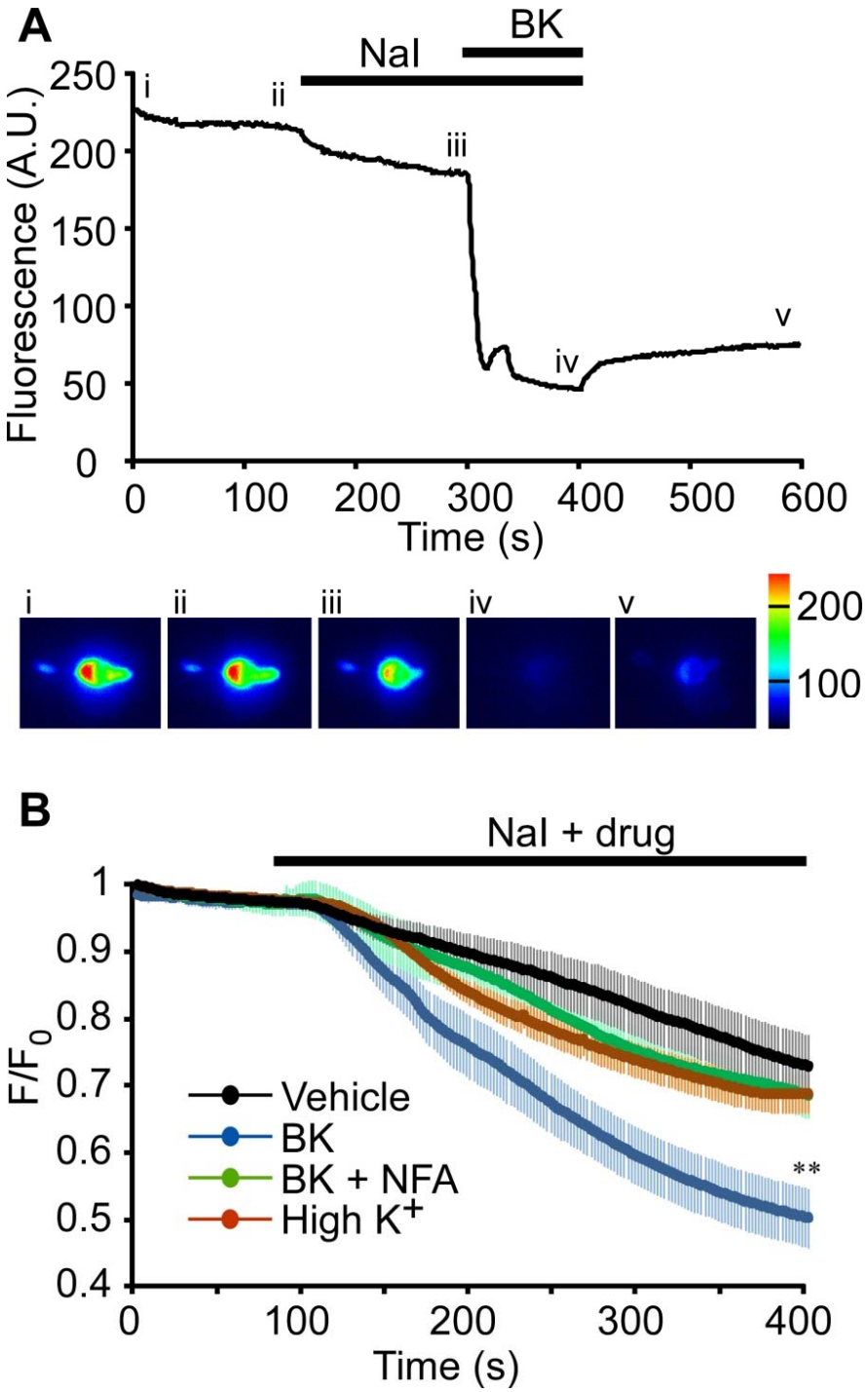

Figure 6.1 Representative images from one neuron (A) and summary of data (B) from experiments carried out with the YFP H148Q/I152L assay on small DRG neurons. Brown, black green and blue traces show the cell fluorescence decrease following I^- addition with vehicle (black; N=10) or with 1 µM BK (blue; N=15), 1 µM BK+100 µM NFA (green; N=8), or with 50 mM KCl (orange; N=27) respectively. Obtained in collaboration with Shihab Shah and Nikita Gamper. From [Jin, X., et al., Sci Signal, 2013. 6(290): p. ra73.] Reprinted with permission from AAAS.

6.3.2 ANO1 is in close proximity to the Ca^{2+} source

Results reported in chapters 4 and 5 have indicated that IP_3-mediated Ca^{2+} release was the main Ca^{2+} source for CaCC activation in small DRG neurons, while VGCC were generally unable to activate CaCC in the majority of DRG neurons. Given the fact that ANO1 has low Ca^{2+} sensitivity, we hypothesized that the Ca^{2+} sources (the IP_3R) must be very close to the CaCCs. To assess this possibility, BK or PAR2-PL-induced Cl^- currents were assessed in recordings with pipette solutions in which we included 10 mM EGTA or 10 mM BAPTA, but this time the dialysis time was set for 4 min to avoid massive ER Ca^{2+} depletion. High concentration of EGTA or BAPTA can deplete the ER of Ca^{2+} if they are present in the cytoplasm for a long time [480]. Accordingly, as has been demonstrated in chapter 4, dialysis of 10 mM EGTA into DRG neurons for 10 min can deplete the ER completely.

The coupling distance between Ca^{2+} sources and their targets can be probed using the exogenous Ca^{2+} chelators EGTA and BAPTA, which have different Ca^{2+} binding rates, but similar Ca^{2+} affinities [481]). The basic principle is simple: if the distance between Ca^{2+} source and its targets is less than ~100 nm, only the fast Ca^{2+} chelator BAPTA will have enough time to capture the Ca^{2+} released from the sources at millimolar concentrations of the chelator. On the other hand, the same concentration of the slow Ca^{2+} chelator EGTA would not be able to capture Ca^{2+}. If, however, the distance between the Ca^{2+} source and the target is larger, both EGTA and BAPTA will capture Ca^{2+}. This approach was first used by Adler and colleagues [460], and subsequent studies have shown that the distance can be further probed by adjusting concentrations of chelators and Ca^{2+} concentrations (when possible) [482].

We found that BAPTA inhibited the induction of CaCC by PAR2-PL, while EGTA was without an effect (Fig. 6.2). Thus, 53% (8/15) of small DRG neurons responded to PAR2-PL in control conditions, while 71% (5/7) of such neurons responded to PAR2-PL when recorded with EGTA-containing pipette solution (215.4 ± 11.2 pA in 5/7 neurons from EGTA vs. 176.5

± 11.2 pA in 8/15 neurons, p>0.05; Fig. 6.2). Conversely, only 11% (1/9) of small DRG neurons responded to PAR2-PL when recorded with EGTA-containing pipette solution (Fig. 6.2). These results clearly indicate that probable Ca^{2+} source (ER) co-localizes with CaCCs in small DRG neurons.

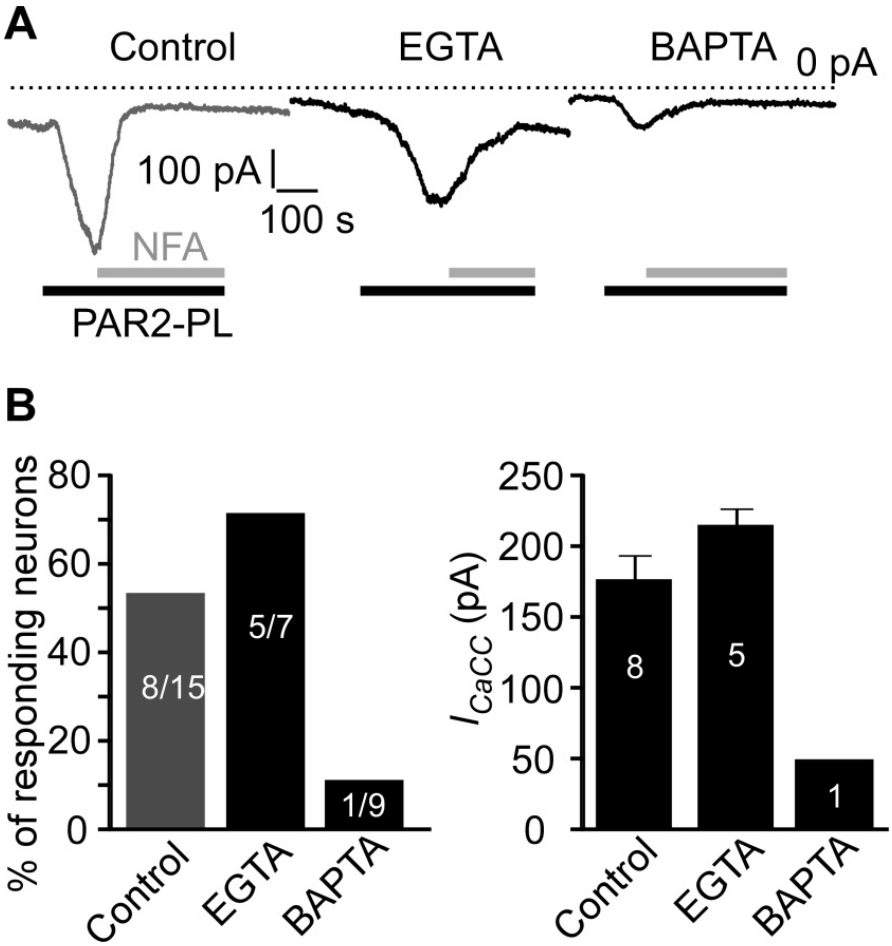

Figure 6.2 Ca^{2+} buffers with different Ca^{2+}-binding dynamics have different effects on CaCC in DRG neurons (A) Whole-cell patch clamp recordings of small DRG neurons were performed after 4 min of intracellular dialysis with 10 mM EGTA or 10 mM BAPTA. Percentage of PAR2-PL responsive neurons and the amplitude of PAR2-PL-induced inward currents were significantly reduced after application of BAPTA, but not after application of EGTA. This suggests close proximity of CaCC and Ca^{2+} stores in neurons. (B) and (C) are summary data for (A). Data are given as mean ± SEM. From [Jin, X., et al., Sci Signal, 2013. 6(290): p. ra73.] Reprinted with permission from AAAS.

6.3.3 ANO1 colocalizes with IP_3R1

I next used an immunostaining technique and confocal microscopy to test if ANO1 indeed colocalizes with IP_3Rs, but not with VGCCs, in small DRG neurons. We first confirmed specificity of ANO1 antibodies. To this end we transfected cDNA constructed for mouse ANO1 together with GFP into HUVECs. HUVECs do not express endogenous ANO1 as tested by RT-PCR. Fig. 6.3A shows that we detected a robust ANO1 antibody binding in cells which also expressed GFP (red arrow), but we detected no ANO1 in cells which did not express GFP (white arrows). ANO1 antibody robustly stained small DRG neurons (Fig. 6.3B, upper panel), but not glia (identified by the GFAB staining). The IP_3R1 antibody labeled characteristic reticular structures in the ANO1-positive neurons (Fig. 6.3B, middle panel). To label VGCC we used a pan-VGCC antibody that recognizes all major VGCC α-subunits. It robustly stained neurons but not glia (Fig. 6.3B, lower panel).

Confocal experiments indicated that ANO1 and IP_3R staining were evident within the cytoplasm and some puncta close to the plasma membrane (Fig. 6.4A and B). The exact location of ANO1 was not possible to ascertain due to the limitation of confocal microscopy. As shown the middle panel of Fig. 6.4A, the same DRG neuron was stained with IP_3R antibody. Thus ANO1 immunoreactivity overlapped with an IP_3R staining in many puncta, as indicated by yellow color in Fig. 6.4A, right panel. Similar results were obtained in 33 small DRG neurons.

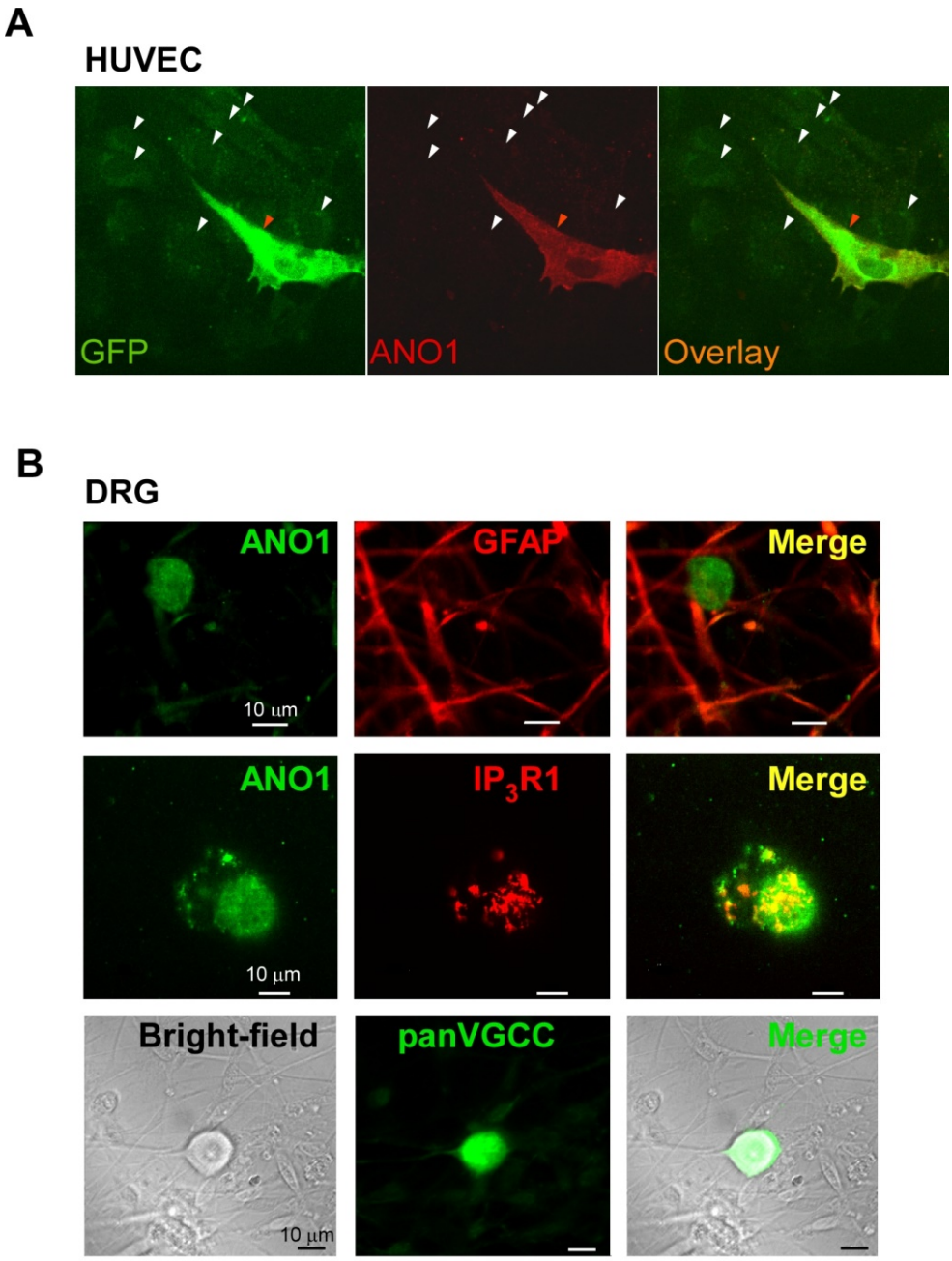

Figure 6.3 Antibody specificity experiments. (A) ANO1 antibody specifically labelled cultured HUVECs co-transfected with ANO1 and GFP (orange arrow); non-transfected cells (white arrows) are not labelled by the antibody. (B) Top row: ANO1 antibody specifically labeled small DRG neuron but not glia (immunolabelled with GFAP antibody). Middle row: IP_3R1 antibody labelled reticular structures in the ANO1-positive DRG neuron cell body. Bottom row: pan-VGCC antibody labeled DRG neuron but not glia (visible using bright-field illumination). From [Jin, X., et al., Sci Signal, 2013. 6(290): p. ra73.] Reprinted with permission from AAAS.

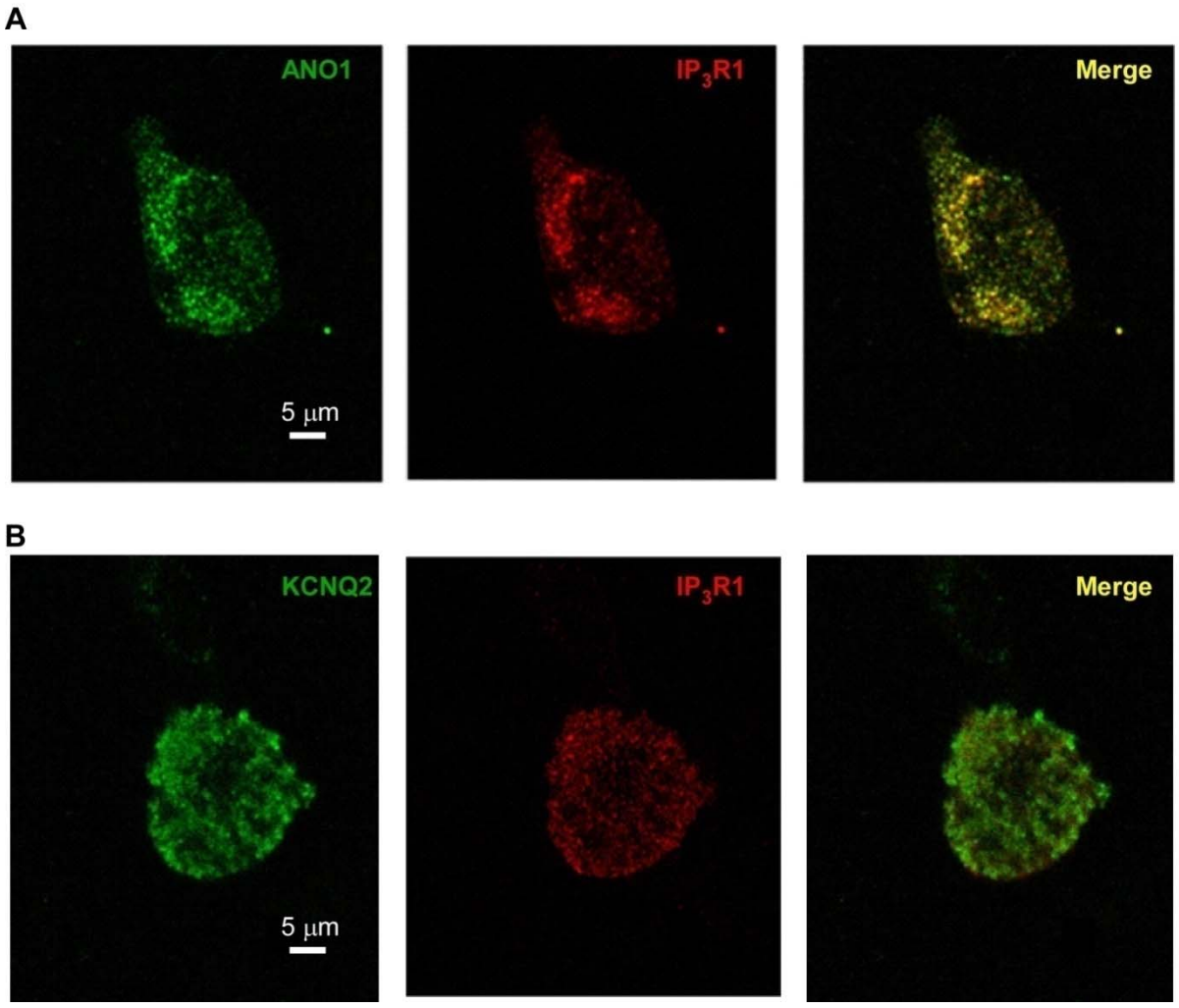

Figure 6.4 Colocalization of endogenous ANO1 with IP_3R. (A) Fluorescence pattern for endogenous ANO1 in small DRG neuron. Cells were labeled with goat polyclonal anti-ANO1 antibody (green) in the left panel. The middle panel shows fluorescence pattern for endogenous IP_3R in the same DRG neuron. Cells were labeled with mouse monoclonal anti-IP_3R1 antibody (red). Right panel shows a combined visualization of IP_3R and ANO1 labeling. Co-localization of both antibodies generates yellow spots. (B) Fluorescence pattern for endogenous KCNQ2 in small DRG neuron. Cells were labeled with goat polyclonal anti-KCNQ2 antibody (green) in the left panel. The middle panel shows fluorescence pattern for endogenous IP_3R in small DRG neuron. Cells were labeled with mouse monoclonal anti-IP_3R1 antibody (red). Right panel shows a combined visualization of IP_3R and KCNQ2 labeling that shows no significant co-localization.

A K^+ channel KCNQ2 which is abundantly expressed in small-diameter DRG neurons [483] was used a negative control because it failed to co-localize with IP_3R. The antibody of

KCNQ2 came from the same species (rabbit) as that for the ANO1 antibody (Fig. 6.4B). Similar results were obtained in 25 small DRG neurons. These data suggest that IP_3Rs may indeed colocalize with ANO1 in small DRG neurons.

To further probe colocalization of ANO1 and IP_3R1 in DRG neurons we employed *in situ* PLA, a highly specific and sensitive proteomics method for detecting the close proximity (less than ~30 nm) of cellular molecules [288]. The method is based on the immunolabeling of two proteins under investigation with specific primary antibodies with subsequent binding of appropriate pairs of secondary antibodies that are conjugates of specific oligonucleotides that can be ligated only if two secondary antibodies are in very close proximity (see Chapter 2 and Fig. 2.2 for method details). If two secondary antibodies are indeed in very close proximity, a punctate PLA staining occurs. PLA staining for ANO1 and IP_3R1 revealed punctate fluorescent signals with a characteristic puncta diameter of ~1 μm [484] in small DRG neurons, but not in glia (Fig. 6.5A). As shown in the left panel of Fig. 6.4A, a small DRG neuron is surrounded by multiple glia cells (labelled with white arrows and also by DAPI staining). The right panel shows that PLA signals appeared in the DRG neuron, but not in glia. No punctate staining was detected in untransfected HUVECs processed in the same way as the DRG cultures (Fig 6.5B). HUVECs do not express ANO1 but express IP_3Rs; thus, lack of PLA signal in HUVECs confirms specificity of the assay. In order to test if VGCC interacts with ANO1, we repeated PLA procedure on DRG cultures using ANO1 and pan-VGCC antibodies. We did not detect punctate fluorescent signals in this experiment (Fig 6.5B). Thus, PLA assay data suggest that at least some ANO1 and IP_3R1 molecules were within 30 nm proximity in small DRG neurons, while no such proximity between ANO1 and VGCC could be detected.

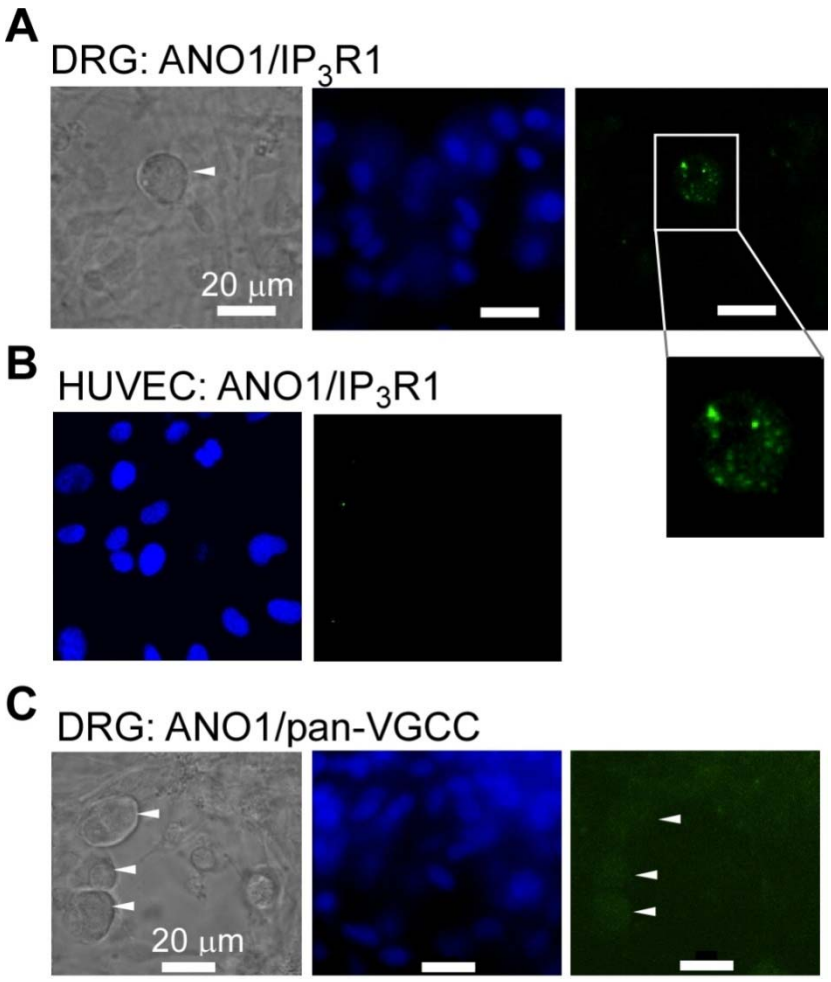

Figure 6.5 Detection of ANO1/IP_3R1 complexes using the proximity ligation assay (PLA). (A) DRG neuron (white arrow) surrounded by glial cells. Right panel shows bright-field illumination, middle panel shows DAPI staining and left panel shows ANO1/IP_3R1 PLA staining (green). (B) PLA ANO1/IP_3R1 staining of HUVEC (right panel) and DAPI (left panel) reveals no PLA signal. (C) DRG neurons (white arrows) surrounded by glial cells. Right panel shows bright-field illumination, middle panel shows DAPI staining, and right panel shows ANO1/IP_3R1 PLA staining which revealed no PLA signal. From [Jin, X., et al., Sci Signal, 2013. 6(290): p. ra73.] Reprinted with permission from AAAS.

6.3.4 ANO1 interacts with IP_3R1

To determine whether IP_3R1 coupling with ANO1 requires a physical interaction, we performed co-immunoprecipitation studies followed by Western blotting. First, the antibody against IP_3R1 was used to immunoprecipitate the total protein from DRG tissue lysate. The presence of ANO1 in the immunoprecipitate was analyzed with Western blotting. IP_3R1 was

detected in no-IP lysates with Western blotting as a loading control (Fig. 6.6A). The data showed that IP_3R1 antibodies can indeed immunoprecipitate ANO1 from native DRG tissue lysates. Next, we performed a reverse experiment: we used the antibody against ANO1 to immunoprecipitate the total proteins and to analyze for IP_3R presence. ANO1 was detected with Western blotting as a loading control. Again, the ANO1 antibody was able to immunoprecipitated IP_3R1 (Fig. 6.6B). This data strongly suggest that ANO1 and IP_3R1 do interact. As a negative control we performed co-immunoprecipitation experiments using HUVEC lysates. We did not detect any co-immunoprecipitation between ANO1 and the IP_3R1 antibody in untransfected HUVECs (Fig. 6.6C). We also failed to detect any interaction between another ER-localized protein, SERCA, and ANO1 in DRG tissue (Fig. 6.6D).

To examine which parts of ANO1 are involved in the interactions with IP_3R1, recombinant GST-fusion plasmids were constructed containing the N terminus, the intracellular loop between TM2 and TM3, and the C terminus of ANO1 (Fig. 6.7A). These constructs (together with GST plasmids as negative controls) were expressed in *E. coli* and purified by GST-agarose beads. These beads were then used to pull down interacting proteins from the whole DRG lysates. The proteins retained on the beads were then separated by SDS-PAGE, and the IP_3R1 were detected by Western blotting using anti-IP_3R1 antibody. As shown in Fig. 6.7B, the intracellular loop between TM2 and TM3 and the C-terminal fragment of ANO1 were indeed able to pull down the IP_3R1 from the DRG lysates. On the other hand, no pull down was detected with the N-terminal construct and the GST on its own.

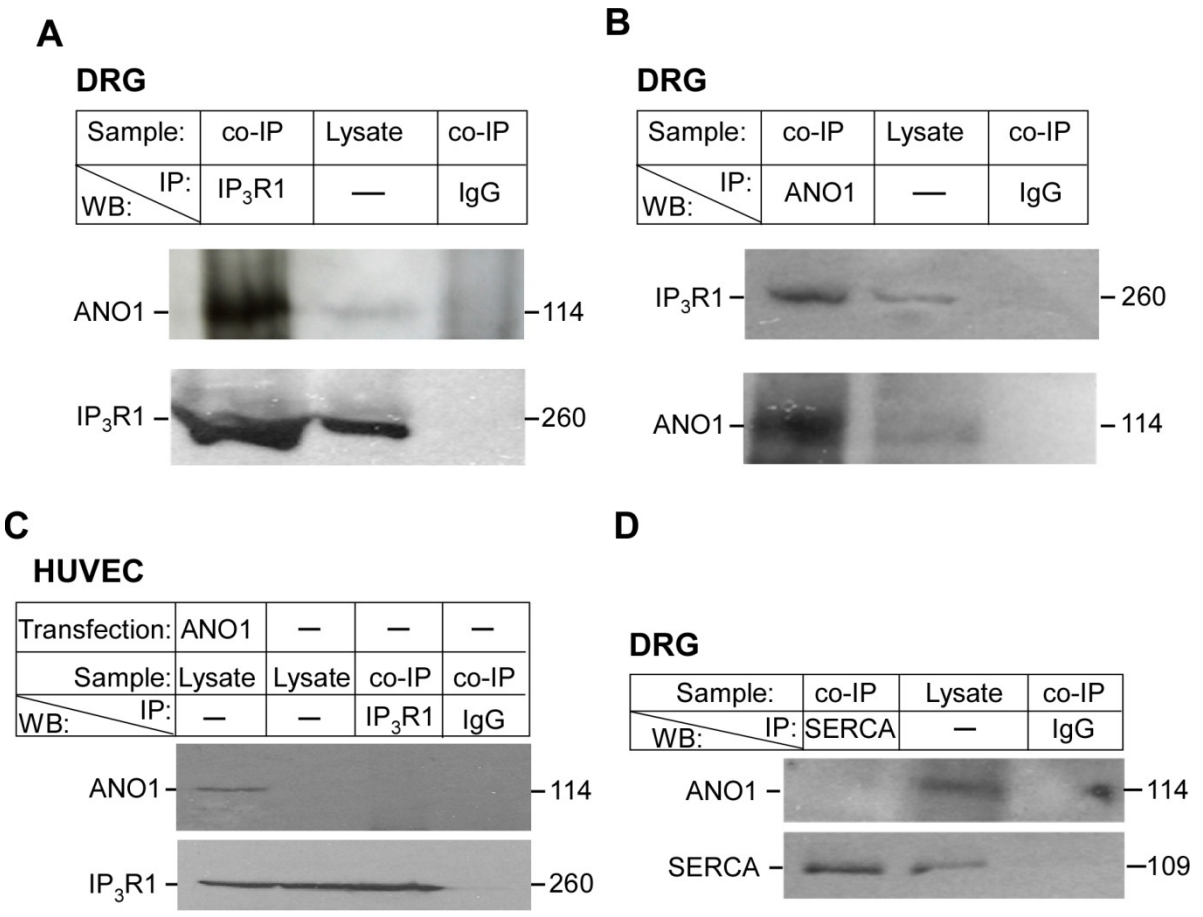

Figure 6.6 ANO1 channels interact with IP_3R. (A) Immunoprecipitation of ANO1 by an antibody against IP_3R1 from the lysates of whole DRG ganglia from rat. (B) Immunoprecipitation of IP_3R1 by an antibody against ANO1. "IP" and "WB" indicate the antibodies used for immunoprecipitation and Western blotting, respectively. Control immunoprecipitations were performed using rabbit (A) or goat (B) IgGs. (C) Lack of immunoprecipitation of ANO1 by an antibody against IP_3R1 from the lysates of untransfected HUVECs. For positive controls, the lysates of HUVECs transfected with ANO1 were probed using ANO1 antibody. (D) Lack of immunoprecipitation of ANO1 by an antibody against SERCA from the lysates of whole DRG ganglia from rats. The gels represent results of 3 independently performed experiments. From [Jin, X., et al., Sci Signal, 2013. 6(290): p. ra73.] Reprinted with permission from AAAS.

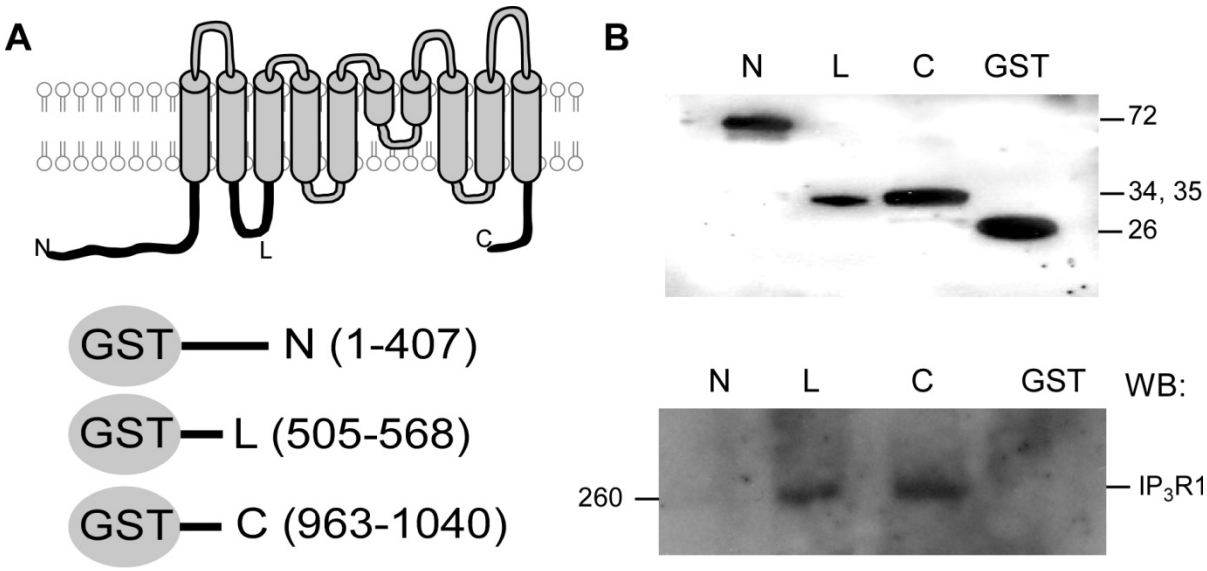

Figure 6.7 GST pull-down experiments. (A) Top panel is a schematic depiction of ANO1 channel. Below left is a schematic depiction of GST-fusion proteins containing the C-terminus (residues 963-1040, "C"), the loop between the second and third transmembrane domains (residues 505-568, 'L'), and the N-terminus (residues 1-407, 'N') of ANO1. (B) Upper panel, Western blotting shows the purified GST-fusion peptides (detected with the antibody against GST); lower panel shows pull-down experiments; GST fusion proteins containing the C terminus ("C") or the loop between the second and third transmembrane domains ("L"), but not the N-terminus ("N") of ANO1 precipitated IP_3R1 from the DRG lysate. All results shown are representative of experiments that were repeated three times independently. From [Jin, X., et al., Sci Signal, 2013. 6(290): p. ra73.] Reprinted with permission from AAAS.

6.3.5 Identification of other constituents of ANO1/ IP_3R1 from signaling complex

Junctional microdomains bringing together B_2R in the plasma membrane and IP_3R in the ER have been reported in sympathetic neurons [485]. Therefore we hypothesized that ANO1-containing plasma membrane microdomains may also contain B_2R and/or PAR2. Further immunoprecipitation experiments demonstrated that IP_3R1 immunoprecipitates also contained both B_2R and PAR2 (Fig. 6.8A). Moreover, we also found that both B_2R and PAR2 immunoprecipitated from DRG lysates by the antibody against the lipid raft protein cavevolin-

1(Fig. 6.8B). Cavevolin-1 was detected in DRG lysates with Western blotting as a loading control.

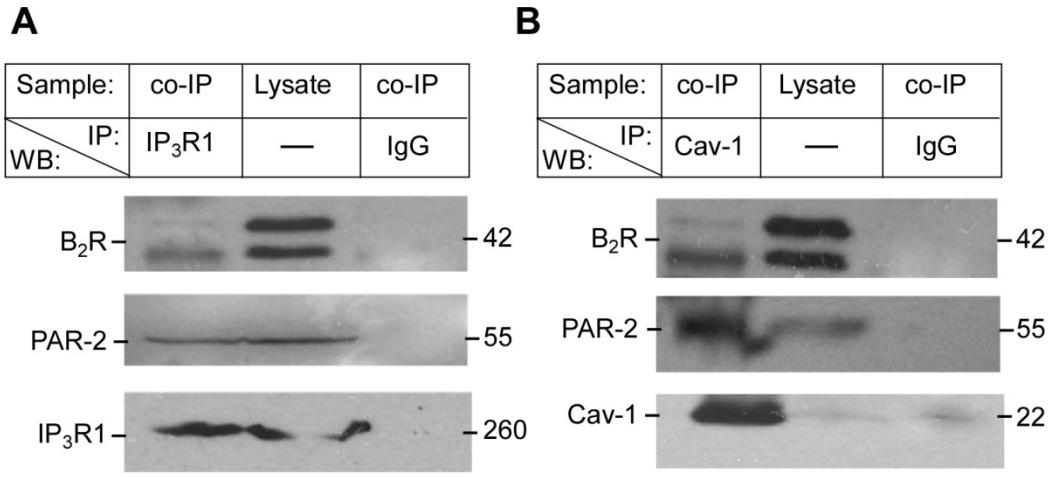

Figure 6.8 Molecular interactions within ANO1-containing junctional microdomains. (A) Immunoprecipitation of B_2R (upper panel) and PAR2 (middle panel) receptors by the antibody against IP_3R1. "IP" and "WB" indicate antibodies used for immunoprecipitation and Western blotting, respectively. Control immunoprecipitations were performed using mouse IgG. (B) Immunoprecipitation of B_2R (upper panel) and PAR2 (middle panel) receptors by the antibody against caveolin-1(Cav-1). Control immunoprecipitations were performed using mouse IgG. The gels represent results of 3 independently performed experiments. From [Jin, X., et al., Sci Signal, 2013. 6(290): p. ra73.] Reprinted with permission from AAAS.

6.4 Discussion

In this chapter we found that GPCR (B_2R and PAR2), cavoelin-1, IP_3R and ANO1 constitute a local Ca^{2+} microdomain, and that such an organization supports spatially discrete local Ca^{2+} signals that activate ANO1. The ER-localized IP_3R may be closely coupled to ANO1, forming part of a hypothetical ER–PM (plasma membrane) junctional complex.

In neurons and many other cell types, Ca^{2+} triggers different Ca^{2+}-dependent signaling pathways. In order to regulate cell function accurately, the Ca^{2+} signals are often restricted to

precise microdomains in which Ca^{2+} concentration can be changed sharply, rapidly and locally. Often the Ca^{2+} signaling microdomains are assembled around the Ca^{2+} sources. This may be achieved either by direct interaction of Ca^{2+}-sensitive proteins with the Ca^{2+} source (i.e. Ca^{2+} permeable ion channels), or by other mechanisms, such as partitioning to lipid rafts [486]. Here, we used a combination of biochemical and optical methods to determine if ANO1 activation in small DRG neurons requires Ca^{2+} microdomains. First, we used YFP indicator to further test coupling of CaCC in small DRG neurons to the Ca^{2+} release from the ER, and to Ca^{2+} influx from VGCC. YFP indicators are based on diffusion-limited collisional quenching. When the Cl^- channel is open, iodide will enter the cell and collide with indicators causing quenching of the fluorescence. We used a YFP based indicator which was mutated to increase the sensitivity of the fluorescent protein to iodide quenching [286]. The results of iodide imaging confirmed previous electrophysiological data (chapter 5), suggesting that ANO1/CaCCs in small DRG neurons are preferentially coupled to the GPCR-induced Ca^{2+} release from the ER.

Next, we tested the proximity of IP_3R1 and ANO1 using the EGTA/BAPTA paradigm. EGTA and BAPTA have similar binding affinities for Ca^{2+}, however, in comparison to EGTA, BAPTA chelate Ca^{2+} 150 times faster [487]. Accordingly, BAPTA is considerably more effective in preventing Ca^{2+} diffusing from a Ca^{2+} source such as a Ca^{2+} channel or Ca^{2+} stores, as compared to EGTA. In general terms, sensitivity of a Ca^{2+}-dependent process to BAPTA and a lack of sensitivity to EGTA is an indicator of the close proximity of a Ca^{2+} sensor to the site of Ca^{2+} entry or release. In my study, I found that EGTA cannot fully inhibit the CaCC activation by PAR2-PLs, while BAPTA reliably inhibits the effect of this agonist in DRG neurons. Dialysis time was restricted to 4 min in these experiments to avoid ER depletion of Ca^{2+}. An early study showed that dialysis of 10 mM EGTA or BAPTA into hippocampal neurons for less than 5 min does not deplete the ER, but longer dialysis time (10 min) resulted in a complete depletion of the ER Ca^{2+} load [480]. These experiments suggest that in small

DRG neurons, ER Ca^{2+} stores are in very close proximity to the ANO1/CaCC channels. In support of this conclusion, confocal imaging revealed that IP_3R1 and ANO1 exhibited punctate staining with largely overlapping patterns, suggesting a significant colocalization of IP_3R1 and IP_3R in neurons. This pattern of ANO1 staining and co-localization with IP_3R1 was specific because it was not observed in neurons stained with KCNQ2 and IP_3R. The antibody to KCNQ2 came from the same species as the antibody to ANO1. In addition, using immunoprecipitation and proximity ligation assays, we demonstrated that IP_3R1 and ANO1 are located in the same protein complexes. Data presented in the previous chapter indicate that Ca^{2+} release from IP_3R1 in ER mediates ANO1 activation. Here we show that IP_3R1 protein in the ER, and GPCR and ANO1 proteins in the plasma membrane, is coupled together, possibly within a junctional microdomain. PLA assay is designed in a way that ensures that only the proteins that are not more than ~30-40 nm apart are detected (see Chapter 2, Fig. 2.2). For negative controls we used secondary antibody diluent without primary antibody and also we performed IP_3R1/ANO1 PLA assay on HUVECs that do not express ANO1 (Fig. 6.3A). Both type of controls returned no PLA puncta, further verifying reliability of the assay.

Coimmunoprecipitation experiments further supported PLA and functional (patch clamp and iodide imaging) data to indicate that IP_3R1 and ANO1 together with the relevant GPCRs are located in the same macromolecular complex. In contrast to data indicating close spatial proximity of IP_3R1 and ANO1 channels, we detected no co-precipitation of SERCA and ANO1 channels in DRG lysates. This result suggests that there is specificity in the way these signaling complexes are assembled (or detected).

To further probe ANO1-IP_3R1 interactions we used a GST pull down assay. We found the TM2-TM3 loop and C-terminus of ANO1 can interact with IP_3R1, but that no such interaction was detected for the ANO1 N-terminus. These experiments do not, however, discriminate between direct or indirect interactions; thus, we cannot exclude the possibility that

ANO1-IP_3R1 interactions are mediated by some other protein(s). There are multiple examples of functional interactions of proteins within junctional ER-PM microdomains, including STIM-Orai interactions that underlie store-operated Ca^{2+} entry [488-490], colocalization of B_2R and IP_3Rs in sympathetic neurons [485], colocalization of Slo1 channels and IP_3Rs in cultured glioma cells [491]. Electron microscopy has shown that the SR and plasma membranes can be located in very close proximity (~20 nm) in arterial SMCs [492]. Conceivably, IP_3R1 and ANO1 channels may be present within macromolecular complexes that bridge the ER and plasma membranes, allowing local molecular communication between these proteins. The physiological function of close localization between IP_3R1 and ANO1 channels will be investigated in the next chapter.

Chapter 7. Role of lipid rafts in the assembly of ANO1-containing signaling complexes.

7.1 Introduction

7.1.1 The structure and function of lipid rafts

Lipid rafts are cholesterol- and sphingomyelin-rich microdomains of cell membranes (Fig. 7.1) [493]. These membrane structures form relatively stable clusters of ~70 nm in diameter [493]. At low temperatures, lipid rafts are resistant to extraction by non-ionic detergents such as Triton X-100. Because of their composition and detergent resistance, lipid rafts float to light fractions when separated by density-gradient centrifugation, a property that enables less separation of lipid rafts from the solubilizable membrane proteins and lipids [494]. Lipid rafts have also been called detergent-insoluble, glycolipid-enriched complexes or DIGs, glycosphingolipid-enriched membranes or detergent-resistant membranes (DRMs) [495]. The DRMs contain 5 times more glycolipids as compared to whole cell membranes. It has been demonstrated that lipid rafts can regulate various cell functions such as cell transport, the intracellular sorting of proteins and lipids, cell-to-cell communication, homeostasis of cholesterol, and signal transduction [496, 497]. The latter role will be discussed in more detail below.

There are two main models for plasma membrane receptor signaling within lipid rafts [493, 498-500]. According to one such model, lipid rafts can act as “signaling platforms,” which connect receptors and coupling factors, affecting enzymes and substrates, to form fully functional signaling complexes. In this way spatial protein-protein proximity produces rapid and efficient signal transduction.

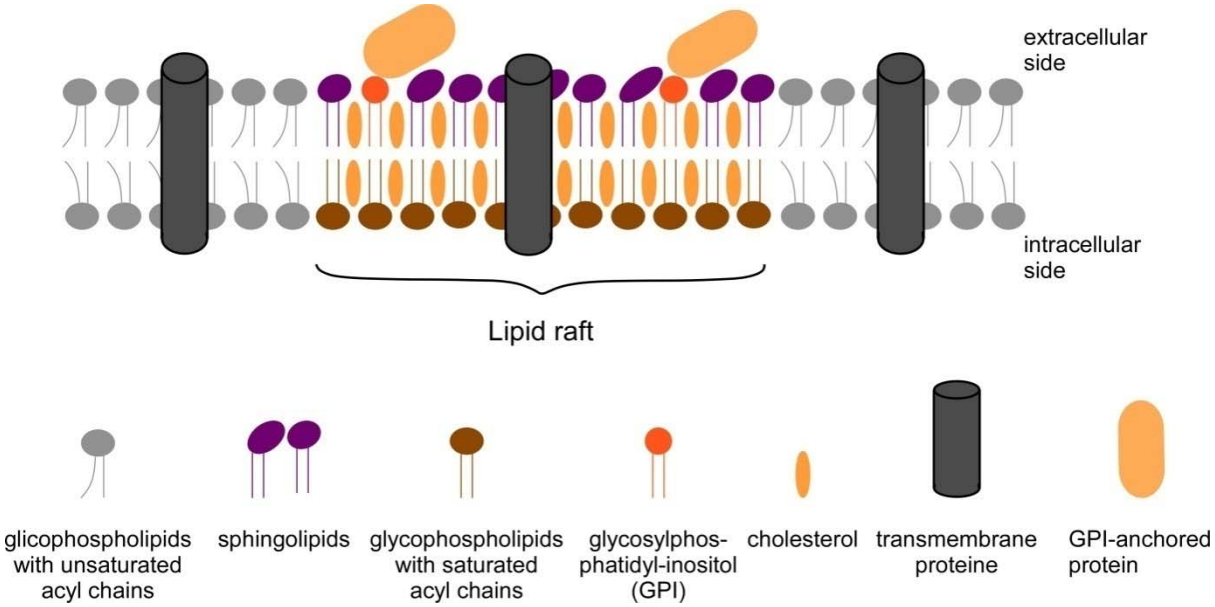

Figure 7.1 The structure of lipid rafts [501]. Rafts are membrane microdomains formed by high concentrations of sphingolipids (purple structures) and cholesterol (yellow structures) immersed in a phospholipid-rich (brown structures) environment. GPI-anchored proteins are anchored to membranes by covalent linkage to glycosyl-phosphatidylinositol (GPI). These proteins located on the extracellular side of the plasma membrane. Sphingomyelin and glycosphingolipids (purple structures) are restricted to the outer leaflet of the membrane bilayer, glycerophospholipids are restricted to the inner leaflet, whereas cholesterol is in both leaflets. Lipids in the rafts usually have saturated fatty acyl chains, whereas those in lipids out of the rafts are unsaturated (grey structures).

In addition, this assembly may represent a way of enhancing signaling specificity. The other model suggests that multiple signaling components can be present in different lipid rafts. Activated receptors could recruit cross linking proteins that bind to proteins in other rafts, and this would result in raft coalescence. In this case, rafts compartmentalization may further facilitate spatial localization. Rafts may also serve to limit the diffusion of signaling molecules and suppress the activity of signaling proteins by inhibiting the interactions.

Because of the small size and the dynamic nature of lipid rafts, it is difficult to study them by conventional approaches. Historically, lipid rafts have been defined functionally by their low density and insolubility in cold 1% Triton X-100. When the whole cell lysates are isolated by density gradient centrifugation, the DRM will float to low-buoyancy fractions.

MβCD can deplete cellular cholesterol which is a property that can be used to study the role of lipid rafts in cellular signaling [502]. Using siRNA to knock down lipid raft protein caveolins can also be used for disruption of raft signaling complexes in some cases (see below).

Lipid rafts are difficult to visualize with the conventional imaging techniques such as confocal microscopy because of their small size. However, some raft markers or fluorescent probes such as 6-acyl-dimethylaminonapthalene can be used to monitor changes of the lipid microenvironments [503]. For some type of rafts (i.e. caveolae), immunogold electron microscopy can be used for direct visualization [503].

7.1.2 Caveolae and caveolin

Caveolae are 50–100-nm invaginations of the plasma membrane in many cell types that are biochemically indistinguishable from lipid rafts (Fig. 7.2). GPI and cholesterol are rich in caveolae. Proteins called caveolins are also abundantly present in the caveolae. There are three different isoforms of caveolins (caveolin-1, -2, and -3). Caveolin-1 and -2 are expressed in many different tissues, whereas caveolin-3 is mostly expressed in muscle tissue, particularly in cardiac myocytes [504-506]. Caveolae and caveolin are involved in such different cellular processes as cell adhesion, cholesterol transport and homeostasis, vesicle trafficking, and signal transduction. Lipid rafts are dynamic assemblies of cholesterol and sphingolipids in the plasma membrane, and caveolae can be viewed specialized lipid rafts or derivatives, because the caveolins involved in their biogenesis are composed of raft-derived components. There are some differences between rafts and caveolae, such as the way either transports cholesterol [507, 508] or performs endocytosis [509], potocytosis [510], and signal transduction [511-514]. The formation of caveolae is associated with the presence of the caveolin-1 protein; indeed, they cannot form without caveolin-1 [515-517]. Caveolar membranes are biochemically similar to other rafts in that they are also resistant to solubilization by Triton X-100 at 4°C, contain

sphingolipids and cholesterol, and have a light, buoyant density.

Caveolin forms hairpin-like structures with cytoplasmic N- and C-termini [518] (Fig. 7.2). The caveolin proteins have an important caveolin scaffolding domain (CSD), which mediates the interaction with various other proteins [519] (Fig 7.2). Caveolins can act as scaffolding proteins recruiting signaling components to keep highly localized and efficient signaling. It is found that some GPCRs, protein kinases A, B and C, steroid hormone receptors, MAP Kinase (p42/44 MAPK), receptor- and non-receptor tyrosine kinases, PI3K, and a range of other signaling molecules localize to caveolae [520, 521]. In addition, downstream molecules including PLC isoforms, $G\alpha_s$, $G\alpha_i$, $G\alpha_q$, $G_{\beta\gamma}$ and some adenylyl cyclase have been detected in caveolae [522]. The caveolin scaffolding domain plays important roles in the formation of these macromolecular signaling complexes. Additionally, other scaffolding proteins such as membrane associated guanylate kinase proteins may also mediate protein-protein interactions within caveolae.

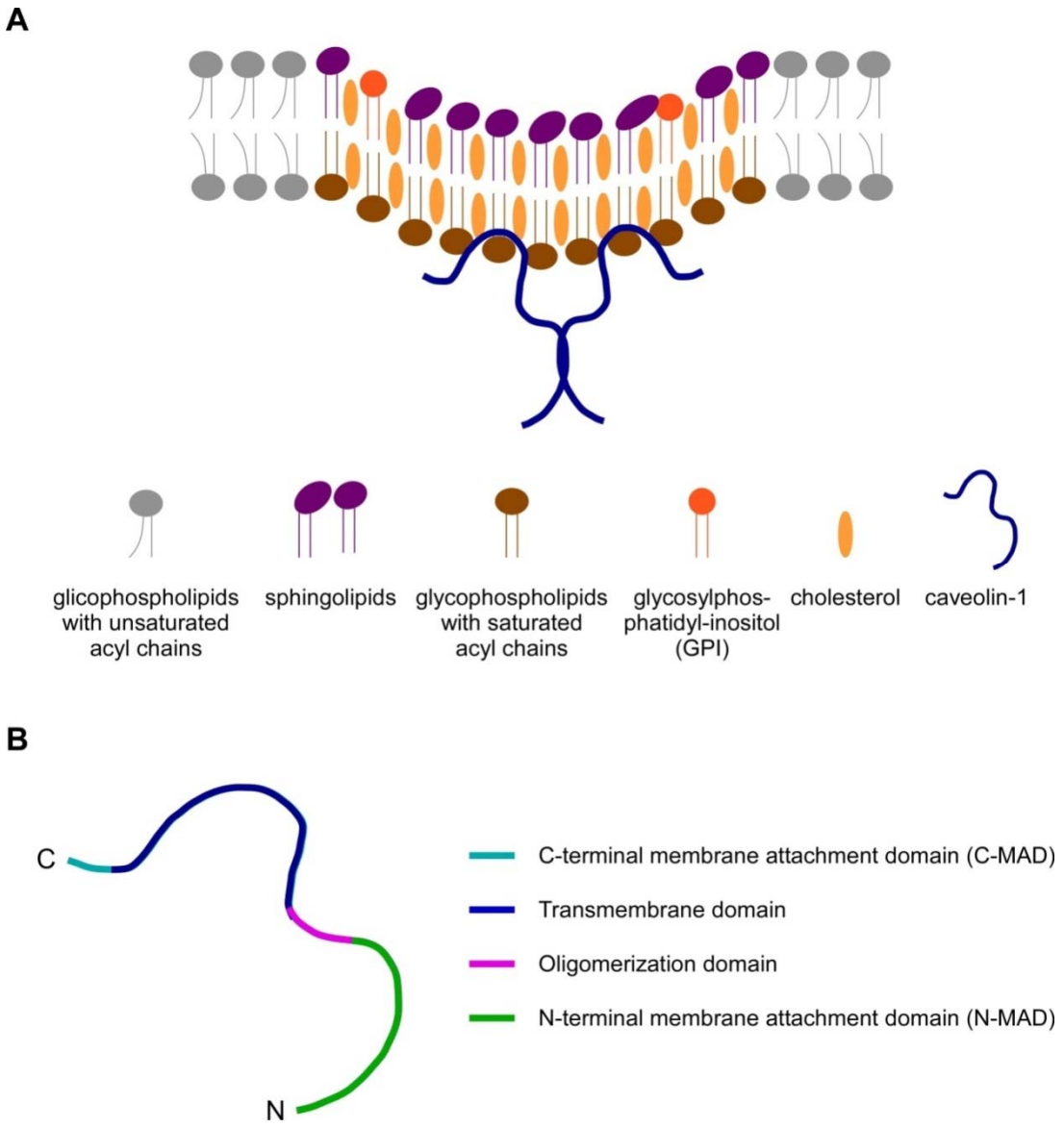

Figure 7.2 Model for the organization caveolae in the plasma membrane. (A) Caveolae is formed from lipid rafts by self-associating caveolin molecules making a hairpin loop in the membrane. The compositions of lipid bilayer from caveolae are similar to lipid rafts. Caveolin-1 exists as a homo-oligomer of ~14 to 16 monomers; a homodimer is shown in picture for clarity. Both the amino- and carboxy-terminal domains are oriented towards the cytosolic face of the plasma membrane, with a hairpin loop structure inserted within the membrane bilayer. Modified from reference [523]. (B) Structural domains present in caveolin-1. The protein is tethered to the plasma membrane via its trans-membrane (TM) domain (blue). The amino-terminal membrane-attachment domain (N-MAD, green) and C-terminal membrane-attachment domain (C-MAD, cyan) are also involved in the membrane interactions. N-MAD is called the caveolin scaffolding domain (CSD). Homo-oligomerization is mediated by 40-amino acids known as the oligomerization domain (OD; purple) [524].

Caveolae provide a platform for regulation of various membrane proteins. Thus, the α-subunit of Na^+/K^+-ATPase has two highly conserved putative caveolin-binding motifs and localize to caveolae [525]. TRPC-1, -3 and -4 are enriched in caveolae and caveolin-1 can directly regulate TRP channel function, particularly the trafficking [526]. MβCD treatment decreases colocalization of caveolin-1 and TRPC1 and prevents Ca^{2+} influx through the latter [527]. Additionally, some voltage- gated K^+ channels are also localized in caveolae and play a major role as modulators of cellular excitability. For example, voltage-gated K^+ channel Kv2.5 is localized to caveolin-rich lipid rafts; depletion of membrane cholesterol influences the functional activities of Kv2.5 [528]. In fibroblasts, the voltage-gated K^+ channel Kv1.5 subunit colocalizes with caveolin-1 on the cell surface. These findings imply that alteration of caveolae and/or caveolin can shift the localization of the channels, thereby altering their functional activity.

7.1.3 Ion channels and lipid rafts

Many ion channels have been reported to function within lipid microdomains. Examples include voltage-gated K^+ channels; CNG channels; TRP channels; P2X receptors; and Cl^- channels [503]. Although there is no direct evidence to suggest that Na^+ channels are located in detergent-insoluble fractions, studies have shown that caveolin-3, Na^+ channels, and $G\alpha_s$ constitute the microdomain in ventricular myocytes [529-532].

VGCC is another type of ion channel that has been found in lipid rafts in some cells. It was, for instance, found that L-type Ca^{2+} channels co-localize with RyR into caveolae, which constitute a microdomain in cardiomyocytes and provide an efficient Ca^{2+}-signal producing excitation-contraction coupling [533, 534]. Moreover, the α1 subunit of the L-type Ca^{2+} channel is found in Triton X-100 insoluble caveolin-enriched fractions in smooth muscle and atrial myocytes [535, 536].

It has been suggested that IP_3R co-precipitates with ankyrin-B and CD44, proteins which are known to concentrate in caveolin-rich detergent-insoluble fractions [537]. All this suggests that plasma membrane lipid rafts can participate in junctional microdomains with intracellular organelles such as the ER.

Many members of various K^+ channels families have been shown to localize to lipid rafts. Thus, Kv2.1 and Kv1.5 localize to cholesterol-enriched microdomains in rat cardiomyocytes or mouse L-cells stably expressing either rat Kv1.5 or Kv2.1 channels [528, 538]. Treatment with MβCD induced a hyperpolarizing shift of Kv2.1 inactivation and Kv1.5 activation and inactivation, suggesting that the plasma membrane environment is important for channel function. Kv1.4 channels have also been found in detergent-insoluble fractions of neurons and HEK293 cells [539]. Kv4.2/4.3 mediate the Ca^{2+}-independent transient outward K^+ currents. These channels were also found in lipid rafts in rat brain and transfected HEK293 cells [539]. The inwardly rectifying K^+ channels (Kir3 and Kir2) appear to localize into detergent insoluble membrane fractions [540]. Increased plasma membrane cholesterol decreases Kir2.1 current density, whereas cholesterol-depletion increases current density. ATP sensitive K^+ channel, Kir6.1, is also expressed in lipid rafts. In rat aortic smooth muscle cells, Kir6.1 colocalizes with adenylyl cyclase in caveolin-enriched low-density membrane fractions [533]. Caveolin co-immunoprecipitates with Kir6.1 from arterial homogenates [541]. Treatment with MβCD reduces Kir6.1 current. Recently, Ca^{2+}-activated K^+ channels have also been shown to interact with caveolin and to localize into lipid rafts [542].

Lipid rafts also modulate ion channels by providing an environment for assembly of macromolecular signaling complexes [543]. Signaling proteins such as GPCRs, various classes of G proteins, adenylyl cyclase, PKC, nitric oxide synthase, tyrosine kinases, H-ras and MAPKs [503, 520] can be recruited to lipid microdomains. Additionally, scaffolding proteins, like caveolin or membrane-associated guanylate kinase proteins such as postsynaptic density

protein-95 (PSD-95) and synapse-associated protein-97 (SAP97), are able to bind to ion channel or several other signaling proteins in order to organize these interacting proteins within the lipid rafts [539, 544]. For example, in cardiac myocytes the β_2-adrenergic pathway includes caveolin-3, $Ca_v1.2$ L-type channels, and a number of other signaling molecules. Disruption of lipid rafts abolishes the response of $Ca_v1.2$ to β_2-adrenergic stimulation [545, 546]. SAP97, a membrane-associated protein with PDZ-domain, interacts with Kv1.5 channels in lipid rafts, and this interaction affects activation and inactivation of Kv1.5 [544, 547, 548]. PSD-95 and voltage-gated K^+ channel-interacting protein (KChIP) also interact with Kv1.5 channels within lipid rafts [549]. PIP_2 has also been found in caveolae and can regulate numerous ion channels [529, 550, 551]. The PIP_2 modulation of ion channels is beyond the scope of this brief introduction.

7.2 Aims

In chapter 6 we found that cavoelin1 interacts with B_2R and PAR2 in small DRG neurons. Therefore I hypothesize that lipid rafts may play some a role in the formation of ANO1-containing junctional microdomains. As evidenced in the introduction to this chapter, lipid rafts often serve as platforms for signal transduction; in many cases these rafts form membrane microdomains. Experiments conducted in this chapter were designed to determine if ANO1 and its signaling complex also reside in the lipid rafts in small DRG neurons. We also tested if such lipid raft-based microdomains facilitate ANO1 activation by Ca^{2+}. Finally, we tested the physiological significance of these microdomains.

7.3 Results

7.3.1 B_2R, PAR2 and ANO1 are located in cholesterol-rich lipid rafts

Informed by the experiments reported in previous chapters, we hypothesized that GPCR, ANO1 and IP_3R1 may be in close proximity in small DRG neurons. We further inferred that the plasma membrane part of this signaling complex could be assembled within lipid rafts. To investigate whether GPCR and ANO1 are colocalized in cholesterol-rich lipid rafts, we isolated lipid rafts from DRG tissue using gradient sucrose ultracentrifugation after solubilization of membranes in buffer containing TritonX-100 (see Chapter 2). The gradient fractions were analyzed by immunoblotting. As shown in Fig. 7.3A, caveolin-1 was distributed mostly in the detergent-insoluble, low-buoyant density fractions, fractions 4 to 6. ANO1, PAR2, and B_2R proteins were also distributed mostly into these same fractions.

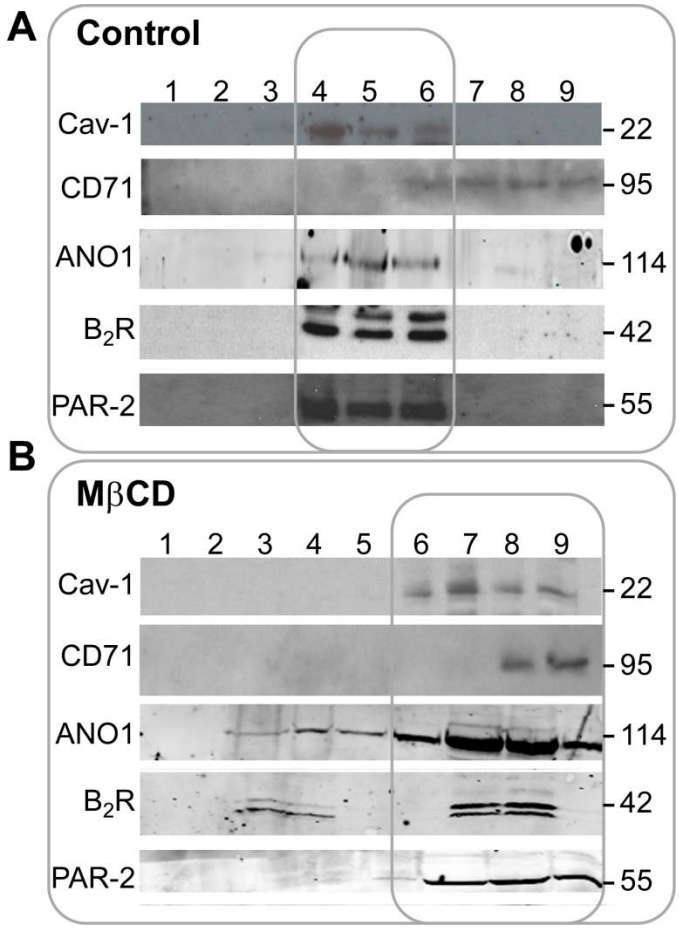

Figure 7.3 ANO1 localizes to lipid rafts in DRG neurons. (A) Sucrose density gradient fractionation of plasma membranes isolated from rat DRG revealed the enrichment of caveolin-1 containing membrane fractions with ANO1, B_2R and PAR2. (B) Disruption of lipid rafts with 50 mM MβCD for 2 hours disrupts the localization of ANO1, B_2R and PAR2. The gels represent results of 3 independently performed experiments. From [Jin, X., et al., Sci Signal, 2013. 6(290): p. ra73.] Reprinted with permission from AAAS.

We used non-raft marker CD71 as a negative control; it localized in high density fractions (7, 8, and 9). However, when DRG tissue was treated with 50 mM MβCD for 2 hr, the ANO1, PAR2, and B_2R peaked in fractions 7, 8 and 9 (heavier fractions). The direct effect of MβCD on cells is extraction of cholesterol from the outer layer of plasma membranes. Atomic force microscopy revealed that MβCD treatment resulted in a reduction in size and eventual dissolution of lipid rafts in a time-dependent manner [552].

7.3.2 Disruption of lipid raft has an effect on DRG excitability

To examine the physiological roles of ANO1/IP_3R/GPCR microdomains located in lipid raft/caveolae, we studied the effects of cholesterol depletion and lipid raft/caveolae disruption on CaCC and on DRG excitability. As shown in Table 7.1 and Fig. 7.4A and B, pretreatment of DRG with 10 mM MβCD analog α-cyclodextrin (αCD), which cannot bind cholesterol [553] for 30 min had no effect on PAR2-PL or BK-induced CaCC (50% *vs*. 46% responsive cells in BK-treated group, 50% *vs*. 53% in PAR2-PL treated group), while MβCD treatment markedly reduced the ability of PAR2-PL or BK to induce CaCC as compared to control conditions (6.7% *vs*. 46% responsive cells in BK-treated group, 6.3% *vs*. 53% in PAR2-PL treated group).

In a series of current clamp experiments we investigated the effect of cholesterol depletion on small DRG neuron excitability. Interestingly, MβCD treatment dramatically increased excitability of small DRG neurons. As shown in Fig. 7.6 and Table 7.1, in control conditions most of DRG neurons only fired one AP in response to 600 pA of depolarizing current injection, and only 3 neurons fired multiple APs. αCD had no effect on DRG AP firing rate, while MβCD treatment markedly increased number of cells firing multiple APs. Thus, in half of the MβCD-treated small DRG neurons (11/22), multiple APs were recorded (Fig. 7.5A). Importantly, when MβCD-treated neurons were recorded under conditions in which intracellular Cl^- was replaced with acetate (and, thus, Cl^- channel opening would result in hyperpolarization, not depolarization), only 3/19 neurons fired multiple APs, indicating that no increase in the proportion of hyperexcitable neurons occurred (Fig. 7.5B, Table 7.1) under these conditions. The latter experiment strongly suggests that the MβCD-induced hyperexcitability depends on the Cl^- conductance.

Table 7.1 Summary of the effects of cholesterol extraction on the coupling of CaCC activity to BK- and PAR2-induced Ca^{2+} release, and to VGCC-mediated Ca^{2+} influx. Shown are proportions of small DRG neurons that displayed properties listed in the right column; data are presented as X/Y where X is number of responsive cells and Y is a total number of neurons tested.

Condition: / **Property:**	**No treatment (Control)**	**MβCD 10 μM**		**αCD 10 μM**
BK-induced cytosolic Ca^{2+} transients	18/31	13/31		N/A
BK-induced CaCC current	16/35	1/15*		7/14
PAR2-PL-induced CaCC current	8/15	1/16*		8/16
CaCC tail current after VGCC activation	1/20	10/20*		1/21
Multiple AP firing	3/18	High $[Cl^-]_i$ 11/22*	Low $[Cl^-]_i$ 3/19$^{\#}$	2/15$^{\&}$

*significantly different from control;

$^{\$}$significantly different from MβCD

$^{\#}$significantly different from high $[Cl^-]_i$;

$^{\&}$significantly different from MβCD with high $[Cl^-]_i$; χ^2 with $p < 0.05$

From [Jin, X., et al., Sci Signal, 2013. 6(290): p. ra73.] Reprinted with permission from AAAS.

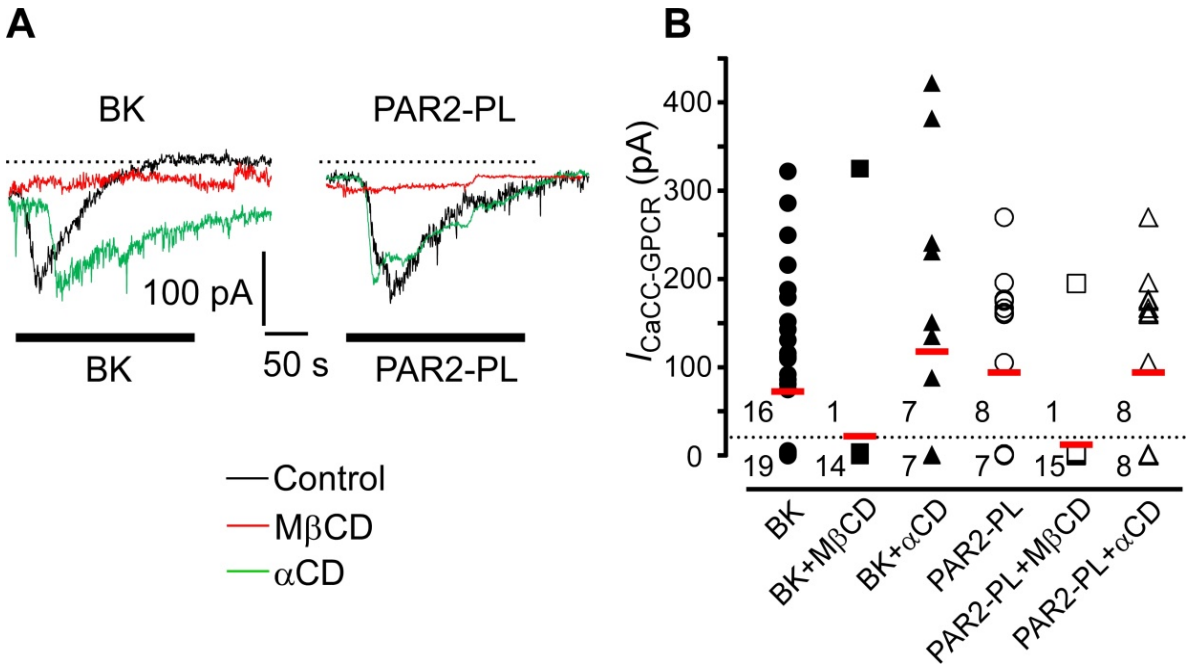

Figure 7.4 Effect of MβCD on the GPCR-induced CaCCs in small DRG neurons. (A) DRG neurons were pretreated with 10 mM MβCD or its analogue that cannot bind cholesterol, αCD, for 30min. Whole-cell patch clamp recordings were performed on the pre-treated neurons and the responses to 1 μM BK or 1 μM PAR2-PL were analyzed. Shown are exemplary current traces. (B) Scatter plot summarizing the experiments like these shown in (A). From [Jin, X., et al., Sci Signal, 2013. 6(290): p. ra73.] Reprinted with permission from AAAS.

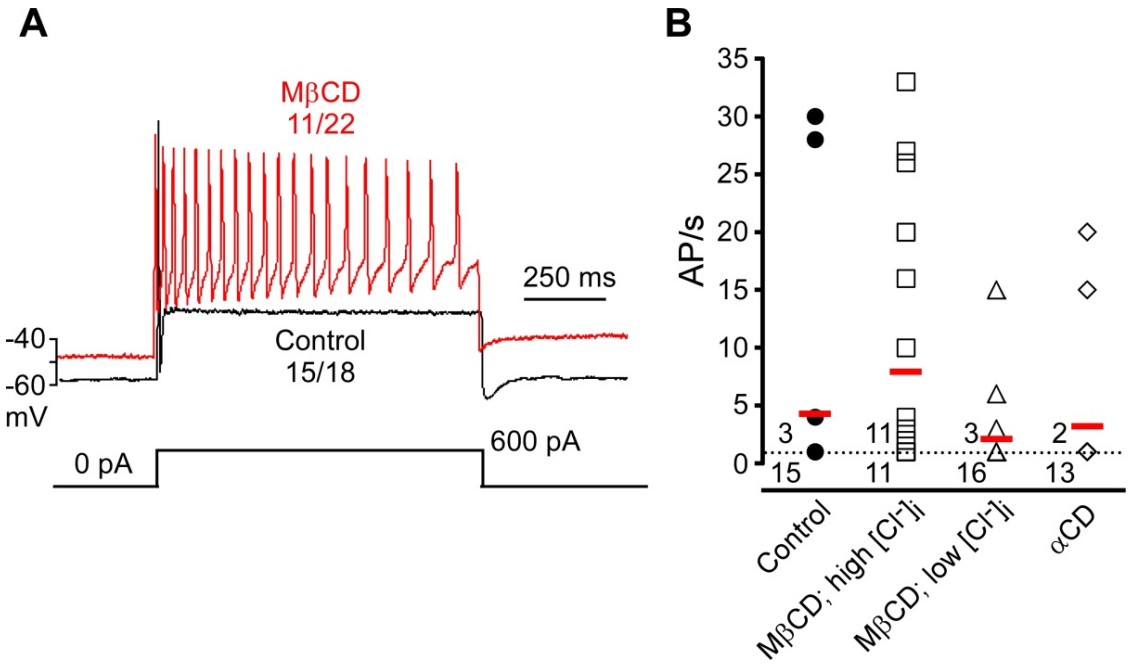

Figure 7.5 MβCD treatment markedly increases DRG excitability. (A) Exemplary AP traces recorded from small DRG neurons in current clamp mode upon injection of 600 pA depolarizing current; control neuron (black trace), MβCD treated neuron (10 mM MβCD for 30 min; red trace). (B) Scatter plot showing number of APs per 1s current injection in various treatment conditions: Control (untreated); MβCD with high intracellular Cl^- concentration; MβCD with low intracellular Cl^- concentration and αCD (10 mM for 10 min). From [Jin, X., et al., Sci Signal, 2013. 6(290): p. ra73.] Reprinted with permission from AAAS.

In experiments reported in previous chapters, we found that VGCC were mostly unable to activate CaCC in small DRG neurons. On the other hands, MβCD treatment dramatically reduced coupling of GPCR to CaCC (Fig. 7.4 and Table 7.1). Therefore we tested if MβCD affected coupling between VGCC and CaCC. As before, we have used double-pulse voltage protocol. Surprisingly, after 10 mM MβCD treatment for 30 min, 50% of the small DRG neurons showed an inward tail current upon repolarization to -80 mV after the first voltage pulse, indicating activation of CaCC (Fig. 7.6). This is a significant increase in percentage of neurons displaying such tail currents compared with the control conditions (5%). The amplitude of the VGCC current was not affected by the MβCD treatment (580 ± 85 pA in control compared to 522 ± 62 pA in MβCD-treated group). Treatment of the neurons with the

MβCD analog αCD, did not significantly change the coupling of CaCCs to VGCCs; the proportion of neurons in which Ca^{2+} influx through VGCCs induced CaCC tail currents (5%) was not different from that seen with untreated neurons and was significantly lower than such proportion in the MβCD-treated group (Fig. 7.6B, Table 7.1).

To confirm this effect of MβCD we performed further imaging experiments using I^--sensitive YFP- H148Q/I152L (Fig 7.7). Application of extracellular solution in which 30 mM NaCl was replaced with 30 mM NaI caused a decrease in normalized fluorescence (F/F0) from unity to 0.77 ± 0.05 (Fig. 7.7), which was not different from the decrease observed in control, MβCD-untreated neurons (Chapter 6, Fig. 6.1; a decrease of F/F0 to 0.76 ± 0.05). However, depolarization with 50 mM KCl induced a significantly greater decrease in fluorescence in MβCD-treated neurons as compared with untreated cells: a decrease of F/F0 to 0.46 ± 0.03 (Fig. 7.7).

Having established that disruption of lipid rafts with MβCD disturbs CaCC activation in small DRG neurons, we next tested if the effect of MβCD is due to disruption of the IP_3R/ANO1/GPCR microdomain. As shown in Fig. 7.8A and C, coimmunoprecipitation experiments showed that MβCD treatment significantly decreased the interaction between IP_3R1 and ANO1, suggesting that the lipid raft is important for the proximity of the ANO1 and IP_3R1. Coimmunoprecipitation of B_2R by IP_3R1 was somewhat reduced by MβCD treatment, but this effect was not statistically significant (Fig. 7.8B). Perhaps the interaction between the B_2R and IP_3R1 in this complex has a different dependency on the lipid raft environment compared to that of ANO1 and IP_3R1.

In the next series of experiments we use PLA assay to test if MβCD treatment of DRG culture reduces the IP_3R1-ANO1 PLA signal. The Carl Zeiss software ZEN was used to automatically detect PLA puncta as local intensity maxima based on the manually set threshold which was kept constant throughout the image analysis. As shown in Fig. 7.9, MβCD treatment

indeed decreased the PLA abundance of the IP_3R-ANO1 puncta, indicating that the ANO1 and IP_3R1 complex was disrupted.

Since MβCD may have non-specific effects, in order to disrupt the microdomain specifically, we took an advantage of the identification of IP_3R1-interacting domains of ANO1 reported in the previous chapter. Therefore, we subcloned the C- and N-terminal hydrophilic regions and the loop between the TM2-TM3 loop of ANO1 into bicistronic pIRES-EGFP vectors and overexpressed these individually into DRG neurons. As shown in Fig. 7.10, application of 10 μM PAR2-PL to small DRG neurons evoked robust inward currents (recorded at -60 mV holding potential) when the DRG neurons were transfected with the N-terminus of ANO1 or the EGFP vector, while PAR2-PL currents were almost abolished when the DRG neurons were transfected with C- terminus or the TM2-TM3 loop of ANO1. These experiments suggest that the C- terminus or the TM2-TM3 loop of ANO1 may have disrupted IP_3R1-ANO1 coupling by a competition mechanism. Together these data suggested the existence of CaCC signaling complexes in DRG neurons that consists of (i) a plasma membrane component containing ANO1, B_2R and/or PAR2 in a cholesterol- and caveolin-1-enriched microdomain; and (ii) a juxtaposed ER region containing IP_3R1. The interactions between ANO1 and the IP_3R1 (mediated by the C-terminus and the TM2-TM3 loop of ANO1) may contribute to linking the two membranes, which is required for CaCC activation by the GPCRs.

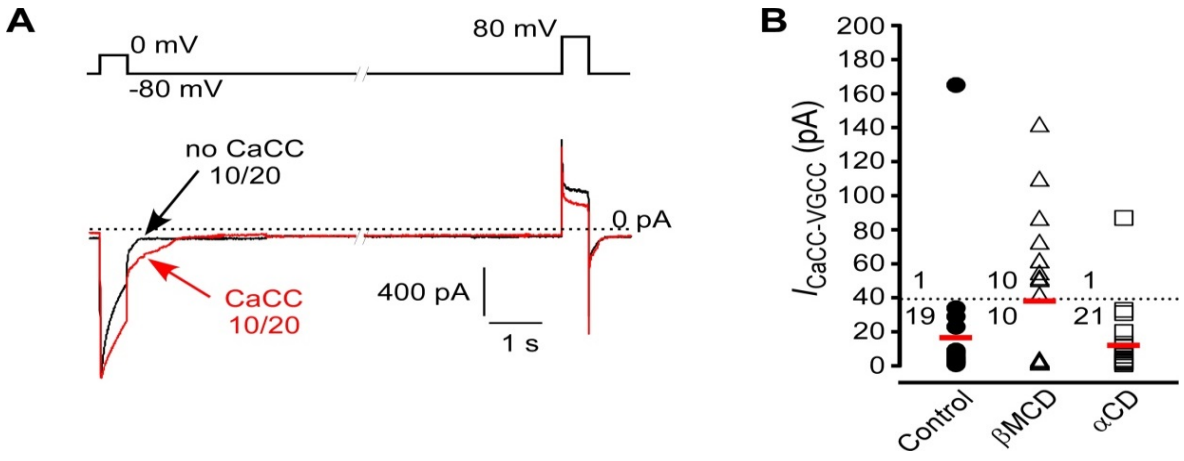

Figure 7.6 VGCC activates CaCC in small DRG neurons after MβCD treatment. (A) Whole-cell patch clamp experiments show that 50% of small DRG neurons (10/20) displayed inward tail current following the activation of VGCC by the voltage steps to 0 mV after 30 min pretreatment with 10 mM MβCD. Voltage protocol is depicted above the traces. (B) Scatter plot of all data from the small DRG neurons tested (vehicle control, 10 mM MβCD and 10 mM αCD, as labelled). CaCC ($I_{CaCC-VGCC}$) was calculated as a difference in peak tail current amplitudes after the depolarizing pulses with and without Ca^{2+} influx; neurons were considered as not displaying activation of CaCC by VGCC when the resulting amplitude was below 40 pA. Red horizontal bars represent mean values of all neurons tested in each group. Numerals above and below the dotted line represent number of neurons with and without VGCC-induced CaCC, respectively. From [Jin, X., et al., Sci Signal, 2013. 6(290): p. ra73.] Reprinted with permission from AAAS.

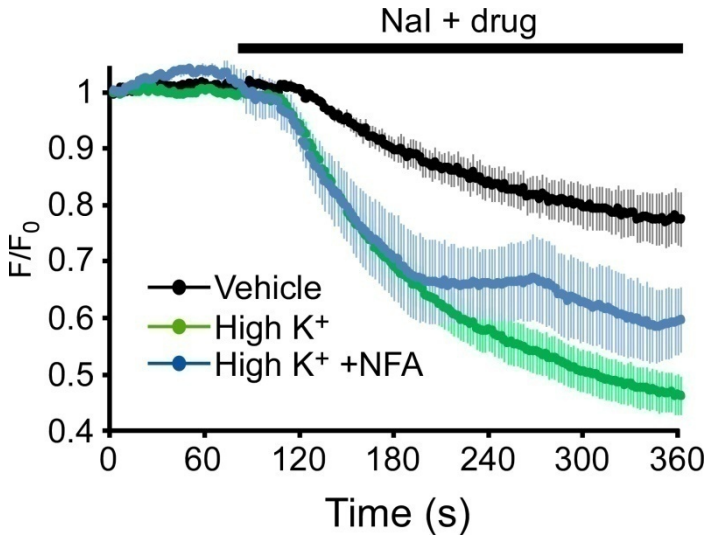

Figure 7.7 Mean time courses from experiments carried out with the EYFP-H148Q/I152L assay on small DRG neurons after MβCD treatment. Effect of MβCD treatment on I^- influx induced by depolarization with 50 mM KCl in DRG neurons. Averaged time courses of normalized fluorescence (F/F_0) of H148Q/I152L EYFP-transfected neurons perfused with 30 mM NaI containing extracellular solution either alone (vehicle, n = 7) or in neurons treated with MβCD (10 mM, 30 min) and then stimulated with 50 mM KCl (High K^+, n = 10) or 50 mM KCl and NFA (100 μM) (High K^+ +NFA, n=5). From [Jin, X., et al., Sci Signal, 2013. 6(290): p. ra73.] Reprinted with permission from AAAS.

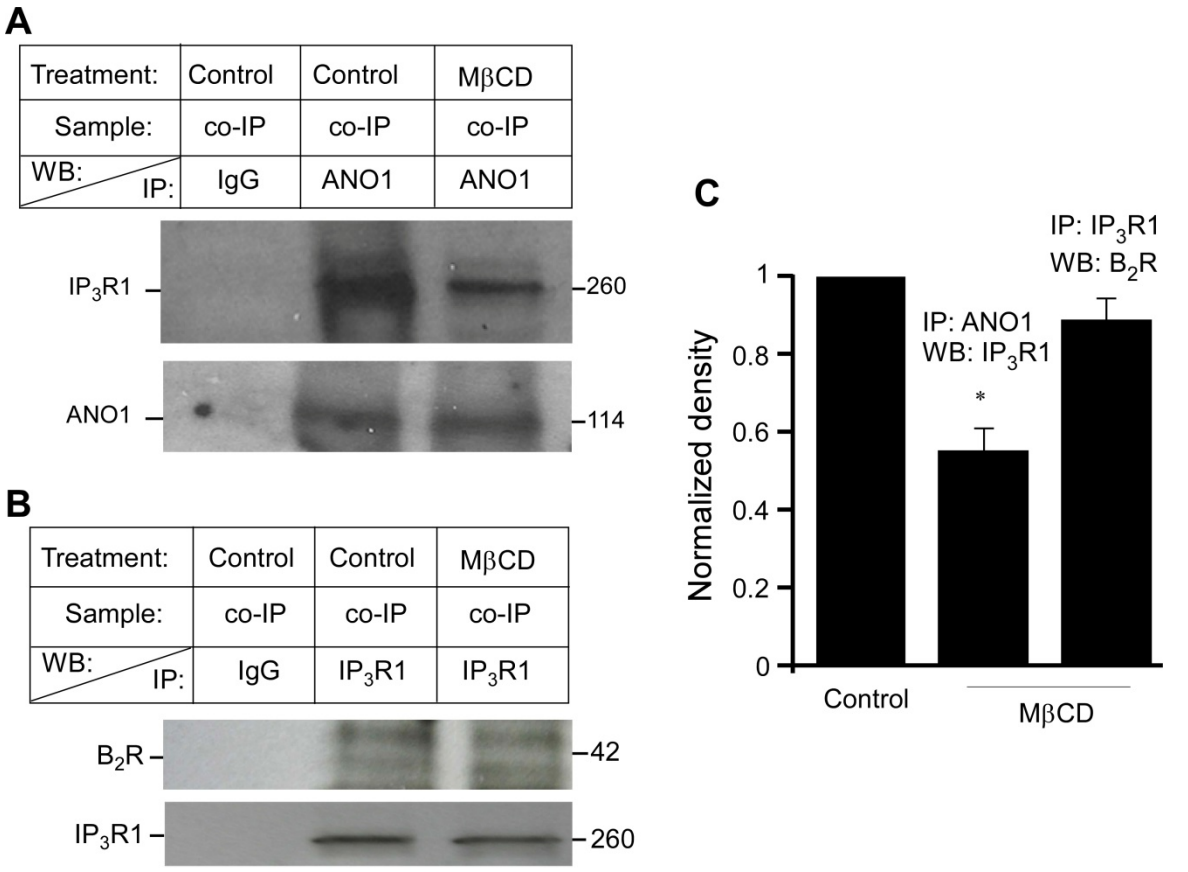

Figure 7.8 MβCD treatment disrupts co-immunoprecipitation of ANO1 with IP_3R1. (A) Using of IP_3R1 by the antibody against ANO1 from DRG lysates was reduced when lysates were treated with MβCD. "IP" and "WB" indicate the antibodies used for immunoprecipitation and Western blotting respectively. Control immunoprecipitations were performed using goat IgG. (B) Experiment similar to (A), but the immunoprecipitation of B_2R by the antibody against the IP_3R1 was tested instead, labeling and conditions as in (A). (C) Densitometry of ANO1/IP_3R1 signals was performed using Nikon Elements 3.2. Bar chart summarizes densitometry data from three independent experiments. Mean optical densities from identical areas around each coimmunoprecipitation band–data from the experiments as these shown on panels (A) and (B) – were normalized to the density of the corresponding WB band (lower blots). The density of the bands in MβCD-treated samples is expressed as a fraction of control; * $p \leq 0.05$ (t-test). From [Jin, X., et al., Sci Signal, 2013. 6(290): p. ra73.] Reprinted with permission from AAAS.

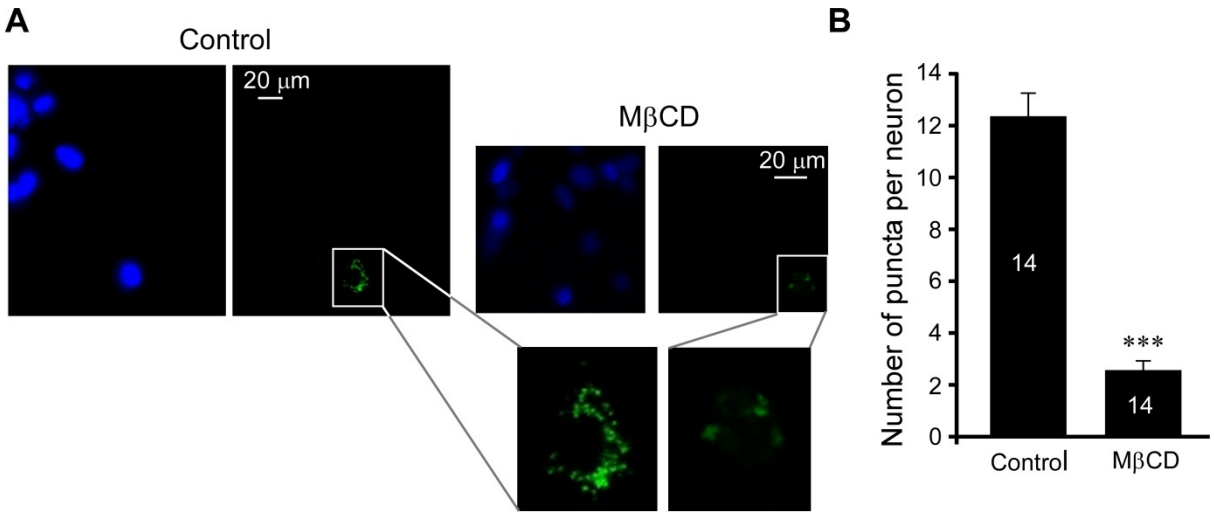

Figure 7.9 MβCD treatment decreases ANO1/IP_3R1 interaction as detected with PLA assay. (A) Detection of ANO1/IP_3R1 complexes (green puncta) in vitro after MβCD treatment (right) or control (left) in small DRG neurons; ANO1/IP_3R1 PLA staining (green), DAPI (blue). Higher magnification images of the boxed areas included. (B) Bar chart summarizes number of puncta per PLA-positive neuron (control, n = 14; MβCD, n = 14). Puncta detected as local intensity maxima in z-stacked imaging planes. Experiments were repeated at least three times. Data are presented as mean ± SEM; ***$p \leq 0.001$ (t-test analysis). From [Jin, X., et al., Sci Signal, 2013. 6(290): p. ra73.] Reprinted with permission from AAAS.

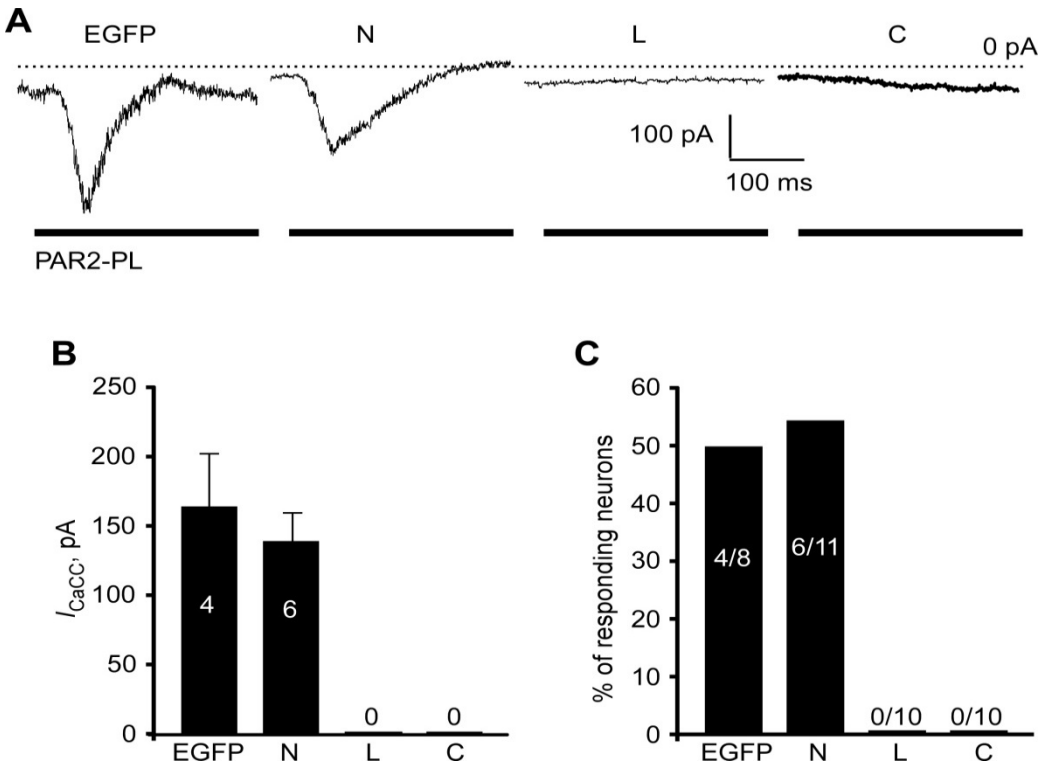

Figure 7.10 Competitive disruption of IP_3R/ANO1 complexes affects activation of ANO1 by PAR2. (A) Effect of the 3 cytosolic domains of ANO1 on PAR2-PL-induced inward currents in DRG neurons. Each ANO1 cytosolic domain was individually overexpressed in DRG neurons, and inward current was tested by patch clamp. Traces are representative recordings from cells transfected with indicated constructs. "EGFP" denotes EGFP-only transfected neurons. Periods of PAR2-PL (10 μM) application indicated by the black bars (B and C). Bar charts summarizing the current amplitudes (B) and proportions (C) of neurons displaying inward current. From [Jin, X., et al., Sci Signal, 2013. 6(290): p. ra73.] Reprinted with permission from AAAS.

7.4 Discussion

In this chapter we found that ANO1 channels in nociceptive neurons are localized to the low density membrane fractions enriched with cholesterol and caveolin-1, characteristics of lipid raft microdomains. In addition, GPCR receptors B_2R and PAR2 in whole DRG lysates were found to localize to the same membrane fractions as well. Because ANO1 has similar distribution with caveolin-1 in DRG neurons, it is likely that the ANO1 resides in caveolae or similar structures in these cells. However, I could not visualize caveolae here due to the limitation of the confocal microscopy. I also found that MβCD disrupted the ANO1 microdomain assembly because MβCD disrupted the coupling between IP_3R and ANO1 as tested with electrophysiology (no CaCC current activation by BK or PAR2-PL in MβCD-treated neurons), coimmunoprecipitation (reduced Co-IP of ANO1 and IP_3R1 after MβCD treatment) and PLA assay. Similarly, GPCR-ANO1 coupling was disrupted by overexpression of IP_3R1-interacting domains of ANO1 identified in the previous chapter. All this evidence suggests that ANO1 and GPCR are localized to lipid rafts and that this localization is important for the functional coupling between the GPCRs, IP_3R1 and ANO1 channels.

Another intriguing finding of the experiments reported in this chapter is that in many MβCD-treated neurons observed CaCC activation coupled to the VGCC activation. Thus, disassociation of the ANO1 signaling complex in a small DRG neuron resulted in a loss of functional coupling between the B_2R/PAR2 and the ANO1 and gain of coupling between ANO1 and VGCCs.

Since CaCC activation is excitatory in nociceptors, and potentially painful [7, 256, 366], there must be mechanisms that control coupling of Ca^{2+} sources to CaCC activation. This is particularly obvious for the case of coupling of CaCCs to VGCCs. Indeed, VGCCs are opened during AP firing, and if Ca^{2+} influx generated during this period would activate CaCCs, this may generate further depolarization and, in turn, more APs [162]. Our current clump

experiments show that most small-diameter DRG neurons fire single APs in control conditions, but MβCD treatment resulted in overexcitable neurons that fire multiple APs. Thus, we hypothesize (see schematic shown in Fig. 7.11) that ANO1 and relevant GPCRs in nociceptive sensory neurons are localized to signaling complexes assembled within lipid rafts at the plasma membrane-ER junctions. The complexes are tethered to the ER in a way that ensures close proximity between ANO1 and IP_3Rs in order to confer efficient activation of the channel by the Ca^{2+} release through the latter. Such assembly may also protect ANO1 from the ambient Ca^{2+} (hence the poor coupling to VGCC). This hypothesis could explain why Ca^{2+} influx via the VGCCs is mostly unable to activate ANO1 in these neurons. It also could provide an explanation to the data reported in Chapter 3, showing that in most small-diameter DRG neurons dialysis of up to 10 μM free Ca^{2+} through the patch pipette was unable to activate CaCC.

Yet, this poor accessibility of ANO1 to global Ca^{2+} (e.g., in this case, Ca^{2+} influx from VGCC or through the patch pipette) is intriguing. While obviously more research is needed to clarify this issue, there are few considerations that may provide an explanation.

i) As said in previous chapters, endogenous Ca^{2+} in cells is buffered by multiple Ca^{2+} binding proteins (e.g. CaM). Such buffering shortens the range of intracellular Ca^{2+} signals.

ii) ANO1 channels have rather low Ca^{2+} affinity, especially at the negative voltages that characterize the resting membranepotential of nociceptive DRG neurons (~ -60 mV [306]) and at such potentials the Ca^{2+} EC_{50} for ANO1 is ~3-5 μM [202, 205]; global Ca^{2+} does therefore not normally reach such levels in cells.

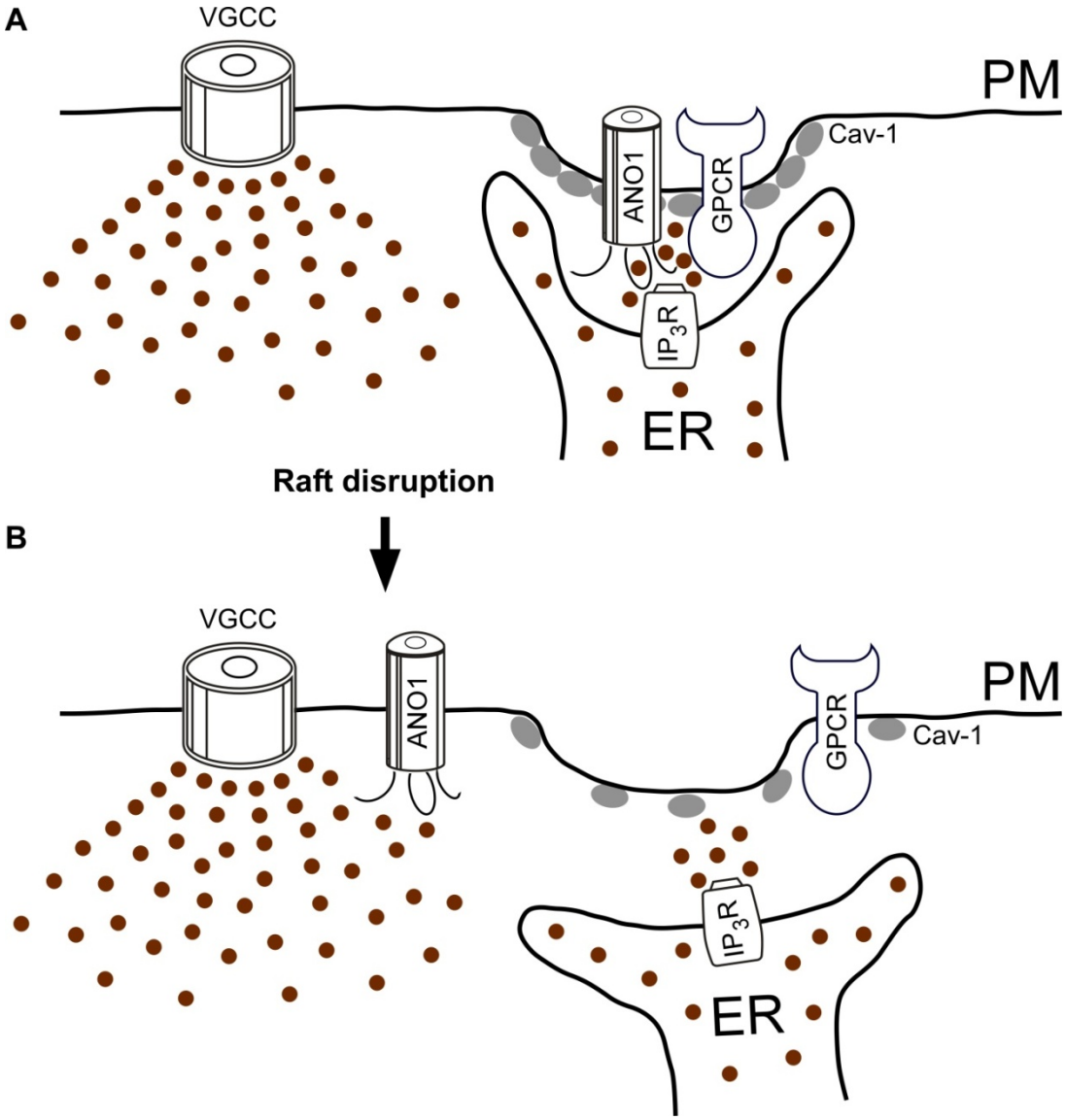

Figure 7.11 Simplified hypothetical scheme of the ANO1-containing junctional signaling microdomain in a nociceptive sensory neuron. (A) Control conditions; (B) Proposed rearrangements after the lipid raft disruption. From [Jin, X., et al., Sci Signal, 2013. 6(290): p. ra73.] Reprinted with permission from AAAS.

iii) Finally, when this thesis was already in a revision stage, a crystal structure of a prokaryotic anoctamin was published [554]. Among several revelations of the structure (including a revised membrane topology of anoctamins which, according to the structure, have ten, not eight TMDs), is the Ca^{2+} binding site of anoctamins. The Ca^{2+} binding site is formed by several aspartate and glutamate residues of transmembrane helices 6, 7 and 8 and, surprisingly, it is situated well within the hydrophobic core of the inner leaflet of the plasma membrane. This feature can explain not only the intrinsically low Ca^{2+} sensitivity of ANO1, but also the poor accessibility of its Ca^{2+} binding site to cytosolic Ca^{2+}. Indeed, it may be that a direct association of ANO1 with the pore vicinity of the IP_3R creates a "dedicated" pathway for Ca^{2+} from the ER to the ANO1 Ca^{2+} binding site. One can further speculate that the accessibility of the Ca^{2+} binding site of ANO1 may depend on the properties and composition of the plasma membrane. For example, ANO1 channels localised to lipid rafts (which are more tightly packed membranes as compared to the non-raft regions) may have more restricted accessibility to Ca^{2+} as compared to non-raft-localized channels. Clearly further research is needed to test this hypothesis.

Another study has demonstrated that, like DRG neurons, ANO1 is enriched within the caveolin-1 containing lipid rafts in murine portal vein myocytes [555]. MβCD treatment resulted in membrane re-distribution of ANO1 and potentiation of ANO1 activation by voltage (at $[Ca^{2+}]_i = 0.5$ μM). Thus, similarly to small DRG neurons, lipid raft-localized microdomains in SMCs may play a dual role: provide a platform for coupling of ANO1 to intracellular stores, and protecting ANO1 from "'global" (i.e., incoming from VGCC) cytosolic Ca^{2+}. Lipid raft disruption in SMCs may expose ANO1 channels to global Ca^{2+}, making them more easily activated. It has to be noted that in murine portal vein myocytes ANO1 resides in less buoyant

fractions as compared to DRG. It is possible that the membrane distribution of ANO1 has tissue-specific differences. Another difference between the study of Sones and colleagues and the present work is that they used lower concentration of MβCD (3 mg/ml) and shorter incubation times (15 min) to treat mouse portal vein cells or portal veins. Here we used 10 mM MβCD for 30 min in the acute experiments and 50 mM for 2 hours in biochemical experiments with native DRG tissue (the higher concentration and incubation time in the latter case is due to the reduced penetration of the reagent in the case of the whole ganglia treatment). I found the concentrations of MβCD that we used did not significantly affect the distribution of a non-lipid raft marker CD71, which was similar to the results reported by Sones and colleagues. Other groups also used 50 mM or higher concentrations of MβCD to treated cells or tissues [556-559]. However, given the possible non-specific effects of cyclodextranes, it is important in the future study to design a more specific ways to disrupt lipid rafts. In this study I used competition peptides (Fig. 7.10) to disrupt ANO1/IP_3R1 complexes more specifically and the results of these experiments are consistent with that where MβCD was used for raft disruption. Moreover, for most MβCD experiments I have performed αCD controls.

In some ways ANO1 channels are similar to the Slo1 Ca^{2+}-activated K^+ channels; both channel types have rather low Ca^{2+} sensitivity and, thus, need to localize closely to the source of Ca^{2+}. Both channels also respond to Ca^{2+} and voltage. In some cells, Slo1 channels were shown to form protein complexes with different Ca^{2+} sources [560]. Interestingly, recent studies have shown that Slo1 channels localize to lipid rafts and couple with IP_3R to ensure their activation inresponse to IP_3-mediated Ca^{2+} release in glioma cells [491]. Thus, while belonging to different protein families, both channels may utilize similar coupling mechanisms.

Chapter 8. Conclusions, General Considerations and Future Directions

The main conclusions of the present study are as follows:

1) In small, TRPV1-expressing (presumed nociceptive) DRG neurons, B_2R, PAR2, cavoelin-1, IP_3R and ANO1 constitute a local Ca^{2+} microdomain and more specifically, an organization that generates spatially discrete local Ca^{2+} signals for activation of ANO1. The sensitivity of ANO1 to global $[Ca^{2+}]_i$ changes is poor, (see Fig.7.11 in the previous chapter) making topological provisions for precisely localized delivery essential.

2) The ER-localized IP_3R may be closely coupled to ANO1, forming part of a theoretical ER–PM (plasma membrane) complex. At least in part this coupling is supported by physical interactions between the C terminus and the first intracellular loop of ANO1 and IP_3R1 (even though it is not yet clear that this interaction is direct). Such junctions may form a diffusionally restricted intervening space that prevents Ca^{2+} from freely diffusing elsewhere into the cytosol, generating locally high enough concentration for activation of poorly Ca^{2+}-sensitive ANO1. At the same time, such junctional microdomains may also shield ANO1 from distal cytosolic Ca^{2+} signals (Fig. 7.11A).

3) The interaction of ANO1 with IP_3R1 and the ability of the local Ca^{2+} signals to stimulate ANO1 activity were lost when lipid microdomains were chemically disrupted. In contrast, ANO1 became receptive to global Ca^{2+} signals, particularly to the Ca^{2+} influx from VGCC, in the absence of lipid rafts. I propose that lipid raft disruption caused a disturbance to the ANO1 signaling complex (Fig. 7.11B) such that the ER Ca^{2+} release sites were no longer close enough to the low-Ca^{2+}-affinity ANO1 channels to supply a sufficient amount of Ca^{2+} to activate the channel. In turn, some delocalized ANO1 channels gain proximity to VGCCs (both of these channels reside within the plasma membrane) when lipid rafts are disrupted and become susceptible to activation following VGCC opening.

4) Disruptions of lipid rafts increases excitability of small-diameter DRG neurons, an effect that depends on the Cl^- channel activity and, thus, is likely to reflect the "acquired" sensitivity of ANO1 channels to global Ca^{2+} signals.

One interesting and important question is the physiological and/or pathophysiological function of this preference of ANO1/CaCC in coupling to a particular Ca^{2+} source in a nociceptive neuron. I speculate that if CaCC were coupled to global Ca^{2+} signals, e.g. through VGCC activation, then a positive feedback loop would be created in which CaCC would induce depolarization which would induce firing of APs and activation of VGCC. That, in turn, would further activate CaCC and cause a self-sustaining depolarization cycle, and a nociceptive neuron firing all the time. This is obviously not a desirable scenario for a nociceptive neuron as it would become a source of constant pain.

While the present work revealed the existence of ANO1-containing junctional microdomains, the exact set-up of these microdomains remains to be elucidated. The peptide competition experiments in which I used three different cytosolic fragments of ANO1 not only confirmed that C terminus and the TM2-TM3 loop of ANO1 interacted with IP_3R1, but also provided a strong evidence that ANO1/IP_3R1/GPCR microdomains are required for ANO1 activation. It is tempting to further speculate that the physical interaction of ANO1 with the IP_3R1 is necessary for delivery of Ca^{2+} to the ANO1 Ca^{2+} binding site which, according to the crystal structure of the fungal ANO1 orthologue [554], is hidden within the lipid bilayer andis therefore relatively inaccessible from cytosol.

My experiments cannot distinguish whether ANO1-IP_3R1 interactions are direct or if additional scaffolding proteins are necessary. Scaffolding proteins play important roles in many signaling pathways. Firstly, they can interact with multiple proteins, tethering them into complexes [561]. Secondly, scaffolding proteins help the signaling components to localize to a specific area in the cell such as the plasma membrane, the nucleus and the Golgi [562]. There

are many different scaffolding proteins such as Spinophilin, NLRP, Pellino, Homer, AHNAK-1, KSR, MEKK1, BCL-10 and many others. In particular, the Homer protein family has been shown to play an important role in Ca^{2+} signaling as it interacts with IP_3Rs and the proteins that are targeted by ER Ca^{2+} release [563]. For example, it has been found that Homer links the glutamate receptors with IP_3Rs in the ER of neurons [564]. Such scaffolding is necessary for signal transduction, synaptogenesis and receptor trafficking [565]. Importantly, Homer proteins are important for assembly of signaling complexes in peripheral sensory neurons [566]. Therefore, I hypothesized that Homer protein may also be involved in formation of ANO1-containing microdomains. Although this is still a hypothesis, in a preliminary experiment I used the antibody against ANO1 to immunoprecipitate the total proteins from native DRG tissue to try to detect the presence of the Homer1b/c presence. I found the ANO1 antibody was able to immunoprecipitate with Homer1b/c (Fig. 8.1); this preliminary data may suggest that Homer1b/c is also involved in the assembly of ANO1-containing signaling complexes in nociceptive neurons. Clearly, however, further experiments are needed to verify and further test this hypothesis.

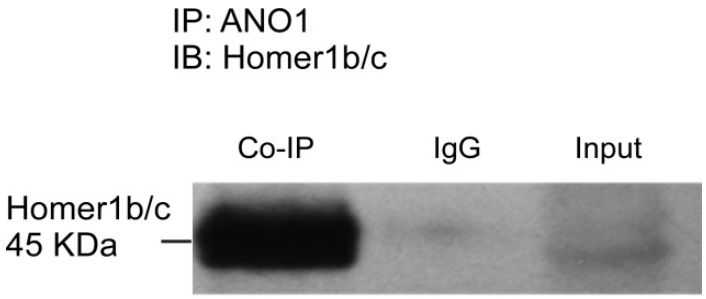

Figure 8.1 Homer1b/c interacts with ANO1. Immunoprecipitation of Homer1b/c by an antibody against ANO1 from the lysates of whole DRG ganglia of four rats. "IP" and "IB" indicate the antibodies used for immunoprecipitation and Western blotting respectively. Control immunoprecipitations were performed using goat IgG.

There may be further components and interactions within the ANO1-containing junctional microdomains which are at present unknown. Such large protein complexes can be supported by cytoskeleton. Indeed, interaction of ANO1 proteins with ezrin-radixin-moesin cytoskeleton network has been reported recently [305]. Depending on the cell type, these microdomains may also contain additional relevant proteins, such as Slo1 channels in SMCs or TRPV1 channels in sensory neurons. Indeed, TRPV1 channels are also modulated by B_2R and PAR2 [365, 567]. In addition, ANO1 [256] and TRPV1 [568] are both activated by noxious heat, making functional coupling between Ca^{2+}-permeable TRPV1 and Ca^{2+}-sensitive ANO1 channels an obvious way to increase the dynamic range of temperature responses in sensory neurons. CRAC may also reside within such microdomains, as CRAC is needed to refill ER Ca^{2+} stores. Furthermore, STIM-Orai1 interactions that underlie CRAC activation may provide a structural link to the plasma membrane [569]. The list of potential candidates can be continued, indicating a large scope for further research that in order to fully elucidate the ANO1 channel's interactome.

Finally, it is still unknown if, like DRG, ANO1-containing junctional microdomains also exist in other tissues. Current literature suggests that this might be the case. For example,

it has been suggested that CaCC in smooth muscles is closely associated with ryanodine receptors [570]. Moreover, ANO1 localizes to lipid rafts in smooth muscle myocytes; and disruption of lipid rafts with MβCD results in the enhanced activation of ANO1/CaCC by voltage at relatively high intracellular Ca^{2+} concentrations (500 nM) [555] (see discussion in the previous chapter). Thus, ANO1-containing microdomains may exist in SMCs, again (like nociceptive sensory neurons), providing a mechanism for specific coupling of ANO1 to intracellular stores and protecting the channels from global Ca^{2+} changes. It is also worth pointing out that lipid rafts provide a scaffold for bringing multiple signaling complexes together. It is therefore possible that ANO1 may partner with different signaling complexes depending on the lipid raft assembly in different cell types.

In conclusion, the data presented in my thesis establish the existence of specific signaling complexes that bring together ANO1, B_2R, PAR2 and ER-localized IP_3Rs. The likely function of these complexes is to ensure the fidelity of acute inflammatory signals in nociceptive DRG neurons. But similar structures may also exist in other cell types.

Reference

1. Loeser, J.D. and R.D. Treede, *The Kyoto protocol of IASP Basic Pain Terminology.* Pain, 2008. **137**(3): p. 473-7.
2. Justins, D.M., *Chronic pain management.* Br J Hosp Med, 1994. **52**(1): p. 12-6.
3. Basbaum, A.I., et al., *Cellular and molecular mechanisms of pain.* Cell, 2009. **139**(2): p. 267-84.
4. Woolf, C.J. and Q. Ma, *Nociceptors--noxious stimulus detectors.* Neuron, 2007. **55**(3): p. 353-64.
5. Dubin, A.E. and A. Patapoutian, *Nociceptors: the sensors of the pain pathway.* J Clin Invest, 2010. **120**(11): p. 3760-72.
6. Linley, J.E., et al., *Inhibition of M current in sensory neurons by exogenous proteases: a signaling pathway mediating inflammatory nociception.* J Neurosci, 2008. **28**(44): p. 11240-9.
7. Liu, B., et al., *The acute nociceptive signals induced by bradykinin in rat sensory neurons are mediated by inhibition of M-type K^+ channels and activation of Ca^{2+}-activated Cl^- channels.* J Clin Invest, 2010. **120**(4): p. 1240-52.
8. Marchand, F., M. Perretti, and S.B. McMahon, *Role of the immune system in chronic pain.* Nat Rev Neurosci, 2005. **6**(7): p. 521-32.
9. Staikopoulos, V., et al., *Localization of P2X2 and P2X3 receptors in rat trigeminal ganglion neurons.* Neuroscience, 2007. **144**(1): p. 208-16.
10. Xu, G.Y. and L.Y. Huang, *Peripheral inflammation sensitizes P2X receptor-mediated responses in rat dorsal root ganglion neurons.* J Neurosci, 2002. **22**(1): p. 93-102.
11. Pankratov Yu, V., et al., *Heterogeneity of the functional expression of P2X3 and P2X2/3 receptors in the primary nociceptive neurons of rat.* Neurochem Res, 2001. **26**(8-9): p. 993-1000.
12. Spicarova, D. and J. Palecek, *The role of spinal cord vanilloid (TRPV1) receptors in pain modulation.* Physiol Res, 2008. **57 Suppl 3**: p. S69-77.
13. Hellwig, N., et al., *TRPV1 acts as proton channel to induce acidification in nociceptive neurons.* J Biol Chem, 2004. **279**(33): p. 34553-61.
14. Fang, X., et al., *trkA is expressed in nociceptive neurons and influences electrophysiological properties via Nav1.8 expression in rapidly conducting nociceptors.* J Neurosci, 2005. **25**(19): p. 4868-78.
15. Josephson, A., et al., *GDNF and NGF family members and receptors in human fetal and adult spinal cord and dorsal root ganglia.* J Comp Neurol, 2001. **440**(2): p. 204-17.
16. Zhu, W., et al., *Activin acutely sensitizes dorsal root ganglion neurons and induces hyperalgesia via PKC-mediated potentiation of transient receptor potential vanilloid I.* J Neurosci, 2007. **27**(50): p. 13770-80.
17. Amadesi, S., et al., *Protease-activated receptor 2 sensitizes TRPV1 by protein kinase Cepsilon- and A-dependent mechanisms in rats and mice.* J Physiol, 2006. **575**(Pt 2): p. 555-71.
18. Fields, H., *Pain*, 1987. New York: McGraw Hill.
19. Lembeck, F. and R. Gamse, *Substance P in peripheral sensory processes.* Ciba Found. Symp., 1982. **91**: p. 35-54.
20. Mantyh, P.W., et al., *Molecular mechanisms of cancer pain.* Nat Rev Cancer, 2002. **2**(3): p. 201-9.

21. Maingret, F., et al., *Inflammatory mediators increase Nav1.9 current and excitability in nociceptors through a coincident detection mechanism.* J Gen Physiol, 2008. **131**(3): p. 211-25.
22. Black, J.A., et al., *Changes in the expression of tetrodotoxin-sensitive sodium channels within dorsal root ganglia neurons in inflammatory pain.* Pain, 2004. **108**(3): p. 237-47.
23. Takeda, M., M. Takahashi, and S. Matsumoto, *Inflammation enhanced brain-derived neurotrophic factor-induced suppression of the voltage-gated potassium currents in small-diameter trigeminal ganglion neurons projecting to the trigeminal nucleus interpolaris/caudalis transition zone.* Neuroscience, 2014. **261**: p. 223-31.
24. Takeda, M., et al., *Peripheral inflammation suppresses inward rectifying potassium currents of satellite glial cells in the trigeminal ganglia.* Pain, 2011. **152**(9): p. 2147-56.
25. Takeda, M., et al., *Activation of interleukin-1beta receptor suppresses the voltage-gated potassium currents in the small-diameter trigeminal ganglion neurons following peripheral inflammation.* Pain, 2008. **139**(3): p. 594-602.
26. Lin, Q., et al., *Roles of TRPV1 and neuropeptidergic receptors in dorsal root reflex-mediated neurogenic inflammation induced by intradermal injection of capsaicin.* Mol Pain, 2007. **3**: p. 30.
27. Mizumura, K., et al., *Excitation and sensitization of nociceptors by bradykinin: what do we know?* Exp Brain Res, 2009. **196**(1): p. 53-65.
28. Rush, A.M., T.R. Cummins, and S.G. Waxman, *Multiple sodium channels and their roles in electrogenesis within dorsal root ganglion neurons.* J Physiol, 2007. **579**(Pt 1): p. 1-14.
29. Gadsby, D.C., *Ion channels versus ion pumps: the principal difference, in principle.* Nat Rev Mol Cell Biol, 2009. **10**(5): p. 344-52.
30. Catterall, W.A., *Structure and function of voltage-gated ion channels.* Trends Neurosci, 1993. **16**(12): p. 500-6.
31. Sands, Z., A. Grottesi, and M.S. Sansom, *Voltage-gated ion channels.* Curr Biol, 2005. **15**(2): p. R44-7.
32. Ahern, C.A. and R. Horn, *Specificity of charge-carrying residues in the voltage sensor of potassium channels.* J Gen Physiol, 2004. **123**(3): p. 205-16.
33. Liman, E.R., et al., *Voltage-sensing residues in the S4 region of a mammalian K+ channel.* Nature, 1991. **353**(6346): p. 752-6.
34. Kukuljan, M., P. Labarca, and R. Latorre, *Molecular determinants of ion conduction and inactivation in K^+ channels.* Am J Physiol, 1995. **268**(3 Pt 1): p. C535-56.
35. Yang, N. and R. Horn, *Evidence for voltage-dependent S4 movement in sodium channels.* Neuron, 1995. **15**(1): p. 213-8.
36. Bezanilla, F., *Voltage-gated ion channels.* IEEE Trans Nanobioscience, 2005. **4**(1): p. 34-48.
37. Payandeh, J., et al., *Crystal structure of a voltage-gated sodium channel in two potentially inactivated states.* Nature, 2012. **486**(7401): p. 135-9.
38. Payandeh, J., et al., *The crystal structure of a voltage-gated sodium channel.* Nature, 2011. **475**(7356): p. 353-8.
39. Long, S.B., E.B. Campbell, and R. Mackinnon, *Crystal structure of a mammalian voltage-dependent Shaker family K^+ channel.* Science, 2005. **309**(5736): p. 897-903.
40. Chen, Y.H., et al., *Structural basis of the alpha1-beta subunit interaction of voltage-gated Ca^{2+} channels.* Nature, 2004. **429**(6992): p. 675-80.
41. Jiang, Y., et al., *X-ray structure of a voltage-dependent K^+ channel.* Nature, 2003. **423**(6935): p. 33-41.

42. Van Petegem, F., et al., *Structure of a complex between a voltage-gated calcium channel beta-subunit and an alpha-subunit domain.* Nature, 2004. **429**(6992): p. 671-5.
43. Craven, K.B. and W.N. Zagotta, *CNG and HCN channels: two peas, one pod.* Annu Rev Physiol, 2006. **68**: p. 375-401.
44. Johnson, J.P., Jr. and W.N. Zagotta, *The carboxyl-terminal region of cyclic nucleotide-modulated channels is a gating ring, not a permeation path.* Proc Natl Acad Sci U S A, 2005. **102**(8): p. 2742-7.
45. Kaupp, U.B. and R. Seifert, *Cyclic nucleotide-gated ion channels.* Physiol Rev, 2002. **82**(3): p. 769-824.
46. Sachs, F. and C.E. Morris, *Mechanosensitive ion channels in nonspecialized cells.* Rev Physiol Biochem Pharmacol, 1998. **132**: p. 1-77.
47. Martinac, B., *Mechanosensitive ion channels: molecules of mechanotransduction.* J Cell Sci, 2004. **117**(Pt 12): p. 2449-60.
48. Coste, B., et al., *Piezo1 and Piezo2 are essential components of distinct mechanically activated cation channels.* Science, 2010. **330**(6000): p. 55-60.
49. Coste, B., et al., *Piezo proteins are pore-forming subunits of mechanically activated channels.* Nature, 2012. **483**(7388): p. 176-81.
50. Hamill, O.P. and D.W. McBride, Jr., *Induced membrane hypo/hyper-mechanosensitivity: a limitation of patch-clamp recording.* Annu Rev Physiol, 1997. **59**: p. 621-31.
51. Lumpkin, E.A. and M.J. Caterina, *Mechanisms of sensory transduction in the skin.* Nature, 2007. **445**(7130): p. 858-65.
52. Corey, D.P. and A.J. Hudspeth, *Kinetics of the receptor current in bullfrog saccular hair cells.* J Neurosci, 1983. **3**(5): p. 962-76.
53. Guharay, F. and F. Sachs, *Stretch-activated single ion channel currents in tissue-cultured embryonic chick skeletal muscle.* J Physiol, 1984. **352**: p. 685-701.
54. Denker, B.M., et al., *Identification, purification, and partial characterization of a novel Mr 28,000 integral membrane protein from erythrocytes and renal tubules.* J Biol Chem, 1988. **263**(30): p. 15634-42.
55. Beitz, E., et al., *Determinants of AQP6 trafficking to intracellular sites versus the plasma membrane in transfected mammalian cells.* Biol Cell, 2006. **98**(2): p. 101-9.
56. Jentsch, T.J., et al., *Molecular structure and physiological function of chloride channels.* Physiol Rev, 2002. **82**(2): p. 503-68.
57. Jentsch, T.J., *Chloride channels are different.* Nature, 2002. **415**(6869): p. 276-7.
58. Friauf, E., et al., *Chloride cotransporters, chloride homeostasis, and synaptic inhibition in the developing auditory system.* Hear Res, 2011. **279**(1-2): p. 96-110.
59. Lu, J., M. Karadsheh, and E. Delpire, *Developmental regulation of the neuronal-specific isoform of K-Cl cotransporter KCC2 in postnatal rat brains.* J Neurobiol, 1999. **39**(4): p. 558-68.
60. Rivera, C., et al., *The K^+/Cl^- co-transporter KCC2 renders GABA hyperpolarizing during neuronal maturation.* Nature, 1999. **397**(6716): p. 251-5.
61. Stein, V., et al., *Expression of the KCl cotransporter KCC2 parallels neuronal maturation and the emergence of low intracellular chloride.* J Comp Neurol, 2004. **468**(1): p. 57-64.
62. Alvarez-Leefmans, F.J., et al., *Immunolocalization of the Na(+)-K(+)-2Cl(-) cotransporter in peripheral nervous tissue of vertebrates.* Neuroscience, 2001. **104**(2): p. 569-82.
63. Kanaka, C., et al., *The differential expression patterns of messenger RNAs encoding K-Cl cotransporters (KCC1,2) and Na-K-2Cl cotransporter (NKCC1) in the rat nervous system.* Neuroscience, 2001. **104**(4): p. 933-46.

64. Blaesse, P., et al., *Cation-chloride cotransporters and neuronal function.* Neuron, 2009. **61**(6): p. 820-38.
65. Payne, J.A., et al., *Cation-chloride co-transporters in neuronal communication, development and trauma.* Trends Neurosci, 2003. **26**(4): p. 199-206.
66. Rivera, C., J. Voipio, and K. Kaila, *Two developmental switches in GABAergic signalling: the K^+-Cl^- cotransporter KCC2 and carbonic anhydrase CAVII.* J Physiol, 2005. **562**(Pt 1): p. 27-36.
67. Yamada, J., et al., *Cl^- uptake promoting depolarizing GABA actions in immature rat neocortical neurones is mediated by NKCC1.* J Physiol, 2004. **557**(Pt 3): p. 829-41.
68. Zhu, L., D. Lovinger, and E. Delpire, *Cortical neurons lacking KCC2 expression show impaired regulation of intracellular chloride.* J Neurophysiol, 2005. **93**(3): p. 1557-68.
69. Gilbert, D., et al., *Differential maturation of chloride homeostasis in primary afferent neurons of the somatosensory system.* Int J Dev Neurosci, 2007. **25**(7): p. 479-89.
70. Kaneko, H., et al., *Chloride accumulation in mammalian olfactory sensory neurons.* J Neurosci, 2004. **24**(36): p. 7931-8.
71. Rocha-Gonzalez, H.I., S. Mao, and F.J. Alvarez-Leefmans, *Na^+,K^+,$2Cl^-$ cotransport and intracellular chloride regulation in rat primary sensory neurons: thermodynamic and kinetic aspects.* J Neurophysiol, 2008. **100**(1): p. 169-84.
72. Billups, D. and D. Attwell, *Control of intracellular chloride concentration and GABA response polarity in rat retinal ON bipolar cells.* J Physiol, 2002. **545**(Pt 1): p. 183-98.
73. Desarmenien, M., et al., *Comparative study of GABA-mediated depolarizations of lumbar A delta and C primary afferent neurones of the rat.* Exp Brain Res, 1984. **54**(3): p. 521-8.
74. Carlton, S.M., S. Zhou, and R.E. Coggeshall, *Peripheral GABA(A) receptors: evidence for peripheral primary afferent depolarization.* Neuroscience, 1999. **93**(2): p. 713-22.
75. Labrakakis, C., et al., *Localization and function of ATP and GABAA receptors expressed by nociceptors and other postnatal sensory neurons in rat.* J Physiol, 2003. **549**(Pt 1): p. 131-42.
76. Willis, W.D., Jr., *Dorsal root potentials and dorsal root reflexes: a double-edged sword.* Exp Brain Res, 1999. **124**(4): p. 395-421.
77. Jentsch, T.J., *CLC chloride channels and transporters: from genes to protein structure, pathology and physiology.* Crit Rev Biochem Mol Biol, 2008. **43**(1): p. 3-36.
78. Pusch, M., et al., *Channel or transporter? The CLC saga continues.* Exp Physiol, 2006. **91**(1): p. 149-52.
79. Miller, C. and M.M. White, *Dimeric structure of single chloride channels from Torpedo electroplax.* Proc Natl Acad Sci U S A, 1984. **81**(9): p. 2772-5.
80. Ludewig, U., M. Pusch, and T.J. Jentsch, *Two physically distinct pores in the dimeric ClC-0 chloride channel.* Nature, 1996. **383**(6598): p. 340-3.
81. Saviane, C., F. Conti, and M. Pusch, *The muscle chloride channel ClC-1 has a double-barreled appearance that is differentially affected in dominant and recessive myotonia.* J Gen Physiol, 1999. **113**(3): p. 457-68.
82. Weinreich, F. and T.J. Jentsch, *Pores formed by single subunits in mixed dimers of different CLC chloride channels.* J Biol Chem, 2001. **276**(4): p. 2347-53.
83. Schmidt-Rose, T. and T.J. Jentsch, *Transmembrane topology of a CLC chloride channel.* Proc Natl Acad Sci U S A, 1997. **94**(14): p. 7633-8.
84. Waldegger, S. and T.J. Jentsch, *From tonus to tonicity: physiology of CLC chloride channels.* J Am Soc Nephrol, 2000. **11**(7): p. 1331-9.
85. Dutzler, R., et al., *X-ray structure of a ClC chloride channel at 3.0 A reveals the molecular basis of anion selectivity.* Nature, 2002. **415**(6869): p. 287-94.

86. de Santiago, J.A., K. Nehrke, and J. Arreola, *Quantitative analysis of the voltage-dependent gating of mouse parotid ClC-2 chloride channel.* J Gen Physiol, 2005. **126**(6): p. 591-603.
87. Steinmeyer, K., C. Ortland, and T.J. Jentsch, *Primary structure and functional expression of a developmentally regulated skeletal muscle chloride channel.* Nature, 1991. **354**(6351): p. 301-4.
88. Duan, D., et al., *A novel anionic inward rectifier in native cardiac myocytes.* Circ Res, 2000. **86**(4): p. E63-71.
89. Ratté, S., et al., *ClC-2 channels regulate neuronal excitability, not intracellular chloride levels*. J Neurosci, 2011. 31(44): p. 15838-43.
90. Duan, D., et al., *Molecular identification of a volume-regulated chloride channel.* Nature, 1997. **390**(6658): p. 417-21.
91. Gunther, W., et al., *ClC-5, the chloride channel mutated in Dent's disease, colocalizes with the proton pump in endocytotically active kidney cells.* Proc Natl Acad Sci U S A, 1998. **95**(14): p. 8075-80.
92. Sakamoto, H., et al., *Cellular and subcellular immunolocalization of ClC-5 channel in mouse kidney: colocalization with H+-ATPase.* Am J Physiol, 1999. **277**(6 Pt 2): p. F957-65.
93. Devuyst, O., et al., *Intra-renal and subcellular distribution of the human chloride channel, CLC-5, reveals a pathophysiological basis for Dent's disease.* Hum Mol Genet, 1999. **8**(2): p. 247-57.
94. Fahlke, C., *Ion permeation and selectivity in ClC-type chloride channels.* Am J Physiol Renal Physiol, 2001. **280**(5): p. F748-57.
95. Kaneda, M., M. Farrant, and S.G. Cull-Candy, *Whole-cell and single-channel currents activated by GABA and glycine in granule cells of the rat cerebellum.* J Physiol, 1995. **485 (Pt 2)**: p. 419-35.
96. Weiss, D.S., *Membrane potential modulates the activation of GABA-gated channels.* J Neurophysiol, 1988. **59**(2): p. 514-27.
97. Birnir, B., A.B. Everitt, and P.W. Gage, *Characteristics of GABAA channels in rat dentate gyrus.* J Membr Biol, 1994. **142**(1): p. 93-102.
98. Gage, P.W. and S.H. Chung, *Influence of membrane potential on conductance sublevels of chloride channels activated by GABA.* Proc Biol Sci, 1994. **255**(1343): p. 167-72.
99. Burgard, E.C., et al., *Properties of recombinant gamma-aminobutyric acid A receptor isoforms containing the alpha 5 subunit subtype.* Mol Pharmacol, 1996. **50**(1): p. 119-27.
100. Eghbali, M., et al., *Hippocampal GABA(A) channel conductance increased by diazepam.* Nature, 1997. **388**(6637): p. 71-5.
101. Mennerick, S., et al., *Effects on gamma-aminobutyric acid (GABA)(A) receptors of a neuroactive steroid that negatively modulates glutamate neurotransmission and augments GABA neurotransmission.* Mol Pharmacol, 2001. **60**(4): p. 732-41.
102. Pytel, M., K. Mercik, and J.W. Mozrzymas, *Membrane voltage modulates the GABA(A) receptor gating in cultured rat hippocampal neurons.* Neuropharmacology, 2006. **50**(2): p. 143-53.
103. Verdoorn, T.A., et al., *Functional properties of recombinant rat GABAA receptors depend upon subunit composition.* Neuron, 1990. **4**(6): p. 919-28.
104. Kuhse, J., et al., *Assembly of the inhibitory glycine receptor: identification of amino acid sequence motifs governing subunit stoichiometry.* Neuron, 1993. **11**(6): p. 1049-56.

105. Kuhse, J., H. Betz, and J. Kirsch, *The inhibitory glycine receptor: architecture, synaptic localization and molecular pathology of a postsynaptic ion-channel complex.* Curr Opin Neurobiol, 1995. **5**(3): p. 318-23.
106. Sontheimer, H., et al., *Functional chloride channels by mammalian cell expression of rat glycine receptor subunit.* Neuron, 1989. **2**(5): p. 1491-7.
107. Bormann, J., et al., *Residues within transmembrane segment M2 determine chloride conductance of glycine receptor homo- and hetero-oligomers.* EMBO J, 1993. **12**(10): p. 3729-37.
108. Trombley, P.Q. and G.M. Shepherd, *Glycine exerts potent inhibitory actions on mammalian olfactory bulb neurons.* J Neurophysiol, 1994. **71**(2): p. 761-7.
109. Gundersen, C.B., R. Miledi, and I. Parker, *Properties of human brain glycine receptors expressed in Xenopus oocytes.* Proc R Soc Lond B Biol Sci, 1984. **221**(1223): p. 235-44.
110. Yadid, G., et al., *Glycine stimulates striatal dopamine release in conscious rats.* Br J Pharmacol, 1993. **110**(1): p. 50-3.
111. Kojovic, M., C. Cordivari, and K. Bhatia, *Myoclonic disorders: a practical approach for diagnosis and treatment.* Ther Adv Neurol Disord, 2011. **4**(1): p. 47-62.
112. Tang, Y.B., J.G. Zhou, and Y.Y. Guan, *Volume-regulated chloride channels and cerebral vascular remodelling.* Clin Exp Pharmacol Physiol, 2010. **37**(2): p. 238-42.
113. Sardini, A., et al., *Cell volume regulation and swelling-activated chloride channels.* Biochim Biophys Acta, 2003. **1618**(2): p. 153-62.
114. Strange, K., F. Emma, and P.S. Jackson, *Cellular and molecular physiology of volume-sensitive anion channels.* Am J Physiol, 1996. **270**(3 Pt 1): p. C711-30.
115. Vandenberg, J.I., et al., *Cell swelling and ion transport pathways in cardiac myocytes.* Cardiovasc Res, 1996. **32**(1): p. 85-97.
116. Okada, Y., *Volume expansion-sensing outward-rectifier Cl^- channel: fresh start to the molecular identity and volume sensor.* Am J Physiol, 1997. **273**(3 Pt 1): p. C755-89.
117. Oz, M.C. and S. Sorota, *Forskolin stimulates swelling-induced chloride current, not cardiac cystic fibrosis transmembrane-conductance regulator current, in human cardiac myocytes.* Circ Res, 1995. **76**(6): p. 1063-70.
118. Sorota, S., *Swelling-induced chloride-sensitive current in canine atrial cells revealed by whole-cell patch-clamp method.* Circ Res, 1992. **70**(4): p. 679-87.
119. Nagasaki, M., et al., *Intracellular cyclic AMP inhibits native and recombinant volume-regulated chloride channels from mammalian heart.* J Physiol, 2000. **523 Pt 3**: p. 705-17.
120. Grunder, S., et al., *Regions involved in the opening of CIC-2 chloride channel by voltage and cell volume.* Nature, 1992. **360**(6406): p. 759-62.
121. Thiemann, A., et al., *A chloride channel widely expressed in epithelial and non-epithelial cells.* Nature, 1992. **356**(6364): p. 57-60.
122. Jordt, S.E. and T.J. Jentsch, *Molecular dissection of gating in the ClC-2 chloride channel.* EMBO J, 1997. **16**(7): p. 1582-92.
123. Duan, D., et al., *A serine residue in ClC-3 links phosphorylation-dephosphorylation to chloride channel regulation by cell volume.* J Gen Physiol, 1999. **113**(1): p. 57-70.
124. Wang, L., L. Chen, and T.J. Jacob, *The role of ClC-3 in volume-activated chloride currents and volume regulation in bovine epithelial cells demonstrated by antisense inhibition.* J Physiol, 2000. **524 Pt 1**: p. 63-75.
125. Hermoso, M., et al., *ClC-3 is a fundamental molecular component of volume-sensitive outwardly rectifying Cl^- channels and volume regulation in HeLa cells and Xenopus laevis oocytes.* J Biol Chem, 2002. **277**(42): p. 40066-74.

126. Xiong, D., et al., *Cardiac-specific overexpression of the human short CLC-3 chloride channel isoform in mice.* Clin Exp Pharmacol Physiol, 2009. **36**(4): p. 386-93.
127. Matsuda, J.J., et al., *Overexpression of CLC-3 in HEK293T cells yields novel currents that are pH dependent.* Am J Physiol Cell Physiol, 2008. **294**(1): p. C251-62.
128. Almaca, J., et al., *TMEM16 proteins produce volume-regulated chloride currents that are reduced in mice lacking TMEM16A.* J Biol Chem, 2009. **284**(42): p. 28571-8.
129. Qiu, Z., et al., *SWELL1, a plasma membrane protein, is an essential component of volume-regulated anion channel.* Cell, 2014. **157**(2): p. 447-58.
130. Voss, F.K., et al., *Identification of LRRC8 heteromers as an essential component of the volume-regulated anion channel VRAC.* Science, 2014. **344**(6184): p. 634-8.
131. Cheadle, J., et al., *Mutation analysis of 184 cystic fibrosis families in Wales.* J Med Genet, 1992. **29**(9): p. 642-6.
132. Sheppard, D.N. and M.J. Welsh, *Structure and function of the CFTR chloride channel.* Physiol Rev, 1999. **79**(1 Suppl): p. S23-45.
133. Hwang, T.C. and D.N. Sheppard, *Gating of the CFTR Cl^- channel by ATP-driven nucleotide-binding domain dimerisation.* J Physiol, 2009. **587**(Pt 10): p. 2151-61.
134. Csanady, L., A.C. Nairn, and D.C. Gadsby, *Thermodynamics of CFTR channel gating: a spreading conformational change initiates an irreversible gating cycle.* J Gen Physiol, 2006. **128**(5): p. 523-33.
135. Bompadre, S.G., et al., *CFTR gating I: Characterization of the ATP-dependent gating of a phosphorylation-independent CFTR channel (DeltaR-CFTR).* J Gen Physiol, 2005. **125**(4): p. 361-75.
136. Gadsby, D.C. and A.C. Nairn, *Control of CFTR channel gating by phosphorylation and nucleotide hydrolysis.* Physiol Rev, 1999. **79**(1 Suppl): p. S77-S107.
137. Cross, N.L., *Initiation of the activation potential by an increase in intracellular calcium in eggs of the frog, Rana pipiens.* Dev Biol, 1981. **85**(2): p. 380-4.
138. Schlichter, L.C. and R.P. Elinson, *Electrical responses of immature and mature Rana pipiens oocytes to sperm and other activating stimuli.* Dev Biol, 1981. **83**(1): p. 33-41.
139. Bader, C.R., D. Bertrand, and E.A. Schwartz, *Voltage-activated and calcium-activated currents studied in solitary rod inner segments from the salamander retina.* J Physiol, 1982. **331**: p. 253-84.
140. Llano, I., N. Leresche, and A. Marty, *Calcium entry increases the sensitivity of cerebellar Purkinje cells to applied GABA and decreases inhibitory synaptic currents.* Neuron, 1991. **6**(4): p. 565-74.
141. Achilles, K., et al., *Kinetic properties of Cl uptake mediated by Na^+-dependent K^+-2Cl cotransport in immature rat neocortical neurons.* J Neurosci, 2007. **27**(32): p. 8616-27.
142. Gamba, G., *Molecular physiology and pathophysiology of electroneutral cation-chloride cotransporters.* Physiol Rev, 2005. **85**(2): p. 423-93.
143. Price, T.J., K.M. Hargreaves, and F. Cervero, *Protein expression and mRNA cellular distribution of the NKCC1 cotransporter in the dorsal root and trigeminal ganglia of the rat.* Brain Res, 2006. **1112**(1): p. 146-58.
144. Alvarez-Leefmans, F.J., et al., *Intracellular chloride regulation in amphibian dorsal root ganglion neurones studied with ion-selective microelectrodes.* J Physiol, 1988. **406**: p. 225-46.
145. Schobel, N., et al., *Trigeminal ganglion neurons of mice show intracellular chloride accumulation and chloride-dependent amplification of capsaicin-induced responses.* PLoS One, 2012. **7**(11): p. e48005.
146. Huang, W.C., et al., *Calcium-activated chloride channels (CaCCs) regulate action potential and synaptic response in hippocampal neurons.* Neuron, 2012. **74**(1): p. 179-92.

147. Funk, K., et al., *Modulation of chloride homeostasis by inflammatory mediators in dorsal root ganglion neurons.* Mol Pain, 2008. **4**: p. 32.
148. Ponissery Saidu, S., et al., *Odorant-induced responses recorded from olfactory receptor neurons using the suction pipette technique.* J Vis Exp, 2012(62): p. e3862.
149. Berg, J., H. Yang, and L.Y. Jan, *Ca^{2+}-activated Cl^- channels at a glance.* J Cell Sci, 2012. **125**(Pt 6): p. 1367-71.
150. Simon Bulley, S.B. and J.H. Jaggar, *$Cl(^-)$ channels in smooth muscle cells.* Pflugers Arch, 2014. **466**(5): p. 861-72.
151. Manoury, B., A. Tamuleviciute, and P. Tammaro, *TMEM16A/anoctamin 1 protein mediates calcium-activated chloride currents in pulmonary arterial smooth muscle cells.* J Physiol, 2010. **588**(Pt 13): p. 2305-14.
152. Thomas-Gatewood, C., et al., *TMEM16A channels generate Ca(2)(+)-activated Cl(-) currents in cerebral artery smooth muscle cells.* Am J Physiol Heart Circ Physiol, 2011. **301**(5): p. H1819-27.
153. Matchkov, V.V., C. Aalkjaer, and H. Nilsson, *A cyclic GMP-dependent calcium-activated chloride current in smooth-muscle cells from rat mesenteric resistance arteries.* J Gen Physiol, 2004. **123**(2): p. 121-34.
154. Matchkov, V.V., C. Aalkjaer, and H. Nilsson, *Distribution of cGMP-dependent and cGMP-independent Ca(2+)-activated Cl(-) conductances in smooth muscle cells from different vascular beds and colon.* Pflugers Arch, 2005. **451**(2): p. 371-9.
155. Matchkov, V.V., et al., *Bestrophin-3 (vitelliform macular dystrophy 2-like 3 protein) is essential for the cGMP-dependent calcium-activated chloride conductance in vascular smooth muscle cells.* Circ Res, 2008. **103**(8): p. 864-72.
156. Aickin, C.C. and N.A. Vermue, *Microelectrode measurement of intracellular chloride activity in smooth muscle cells of guinea-pig ureter.* Pflugers Arch, 1983. **397**(1): p. 25-8.
157. Owen, N.E., *Regulation of Na/K/Cl cotransport in vascular smooth muscle cells.* Biochem Biophys Res Commun, 1984. **125**(2): p. 500-8.
158. Meyer, J.W., et al., *Decreased blood pressure and vascular smooth muscle tone in mice lacking basolateral Na(+)-K(+)-2Cl(-) cotransporter.* Am J Physiol Heart Circ Physiol, 2002. **283**(5): p. H1846-55.
159. Jang, Y. and U. Oh, *Anoctamin 1 in secretory epithelia.* Cell Calcium, 2014. **55**(6): p. 355-61.
160. Pedemonte, N. and L.J. Galietta, *Structure and function of TMEM16 proteins (anoctamins).* Physiol Rev, 2014. **94**(2): p. 419-59.
161. Huang, F., X. Wong, and L.Y. Jan, *International Union of Basic and Clinical Pharmacology. LXXXV: calcium-activated chloride channels.* Pharmacol Rev, 2012. **64**(1): p. 1-15.
162. Hartzell, C., I. Putzier, and J. Arreola, *Calcium-activated chloride channels.* Annu Rev Physiol, 2005. **67**: p. 719-58.
163. Large, W.A. and Q. Wang, *Characteristics and physiological role of the Ca(2+)-activated Cl^- conductance in smooth muscle.* Am J Physiol, 1996. **271**(2 Pt 1): p. C435-54.
164. Qu, Z. and H.C. Hartzell, *Anion permeation in Ca(2+)-activated Cl(-) channels.* J Gen Physiol, 2000. **116**(6): p. 825-44.
165. Kuruma, A. and H.C. Hartzell, *Bimodal control of a Ca(2+)-activated Cl(-) channel by different Ca(2+) signals.* J Gen Physiol, 2000. **115**(1): p. 59-80.
166. Salzer, I., et al., *Excitation of rat sympathetic neurons via M muscarinic receptors independently of K 7 channels.* Pflugers Arch, 2014.

167. Arreola, J., J.E. Melvin, and T. Begenisich, *Activation of calcium-dependent chloride channels in rat parotid acinar cells.* J Gen Physiol, 1996. **108**(1): p. 35-47.
168. Nilius, B., et al., *Kinetic and pharmacological properties of the calcium-activated chloride-current in macrovascular endothelial cells.* Cell Calcium, 1997. **22**(1): p. 53-63.
169. Qu, Z., R.W. Wei, and H.C. Hartzell, *Characterization of Ca^{2+}-activated Cl^- currents in mouse kidney inner medullary collecting duct cells.* Am J Physiol Renal Physiol, 2003. **285**(2): p. F326-35.
170. Angermann, J.E., et al., *Mechanism of the inhibition of Ca^{2+}-activated Cl^- currents by phosphorylation in pulmonary arterial smooth muscle cells.* J Gen Physiol, 2006. **128**(1): p. 73-87.
171. Ishikawa, T. and D.I. Cook, *A Ca(2+)-activated Cl^- current in sheep parotid secretory cells.* J Membr Biol, 1993. **135**(3): p. 261-71.
172. Leblanc, N., et al., *Regulation of calcium-activated chloride channels in smooth muscle cells: a complex picture is emerging.* Can J Physiol Pharmacol, 2005. **83**(7): p. 541-56.
173. Piper, A.S., I.A. Greenwood, and W.A. Large, *Dual effect of blocking agents on Ca^{2+}-activated Cl(-) currents in rabbit pulmonary artery smooth muscle cells.* J Physiol, 2002. **539**(Pt 1): p. 119-31.
174. Ledoux, J., I.A. Greenwood, and N. Leblanc, *Dynamics of Ca^{2+}-dependent Cl^- channel modulation by niflumic acid in rabbit coronary arterial myocytes.* Mol Pharmacol, 2005. **67**(1): p. 163-73.
175. Cruickshank, S.F., L.M. Baxter, and R.M. Drummond, *The Cl(-) channel blocker niflumic acid releases Ca(2+) from an intracellular store in rat pulmonary artery smooth muscle cells.* Br J Pharmacol, 2003. **140**(8): p. 1442-50.
176. Cunningham, S.A., et al., *Cloning of an epithelial chloride channel from bovine trachea.* J Biol Chem, 1995. **270**(52): p. 31016-26.
177. Huang, P., et al., *Regulation of human CLC-3 channels by multifunctional Ca^{2+}/calmodulin-dependent protein kinase.* J Biol Chem, 2001. **276**(23): p. 20093-100.
178. Loewen, M.E. and G.W. Forsyth, *Structure and function of CLCA proteins.* Physiol Rev, 2005. **85**(3): p. 1061-92.
179. Gandhi, R., et al., *Molecular and functional characterization of a calcium-sensitive chloride channel from mouse lung.* J Biol Chem, 1998. **273**(48): p. 32096-101.
180. Gruber, A.D., et al., *Genomic cloning, molecular characterization, and functional analysis of human CLCA1, the first human member of the family of Ca^{2+}-activated Cl^- channel proteins.* Genomics, 1998. **54**(2): p. 200-14.
181. Gruber, A.D., et al., *Molecular cloning and transmembrane structure of hCLCA2 from human lung, trachea, and mammary gland.* Am J Physiol, 1999. **276**(6 Pt 1): p. C1261-70.
182. Elble, R.C., et al., *Molecular and functional characterization of a murine calcium-activated chloride channel expressed in smooth muscle.* J Biol Chem, 2002. **277**(21): p. 18586-91.
183. Cliff, W.H. and R.A. Frizzell, *Separate Cl^- conductances activated by cAMP and Ca^{2+} in Cl(-)-secreting epithelial cells.* Proc Natl Acad Sci U S A, 1990. **87**(13): p. 4956-60.
184. Britton, F.C., et al., *Comparison of the properties of CLCA1 generated currents and I(Cl(Ca)) in murine portal vein smooth muscle cells.* J Physiol, 2002. **539**(Pt 1): p. 107-17.
185. Greenwood, I.A., et al., *The large conductance potassium channel beta-subunit can interact with and modulate the functional properties of a calcium-activated chloride channel, CLCA1.* J Biol Chem, 2002. **277**(25): p. 22119-22.

186. Gibson, A., et al., *hCLCA1 and mCLCA3 are secreted non-integral membrane proteins and therefore are not ion channels.* J Biol Chem, 2005. **280**(29): p. 27205-12.
187. Arreola, J., et al., *Secretion and cell volume regulation by salivary acinar cells from mice lacking expression of the Clcn3 Cl^- channel gene.* J Physiol, 2002. **545**(Pt 1): p. 207-16.
188. Stohr, H., et al., *Three novel human VMD2-like genes are members of the evolutionary highly conserved RFP-TM family.* Eur J Hum Genet, 2002. **10**(4): p. 281-4.
189. Tsunenari, T., et al., *Structure-function analysis of the bestrophin family of anion channels.* J Biol Chem, 2003. **278**(42): p. 41114-25.
190. Hartzell, H.C., et al., *Molecular physiology of bestrophins: multifunctional membrane proteins linked to best disease and other retinopathies.* Physiol Rev, 2008. **88**(2): p. 639-72.
191. Qu, Z., et al., *Two bestrophins cloned from Xenopus laevis oocytes express Ca(2+)-activated Cl(-) currents.* J Biol Chem, 2003. **278**(49): p. 49563-72.
192. Sun, H., et al., *The vitelliform macular dystrophy protein defines a new family of chloride channels.* Proc Natl Acad Sci U S A, 2002. **99**(6): p. 4008-13.
193. Xiao, Q., et al., *Regulation of bestrophin Cl channels by calcium: role of the C terminus.* J Gen Physiol, 2008. **132**(6): p. 681-92.
194. O'Driscoll, K.E., et al., *Functional properties of murine bestrophin 1 channel.* Biochem Biophys Res Commun, 2009. **384**(4): p. 476-81.
195. Liu, Y., et al., *Characterization of the effects of Cl channel modulators on TMEM16A and bestrophin-1 Ca activated Cl channels.* Pflugers Arch, 2014.
196. Qu, Z., R. Fischmeister, and C. Hartzell, *Mouse bestrophin-2 is a bona fide Cl(-) channel: identification of a residue important in anion binding and conduction.* J Gen Physiol, 2004. **123**(4): p. 327-40.
197. Hartzell, H.C., et al., *Anoctamin/TMEM16 family members are Ca^{2+}-activated Cl^- channels.* J Physiol, 2009. **587**(Pt 10): p. 2127-39.
198. Marmorstein, L.Y., et al., *The light peak of the electroretinogram is dependent on voltage-gated calcium channels and antagonized by bestrophin (best-1).* J Gen Physiol, 2006. **127**(5): p. 577-89.
199. Barro-Soria, R., R. Schreiber, and K. Kunzelmann, *Bestrophin 1 and 2 are components of the Ca(2+) activated Cl(-) conductance in mouse airways.* Biochim Biophys Acta, 2008. **1783**(10): p. 1993-2000.
200. Rosenthal, R., et al., *Expression of bestrophin-1, the product of the VMD2 gene, modulates voltage-dependent Ca^{2+} channels in retinal pigment epithelial cells.* FASEB J, 2006. **20**(1): p. 178-80.
201. Gomez, N.M., E.R. Tamm, and O. Straubeta, *Role of bestrophin-1 in store-operated calcium entry in retinal pigment epithelium.* Pflugers Arch, 2013. **465**(4): p. 481-95.
202. Yang, Y.D., et al., *TMEM16A confers receptor-activated calcium-dependent chloride conductance.* Nature, 2008. **455**(7217): p. 1210-5.
203. Caputo, A., et al., *TMEM16A, a membrane protein associated with calcium-dependent chloride channel activity.* Science, 2008. **322**(5901): p. 590-4.
204. Schroeder, B.C., et al., *Expression cloning of TMEM16A as a calcium-activated chloride channel subunit.* Cell, 2008. **134**(6): p. 1019-29.
205. Xiao, Q., et al., *Voltage- and calcium-dependent gating of TMEM16A/Ano1 chloride channels are physically coupled by the first intracellular loop.* Proc Natl Acad Sci U S A, 2011. **108**(21): p. 8891-6.
206. Yu, K., et al., *Explaining calcium-dependent gating of anoctamin-1 chloride channels requires a revised topology.* Circ Res, 2012. **110**(7): p. 990-9.

207. Adomaviciene, A., et al., *Putative pore-loops of TMEM16/anoctamin channels affect channel density in cell membranes.* J Physiol, 2013. **591**(Pt 14): p. 3487-505.
208. Romanenko, V.G., et al., *Tmem16A encodes the Ca^{2+}-activated Cl^- channel in mouse submandibular salivary gland acinar cells.* J Biol Chem, 2010. **285**(17): p. 12990-3001.
209. El Chemaly, A., et al., *ANO1 contributes to angiotensin-II-activated Ca^{2+}-dependent Cl^- current in human atrial fibroblasts.* J Mol Cell Cardiol, 2014. **68**: p. 12-9.
210. Dam, V.S., et al., *TMEM16A knockdown abrogates two different $Ca(^{2+})$-activated Cl (-) currents and contractility of smooth muscle in rat mesenteric small arteries.* Pflugers Arch, 2014. **466**(7): p. 1391-409.
211. Dutta, A.K., et al., *Identification and functional characterization of TMEM16A, a Ca^{2+}-activated Cl^- channel activated by extracellular nucleotides, in biliary epithelium.* J Biol Chem, 2011. **286**(1): p. 766-76.
212. Grubb, B.R., et al., *Intestinal ion transport in NKCC1-deficient mice.* Am J Physiol Gastrointest Liver Physiol, 2000. **279**(4): p. G707-18.
213. Grubb, B.R., et al., *Alterations in airway ion transport in NKCC1-deficient mice.* Am J Physiol Cell Physiol, 2001. **281**(2): p. C615-23.
214. Petersen, O.H. and A.V. Tepikin, *Polarized calcium signaling in exocrine gland cells.* Annu Rev Physiol, 2008. **70**: p. 273-99.
215. Melvin, J.E., et al., *Regulation of fluid and electrolyte secretion in salivary gland acinar cells.* Annu Rev Physiol, 2005. **67**: p. 445-69.
216. Rock, J.R., et al., *Transmembrane protein 16A (TMEM16A) is a Ca^{2+}-regulated Cl^- secretory channel in mouse airways.* J Biol Chem, 2009. **284**(22): p. 14875-80.
217. Ousingsawat, J., et al., *Loss of TMEM16A causes a defect in epithelial Ca^{2+}-dependent chloride transport.* J Biol Chem, 2009. **284**(42): p. 28698-703.
218. Namkung, W., P.W. Phuan, and A.S. Verkman, *TMEM16A inhibitors reveal TMEM16A as a minor component of calcium-activated chloride channel conductance in airway and intestinal epithelial cells.* J Biol Chem, 2011. **286**(3): p. 2365-74.
219. Mroz, M.S. and S.J. Keely, *Epidermal growth factor chronically upregulates Ca(2+)-dependent Cl(-) conductance and TMEM16A expression in intestinal epithelial cells.* J Physiol, 2012. **590**(Pt 8): p. 1907-20.
220. Byrne, N.G. and W.A. Large, *Action of noradrenaline on single smooth muscle cells freshly dispersed from the rat anococcygeus muscle.* J Physiol, 1987. **389**: p. 513-25.
221. Piper, A.S. and W.A. Large, *Multiple conductance states of single Ca^{2+}-activated Cl^- channels in rabbit pulmonary artery smooth muscle cells.* J Physiol, 2003. **547**(Pt 1): p. 181-96.
222. Greenwood, I.A., J. Ledoux, and N. Leblanc, *Differential regulation of Ca(2+)-activated Cl(-) currents in rabbit arterial and portal vein smooth muscle cells by Ca(2+)-calmodulin-dependent kinase.* J Physiol, 2001. **534**(Pt. 2): p. 395-408.
223. Greenwood, I.A., et al., *Calcineurin Aalpha but not Abeta augments ICl(Ca) in rabbit pulmonary artery smooth muscle cells.* J Biol Chem, 2004. **279**(37): p. 38830-7.
224. Bulley, S., et al., *TMEM16A/ANO1 channels contribute to the myogenic response in cerebral arteries.* Circ Res, 2012. **111**(8): p. 1027-36.
225. Kitamura, K. and J. Yamazaki, *Chloride channels and their functional roles in smooth muscle tone in the vasculature.* Jpn J Pharmacol, 2001. **85**(4): p. 351-7.
226. Pollock, N.S., M.E. Kargacin, and G.J. Kargacin, *Chloride channel blockers inhibit Ca^{2+} uptake by the smooth muscle sarcoplasmic reticulum.* Biophys J, 1998. **75**(4): p. 1759-66.
227. Wang, M., et al., *Downregulation of TMEM16A calcium-activated chloride channel contributes to cerebrovascular remodeling during hypertension by promoting basilar smooth muscle cell proliferation.* Circulation, 2012. **125**(5): p. 697-707.

228. Sun, H., et al., *Chronic hypoxia-induced upregulation of Ca^{2+}-activated Cl^- channel in pulmonary arterial myocytes: a mechanism contributing to enhanced vasoreactivity.* J Physiol, 2012. **590**(Pt 15): p. 3507-21.
229. Forrest, A.S., et al., *Increased TMEM16A-encoded calcium-activated chloride channel activity is associated with pulmonary hypertension.* Am J Physiol Cell Physiol, 2012. **303**(12): p. C1229-43.
230. Zhang, C.H., et al., *The transmembrane protein 16A Ca(2+)-activated Cl^- channel in airway smooth muscle contributes to airway hyperresponsiveness.* Am J Respir Crit Care Med, 2013. **187**(4): p. 374-81.
231. Davis, A.J., et al., *Potent vasorelaxant activity of the TMEM16A inhibitor T16A(inh) - A01.* Br J Pharmacol, 2013. **168**(3): p. 773-84.
232. Fallah, G., et al., *TMEM16A(a)/anoctamin-1 shares a homodimeric architecture with CLC chloride channels.* Mol Cell Proteomics, 2011. **10**(2): p. M110. 004697.
233. Sheridan, J.T., et al., *Characterization of the oligomeric structure of the Ca(2+)-activated Cl^- channel Ano1/TMEM16A.* J Biol Chem, 2011. **286**(2): p. 1381-8.
234. Tien, J., et al., *Identification of a dimerization domain in the TMEM16A calcium-activated chloride channel (CaCC).* Proc Natl Acad Sci U S A, 2013. **110**(16): p. 6352-7.
235. Adomaviciene, A., et al., *Putative pore-loops of TMEM16/Anoctamin channels affect channel density in cell membranes.* J Physiol, 2013. **591**(Pt 14): p. 3487-505.
236. Jung, J., et al., *Dynamic modulation of ANO1/TMEM16A HCO3(-) permeability by Ca^{2+}/calmodulin.* Proc Natl Acad Sci U S A, 2013. **110**(1): p. 360-5.
237. Chan, H.C., et al., *Annexin IV inhibits calmodulin-dependent protein kinase II-activated chloride conductance. A novel mechanism for ion channel regulation.* J Biol Chem, 1994. **269**(51): p. 32464-8.
238. Ho, M.W., et al., *Regulation of a human chloride channel. a paradigm for integrating input from calcium, type ii calmodulin-dependent protein kinase, and inositol 3,4,5,6-tetrakisphosphate.* J Biol Chem, 2001. **276**(22): p. 18673-80.
239. Wagner, J.A., et al., *Activation of chloride channels in normal and cystic fibrosis airway epithelial cells by multifunctional calcium/calmodulin-dependent protein kinase.* Nature, 1991. **349**(6312): p. 793-6.
240. Xie, W., et al., *Inositol 3,4,5,6-tetrakisphosphate inhibits the calmodulin-dependent protein kinase II-activated chloride conductance in T84 colonic epithelial cells.* J Biol Chem, 1996. **271**(24): p. 14092-7.
241. Wang, Y.X. and M.I. Kotlikoff, *Inactivation of calcium-activated chloride channels in smooth muscle by calcium/calmodulin-dependent protein kinase.* Proc Natl Acad Sci U S A, 1997. **94**(26): p. 14918-23.
242. Tian, Y., et al., *Calmodulin-dependent activation of the epithelial calcium-dependent chloride channel TMEM16A.* FASEB J, 2011. **25**(3): p. 1058-68.
243. Praetorius, J., et al., *Molecular and functional evidence for electrogenic and electroneutral Na(+)-HCO(3)(-) cotransporters in murine duodenum.* Am J Physiol Gastrointest Liver Physiol, 2001. **280**(3): p. G332-43.
244. Nickell, W.T., N.K. Kleene, and S.J. Kleene, *Mechanisms of neuronal chloride accumulation in intact mouse olfactory epithelium.* J Physiol, 2007. **583**(Pt 3): p. 1005-20.
245. Qu, Z. and H.C. Hartzell, *Functional geometry of the permeation pathway of Ca^{2+}-activated Cl^-channels inferred from analysis of voltage-dependent block.* J Biol Chem, 2001. **276**(21): p. 18423-9.

246. Hogg, R.C., Q. Wang, and W.A. Large, *Action of niflumic acid on evoked and spontaneous calcium-activated chloride and potassium currents in smooth muscle cells from rabbit portal vein.* Br J Pharmacol, 1994. **112**(3): p. 977-84.
247. Bradley, E., et al., *Pharmacological characterization of TMEM16A currents.* Channels (Austin), 2014. **8**(3).
248. Piper, A.S. and I.A. Greenwood, *Anomalous effect of anthracene-9-carboxylic acid on calcium-activated chloride currents in rabbit pulmonary artery smooth muscle cells.* Br J Pharmacol, 2003. **138**(1): p. 31-8.
249. Saleh, S.N., et al., *Stimulation of Ca^{2+}-gated Cl^- currents by the calcium-dependent K^+ channel modulators NS1619 [1,3-dihydro-1-[2-hydroxy-5-(trifluoromethyl)phenyl]-5-(trifluoromethyl)-2H-benzi midazol-2-one] and isopimaric acid.* J Pharmacol Exp Ther, 2007. **321**(3): p. 1075-84.
250. Ai, T., et al., *Direct effects of 9-anthracene compounds on cystic fibrosis transmembrane conductance regulator gating.* Pflugers Arch, 2004. **449**(1): p. 88-95.
251. De La Fuente, R., et al., *Small-molecule screen identifies inhibitors of a human intestinal calcium-activated chloride channel.* Mol Pharmacol, 2008. **73**(3): p. 758-68.
252. Namkung, W., et al., *Small-molecule activators of TMEM16A, a calcium-activated chloride channel, stimulate epithelial chloride secretion and intestinal contraction.* FASEB J, 2011. **25**(11): p. 4048-62.
253. Duvvuri, U., et al., *TMEM16A induces MAPK and contributes directly to tumorigenesis and cancer progression.* Cancer Res, 2012. **72**(13): p. 3270-81.
254. Okada, Y., *Cell volume-sensitive chloride channels: phenotypic properties and molecular identity.* Contrib Nephrol, 2006. **152**: p. 9-24.
255. Reuter, D., et al., *A depolarizing chloride current contributes to chemoelectrical transduction in olfactory sensory neurons in situ.* J Neurosci, 1998. **18**(17): p. 6623-30.
256. Cho, H., et al., *The calcium-activated chloride channel anoctamin 1 acts as a heat sensor in nociceptive neurons.* Nat Neurosci, 2012. **15**(7): p. 1015-21.
257. Andre, S., et al., *Axotomy-induced expression of calcium-activated chloride current in subpopulations of mouse dorsal root ganglion neurons.* J Neurophysiol, 2003. **90**(6): p. 3764-73.
258. Boudes, M., et al., *Best1 is a gene regulated by nerve injury and required for Ca^{2+}-activated Cl^- current expression in axotomized sensory neurons.* J Neurosci, 2009. **29**(32): p. 10063-71.
259. Britschgi, A., et al., *Calcium-activated chloride channel ANO1 promotes breast cancer progression by activating EGFR and CAMK signaling.* Proc Natl Acad Sci U S A, 2013. **110**(11): p. E1026-34.
260. Huang, F., et al., *Studies on expression and function of the TMEM16A calcium-activated chloride channel.* Proc Natl Acad Sci U S A, 2009. **106**(50): p. 21413-8.
261. Ruiz, C., et al., *Enhanced expression of ANO1 in head and neck squamous cell carcinoma causes cell migration and correlates with poor prognosis.* PLoS One, 2012. **7**(8): p. e43265.
262. Liu, W., et al., *Inhibition of Ca(2+)-activated Cl(-) channel ANO1/TMEM16A expression suppresses tumor growth and invasiveness in human prostate carcinoma.* Cancer Lett, 2012. **326**(1): p. 41-51.
263. Scudieri, P., et al., *Association of TMEM16A chloride channel overexpression with airway goblet cell metaplasia.* J Physiol, 2012. **590**(Pt 23): p. 6141-55.
264. Pifferi, S., M. Dibattista, and A. Menini, *TMEM16B induces chloride currents activated by calcium in mammalian cells.* Pflugers Arch, 2009. **458**(6): p. 1023-38.

265. Stephan, A.B., et al., *ANO2 is the cilial calcium-activated chloride channel that may mediate olfactory amplification.* Proc Natl Acad Sci U S A, 2009. **106**(28): p. 11776-81.
266. Cenedese, V., et al., *The voltage dependence of the TMEM16B/anoctamin2 calcium-activated chloride channel is modified by mutations in the first putative intracellular loop.* J Gen Physiol, 2012. **139**(4): p. 285-94.
267. Ferrera, L., et al., *Regulation of TMEM16A chloride channel properties by alternative splicing.* J Biol Chem, 2009. **284**(48): p. 33360-8.
268. Pifferi, S., V. Cenedese, and A. Menini, *Anoctamin 2/TMEM16B: a calcium-activated chloride channel in olfactory transduction.* Exp Physiol, 2012. **97**(2): p. 193-9.
269. Stohr, H., et al., *TMEM16B, a novel protein with calcium-dependent chloride channel activity, associates with a presynaptic protein complex in photoreceptor terminals.* J Neurosci, 2009. **29**(21): p. 6809-18.
270. Frings, S., D. Reuter, and S.J. Kleene, *Neuronal Ca^{2+} -activated Cl^- channels--homing in on an elusive channel species.* Prog Neurobiol, 2000. **60**(3): p. 247-89.
271. Kleene, S.J., *The electrochemical basis of odor transduction in vertebrate olfactory cilia.* Chem Senses, 2008. **33**(9): p. 839-59.
272. Dibattista, M., et al., *Calcium-activated chloride channels in the apical region of mouse vomeronasal sensory neurons.* J Gen Physiol, 2012. **140**(1): p. 3-15.
273. Billig, G.M., et al., *Ca^{2+}-activated Cl^- currents are dispensable for olfaction.* Nat Neurosci, 2011. **14**(6): p. 763-9.
274. Duran, C., et al., *ANOs 3-7 in the anoctamin/Tmem16 Cl^- channel family are intracellular proteins.* Am J Physiol Cell Physiol, 2012. **302**(3): p. C482-93.
275. Schreiber, R., et al., *Expression and function of epithelial anoctamins.* J Biol Chem, 2010. **285**(10): p. 7838-45.
276. Suzuki, J., et al., *Calcium-dependent phospholipid scrambling by TMEM16F.* Nature, 2010. **468**(7325): p. 834-8.
277. Yang, H., et al., *TMEM16F forms a Ca^{2+}-activated cation channel required for lipid scrambling in platelets during blood coagulation.* Cell, 2012. **151**(1): p. 111-22.
278. Suzuki, J., et al., *Calcium-dependent Phospholipid Scramblase Activity of TMEM16 Family Members.* J Biol Chem, 2013.
279. Martins, J.R., et al., *Anoctamin 6 is an essential component of the outwardly rectifying chloride channel.* Proc Natl Acad Sci U S A, 2011. **108**(44): p. 18168-72.
280. Shimizu, T., et al., *TMEM16F is a component of a Ca^{2+}-activated Cl^- channel but not a volume-sensitive outwardly rectifying Cl^- channel.* Am J Physiol Cell Physiol, 2013. **304**(8): p. C748-59.
281. Huang, F., et al., *TMEM16C facilitates Na(+)-activated K^+ currents in rat sensory neurons and regulates pain processing.* Nat Neurosci, 2013. **16**(9): p. 1284-90.
282. Jin, X., et al., *Blockade of AP-1 activity by dominant-negative TAM67 can abrogate the oncogenic phenotype in latent membrane protein 1-positive human nasopharyngeal carcinoma.* Mol Carcinog, 2007. **46**(11): p. 901-11.
283. Jin, X., et al., *Expression and function of osteopontin in vascular adventitial fibroblasts and pathological vascular remodeling.* PLoS One, 2011. **6**(9): p. e23558.
284. Oldfield, S., et al., *Receptor-mediated suppression of potassium currents requires colocalization within lipid rafts.* Mol Pharmacol, 2009. **76**(6): p. 1279-89.
285. Singh, R.K., et al., *An MHC-I cytoplasmic domain/HIV-1 Nef fusion protein binds directly to the mu subunit of the AP-1 endosomal coat complex.* PLoS One, 2009. **4**(12): p. e8364.

286. Galietta, L.J., P.M. Haggie, and A.S. Verkman, *Green fluorescent protein-based halide indicators with improved chloride and iodide affinities.* FEBS Lett, 2001. **499**(3): p. 220-4.
287. Linley, J.E., et al., *Reactive oxygen species are second messengers of neurokinin signaling in peripheral sensory neurons.* Proc Natl Acad Sci U S A, 2012. **109**: p. E1578-E1586.
288. Soderberg, O., et al., *Direct observation of individual endogenous protein complexes in situ by proximity ligation.* Nat Methods, 2006. **3**(12): p. 995-1000.
289. Weibrecht, I., et al., *Proximity ligation assays: a recent addition to the proteomics toolbox.* Expert Rev Proteomics, 2010. **7**(3): p. 401-9.
290. Mahen, R., et al., *A-type lamins maintain the positional stability of DNA damage repair foci in mammalian nuclei.* PLoS One, 2013. **8**(5): p. e61893.
291. Jarvius, M., et al., *In situ detection of phosphorylated platelet-derived growth factor receptor beta using a generalized proximity ligation method.* Mol Cell Proteomics, 2007. **6**(9): p. 1500-9.
292. Raghuram, V., Y. Sharma, and M.R. Kreutz, *Ca(2+) sensor proteins in dendritic spines: a race for Ca(2+).* Front Mol Neurosci, 2012. **5**: p. 61.
293. Schreiber, M. and L. Salkoff, *A novel calcium-sensing domain in the BK channel.* Biophys J, 1997. **73**(3): p. 1355-63.
294. Bian, S., I. Favre, and E. Moczydlowski, *Ca^{2+}-binding activity of a COOH-terminal fragment of the Drosophila BK channel involved in Ca^{2+}-dependent activation.* Proc Natl Acad Sci U S A, 2001. **98**(8): p. 4776-81.
295. Bao, L., et al., *Mapping the BKCa channel's "Ca^{2+} bowl": side-chains essential for Ca^{2+} sensing.* J Gen Physiol, 2004. **123**(5): p. 475-89.
296. Xia, X.M., X. Zeng, and C.J. Lingle, *Multiple regulatory sites in large-conductance calcium-activated potassium channels.* Nature, 2002. **418**(6900): p. 880-4.
297. Shi, J., et al., *Mechanism of magnesium activation of calcium-activated potassium channels.* Nature, 2002. **418**(6900): p. 876-80.
298. Vocke, K., et al., *Calmodulin-dependent activation and inactivation of anoctamin calcium-gated chloride channels.* J Gen Physiol, 2013. **142**(4): p. 381-404.
299. Ferrera, L., A. Caputo, and L.J. Galietta, *TMEM16A protein: a new identity for Ca(2+)-dependent Cl(-) channels.* Physiology (Bethesda), 2010. **25**(6): p. 357-63.
300. Yuan, P., et al., *Structure of the human BK channel Ca^{2+}-activation apparatus at 3.0 A resolution.* Science, 2010. **329**(5988): p. 182-6.
301. Scudieri, P., et al., *TMEM16A-TMEM16B chimeras to investigate the structure-function relationship of calcium-activated chloride channels.* Biochem J, 2013. **452**(3): p. 443-55.
302. Terashima, H., A. Picollo, and A. Accardi, *Purified TMEM16A is sufficient to form Ca^{2+}-activated Cl^- channels.* Proc Natl Acad Sci U S A, 2013. **110**(48): p. 19354-9.
303. Yu, K., et al., *Activation of the Ano1 (TMEM16A) chloride channel by calcium is not mediated by calmodulin.* J Gen Physiol, 2014. **143**(2): p. 253-67.
304. Bandell, M. and A. Patapoutian, *A hot new channel.* Nat Neurosci, 2012. **15**(7): p. 931-3.
305. Perez-Cornejo, P., et al., *Anoctamin 1 (Tmem16A) Ca^{2+}-activated chloride channel stoichiometrically interacts with an ezrin-radixin-moesin network.* Proc Natl Acad Sci U S A, 2012. **109**(26): p. 10376-81.
306. Du, X., et al., *Control of somatic membrane potential in nociceptive neurons and its implications for peripheral nociceptive transmission.* Pain, 2014. **155**(11): p. 2306-22.
307. Davis, A.J., et al., *Expression profile and protein translation of TMEM16A in murine smooth muscle.* Am J Physiol Cell Physiol, 2010. **299**(5): p. C948-59.

308. Gallos, G., et al., *Functional expression of the TMEM16 family of calcium-activated chloride channels in airway smooth muscle.* Am J Physiol Lung Cell Mol Physiol, 2013. **305**(9): p. L625-34.
309. McGahon, M.K., et al., *Ca^{2+}-activated Cl^- current in retinal arteriolar smooth muscle.* Invest Ophthalmol Vis Sci, 2009. **50**(1): p. 364-71.
310. Ni, Y.L., A.S. Kuan, and T.Y. Chen, *Activation and inhibition of TMEM16A calcium-activated chloride channels.* PLoS One, 2014. **9**(1): p. e86734.
311. Yuan, X.J., *Role of calcium-activated chloride current in regulating pulmonary vasomotor tone.* Am J Physiol, 1997. **272**(5 Pt 1): p. L959-68.
312. Kunzelmann, K., et al., *Bestrophin and TMEM16-Ca(2+) activated Cl(-) channels with different functions.* Cell Calcium, 2009. **46**(4): p. 233-41.
313. Gamper, N. and T. Rohacs, *Phosphoinositide sensitivity of ion channels, a functional perspective.* Subcell Biochem, 2012. **59**: p. 289-333.
314. Pritchard, H.A., et al., *Inhibitory role of phosphatidylinositol 4,5-bisphosphate on TMEM16A-encoded calcium-activated chloride channels in rat pulmonary artery.* Br J Pharmacol, 2014. **171**(18): p. 4311-21.
315. Bader, C.R., D. Bertrand, and R. Schlichter, *Calcium-activated chloride current in cultured sensory and parasympathetic quail neurones.* J Physiol, 1987. **394**: p. 125-48.
316. Sanchez-Vives, M.V. and R. Gallego, *Calcium-dependent chloride current induced by axotomy in rat sympathetic neurons.* J Physiol, 1994. **475**(3): p. 391-400.
317. Lancaster, E., et al., *Calcium and calcium-activated currents in vagotomized rat primary vagal afferent neurons.* J Physiol, 2002. **540**(Pt 2): p. 543-56.
318. Yeagle, P.L. and A.D. Albert, *G-protein coupled receptor structure.* Biochim Biophys Acta, 2007. **1768**(4): p. 808-24.
319. Wess, J., *G-protein-coupled receptors: molecular mechanisms involved in receptor activation and selectivity of G-protein recognition.* FASEB J, 1997. **11**(5): p. 346-54.
320. Hamm, H.E. and A. Gilchrist, *Heterotrimeric G proteins.* Curr Opin Cell Biol, 1996. **8**(2): p. 189-96.
321. Engelhardt, S. and F. Rochais, *G proteins: more than transducers of receptor-generated signals?* Circ Res, 2007. **100**(8): p. 1109-11.
322. Gilman, A.G., *G proteins: transducers of receptor-generated signals.* Annu Rev Biochem, 1987. **56**: p. 615-49.
323. Clapham, D.E. and E.J. Neer, *G protein beta gamma subunits.* Annu Rev Pharmacol Toxicol, 1997. **37**: p. 167-203.
324. Solinski, H.J., et al., *Human sensory neuron-specific Mas-related G protein-coupled receptors-X1 sensitize and directly activate transient receptor potential cation channel V1 via distinct signaling pathways.* J Biol Chem, 2012. **287**(49): p. 40956-71.
325. Dai, Y., et al., *Sensitization of TRPA1 by PAR2 contributes to the sensation of inflammatory pain.* J Clin Invest, 2007. **117**(7): p. 1979-87.
326. Song, S.O. and J. Varner, *Modeling and analysis of the molecular basis of pain in sensory neurons.* PLoS One, 2009. **4**(9): p. e6758.
327. Altier, C., *GPCR and Voltage-Gated Calcium Channels (VGCC) Signaling Complexes.* Subcell Biochem, 2012. **63**: p. 241-62.
328. Linley, J.E., et al., *M channel enhancers and physiological M channel block.* J Physiol, 2012. **590**(Pt 4): p. 793-807.
329. Amaya, F., et al., *The voltage-gated sodium channel Na(v)1.9 is an effector of peripheral inflammatory pain hypersensitivity.* J Neurosci, 2006. **26**(50): p. 12852-60.
330. Petho, G. and P.W. Reeh, *Sensory and signaling mechanisms of bradykinin, eicosanoids, platelet-activating factor, and nitric oxide in peripheral nociceptors.* Physiol Rev, 2012. **92**(4): p. 1699-775.

331. Blais, C., Jr., et al., *The kallikrein-kininogen-kinin system: lessons from the quantification of endogenous kinins.* Peptides, 2000. **21**(12): p. 1903-40.
332. Ni, A., et al., *Molecular cloning and expression of rat bradykinin B1 receptor.* Biochim Biophys Acta, 1998. **1442**(2-3): p. 177-85.
333. Sardi, S.P., et al., *Bradykinin B1 receptors in human umbilical vein: pharmacological evidence of up-regulation, and induction by interleukin-1 beta.* Eur J Pharmacol, 1998. **358**(3): p. 221-7.
334. Medeiros, R., et al., *Bradykinin B1 receptor expression induced by tissue damage in the rat portal vein: a critical role for mitogen-activated protein kinase and nuclear factor-kappaB signaling pathways.* Circ Res, 2004. **94**(10): p. 1375-82.
335. Clark, M.A., et al., *Islet-activating protein inhibits leukotriene D4- and leukotriene C4- but not bradykinin- or calcium ionophore-induced prostacyclin synthesis in bovine endothelial cells.* Proc Natl Acad Sci U S A, 1986. **83**(19): p. 7320-4.
336. Hong, S.L. and D. Deykin, *Activation of phospholipases A2 and C in pig aortic endothelial cells synthesizing prostacyclin.* J Biol Chem, 1982. **257**(12): p. 7151-4.
337. Smith, J.A., et al., *Signal transduction pathways for B1 and B2 bradykinin receptors in bovine pulmonary artery endothelial cells.* Mol Pharmacol, 1995. **47**(3): p. 525-34.
338. Regoli, D., et al., *Bradykinin receptors and their antagonists.* Eur J Pharmacol, 1998. **348**(1): p. 1-10.
339. Bhoola, K., et al., *Kallikrein and kinin receptor expression in inflammation and cancer.* Biol Chem, 2001. **382**(1): p. 77-89.
340. Leeb-Lundberg, L.M., et al., *International union of pharmacology. XLV. Classification of the kinin receptor family: from molecular mechanisms to pathophysiological consequences.* Pharmacol Rev, 2005. **57**(1): p. 27-77.
341. Kuoppala, A., et al., *Inactivation of bradykinin by angiotensin-converting enzyme and by carboxypeptidase N in human plasma.* Am J Physiol Heart Circ Physiol, 2000. **278**(4): p. H1069-74.
342. Dray, A. and M. Perkins, *Bradykinin and inflammatory pain.* Trends Neurosci, 1993. **16**(3): p. 99-104.
343. Steranka, L.R., et al., *Bradykinin as a pain mediator: receptors are localized to sensory neurons, and antagonists have analgesic actions.* Proc Natl Acad Sci U S A, 1988. **85**(9): p. 3245-9.
344. Dray, A., et al., *Bradykinin-induced activation of nociceptors: receptor and mechanistic studies on the neonatal rat spinal cord-tail preparation in vitro.* Br J Pharmacol, 1992. **107**(4): p. 1129-34.
345. Haley, J.E., A.H. Dickenson, and M. Schachter, *Electrophysiological evidence for a role of bradykinin in chemical nociception in the rat.* Neurosci Lett, 1989. **97**(1-2): p. 198-202.
346. Geppetti, P., et al., *Bradykinin-induced release of calcitonin gene-related peptide from capsaicin-sensitive nerves in guinea-pig atria: mechanism of action and calcium requirements.* Neuroscience, 1990. **38**(3): p. 687-92.
347. Scholz, J. and C.J. Woolf, *The neuropathic pain triad: neurons, immune cells and glia.* Nat Neurosci, 2007. **10**(11): p. 1361-8.
348. Davis, A.J. and M.N. Perkins, *The involvement of bradykinin B1 and B2 receptor mechanisms in cytokine-induced mechanical hyperalgesia in the rat.* Br J Pharmacol, 1994. **113**(1): p. 63-8.
349. Petersen, M., et al., *Plasticity in the expression of bradykinin binding sites in sensory neurons after mechanical nerve injury.* Neuroscience, 1998. **83**(3): p. 949-59.

350. Eckert, A., et al., *Spatio-temporal pattern of induction of bradykinin receptors and inflammation in rat dorsal root ganglia after unilateral nerve ligation.* Pain, 1999. **83**(3): p. 487-97.
351. Pesquero, J.B., et al., *Hypoalgesia and altered inflammatory responses in mice lacking kinin B1 receptors.* Proc Natl Acad Sci U S A, 2000. **97**(14): p. 8140-5.
352. Rupniak, N.M., et al., *Effects of the bradykinin B1 receptor antagonist des-Arg9[Leu8]bradykinin and genetic disruption of the B2 receptor on nociception in rats and mice.* Pain, 1997. **71**(1): p. 89-97.
353. Macfarlane, S.R., et al., *Proteinase-activated receptors.* Pharmacol Rev, 2001. **53**(2): p. 245-82.
354. O'Brien, P.J., et al., *Protease activated receptors: theme and variations.* Oncogene, 2001. **20**(13): p. 1570-81.
355. Kahn, M.L., et al., *A dual thrombin receptor system for platelet activation.* Nature, 1998. **394**(6694): p. 690-4.
356. Xu, W.F., et al., *Cloning and characterization of human protease-activated receptor 4.* Proc Natl Acad Sci U S A, 1998. **95**(12): p. 6642-6.
357. Nakanishi-Matsui, M., et al., *PAR3 is a cofactor for PAR4 activation by thrombin.* Nature, 2000. **404**(6778): p. 609-13.
358. Chow, J.M., J.D. Moffatt, and T.M. Cocks, *Effect of protease-activated receptor (PAR)-1, -2 and -4-activating peptides, thrombin and trypsin in rat isolated airways.* Br J Pharmacol, 2000. **131**(8): p. 1584-91.
359. Vergnolle, N., *Modulation of visceral pain and inflammation by protease-activated receptors.* Br J Pharmacol, 2004. **141**(8): p. 1264-74.
360. Dinh, Q.T., et al., *Protease-activated receptor 2 expression in trigeminal neurons innervating the rat nasal mucosa.* Neuropeptides, 2005. **39**(5): p. 461-6.
361. Steinhoff, M., et al., *Agonists of proteinase-activated receptor 2 induce inflammation by a neurogenic mechanism.* Nat Med, 2000. **6**(2): p. 151-8.
362. Vergnolle, N., et al., *Proteinase-activated receptor-2 and hyperalgesia: A novel pain pathway.* Nat Med, 2001. **7**(7): p. 821-6.
363. Ikehara, O., et al., *Proteinase-activated receptors-1 and 2 induce electrogenic Cl^- secretion in the mouse cecum by distinct mechanisms.* Am J Physiol Gastrointest Liver Physiol, 2010. **299**(1): p. G115-25.
364. Dai, Y., et al., *Proteinase-activated receptor 2-mediated potentiation of transient receptor potential vanilloid subfamily 1 activity reveals a mechanism for proteinase-induced inflammatory pain.* J Neurosci, 2004. **24**(18): p. 4293-9.
365. Amadesi, S., et al., *Protease-activated receptor 2 sensitizes the capsaicin receptor transient receptor potential vanilloid receptor 1 to induce hyperalgesia.* J Neurosci, 2004. **24**(18): p. 4300-12.
366. Lee, B., et al., *Anoctamin 1 contributes to inflammatory and nerve-injury induced hypersensitivity.* Mol Pain, 2014. **10**: p. 5.
367. Vergnolle, N., *Protease-activated receptors and inflammatory hyperalgesia.* Mem Inst Oswaldo Cruz, 2005. **100 Suppl 1**: p. 173-6.
368. Chen, Y., C. Yang, and Z.J. Wang, *Proteinase-activated receptor 2 sensitizes transient receptor potential vanilloid 1, transient receptor potential vanilloid 4, and transient receptor potential ankyrin 1 in paclitaxel-induced neuropathic pain.* Neuroscience, 2011. **193**: p. 440-51.
369. Parekh, A.B. and J.W. Putney, Jr., *Store-operated calcium channels.* Physiol Rev, 2005. **85**(2): p. 757-810.
370. Parekh, A.B. and R. Penner, *Store depletion and calcium influx.* Physiol Rev, 1997. **77**(4): p. 901-30.

371. Ramachandran, R. and M.D. Hollenberg, *Proteinases and signalling: pathophysiological and therapeutic implications via PARs and more.* Br J Pharmacol, 2008. **153 Suppl 1**: p. S263-82.
372. Shimazaki, A., et al., *Gangliosides and chondroitin sulfate desensitize and internalize B2 bradykinin receptors.* Biochem Biophys Res Commun, 2012. **420**(1): p. 193-8.
373. Bawolak, M.T., et al., *Effects of inactivation-resistant agonists on the signalling, desensitization and down-regulation of bradykinin B(2) receptors.* Br J Pharmacol, 2009. **158**(5): p. 1375-86.
374. Simaan, M., et al., *Dissociation of beta-arrestin from internalized bradykinin B2 receptor is necessary for receptor recycling and resensitization.* Cell Signal, 2005. **17**(9): p. 1074-83.
375. Ricks, T.K. and J. Trejo, *Phosphorylation of protease-activated receptor-2 differentially regulates desensitization and internalization.* J Biol Chem, 2009. **284**(49): p. 34444-57.
376. D'Andrea, M.R., et al., *Characterization of protease-activated receptor-2 immunoreactivity in normal human tissues.* J Histochem Cytochem, 1998. **46**(2): p. 157-64.
377. von Banchet, G.S., et al., *Monoarticular antigen-induced arthritis leads to pronounced bilateral upregulation of the expression of neurokinin 1 and bradykinin 2 receptors in dorsal root ganglion neurons of rats.* Arthritis Res, 2000. **2**(5): p. 424-7.
378. Darszon, A., et al., *Calcium channels in the development, maturation, and function of spermatozoa.* Physiol Rev, 2011. **91**(4): p. 1305-55.
379. Cao, Y.Q., *Voltage-gated calcium channels and pain.* Pain, 2006. **126**(1-3): p. 5-9.
380. Catterall, W.A., et al., *International Union of Pharmacology. XLVIII. Nomenclature and structure-function relationships of voltage-gated calcium channels.* Pharmacol Rev, 2005. **57**(4): p. 411-25.
381. Buraei, Z. and J. Yang, *The ss subunit of voltage-gated Ca^{2+} channels.* Physiol Rev, 2010. **90**(4): p. 1461-506.
382. Guy, H.R. and S.R. Durell, *Structural models of Na^{+}, Ca^{2+}, and K^{+} channels.* Soc Gen Physiol Ser, 1995. **50**: p. 1-16.
383. Catterall, W.A., *Voltage-gated calcium channels.* Cold Spring Harb Perspect Biol, 2011. **3**(8): p. a003947.
384. Lehmann-Horn, F. and K. Jurkat-Rott, *Voltage-gated ion channels and hereditary disease.* Physiol Rev, 1999. **79**(4): p. 1317-72.
385. Nargeot, J., P. Lory, and S. Richard, *Molecular basis of the diversity of calcium channels in cardiovascular tissues.* Eur Heart J, 1997. **18 Suppl A**: p. A15-26.
386. Hemond, P.J., et al., *Simulated GABA synaptic input and L-type calcium channels form functional microdomains in hypothalamic gonadotropin-releasing hormone neurons.* J Neurosci, 2012. **32**(26): p. 8756-66.
387. Bito, H., K. Deisseroth, and R.W. Tsien, *Ca^{2+}-dependent regulation in neuronal gene expression.* Curr Opin Neurobiol, 1997. **7**(3): p. 419-29.
388. Rola, R., P.J. Szulczyk, and G. Witkowski, *Voltage-dependent Ca^{2+} currents in rat cardiac dorsal root ganglion neurons.* Brain Res, 2003. **961**(1): p. 171-8.
389. Heinke, B., E. Balzer, and J. Sandkuhler, *Pre- and postsynaptic contributions of voltage-dependent Ca^{2+} channels to nociceptive transmission in rat spinal lamina I neurons.* Eur J Neurosci, 2004. **19**(1): p. 103-11.
390. Fioretti, B., et al., *Trigeminal ganglion neuron subtype-specific alterations of Ca(V)2.1 calcium current and excitability in a Cacna1a mouse model of migraine.* J Physiol, 2011. **589**(Pt 23): p. 5879-95.

391. Molderings, G.J., J. Likungu, and M. Gothert, *N-Type calcium channels control sympathetic neurotransmission in human heart atrium.* Circulation, 2000. **101**(4): p. 403-7.
392. Rose, K.E., et al., *Immunohistological demonstration of CaV3.2 T-type voltage-gated calcium channel expression in soma of dorsal root ganglion neurons and peripheral axons of rat and mouse.* Neuroscience, 2013. **250**: p. 263-74.
393. Perez-Reyes, E., *Molecular physiology of low-voltage-activated t-type calcium channels.* Physiol Rev, 2003. **83**(1): p. 117-61.
394. Chan, J., et al., *Structural studies of inositol 1,4,5-trisphosphate receptor: coupling ligand binding to channel gating.* J Biol Chem, 2010. **285**(46): p. 36092-9.
395. da Fonseca, P.C., et al., *Domain organization of the type 1 inositol 1,4,5-trisphosphate receptor as revealed by single-particle analysis.* Proc Natl Acad Sci U S A, 2003. **100**(7): p. 3936-41.
396. Taylor, C.W., P.C. da Fonseca, and E.P. Morris, *IP(3) receptors: the search for structure.* Trends Biochem Sci, 2004. **29**(4): p. 210-9.
397. Galvan, D.L., et al., *Subunit oligomerization, and topology of the inositol 1,4, 5-trisphosphate receptor.* J Biol Chem, 1999. **274**(41): p. 29483-92.
398. Parker, A.K., F.V. Gergely, and C.W. Taylor, *Targeting of inositol 1,4,5-trisphosphate receptors to the endoplasmic reticulum by multiple signals within their transmembrane domains.* J Biol Chem, 2004. **279**(22): p. 23797-805.
399. Bezprozvanny, I., *The inositol 1,4,5-trisphosphate receptors.* Cell Calcium, 2005. **38**(3-4): p. 261-72.
400. Zhang, S., et al., *Inositol 1,4,5-trisphosphate receptor subtype-specific regulation of calcium oscillations.* Neurochem Res, 2011. **36**(7): p. 1175-85.
401. Allbritton, N.L., T. Meyer, and L. Stryer, *Range of messenger action of calcium ion and inositol 1,4,5-trisphosphate.* Science, 1992. **258**(5089): p. 1812-5.
402. Scheff, N.N., S.G. Lu, and M.S. Gold, *Contribution of endoplasmic reticulum Ca(2+) regulatory mechanisms to the inflammation-induced increase in the evoked Ca(2+) transient in rat cutaneous dorsal root ganglion neurons.* Cell Calcium, 2013. **54**(1): p. 46-56.
403. Lai, F.A., et al., *Purification and reconstitution of the calcium release channel from skeletal muscle.* Nature, 1988. **331**(6154): p. 315-9.
404. Inui, M., A. Saito, and S. Fleischer, *Purification of the ryanodine receptor and identity with feet structures of junctional terminal cisternae of sarcoplasmic reticulum from fast skeletal muscle.* J Biol Chem, 1987. **262**(4): p. 1740-7.
405. Avila, G., et al., *FKBP12 binding to RyR1 modulates excitation-contraction coupling in mouse skeletal myotubes.* J Biol Chem, 2003. **278**(25): p. 22600-8.
406. Stutzmann, G.E. and M.P. Mattson, *Endoplasmic reticulum Ca(2+) handling in excitable cells in health and disease.* Pharmacol Rev, 2011. **63**(3): p. 700-27.
407. Hertle, D.N. and M.F. Yeckel, *Distribution of inositol-1,4,5-trisphosphate receptor isotypes and ryanodine receptor isotypes during maturation of the rat hippocampus.* Neuroscience, 2007. **150**(3): p. 625-38.
408. Dulhunty, A.F., N.A. Beard, and A.D. Hanna, *Regulation and dysregulation of cardiac ryanodine receptor (RyR2) open probability during diastole in health and disease.* J Gen Physiol, 2012. **140**(2): p. 87-92.
409. Fill, M. and J.A. Copello, *Ryanodine receptor calcium release channels.* Physiol Rev, 2002. **82**(4): p. 893-922.
410. Rybalchenko, V., et al., *The cytosolic N-terminus of presenilin-1 potentiates mouse ryanodine receptor single channel activity.* Int J Biochem Cell Biol, 2008. **40**(1): p. 84-97.

411. Zhang, H., et al., *Role of presenilins in neuronal calcium homeostasis.* J Neurosci, 2010. **30**(25): p. 8566-80.
412. Van Petegem, F., *Ryanodine receptors: structure and function.* J Biol Chem, 2012. **287**(38): p. 31624-32.
413. Goswami, C., et al., *Importance of non-selective cation channel TRPV4 interaction with cytoskeleton and their reciprocal regulations in cultured cells.* PLoS One, 2010. **5**(7): p. e11654.
414. Shim, S., et al., *XTRPC1-dependent chemotropic guidance of neuronal growth cones.* Nat Neurosci, 2005. **8**(6): p. 730-5.
415. Di, A., et al., *The redox-sensitive cation channel TRPM2 modulates phagocyte ROS production and inflammation.* Nat Immunol, 2012. **13**(1): p. 29-34.
416. Simon, F., et al., *Non-selective cation channels and oxidative stress-induced cell swelling.* Biol Res, 2002. **35**(2): p. 215-22.
417. Venkatachalam, K., et al., *The cellular and molecular basis of store-operated calcium entry.* Nat Cell Biol, 2002. **4**(11): p. E263-72.
418. Minke, B., *The TRP channel and phospholipase C-mediated signaling.* Cell Mol Neurobiol, 2001. **21**(6): p. 629-43.
419. Gottlieb, P., et al., *Revisiting TRPC1 and TRPC6 mechanosensitivity.* Pflugers Arch, 2008. **455**(6): p. 1097-103.
420. Caterina, M.J. and D. Julius, *The vanilloid receptor: a molecular gateway to the pain pathway.* Annu Rev Neurosci, 2001. **24**: p. 487-517.
421. Julius, D. and A.I. Basbaum, *Molecular mechanisms of nociception.* Nature, 2001. **413**(6852): p. 203-10.
422. Rosenbaum, T. and S.A. Simon, *TRPV1 Receptors and Signal Transduction*, in *TRP Ion Channel Function in Sensory Transduction and Cellular Signaling Cascades*, W.B. Liedtke and S. Heller, Editors. 2007: Boca Raton (FL).
423. Caterina, M.J., et al., *A capsaicin-receptor homologue with a high threshold for noxious heat.* Nature, 1999. **398**(6726): p. 436-41.
424. Peier, A.M., et al., *A heat-sensitive TRP channel expressed in keratinocytes.* Science, 2002. **296**(5575): p. 2046-9.
425. Peier, A.M., et al., *A TRP channel that senses cold stimuli and menthol.* Cell, 2002. **108**(5): p. 705-15.
426. Story, G.M., et al., *ANKTM1, a TRP-like channel expressed in nociceptive neurons, is activated by cold temperatures.* Cell, 2003. **112**(6): p. 819-29.
427. Torres, G.E., T.M. Egan, and M.M. Voigt, *Identification of a domain involved in ATP-gated ionotropic receptor subunit assembly.* J Biol Chem, 1999. **274**(32): p. 22359-65.
428. Jarvis, M.F. and B.S. Khakh, *ATP-gated P2X cation-channels.* Neuropharmacology, 2009. **56**(1): p. 208-15.
429. Nicke, A., *Homotrimeric complexes are the dominant assembly state of native P2X7 subunits.* Biochem Biophys Res Commun, 2008. **377**(3): p. 803-8.
430. Mo, G., et al., *Subtype-specific regulation of P2X3 and P2X2/3 receptors by phosphoinositides in peripheral nociceptors.* Mol Pain, 2009. **5**: p. 47.
431. Boudes, M. and F. Scamps, *Calcium-activated chloride current expression in axotomized sensory neurons: what for?* Front Mol Neurosci, 2012. **5**: p. 35.
432. Courjaret, R. and K. Machaca, *Mid-range Ca^{2+} signalling mediated by functional coupling between store-operated Ca^{2+} entry and IP_3-dependent Ca^{2+} release.* Nat Commun, 2014. **5**: p. 3916.
433. Dent, M.A., G. Raisman, and F.A. Lai, *Expression of type 1 inositol 1,4,5-trisphosphate receptor during axogenesis and synaptic contact in the central and peripheral nervous system of developing rat.* Development, 1996. **122**(3): p. 1029-39.

434. Lu, L., et al., *Molecular coupling of a Ca^{2+}-activated K^+ channel to L-type Ca^{2+} channels via alpha-actinin2.* Circ Res, 2007. **100**(1): p. 112-20.
435. Yan, J. and R.W. Aldrich, *LRRC26 auxiliary protein allows BK channel activation at resting voltage without calcium.* Nature, 2010. **466**(7305): p. 513-6.
436. Berridge, M.J., P. Lipp, and M.D. Bootman, *The versatility and universality of calcium signalling.* Nat Rev Mol Cell Biol, 2000. **1**(1): p. 11-21.
437. Berridge, M.J., *Calcium microdomains: organization and function.* Cell Calcium, 2006. **40**(5-6): p. 405-12.
438. Braet, K., et al., *Calcium signal communication in the central nervous system.* Biol Cell, 2004. **96**(1): p. 79-91.
439. Demuro, A. and I. Parker, *Imaging single-channel calcium microdomains.* Cell Calcium, 2006. **40**(5-6): p. 413-22.
440. Oheim, M., F. Kirchhoff, and W. Stuhmer, *Calcium microdomains in regulated exocytosis.* Cell Calcium, 2006. **40**(5-6): p. 423-39.
441. Berkefeld, H., et al., *BKCa-Cav channel complexes mediate rapid and localized Ca^{2+}-activated K^+ signaling.* Science, 2006. **314**(5799): p. 615-20.
442. Grunnet, M. and W.A. Kaufmann, *Coassembly of big conductance Ca^{2+}-activated K^+ channels and L-type voltage-gated Ca^{2+} channels in rat brain.* J Biol Chem, 2004. **279**(35): p. 36445-53.
443. Eggermann, E., et al., *Nanodomain coupling between Ca(2)(+) channels and sensors of exocytosis at fast mammalian synapses.* Nat Rev Neurosci, 2012. **13**(1): p. 7-21.
444. Shin, D.M., et al., *Homer 2 tunes G protein-coupled receptors stimulus intensity by regulating RGS proteins and PLCbeta GAP activities.* J Cell Biol, 2003. **162**(2): p. 293-303.
445. van den Bogaart, G., T. Lang, and R. Jahn, *Microdomains of SNARE proteins in the plasma membrane.* Curr Top Membr, 2013. **72**: p. 193-230.
446. Missler, M., et al., *Alpha-neurexins couple Ca^{2+} channels to synaptic vesicle exocytosis.* Nature, 2003. **423**(6943): p. 939-48.
447. Chang, W.C. and A.B. Parekh, *Close functional coupling between Ca2+ release-activated Ca^{2+} channels, arachidonic acid release, and leukotriene C4 secretion.* J Biol Chem, 2004. **279**(29): p. 29994-9.
448. Chang, W.C., et al., *All-or-none activation of CRAC channels by agonist elicits graded responses in populations of mast cells.* J Immunol, 2007. **179**(8): p. 5255-63.
449. Bautista, D.M. and R.S. Lewis, *Modulation of plasma membrane calcium-ATPase activity by local calcium microdomains near CRAC channels in human T cells.* J Physiol, 2004. **556**(Pt 3): p. 805-17.
450. Tsunoda, S., et al., *A multivalent PDZ-domain protein assembles signalling complexes in a G-protein-coupled cascade.* Nature, 1997. **388**(6639): p. 243-9.
451. Chevesich, J., A.J. Kreuz, and C. Montell, *Requirement for the PDZ domain protein, INAD, for localization of the TRP store-operated channel to a signaling complex.* Neuron, 1997. **18**(1): p. 95-105.
452. Kiselyov, K., D.M. Shin, and S. Muallem, *Signalling specificity in GPCR-dependent Ca^{2+} signalling.* Cell Signal, 2003. **15**(3): p. 243-53.
453. Kammermeier, P.J., et al., *Homer proteins regulate coupling of group I metabotropic glutamate receptors to N-type calcium and M-type potassium channels.* J Neurosci, 2000. **20**(19): p. 7238-45.
454. Duncan, R.S., S.Y. Hwang, and P. Koulen, *Effects of Vesl/Homer proteins on intracellular signaling.* Exp Biol Med (Maywood), 2005. **230**(8): p. 527-35.
455. Becherer, U., et al., *Calcium regulates exocytosis at the level of single vesicles.* Nat Neurosci, 2003. **6**(8): p. 846-53.

456. Zenisek, D., et al., *Imaging calcium entry sites and ribbon structures in two presynaptic cells.* J Neurosci, 2003. **23**(7): p. 2538-48.
457. Llinas, R., M. Sugimori, and R.B. Silver, *Microdomains of high calcium concentration in a presynaptic terminal.* Science, 1992. **256**(5057): p. 677-9.
458. DiGregorio, D.A. and J.L. Vergara, *Localized detection of action potential-induced presynaptic calcium transients at a Xenopus neuromuscular junction.* J Physiol, 1997. **505 (Pt 3)**: p. 585-92.
459. Skiteva, O.I., V.I. Lapteva, and O.P. Balezina, *Effect of fast and slow calcium buffers on induced secretion of neurotransmitter.* Bull Exp Biol Med, 2010. **149**(3): p. 276-9.
460. Adler, E.M., et al., *Alien intracellular calcium chelators attenuate neurotransmitter release at the squid giant synapse.* J Neurosci, 1991. **11**(6): p. 1496-507.
461. Borst, J.G. and B. Sakmann, *Calcium influx and transmitter release in a fast CNS synapse.* Nature, 1996. **383**(6599): p. 431-4.
462. Rozov, A., et al., *Transmitter release modulation by intracellular Ca^{2+} buffers in facilitating and depressing nerve terminals of pyramidal cells in layer 2/3 of the rat neocortex indicates a target cell-specific difference in presynaptic calcium dynamics.* J Physiol, 2001. **531**(Pt 3): p. 807-26.
463. Chiono, M., et al., *Capacitative Ca^{2+} entry exclusively inhibits cAMP synthesis in C6-2B glioma cells. Evidence that physiologically evoked Ca^{2+} entry regulates $Ca(^{2+})$-inhibitable adenylyl cyclase in non-excitable cells.* J Biol Chem, 1995. **270**(3): p. 1149-55.
464. Fagan, K.A., R. Mahey, and D.M. Cooper, *Functional co-localization of transfected Ca(2+)-stimulable adenylyl cyclases with capacitative Ca^{2+} entry sites.* J Biol Chem, 1996. **271**(21): p. 12438-44.
465. Hardingham, G.E., et al., *Distinct functions of nuclear and cytoplasmic calcium in the control of gene expression.* Nature, 1997. **385**(6613): p. 260-5.
466. Deisseroth, K., H. Bito, and R.W. Tsien, *Signaling from synapse to nucleus: postsynaptic CREB phosphorylation during multiple forms of hippocampal synaptic plasticity.* Neuron, 1996. **16**(1): p. 89-101.
467. Dolmetsch, R.E., et al., *Signaling to the nucleus by an L-type calcium channel-calmodulin complex through the MAP kinase pathway.* Science, 2001. **294**(5541): p. 333-9.
468. Hardingham, G.E., F.J. Arnold, and H. Bading, *A calcium microdomain near NMDA receptors: on switch for ERK-dependent synapse-to-nucleus communication.* Nat Neurosci, 2001. **4**(6): p. 565-6.
469. Zhang, J. and M.S. Shapiro, *Activity-dependent transcriptional regulation of M-Type (Kv7) K(+) channels by AKAP79/150-mediated NFAT actions.* Neuron, 2012. **76**(6): p. 1133-46.
470. Nowycky, M.C. and M.J. Pinter, *Time courses of calcium and calcium-bound buffers following calcium influx in a model cell.* Biophys J, 1993. **64**(1): p. 77-91.
471. Parekh, A.B., *Ca^{2+} microdomains near plasma membrane Ca^{2+} channels: impact on cell function.* J Physiol, 2008. **586**(13): p. 3043-54.
472. Roberts, W.M., R.A. Jacobs, and A.J. Hudspeth, *Colocalization of ion channels involved in frequency selectivity and synaptic transmission at presynaptic active zones of hair cells.* J Neurosci, 1990. **10**(11): p. 3664-84.
473. Prakriya, M., C.R. Solaro, and C.J. Lingle, *$[Ca^{2+}]i$ elevations detected by BK channels during Ca^{2+} influx and muscarine-mediated release of Ca2+ from intracellular stores in rat chromaffin cells.* J Neurosci, 1996. **16**(14): p. 4344-59.

474. Robitaille, R., E.M. Adler, and M.P. Charlton, *Strategic location of calcium channels at transmitter release sites of frog neuromuscular synapses.* Neuron, 1990. **5**(6): p. 773-9.
475. Lemonnier, L., et al., *Direct modulation of volume-regulated anion channels by Ca(2+) chelating agents.* FEBS Lett, 2002. **521**(1-3): p. 152-6.
476. Lemonnier, L., et al., *Protection of TRPC7 cation channels from calcium inhibition by closely associated SERCA pumps.* FASEB J, 2006. **20**(3): p. 503-5.
477. Brakemeier, S., et al., *Modulation of Ca^{2+}-activated K^+ channel in renal artery endothelium in situ by nitric oxide and reactive oxygen species.* Kidney Int, 2003. **64**(1): p. 199-207.
478. Verkman, A.S., *Development and biological applications of chloride-sensitive fluorescent indicators.* Am J Physiol, 1990. **259**(3 Pt 1): p. C375-88.
479. Huang, F., et al., *Calcium-activated chloride channel TMEM16A modulates mucin secretion and airway smooth muscle contraction.* Proc Natl Acad Sci U S A, 2012. **109**(40): p. 16354-9.
480. Storm, J.F., *Intracellular injection of a Ca^{2+} chelator inhibits spike repolarization in hippocampal neurons.* Brain Res, 1987. **435**(1-2): p. 387-92.
481. Naraghi, M. and E. Neher, *Linearized buffered Ca^{2+} diffusion in microdomains and its implications for calculation of $[Ca^{2+}]$ at the mouth of a calcium channel.* J Neurosci, 1997. **17**(18): p. 6961-73.
482. Neher, E., *Usefulness and limitations of linear approximations to the understanding of Ca++ signals.* Cell Calcium, 1998. **24**(5-6): p. 345-57.
483. Rose, K., et al., *Transcriptional repression of the M channel subunit Kv7.2 in chronic nerve injury.* Pain, 2011. **152**(4): p. 742-54.
484. Jarvius, M., et al., *In situ detection of phosphorylated platelet-derived growth factor receptor beta using a generalized proximity ligation method.* Molecular & Cellular Proteomics, 2007. **6**(9): p. 1500-1509.
485. Delmas, P., et al., *Signaling microdomains define the specificity of receptor-mediated InsP(3) pathways in neurons.* Neuron, 2002. **34**(2): p. 209-20.
486. Fakler, B. and J.P. Adelman, *Control of K(Ca) channels by calcium nano/microdomains.* Neuron, 2008. **59**(6): p. 873-81.
487. Willoughby, D., et al., *Direct demonstration of discrete Ca^{2+} microdomains associated with different isoforms of adenylyl cyclase.* J Cell Sci, 2010. **123**(Pt 1): p. 107-17.
488. Park, C.Y., et al., *STIM1 clusters and activates CRAC channels via direct binding of a cytosolic domain to Orai1.* Cell, 2009. **136**(5): p. 876-90.
489. Yuan, J.P., et al., *SOAR and the polybasic STIM1 domains gate and regulate Orai channels.* Nat Cell Biol, 2009. **11**(3): p. 337-43.
490. Pani, B., et al., *Activation of TRPC1 by STIM1 in ER-PM microdomains involves release of the channel from its scaffold caveolin-1.* Proc Natl Acad Sci U S A, 2009. **106**(47): p. 20087-92.
491. Weaver, A.K., et al., *BK channels are linked to inositol 1,4,5-triphosphate receptors via lipid rafts: a novel mechanism for coupling [Ca(2+)](i) to ion channel activation.* J Biol Chem, 2007. **282**(43): p. 31558-68.
492. Devine, C.E., A.V. Somlyo, and A.P. Somlyo, *Sarcoplasmic reticulum and excitation-contraction coupling in mammalian smooth muscles.* J Cell Biol, 1972. **52**(3): p. 690-718.
493. Pike, L.J., *Lipid rafts: bringing order to chaos.* J Lipid Res, 2003. **44**(4): p. 655-67.
494. Zeyda, M. and T.M. Stulnig, *Lipid Rafts & Co.: an integrated model of membrane organization in T cell activation.* Prog Lipid Res, 2006. **45**(3): p. 187-202.

495. Fivaz, M., L. Abrami, and F.G. van der Goot, *Landing on lipid rafts.* Trends Cell Biol, 1999. **9**(6): p. 212-3.
496. Korade, Z. and A.K. Kenworthy, *Lipid rafts, cholesterol, and the brain.* Neuropharmacology, 2008. **55**(8): p. 1265-73.
497. Pike, L.J., *The challenge of lipid rafts.* J Lipid Res, 2009. **50 Suppl**: p. S323-8.
498. Rimmerman, N., et al., *Compartmentalization of endocannabinoids into lipid rafts in a dorsal root ganglion cell line.* Br J Pharmacol, 2008. **153**(2): p. 380-9.
499. Hicks, D.A., N.N. Nalivaeva, and A.J. Turner, *Lipid rafts and Alzheimer's disease: protein-lipid interactions and perturbation of signaling.* Front Physiol. **3**: p. 189.
500. Jury, E.C., F. Flores-Borja, and P.S. Kabouridis, *Lipid rafts in T cell signalling and disease.* Semin Cell Dev Biol, 2007. **18**(5): p. 608-15.
501. Waheed, A.A. and E.O. Freed, *Lipids and membrane microdomains in HIV-1 replication.* Virus Res, 2009. **143**(2): p. 162-76.
502. Rodal, S.K., et al., *Extraction of cholesterol with methyl-beta-cyclodextrin perturbs formation of clathrin-coated endocytic vesicles.* Mol Biol Cell, 1999. **10**(4): p. 961-74.
503. Dart, C., *Lipid microdomains and the regulation of ion channel function.* J Physiol, 2010. **588**(Pt 17): p. 3169-78.
504. Parton, R.G., *Caveolae and caveolins.* Curr Opin Cell Biol, 1996. **8**(4): p. 542-8.
505. Kurzchalia, T.V. and R.G. Parton, *Membrane microdomains and caveolae.* Curr Opin Cell Biol, 1999. **11**(4): p. 424-31.
506. Anderson, R.G., *The caveolae membrane system.* Annu Rev Biochem, 1998. **67**: p. 199-225.
507. Fielding, P.E. and C.J. Fielding, *Plasma membrane caveolae mediate the efflux of cellular free cholesterol.* Biochemistry, 1995. **34**(44): p. 14288-92.
508. Smart, E.J., et al., *A role for caveolin in transport of cholesterol from endoplasmic reticulum to plasma membrane.* J Biol Chem, 1996. **271**(46): p. 29427-35.
509. Schnitzer, J.E., P. Oh, and D.P. McIntosh, *Role of GTP hydrolysis in fission of caveolae directly from plasma membranes.* Science, 1996. **274**(5285): p. 239-42.
510. Anderson, R.G., et al., *Potocytosis: sequestration and transport of small molecules by caveolae.* Science, 1992. **255**(5043): p. 410-1.
511. Lisanti, M.P., et al., *Characterization of caveolin-rich membrane domains isolated from an endothelial-rich source: implications for human disease.* J Cell Biol, 1994. **126**(1): p. 111-26.
512. Okamoto, C.T., *Endocytosis and transcytosis.* Adv Drug Deliv Rev, 1998. **29**(3): p. 215-228.
513. Shaul, P.W. and R.G. Anderson, *Role of plasmalemmal caveolae in signal transduction.* Am J Physiol, 1998. **275**(5 Pt 1): p. L843-51.
514. Kurzchalia, T.V., et al., *VIP21, a 21-kD membrane protein is an integral component of trans-Golgi-network-derived transport vesicles.* J Cell Biol, 1992. **118**(5): p. 1003-14.
515. Drab, M., et al., *Loss of caveolae, vascular dysfunction, and pulmonary defects in caveolin-1 gene-disrupted mice.* Science, 2001. **293**(5539): p. 2449-52.
516. Razani, B., et al., *Caveolin-1 null mice are viable but show evidence of hyperproliferative and vascular abnormalities.* J Biol Chem, 2001. **276**(41): p. 38121-38.
517. Hong, S., et al., *Insulin-like growth factor-1 receptor signaling in 3T3-L1 adipocyte differentiation requires lipid rafts but not caveolae.* Cell Death Differ, 2004. **11**(7): p. 714-23.
518. Krajewska, W.M. and I. Maslowska, *Caveolins: structure and function in signal transduction.* Cell Mol Biol Lett, 2004. **9**(2): p. 195-220.

519. Silva, A.R., et al., *Lipid bodies in oxidized LDL-induced foam cells are leukotriene-synthesizing organelles: a MCP-1/CCL2 regulated phenomenon.* Biochim Biophys Acta, 2009. **1791**(11): p. 1066-75.
520. Patel, H.H., F. Murray, and P.A. Insel, *Caveolae as organizers of pharmacologically relevant signal transduction molecules.* Annu Rev Pharmacol Toxicol, 2008. **48**: p. 359-91.
521. Steinberg, S.F., *beta(2)-Adrenergic receptor signaling complexes in cardiomyocyte caveolae/lipid rafts.* J Mol Cell Cardiol, 2004. **37**(2): p. 407-15.
522. Insel, P.A., et al., *Caveolae and lipid rafts: G protein-coupled receptor signaling microdomains in cardiac myocytes.* Ann N Y Acad Sci, 2005. **1047**: p. 166-72.
523. Razani, B., S.E. Woodman, and M.P. Lisanti, *Caveolae: from cell biology to animal physiology.* Pharmacol Rev, 2002. **54**(3): p. 431-67.
524. Williams, T.M. and M.P. Lisanti, *The caveolin proteins.* Genome Biol, 2004. **5**(3): p. 214.
525. Fagan, K.A., K.E. Smith, and D.M. Cooper, *Regulation of the Ca^{2+}-inhibitable adenylyl cyclase type VI by capacitative Ca2+ entry requires localization in cholesterol-rich domains.* J Biol Chem, 2000. **275**(34): p. 26530-7.
526. Kwiatek, A.M., et al., *Caveolin-1 regulates store-operated Ca^{2+} influx by binding of its scaffolding domain to transient receptor potential channel-1 in endothelial cells.* Mol Pharmacol, 2006. **70**(4): p. 1174-83.
527. Bergdahl, A., et al., *Cholesterol depletion impairs vascular reactivity to endothelin-1 by reducing store-operated Ca^{2+} entry dependent on TRPC1.* Circ Res, 2003. **93**(9): p. 839-47.
528. Martens, J.R., et al., *Isoform-specific localization of voltage-gated K^+ channels to distinct lipid raft populations. Targeting of Kv1.5 to caveolae.* J Biol Chem, 2001. **276**(11): p. 8409-14.
529. Balijepalli, R.C. and T.J. Kamp, *Caveolae, ion channels and cardiac arrhythmias.* Prog Biophys Mol Biol, 2008. **98**(2-3): p. 149-60.
530. Palygin, O.A., J.M. Pettus, and E.F. Shibata, *Regulation of caveolar cardiac sodium current by a single Gsalpha histidine residue.* Am J Physiol Heart Circ Physiol, 2008. **294**(4): p. H1693-9.
531. Shibata, E.F., et al., *Autonomic regulation of voltage-gated cardiac ion channels.* J Cardiovasc Electrophysiol, 2006. **17 Suppl 1**: p. S34-S42.
532. Yarbrough, T.L., et al., *Localization of cardiac sodium channels in caveolin-rich membrane domains: regulation of sodium current amplitude.* Circ Res, 2002. **90**(4): p. 443-9.
533. Maguy, A., T.E. Hebert, and S. Nattel, *Involvement of lipid rafts and caveolae in cardiac ion channel function.* Cardiovasc Res, 2006. **69**(4): p. 798-807.
534. Lopez-Lopez, J.R., et al., *Local calcium transients triggered by single L-type calcium channel currents in cardiac cells.* Science, 1995. **268**(5213): p. 1042-5.
535. Darby, P.J., C.Y. Kwan, and E.E. Daniel, *Caveolae from canine airway smooth muscle contain the necessary components for a role in Ca(2+) handling.* Am J Physiol Lung Cell Mol Physiol, 2000. **279**(6): p. L1226-35.
536. O'Connell, K.M., J.R. Martens, and M.M. Tamkun, *Localization of ion channels to lipid Raft domains within the cardiovascular system.* Trends Cardiovasc Med, 2004. **14**(2): p. 37-42.
537. Singleton, P.A. and L.Y. Bourguignon, *CD44 interaction with ankyrin and IP_3 receptor in lipid rafts promotes hyaluronan-mediated Ca^{2+} signaling leading to nitric oxide production and endothelial cell adhesion and proliferation.* Exp Cell Res, 2004. **295**(1): p. 102-18.

538. Abi-Char, J., et al., *Membrane cholesterol modulates Kv1.5 potassium channel distribution and function in rat cardiomyocytes.* J Physiol, 2007. **582**(Pt 3): p. 1205-17.
539. Wong, W. and L.C. Schlichter, *Differential recruitment of Kv1.4 and Kv4.2 to lipid rafts by PSD-95.* J Biol Chem, 2004. **279**(1): p. 444-52.
540. Hibino, H., et al., *Inwardly rectifying potassium channels: their structure, function, and physiological roles.* Physiol Rev, 2010. **90**(1): p. 291-366.
541. Sampson, L.J., et al., *Caveolae localize protein kinase A signaling to arterial ATP-sensitive potassium channels.* Circ Res, 2004. **95**(10): p. 1012-8.
542. Tajima, N., et al., *Activity of BK(Ca) channel is modulated by membrane cholesterol content and association with Na^+/K^+-ATPase in human melanoma IGR39 cells.* J Biol Chem, 2011. **286**(7): p. 5624-38.
543. Pani, B. and B.B. Singh, *Lipid rafts/caveolae as microdomains of calcium signaling.* Cell Calcium, 2009. **45**(6): p. 625-33.
544. Folco, E.J., G.X. Liu, and G. Koren, *Caveolin-3 and SAP97 form a scaffolding protein complex that regulates the voltage-gated potassium channel Kv1.5.* Am J Physiol Heart Circ Physiol, 2004. **287**(2): p. H681-90.
545. Calaghan, S. and E. White, *Caveolae modulate excitation-contraction coupling and beta2-adrenergic signalling in adult rat ventricular myocytes.* Cardiovasc Res, 2006. **69**(4): p. 816-24.
546. Balijepalli, R.C., et al., *Localization of cardiac L-type Ca(2+) channels to a caveolar macromolecular signaling complex is required for beta(2)-adrenergic regulation.* Proc Natl Acad Sci U S A, 2006. **103**(19): p. 7500-5.
547. Abi-Char, J., et al., *The anchoring protein SAP97 retains Kv1.5 channels in the plasma membrane of cardiac myocytes.* Am J Physiol Heart Circ Physiol, 2008. **294**(4): p. H1851-61.
548. Murata, M., et al., *SAP97 interacts with Kv1.5 in heterologous expression systems.* Am J Physiol Heart Circ Physiol, 2001. **281**(6): p. H2575-84.
549. Pike, L.J., *Lipid rafts: heterogeneity on the high seas.* Biochem J, 2004. **378**(Pt 2): p. 281-92.
550. Suh, B.C. and B. Hille, *Regulation of ion channels by phosphatidylinositol 4,5-bisphosphate.* Curr Opin Neurobiol, 2005. **15**(3): p. 370-8.
551. Gamper, N. and M.S. Shapiro, *Target-specific PIP(2) signalling: how might it work?* J Physiol, 2007. **582**(Pt 3): p. 967-75.
552. Lawrence, J.C., et al., *Real-time analysis of the effects of cholesterol on lipid raft behavior using atomic force microscopy.* Biophys J, 2003. **84**(3): p. 1827-32.
553. Ohtani, Y., et al., *Differential effects of alpha-, beta- and gamma-cyclodextrins on human erythrocytes.* Eur J Biochem, 1989. **186**(1-2): p. 17-22.
554. Brunner, J.D., et al., *X-ray structure of a calcium-activated TMEM16 lipid scramblase.* Nature, 2014. **516**(7530): p. 207-12.
555. Sones, W.R., et al., *Cholesterol depletion alters amplitude and pharmacology of vascular calcium-activated chloride channels.* Cardiovasc Res, 2010. **87**(3): p. 476-84.
556. Sun, X. and G.R. Whittaker, *Role for influenza virus envelope cholesterol in virus entry and infection.* J Virol, 2003. **77**(23): p. 12543-51.
557. Absi, M., et al., *Effects of methyl beta-cyclodextrin on EDHF responses in pig and rat arteries; association between SK(Ca) channels and caveolin-rich domains.* Br J Pharmacol, 2007. **151**(3): p. 332-40.
558. Brainard, A.M., et al., *Maxi-K channels localize to caveolae in human myometrium: a role for an actin-channel-caveolin complex in the regulation of myometrial smooth muscle K^+ current.* Am J Physiol Cell Physiol, 2005. **289**(1): p. C49-57.

559. Vial, C. and R.J. Evans, *Disruption of lipid rafts inhibits P2X1 receptor-mediated currents and arterial vasoconstriction.* J Biol Chem, 2005. **280**(35): p. 30705-11.
560. Berkefeld, H., B. Fakler, and U. Schulte, *Ca^{2+}-activated K^+ channels: from protein complexes to function.* Physiol Rev, 2010. **90**(4): p. 1437-59.
561. Good, M.C., J.G. Zalatan, and W.A. Lim, *Scaffold proteins: hubs for controlling the flow of cellular information.* Science, 2011. **332**(6030): p. 680-6.
562. Shaw, A.S. and E.L. Filbert, *Scaffold proteins and immune-cell signalling.* Nat Rev Immunol, 2009. **9**(1): p. 47-56.
563. Gasperini, R., et al., *Homer regulates calcium signalling in growth cone turning.* Neural Dev, 2009. **4**: p. 29.
564. Tu, J.C., et al., *Homer binds a novel proline-rich motif and links group 1 metabotropic glutamate receptors with IP_3 receptors.* Neuron, 1998. **21**(4): p. 717-26.
565. Xiao, B., J.C. Tu, and P.F. Worley, *Homer: a link between neural activity and glutamate receptor function.* Curr Opin Neurobiol, 2000. **10**(3): p. 370-4.
566. Jeske, N.A., *Somatosensory scaffolding structures.* Front Mol Neurosci, 2012. **5**: p. 2.
567. Chuang, H.H., et al., *Bradykinin and nerve growth factor release the capsaicin receptor from PtdIns(4,5)P2-mediated inhibition.* Nature, 2001. **411**(6840): p. 957-62.
568. Caterina, M.J., et al., *The capsaicin receptor: a heat-activated ion channel in the pain pathway.* Nature, 1997. **389**(6653): p. 816-24.
569. Cahalan, M.D. and K.G. Chandy, *The functional network of ion channels in T lymphocytes.* Immunol Rev, 2009. **231**(1): p. 59-87.
570. Bao, R., et al., *A close association of RyRs with highly dense clusters of Ca^{2+} activated Cl^- channels underlies the activation of STICs by Ca^{2+} sparks in mouse airway smooth muscle*. J Gen Physiol, 2008. **132**(1): p. 145-60.
571. Jentsch, T.J., K. Steinmeyer, and G. Schwarz, *Primary structure of Torpedo marmorata chloride channel isolated by expression cloning in Xenopus oocytes*. Nature, 1990. **348**(6301): p. 510-4.
572. Greenwood, I.A. and N. Leblanc, *Overlapping pharmacology of Ca^{2+}-activated Cl^- and K^+ channels.* Trends Pharmacol Sci, 2007. **28**(1): p. 1-5.
573. Liantonio, A., et al., *Activation and inhibition of kidney CLC-K chloride channels by fenamates*. Mol Pharmacol, 2006. **69**(1): p. 165-73.
574. Duranton, C., et al., *Organic osmolyte permeabilities of the malaria-induced anion conductances in human erythrocytes*. J Gen Physiol, 2004. **123**(4): p. 417-26.

Publications

1. Jin X, Shah S, Du X, Zhang H, Gamper N. Activation of Ca^{2+}-activated Cl^- channel ANO1 by localized Ca^{2+} signals. J Physiol. 2014 Nov 14.
2. Jin X, Shah S, Liu Y, Zhang H, Lees M, Fu Z, Lippiat JD, Beech DJ, Sivaprasadarao A, Baldwin SA, Zhang H, Gamper N. Activation of the Cl^- channel ANO1 by localized calcium signals in nociceptive sensory neurons requires coupling with the IP_3 receptor. Sci Signal. 2013 Aug 27;6(290):ra73.